National Technical University of Athens

School of Civil Engineering

M.Sc. Thesis

3D EXPERIMENTAL AND NUMERICAL ANALYSIS OF FAULT RUPTURE - SOIL - FOUNDATION - STRUCTURE INTERACTION

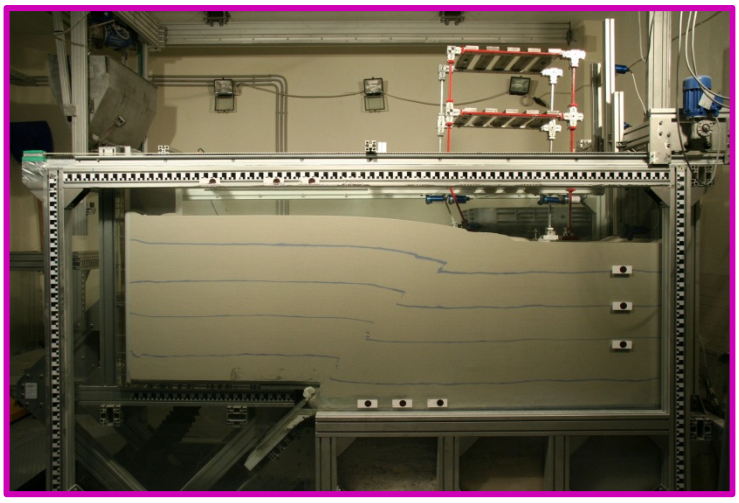

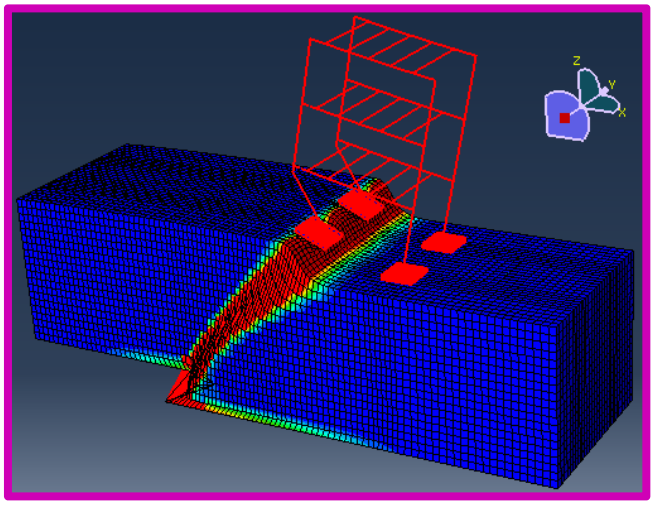

Kiana Hashemi

Supervisor: Prof. George. Gazetas

Dr. I. Anastasopoulos

October 2012

ΕΘΝΙΚΟ ΜΕΤΣΟΒΙΟ ΠΟΛΥΤΕΧΝΕΙΟ
ΔΙΑΤΜΗΜΑΤΙΚΟ ΠΡΟΓΡΑΜΜΑ ΜΕΤΑΠΤΥΧΙΑΚΩΝ ΣΠΟΥΔΩΝ
"ΔΟΜΟΣΤΑΤΙΚΟΣ ΣΧΕΔΙΑΣΜΟΣ ΚΑΙ ΑΝΑΛΥΣΗ ΚΑΤΑΣΚΕΥΩΝ"

Ακαδημαϊκό έτος 2010-2011

Εξεταστική Περίοδος Οκτωβρίου 2011

ΔΕΛΤΙΟ ΒΑΘΜΟΛΟΓΙΑΣ
ΜΕΤΑΠΤΥΧΙΑΚΗΣ ΕΡΓΑΣΙΑΣ

Ονοματεπώνυμο:

Θεματική περιοχή: Γεωτεχνική Δυναμική Μηχ.

Τίτλος: 3D Experimental and Numerical Analysis of Fault Rupture Foundation Interaction

Ημερομηνία έναρξης εκπόνησης:

Τριμελής Επιτροπή:
1. Γ. ΓΚΑΖΕΤΑΣ (Επιβλέπων)
2. Β. ΚΟΥΜΟΥΣΗΣ
3. Ν. ΓΕΡΟΛΥΜΟΣ

Τόπος και ημερομηνία παρουσίασης: 26/10/12

Για την διαμόρφωση του τελικού βαθμού λήφθηκαν υπόψη οι ακόλουθοι επιμέρους βαθμοί με τα αντίστοιχα κριτήρια βαρύτητας:
α) Για την επιστημονική επάρκεια, πληρότητα και πρωτοτυπία (50%): 10 (Βαθμός)
β) Για την εφαρμογή σε προβλήματα δομοστατικού σχεδιασμού (30%): 10 (Βαθμός)
γ) Για την παρουσίαση (20%): 10 (Βαθμός)

Τελικός βαθμός: 10 δέκα

Αθήνα / /
Η Τριμελής Επιτροπή
(υπογραφές)

National Technical University of Athens

School of Civil Engineering

M.Sc. Thesis

3D EXPERIMENTAL AND NUMERICAL ANALYSIS OF FAULT RUPTURE-SOIL-FOUNDATION-STRUCTURE INTERACTION

Kiana Hashemi

Supervisor: Prof. George. Gazetas

Dr. I. Anastasopoulos

October 2012

Dedicated to my parents who were deprived from continuing their studies in Medical School of University of Shiraz just because of their faith in 1981

ABSTRACT

In an earthquake, the rupture of an active fault generates two types of ground displacement: transient dynamic waves away from the fault and permanent quasi-static offsets on the fault itself [Ambraseys and Jackson, 1984; Jackson, 2001]. In past decades, earthquake engineering research and practice has generally concentrated on the dynamic response of structures and soil–structure interaction during seismic shaking and less consideration has been paid to the most direct consequence of the faulting process. This is because of the fact that the seismic waves propagate over large distances in the earth and therefore they always affect the ground surface. By contrast, permanent surface ruptures are only important near the fault trace and when rupture extends all the way to the surface. However, in large magnitude earthquakes the fault rupture may be important, imposing significant deformation to overlying structures.

The 1999 earthquakes in Turkey and Taiwan, offering a variety of case histories with structures subjected to large tectonic displacements, have prompted the increased interest of the earthquake engineering community on the subject. While several structures were severely damaged or even collapsed, there were numerous examples of satisfactory performance. Surprisingly, in specific cases the surface fault rupture was effectively diverted due to the presence of a structure.

In order to develop deeper insight into main mechanisms controlling this interlay, this research studies the effects of thrust fault rupture on foundation - structure systems founded on top of a sand soil deposit. This is done through 2-step procedure: The first step is to model the propagation of fault rupture through the soil layers and reaching the ground surface, and the second is simulating the effects of presence of structure founded on top of outcropping fault. Through these two steps, a 3D nonlinear finite element analysis with ABAQUS is performed in order to investigate the response of both a 3-story structure and the foundation to the fault rupture.

The soil constitutive model is calibrated by performing direct shear test. The model in ABAQUS has been verified by experiments which taken place in Laboratory of Soil Mechanics in N.T.U.A. The foundation is modeled as solid element and the columns and beams are modeled as flexural beam elements, while the possibility of sliding and detachment between the foundation and the underlying soil is considered through the use of special interface elements.

The numerical finite element which was verified by some small-scale experiments has been used to study the effects of different parameters like the magnitude of the fault offset and its location on the behaviour of both structure and foundation. The main results for our fault rupture soil-foundation-structure interaction analysis are discussed in terms of the distribution of plastic strains, the vertical displacement profile Δy, the foundation horizontal displacement, the structural drift ratio, structural moment, the foundation and structure rotation, the rigid body rotation in foundation and structure level and the rigid body settlement.

In this dissertation, we achieved good agreement between numerical and experimental results with the presence of the structure especially for larger base vertical displacement. As in the prototype structure which wasn't comply with capacity design principles and was prone to soft-story collapse mechanism, our reduced-scale model in ABAQUS also shows this soft-story failure and having plastic hinges in columns. We also observe that buildings on isolated footings are unable to avoid the direct hit of an underneath outcropping surface rupture. Consequently, the dislocation emerges within the structure causing significant deformation and distress.

Table of Contents

Chapter 1

1. Introduction

1.1. Background

When an earthquake acts on a structural system founded on the soil, neither the structural deformation nor the ground displacement, are independent of each other. Observations from recent earthquakes, such as the 1995 Kobe Earthquake, have shown that the response of a structure during earthquake is affected by interactions between three linked systems: the structure, the foundation, and the geologic media underlying and surrounding the foundation. The process in which the soil response affects the behavior of the structure and behavior of the structure affects the response of the soil is known as **Soil-Foundation-Structure-Interaction (SFSI)**.

During an earthquake, we observe two types of ground movements: static offset on the fault and transient dynamic vibration away from the fault [Ambraseys and Jackson, 1984; Jackson, 2001]. Much efforts have been devoted to the dynamic response of soil and structure to the transient dynamic oscillations as such waves always affect the ground surface compared to static dislocation which just affects the surface when the rupture extends all the way to reach the surface. However, the recent earthquakes (.g., Kocaeli 1999; Düzce 1999; Chi-Chi 1999; Wenchuan 2008) showed the significant effects of surface ruptures on structures. One of the best examples of faulting hazard has been presented in the 1999 Chi-Chi earthquake in Taiwan with a total length of the fault be almost 90 km, the fault of the Mw 7.6 earthquake spread all the way to the ground surface, creating a multitude of fault scarps of vertical offset of up to 10 m (**Fig.1.1)** while in the same earthquake there weren't any detrimental damages in the structure of **Fig.1.2** due to rigid body rotation of whole structure. Finally in **Fig.1.3** of Kocaeli (Turkey) earthquake of 1999, we can see no damages due to diversion of rupture as if to avoid rupturing directly underneath the structure.

Most seismic codes demand to not build structures in vicinity of active faults but this prohibition is sometimes difficult to obey. One important reason is that the existence of a structure on soil deposit would modify the path of the rupture depending on the rigidity of the foundation and the weight of the structure. Therefore, in addition to Soil-Structure Interaction, there would be also interplay between the propagating fault rupture, the deformed soil deposit and the displaced structure.

1.2. Scope and Objectives

The primary objective of this research is the investigation of the above mentioned interaction between soil and the structure hit by thrust fault rupture. This is done through 2-step procedure: The first step is to model the propagation of fault rupture through the soil layers and reaching the ground surface, and the second is simulating the effects of presence of structure founded on top of outcropping fault. Through these two steps, a 3D numerical model is verified by some reduced-scale experiments which were done in Laboratory of Soil Mechanics of National Technical University of Athens and then that verified model is used for some parametric analysis on the Fault Rupture Soil-Foundation-Structure Interaction (FR-SFSI).

This dissertation consists of six chapters. Apart from the first one which was the introduction to the problem and clarifying the objectives of this research, the second chapter will present the literature review of different researched have been conducted on this subject.

Chapter 3 and 4 will deal with the analysis of fault rupture propagation in the free field by ignoring the presence of the structure and then by considering also the structure on soil deposit respectively. This two-step analysis will be done both numerically and experimentally.

Chapter 5 undertakes a parametric investigation on the influence of magnitude of rupture offset and also on rupture location on the soil-structure interaction.

Finally, chapter 6 summarizes the main conclusions of this study.

Figures of **Chapter 1**

∞ **Figure 1.1** Substantial damages due to surface rupture from Chi-Chi Earthquake of 1999 (Taiwan)

Figure 1.2 No damages due to rigid body rotation of structure -Chi-Chi Earthquake 1999 (Taiwan)

Figure 1.3 No damages due to diversion of rupture – Kokaeli Earthquake 1999 (Turkey)

Chapter 2

2. Literature Review

In literature, the problem of fault rupture propagation through soil has been investigated in three main fields: (a) Studying the real case histories, (b) small-scale modeling, and (c) Numerical and analytical analysis. From the analysis of real case histories, it is observed that the surface rupture caused many structures to collapse or substantial damages while in some cases there is diversion of rupture path due to presence of the structure and its heavy load. In another examples, the rigid and continues foundations behave better against rupture compared to spread footings. [Ulusay et al, 2001; Faccioli et al, 2008; Anastasopoulos, et al., 2007].

The second method for the experimental research in the field of fault rupture propagation is quite significant and it has two branches: 1g testing [Cole and Lade, 1984; Lade et al., 1984; Bray et al., 1994a,b, Bray, 2001; Lee and Hamada, 2005; Lin et al., 2005, 2006a] and centrifuge experiments [Bransby et al 2008a,b; Lee et al, 2005]. Although these efforts in small-scale experiments offer in-deep insight on the mechanics of rupturing, the extrapolation from the small-scale to reality is needed to be completely investigated.

By using the results of aforementioned studies, many researchers have utilized Finite Element Method and Finite Difference Method [Bray, 1990; Bray, 2001; Anastasopoulos, 2005,2008,2009,2010; Lin et al., 2005; Lin et al., 2005, 2006b] as well as analytical methods [Yilmaz and Paolucci, 2007] to simulate the fault rupture propagation through soil. These studies have been conducted to investigate the effects of load and rigidity of foundation, the stiffness of foundation system, and the relative outcropping position of the rupture as well as soil deformability (loos vs. dense sand). However, most of these researches evaluated fault rupture-soil-structure interaction by analyzing a rigid foundation located on top of soil deposit and the only effort to investigate the influence of a building and investigate the effects of rigidity of structure on fault rupture propagation by Anastasopoulos et al., 2007 was done by utilizing 2D finite element modeling.

Chapter 3

3. Free Field Fault Rupture Propagation

3.1. Introduction

Analysis of free field rupture propagation is the first step of Fault Rupture-Soil-Foundation-Structure Interaction analysis. Although the complete analysis of fault rupture propagation in the free field is not in the scope of this research, its realistic simulation is important for the second step of our analysis. It is prerequisite for our analysis that first we verify our model in free field fault rupture propagation and then go forward to consideration of the presence of the structure. This analysis shows for small rupture amplitude, h, the rupture cannot propagate all the way to reach the surface. The required h/H ratio for the rupture to outcrop is a function of soil ductility which is considered in our Mohr-Coulomb constitutive law, through the yield strain γ_y. The results show satisfactory agreement between the numerical analysis and experimental studies.

3.2. Analysis Methodology

For performing the first step of our methodology which is free field analysis, a small-scale experiment was conducted in Laboratory of Soil Mechanics of N.T.U.A for simulating the thrust fault rupture propagating through soil layers and reaching the ground surface. Then a 3D nonlinear finite element analysis is done to simulate the reduced-scale experiment in ABAQUS. Finally the results are compared in order to verify the free field model in ABAQUS for using it for the next step of our analysis which is going to consider the presence of the structure on the soil deposit.

3.3. Reduced-Scale Experiments

3.3.1. Fault Rupture Apparatus

The free field fault rupture small-scale experiment was done in the Laboratory of Soil Mechanics of N.T.U.A through the apparatus of **Fig.3.1.a**. This apparatus contains a sand box with the internal dimensions of $1.48\text{m} \times 0.78\text{m} \times 0.645\text{m}$ (**Fig.3.1.b**) which has two transparent barriers which have been installed at the two opposite bigger sides of the box for the better observation of the experiment. The internal sides of these barriers are from glass which minimize the friction inside and the external sides are from Plexiglas for rigidity and durability of the outside [Nonika Antonaki, 2012].

3.3.2. Sand Properties

The transparent soil container was filled with dry ‘‘Longstone’’ sand, a very fine and uniform quartz sand with a mean grain size of $D_{50} = 0.15\ \text{mm}$ [Anastasopoulos et al., 2010b]. The grain size distribution of this sand is shown in **Fig.3.2**. The maximum and minimum void ratios measured in laboratory are $e_{max} = 0.954$ and $e_{min} = 0.572$ with $G_s = 2.63$. In order to have a constant D_r during raining the sand to the container, a custom raining system has been used (**Fig.3.3.a**). Through this system, it is possible to control the mass flow rate and rain the sand from specific height in order to have a constant density during filling the container with different layers of soil and achieve reproducibility and repeatability of the soil model properties (**Fig.3.3.b**).

For this experiment, the sand box was filled with 10 layers of loose sand (**Fig.3.4**) with the approximate thickness of 0.075 m in order to have a total thickness of 0.75 m soil deposit.

3.3.3. Fault Rupture Simulation

For simulating the thrust fault rupture, a machine at the bottom of this box produced vertical displacement at the base of the soil layer with a defined dip angle. This vertical displacement was increased gradually until reaching the desired value. For this experiment the vertical displacement began from 5 mm and increased in each step for 5 mm to reach the total vertical displacement of 100 mm (**Fig.3.5**).

3.4. Finite Element Model

3.4.1. Model Geometry

The finite element model for the simulation of the free field motion is displayed in **Fig.3.6**. It refers to a $H = 750$ mm thick soil layer at the base of which a reverse fault with dip angle α ruptures and produces an upward movement with vertical amplitude h. The model has a total length of $L = 2.6$ m and width of $B = 0.9$ m as shown in **Fig.3.6.b**. The discretization in x direction from $x = 0.9$ m to $x = 1.65$ m and from $x = 2.1$ m to $x = 2.25$ m and in y direction from $y = -0.275$ m to $y = -0.125$ m and from $y = 0.125$ m to $y = 0.275$ m where is in the neighborhood of potential rupture and where the foundations will be located in the next step is finer as it is illustrated in **Fig.3.7**. At other locations, where the deformation is expected to be limited, the mesh is coarser. The octahedral elements dimensions in z direction is constant and is 0.035 m.

3.4.2. Soil Properties

Many experimental and numerical studies have shown that the behavior of soil after reaching failure is an important factor in problems related to shear-band formation (Bray 1990; Bray et al. 1994a, b). For our analysis in ABAQUS, a nonlinear finite element method with an elastoplastic constitutive model with Mohr-Coulomb failure criterion and an isotropic strain softening characteristics is used which have been shown to be effective in the simulation of fault rupture propagation through soil (Roth et al. 1981, 1982; Loukidis 1999; Erickson et al. 2001). In our modeling, strain softening is applied to friction angle φ and dilation ψ as $c = 0$ for sand. These soil parameters are linearly decreasing with the total plastic strain down to their residual values φ_{res} and ψ_{res} at γ_f which is the plastic shear strain at which soil reaches its residual strength.

For verification of the capability of the constitutive model which we are going to use in our model in ABAQUS for simulating the actual behavior of the soil, several

analysis of idealized soil samples tested in direct shear are performed. In **Fig.3.8**, the results of the simulation of a direct shear test on our specimen are compared with experiment data. As a result, we use $\varphi_{peak} = 46°, \varphi_{res} = 35°, \psi_{peak} = 13°, \psi_{res} = 1°, \gamma_y = 3\%, \text{and } \gamma_f = 7\%$ for our soil parameters. Although our soil sample is loos sand, it shows peak values, as we can see in this figure. Therefore, it seems that it has high value of dilation even though it is loos sand. That's because of low confining pressure due to performing small-scale experiment.

The soil is modeled in ABAQUS, with rectangular, octahedral, plane-strain elements. Each element is defined with 8 nodes with 3 degrees of freedom at each node.

3.4.3. Fault Rupture Simulation

The differential displacement is applied to the left part of the model (until $x = 0.90$ m) in small constitutive steps of 5mm until reaching the total vertical displacement of 0.1 m.

The deformed mesh and the location of outcropping rupture are displayed in **Fig.3.10**. Vertical displacement at the surface for normalized bedrock displacement ranging from h/H=2% to 12% is shown in **Fig.3.11**.

3.5. Verification of Model

By comparing the experimental and numerical results as represented in **Fig.3.12** and **Fig.3.13**, we can see a satisfactory agreement between the experiment and numerical model in ABAQUS. The comparison of the results have been done for normalized bedrock displacement of $h/H = 2\%, 5\%, 6\%, 10\%$, and 12%.

Figures of **Chapter 3**

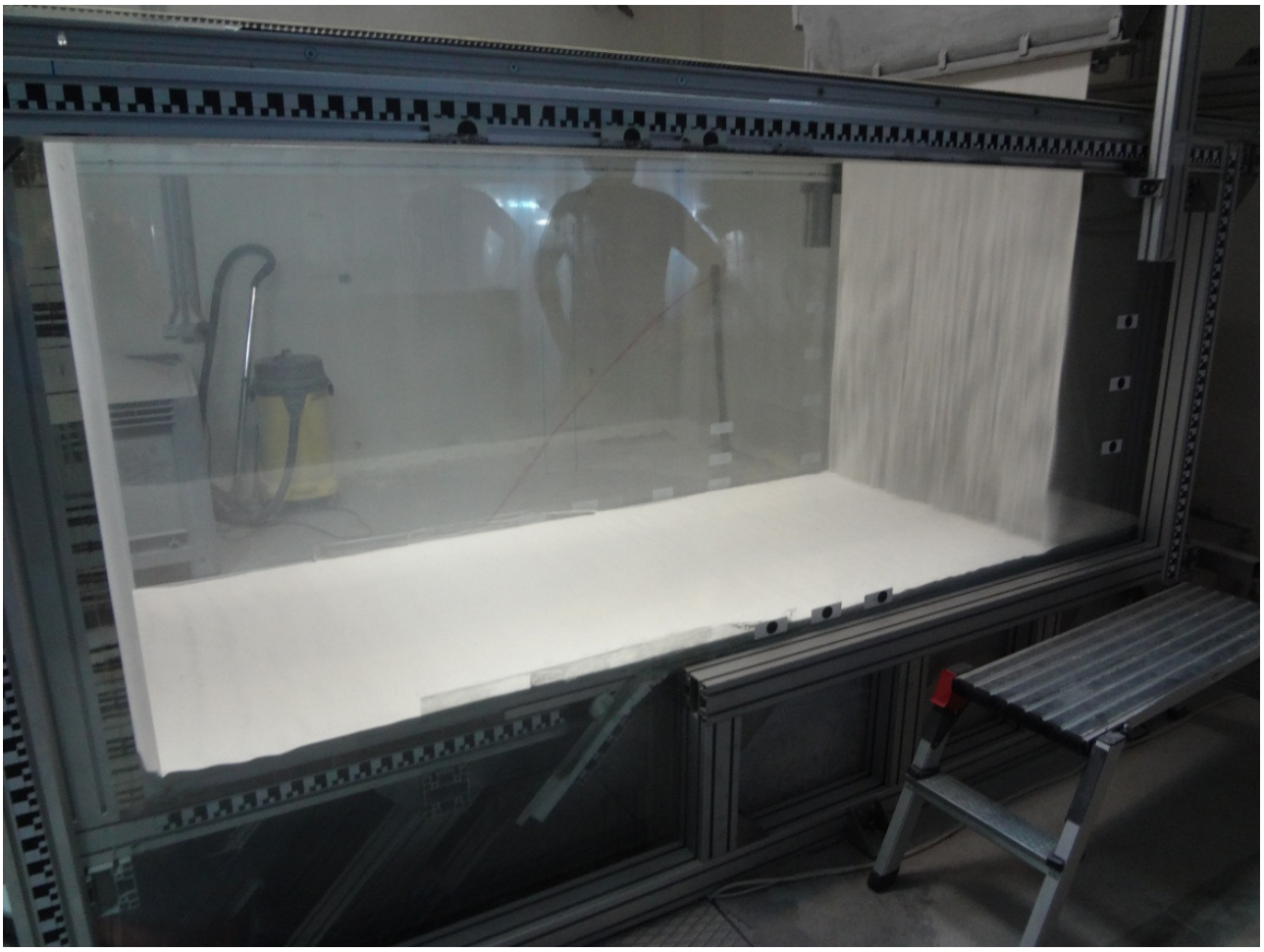

Figure 3.1 (Fault Rupture Apparatus in Laboratory of Soil Mechanics of N.T.U.A

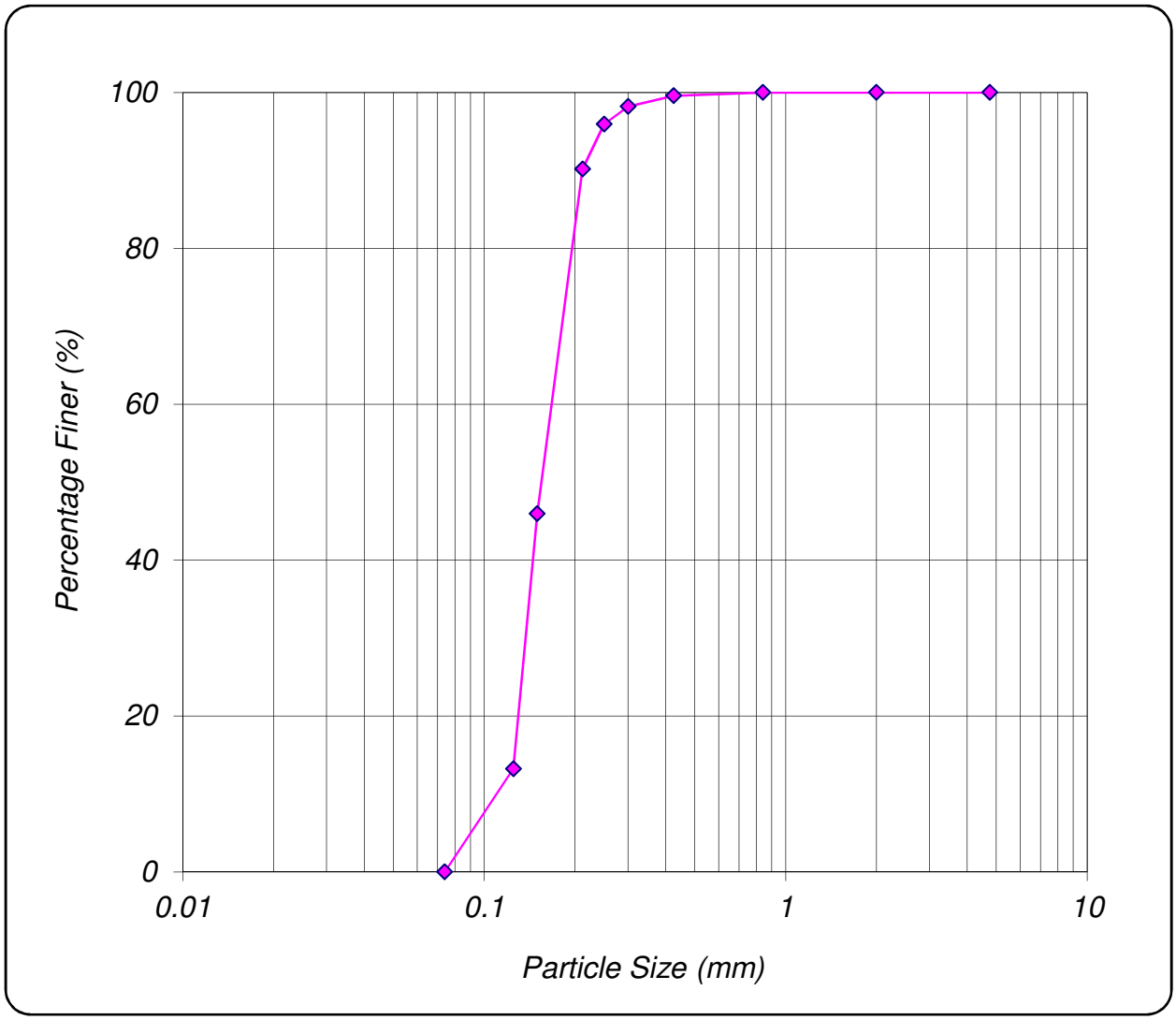

Figure 3.2 The grain size distribution of sand

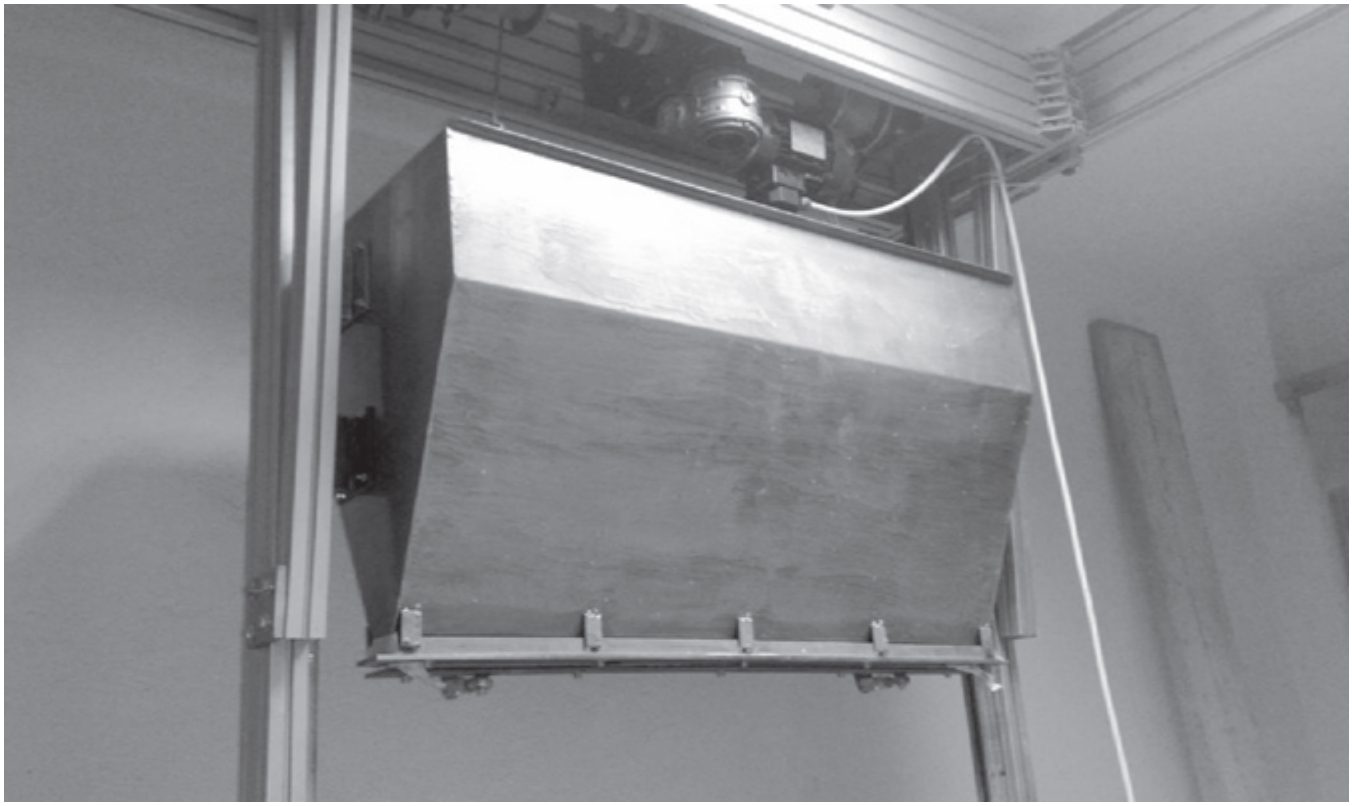

(a)

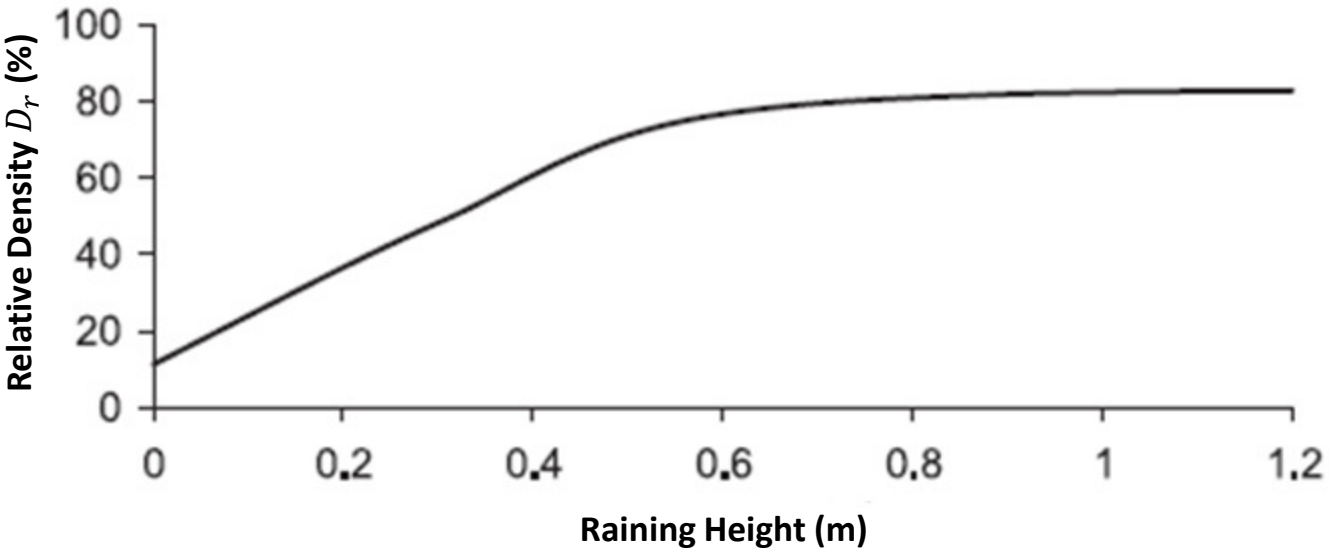

(b)

Figure 3.3 (a) Electronically controlled sand raining system used for preparation of the models. (b) Relative density D_r with respect to the raining height for a constant velocity. [Anastasopoulos et. al. 2010]

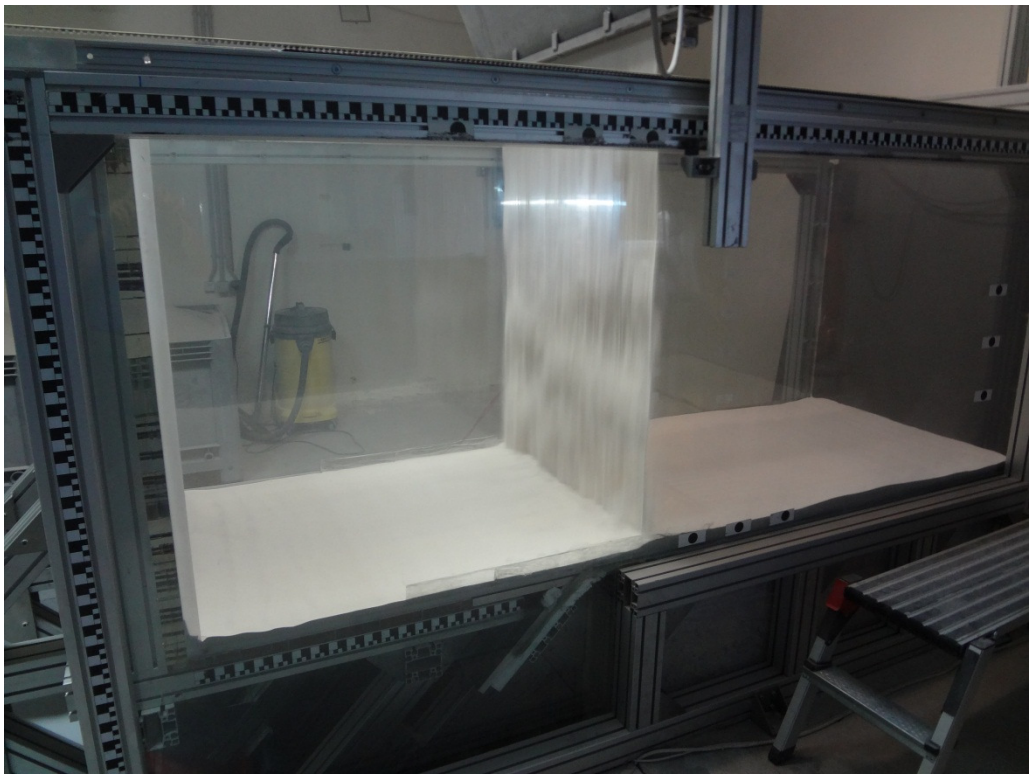

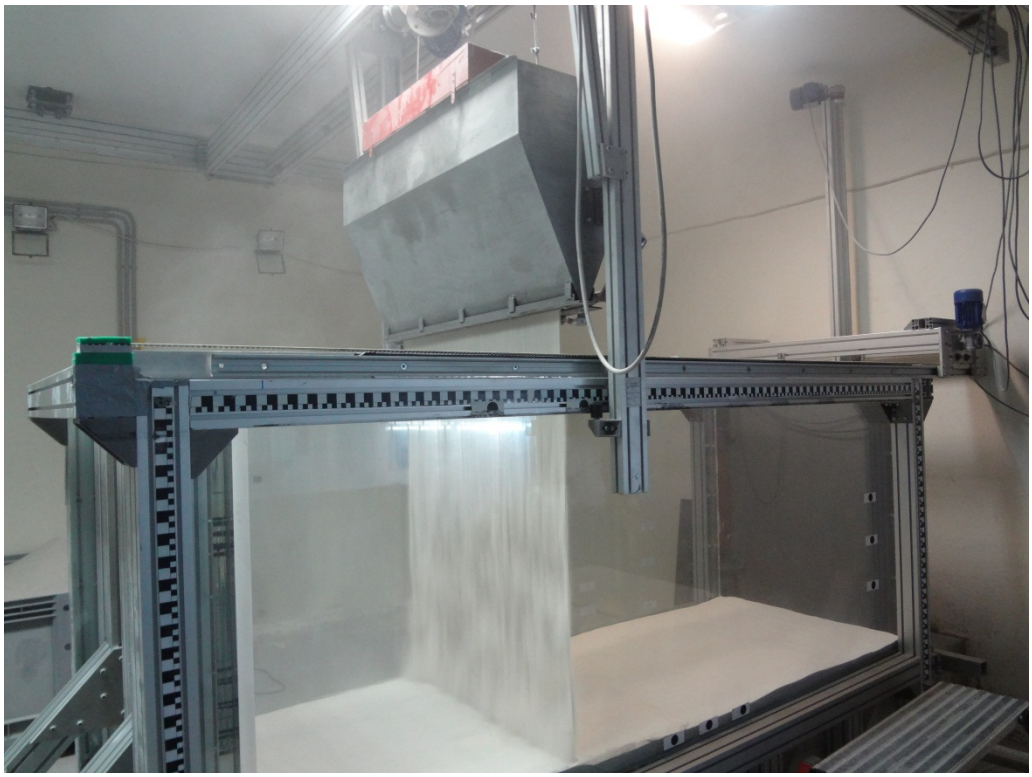

Figure 3.4 Preparing the sand box for free field experiment in the Laboratory of Soil Mechanics of N.T.U.A

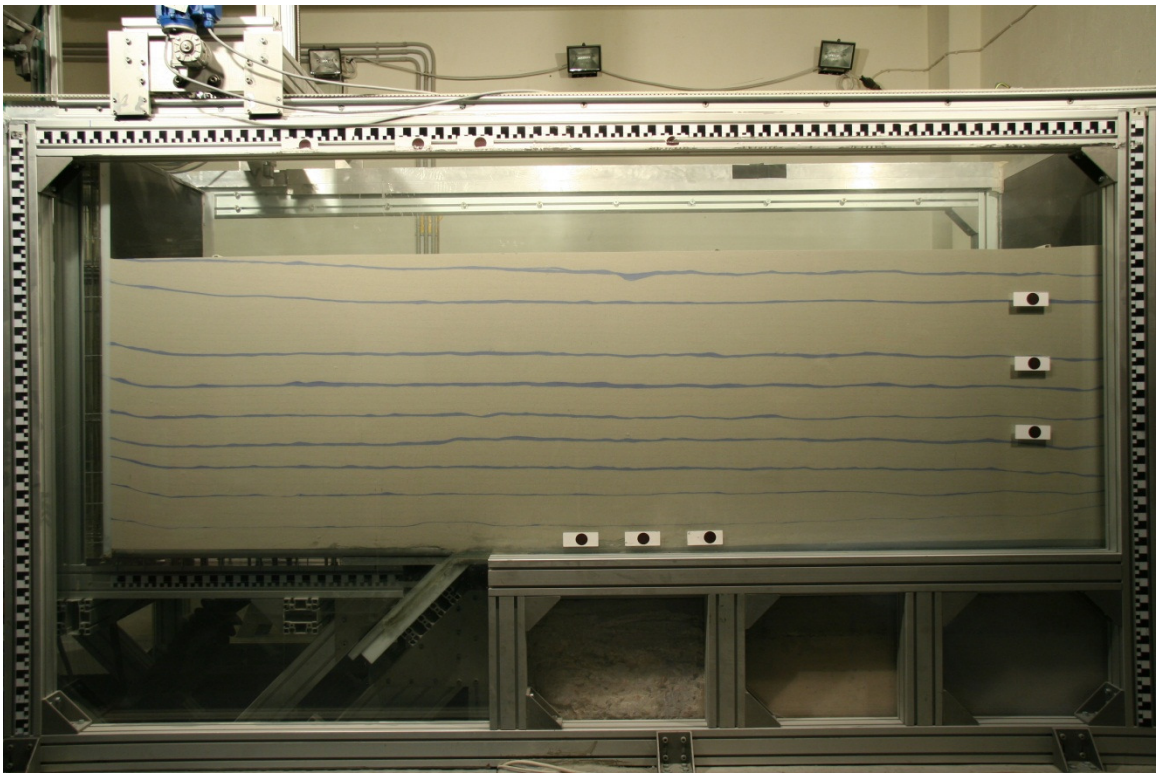

(a)

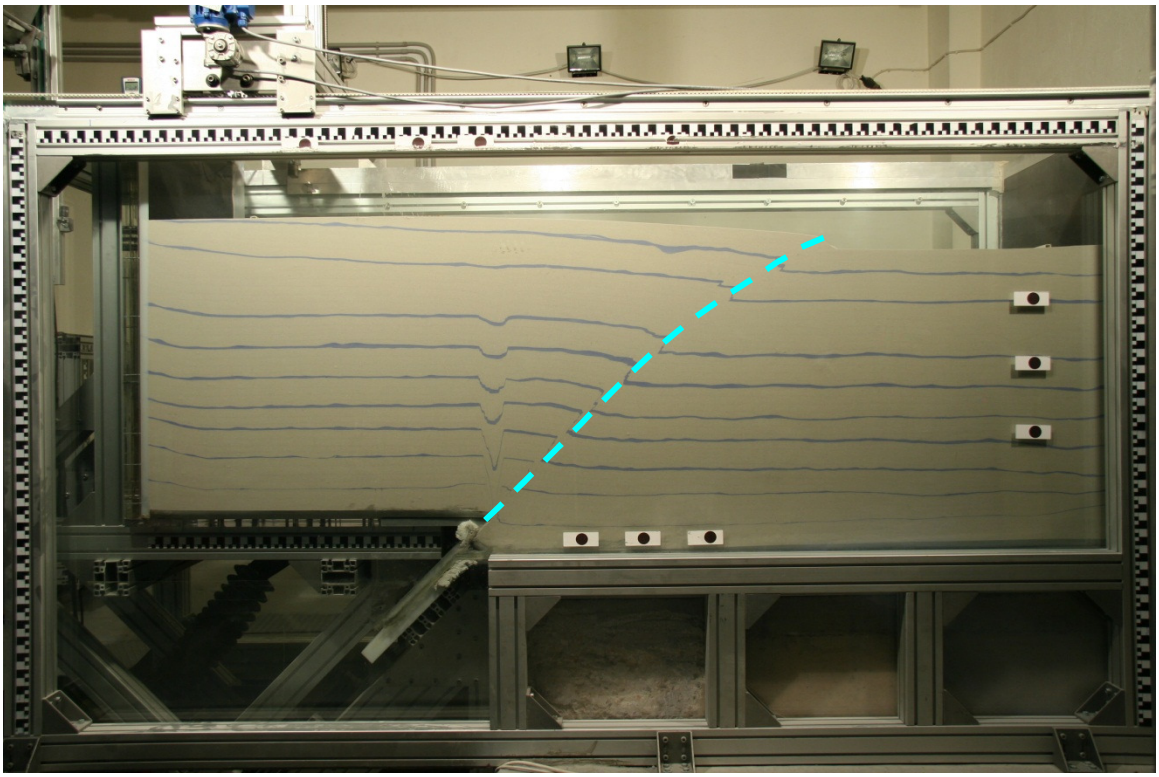

(b)

Figure 3.5 Fault rupture experiment on sand soil for Free Field in Soil Mechanic Laboratory of N.T.U.A: (a) Before applying the rupture, and (b) after applying rupture with final amplitude of 0.1m

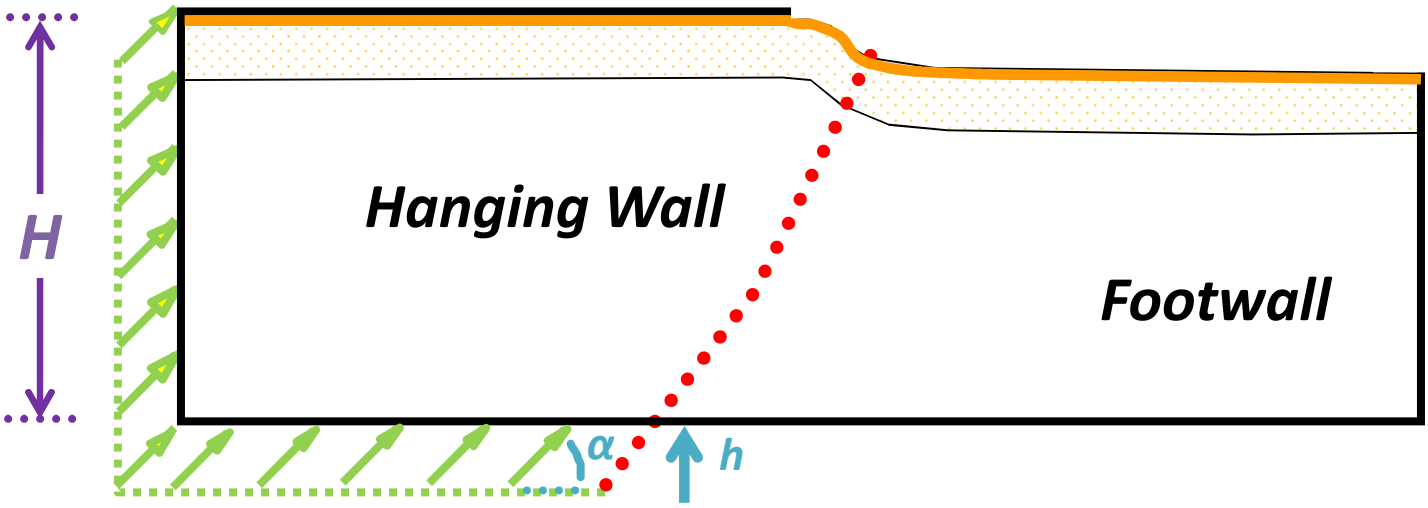

(a)

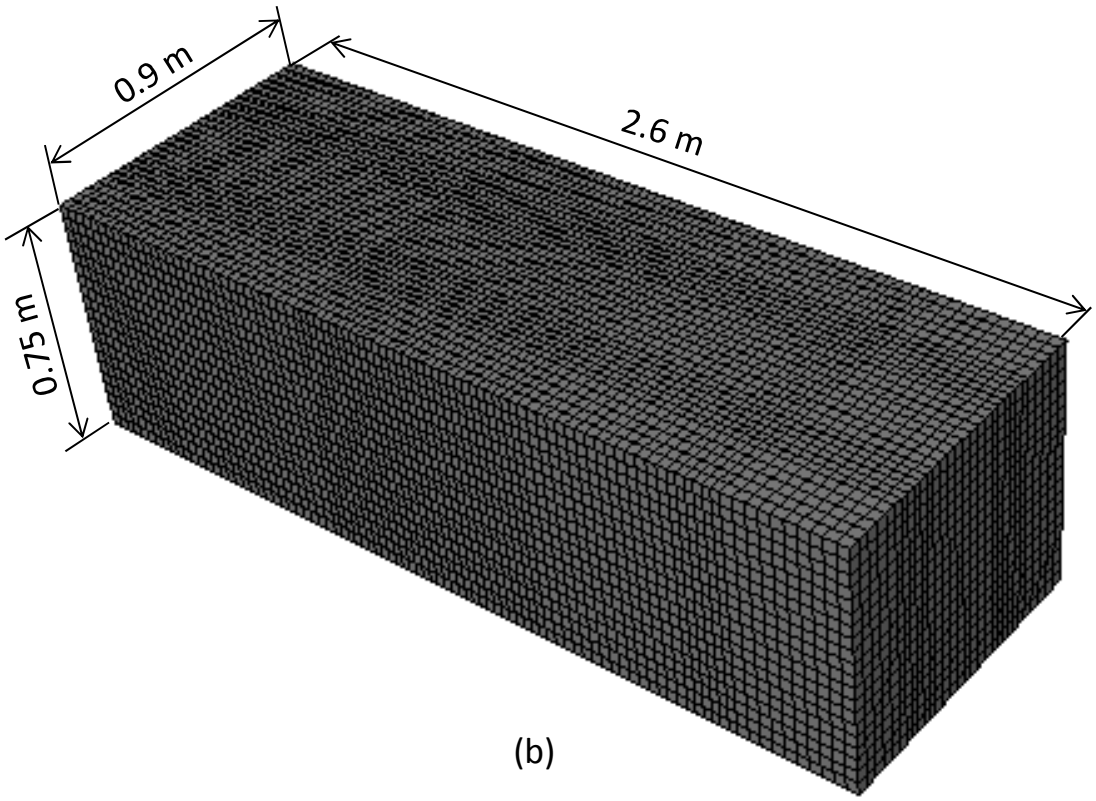

(b)

Figure 3.6 (a) Schematic illustration of thrust fault rupture with amplitude h in free field motion (b) Finite element model dimensions in ABAQUS

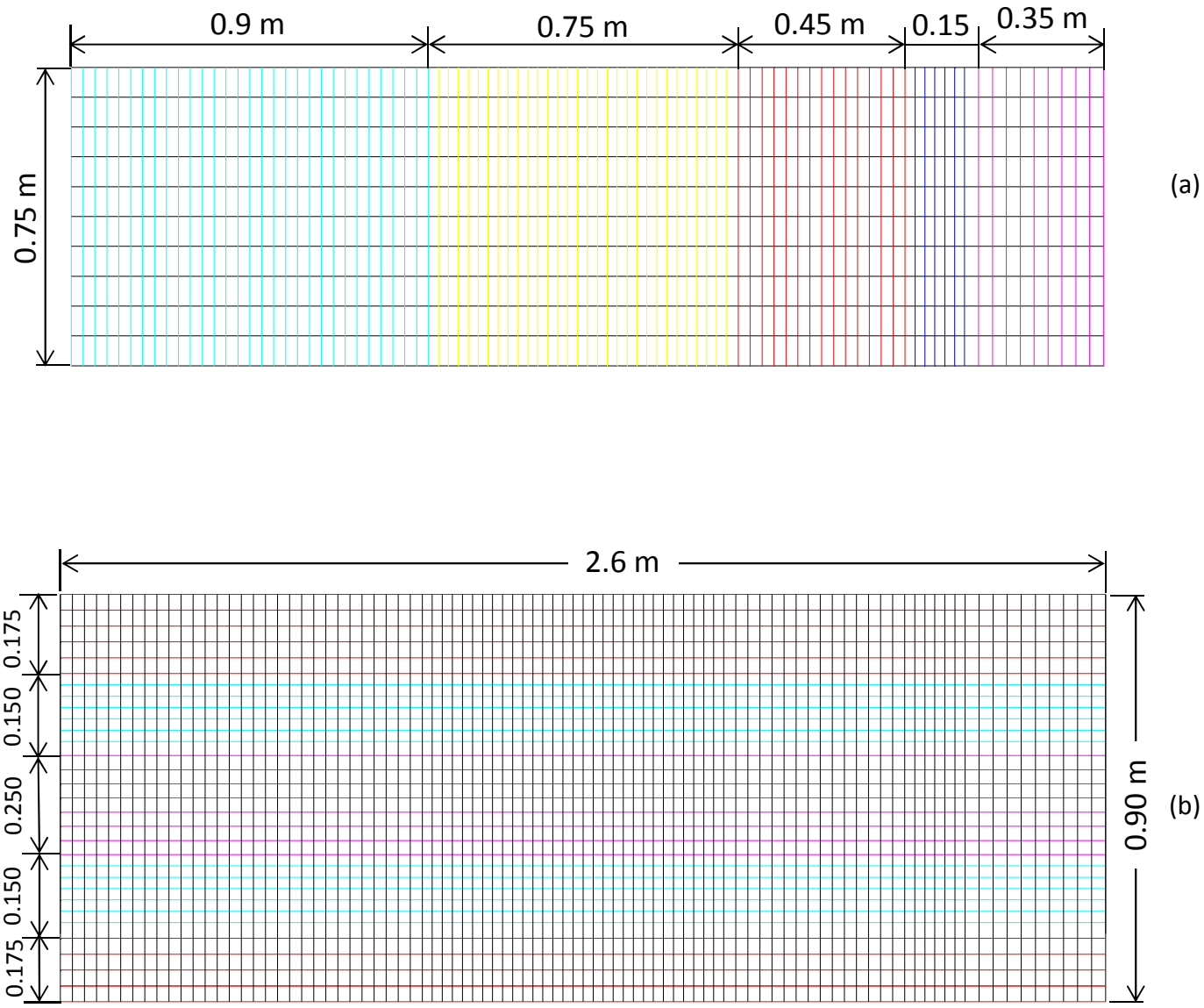

Figure 3.7 Finite Element model discretization in (a) x, and (b) y direction

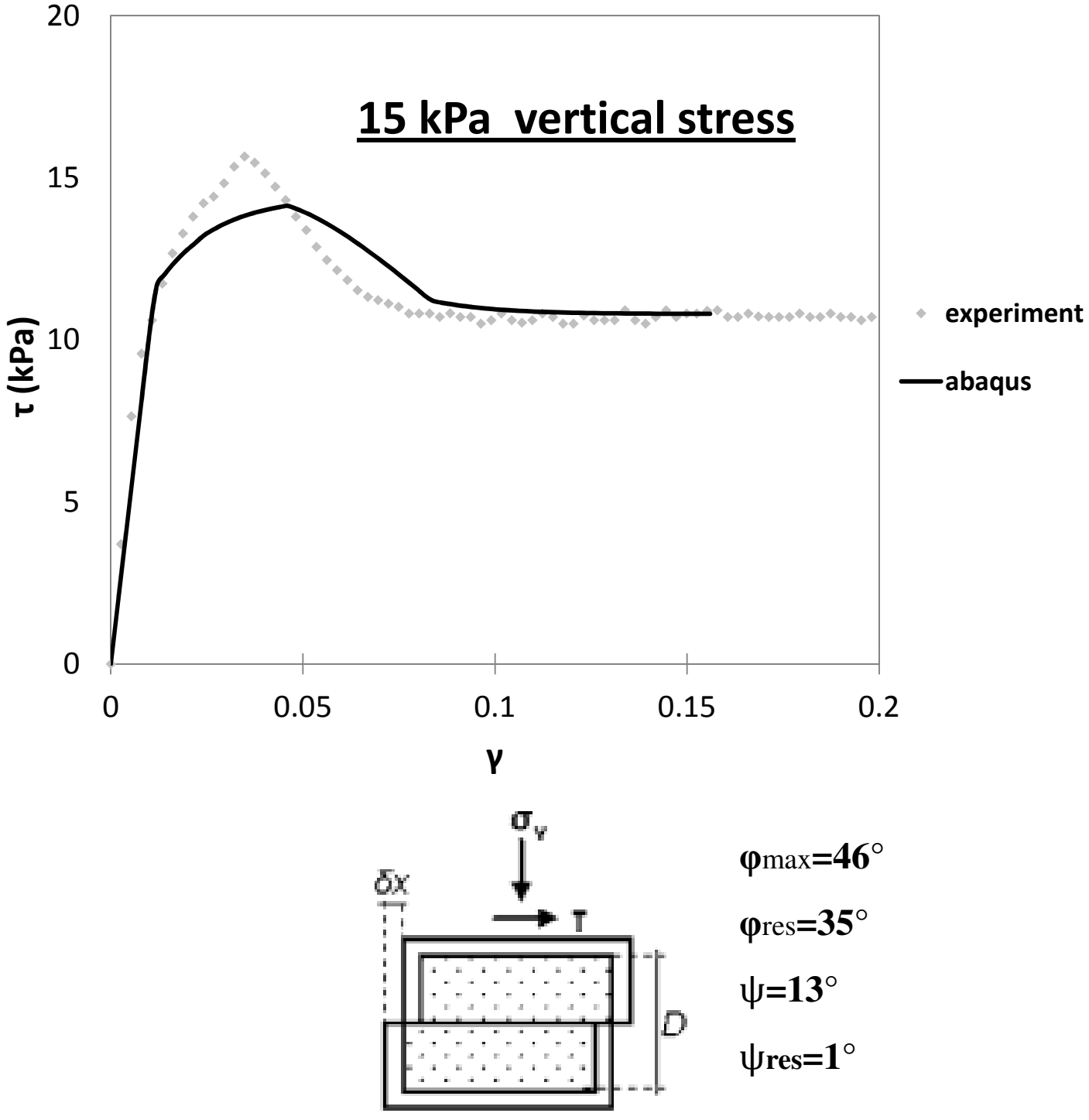

Figure 3.8 Comparison of direct shear test experimental data and the constitutive model in ABAQUS

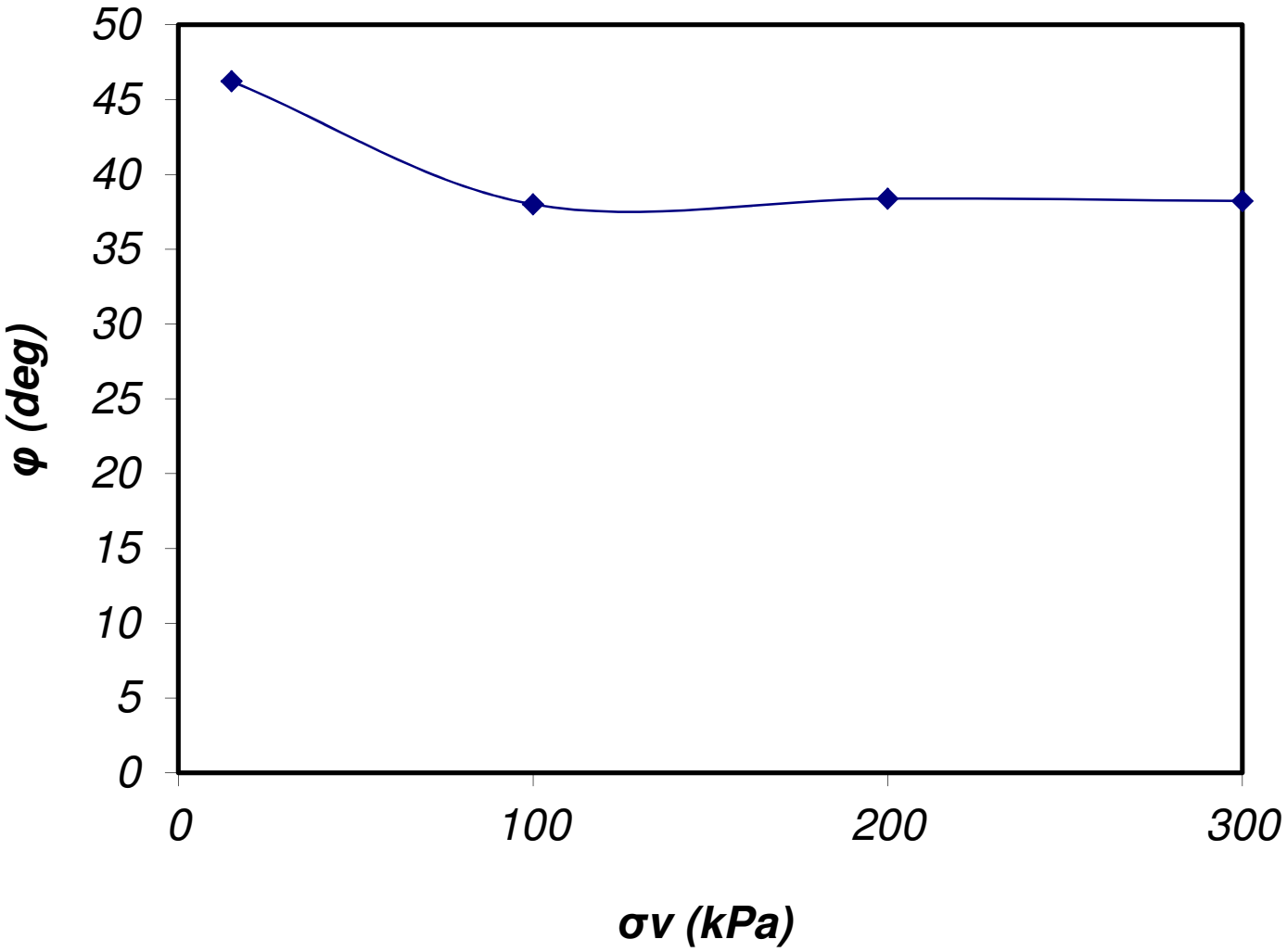

Figure 3.9 Variation of φ of our soil sample with vertical compressive pressure.

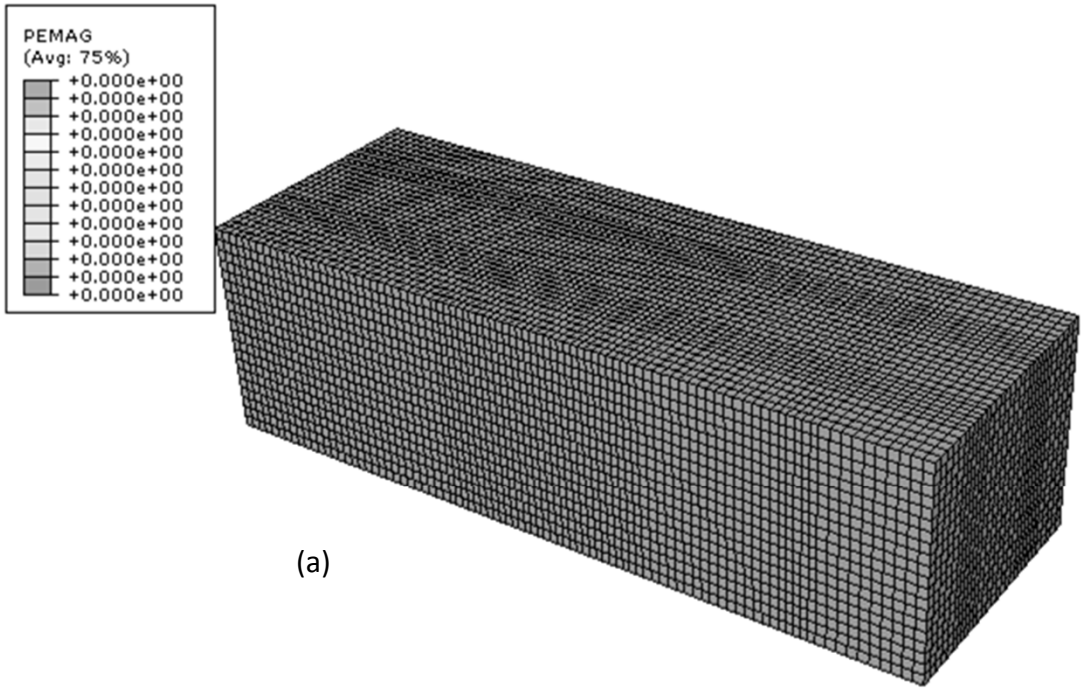

(a)

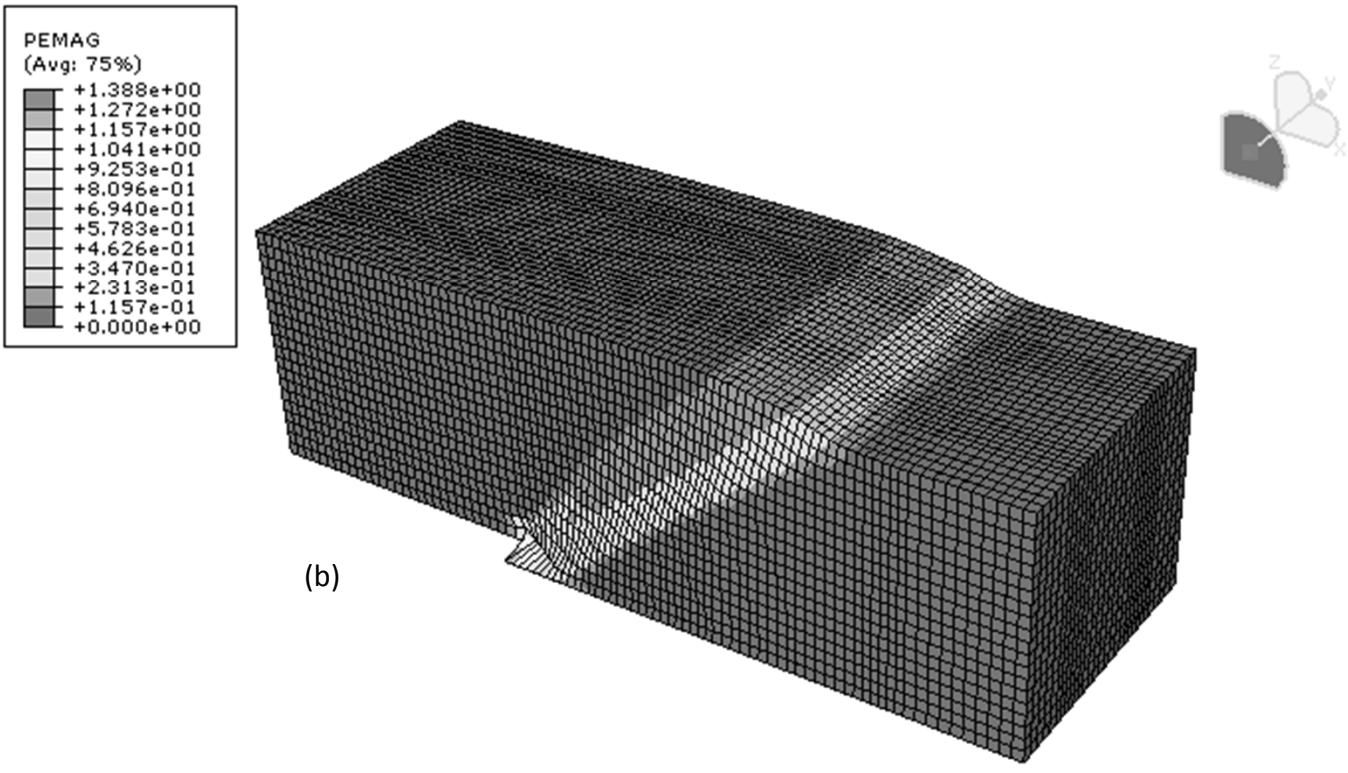

(b)

Figure 3.10 Free Field model in ABAQUS: (a) Before applying rupture, and (b) After applying rupture with total amplitude of 0.1 m

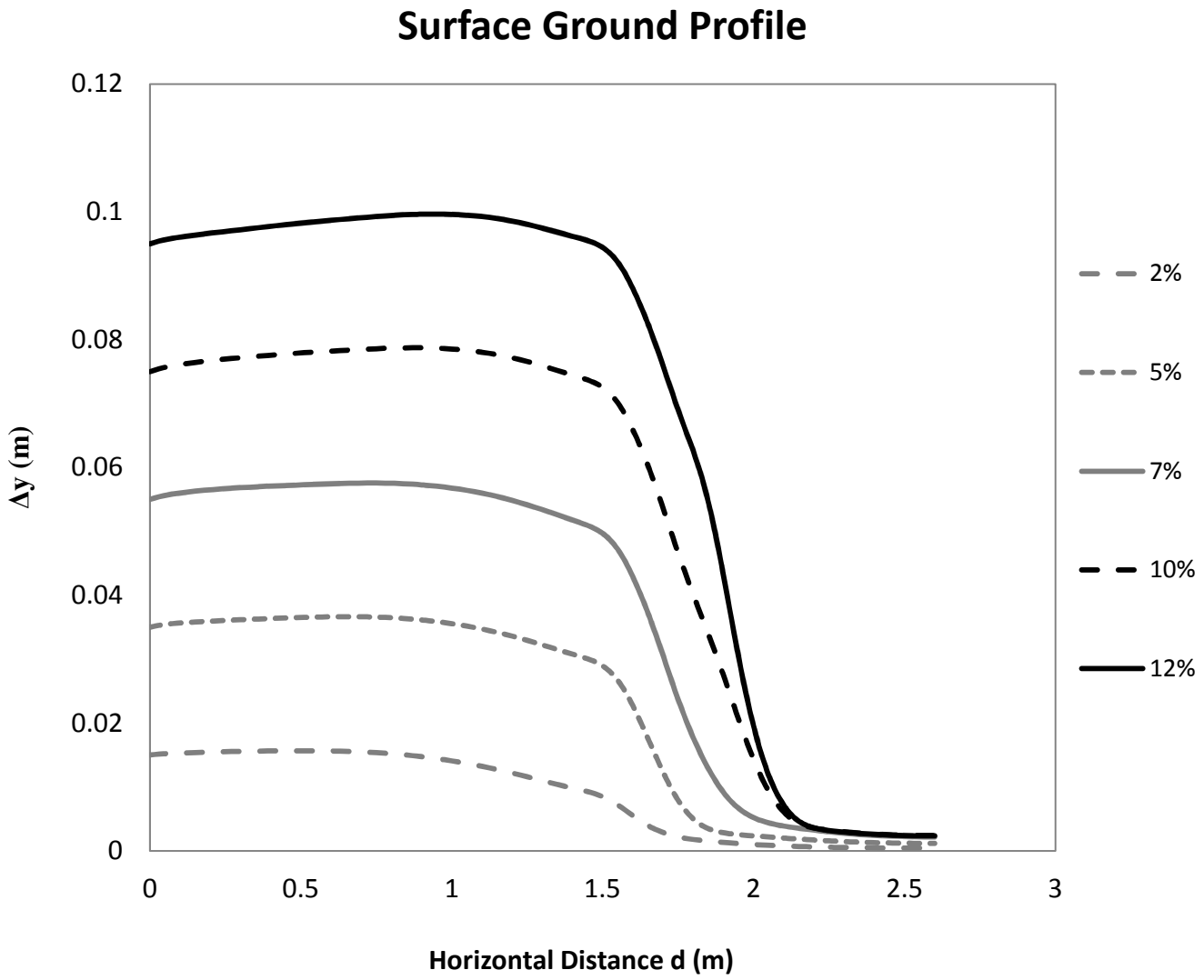

Figure 3.11 Vertical displacement at the surface for normalized bedrock displacement ranging from h/H=2% to 12%

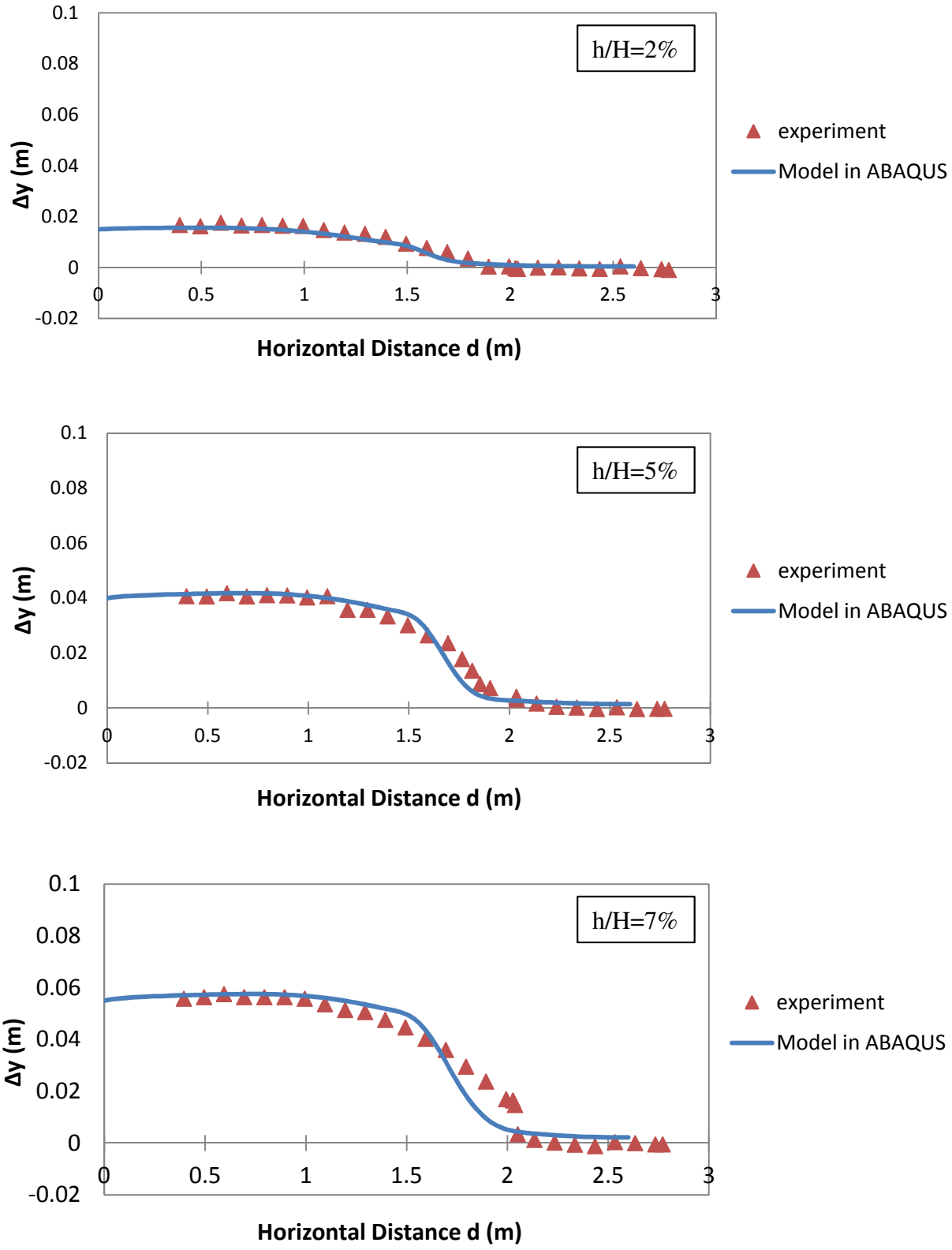

Figure 3.12 Comparison of vertical displacement at the surface for free field experiment and the model in ABAQUS for normalized bedrock displacement of: (a) h/H=2% (b) h/H=5%, and (c) h/H=7%

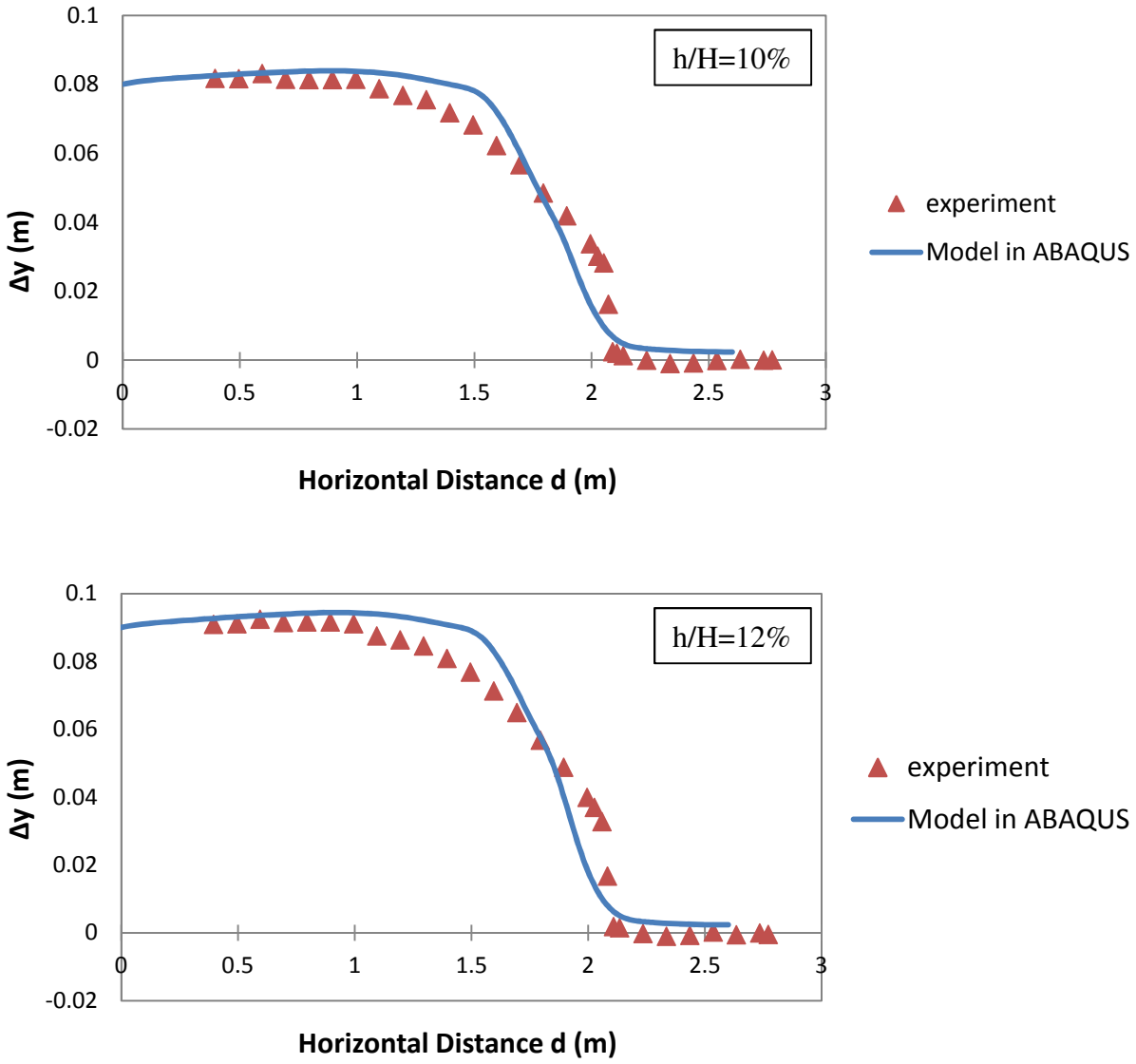

Figure 3.13 Comparison of vertical displacement at the surface for free field experiment and the model in ABAQUS for normalized bedrock displacement of: (a) h/H=10% , and (b) h/H=12%

Chapter 4

4. Fault Rupture-Soil-Foundation-Structure Interaction

4.1. Introduction

The second step of the Soil-Foundation-Structure interaction during fault rupture propagation is simulating the effect of presence of a structure founded on top of the outcropping fault. Main goal of this chapter is to present an in-depth analysis of behavior of foundations and structures sitting directly on a rupturing thrust fault both experimentally and numerically. The results show satisfactory agreement between the numerical analysis and experimental studies.

4.2. Analysis Methodology

In this chapter, the results of a reduced-scale experiment which was conducted in Laboratory of Soil Mechanics of N.T.U.A for simulating the thrust fault rupture soil-foundation-structure interaction are presented. Then a 3D nonlinear finite element analysis is done to simulate the small-scale experiment in ABAQUS. Finally the results are compared in order to verify the model in ABAQUS which considers the effects of presence of the structure on top of soil layers.

4.3. Reduced-Scale Experiments

4.3.1. Structure Geometry

The reduce-scale experiment for investigation of Soil-Foundation-Structure interaction was done in Laboratory of Soil Mechanics of N.T.U.A. The structure model which was used for this experiment is the reduced-scale model of a real typical 3-storey building of Southern Europe which was designed and constructed during the 70's. The real model weren't designed according to capacity design principles and therefore it is prone to soft – story collapse [Nonika Antonaki, 2012]. For this experiment, the scale factor of N = 10 has been chosen. The physical model consists of two 3-story identical frames connected together with steel plates which were distributed evenly (**Fig.4.1**, **Fig.4.2**, and **Fig.4.3**). The columns and beams have $30\ \text{mm} \times 8\ \text{mm}$ and $60\text{mm} \times 8\text{mm}$ cross sections respectively and they are made of aluminum. The steel plates have cross section of $64\ \text{mm} \times 20\text{mm}$. The foundations consist of square plates of width $\text{B} = 150\ \text{mm}$. Plastic artificial joints are displayed in **Fig.4.4**. All structural members are shown in detail in Appendix A.

4.3.2. Artificial Plastic Hinges

In order to model the stiffness of elements correctly and get the desired bending moment capacity of the structural members, the beam-column joints are modeled with artificial plastic hinges. Bending moment capacity of each plastic hinge (M_{ult}) is calibrated through adjustment of the applied torque. This is done by performing static and slow-cyclic pushover tests with screw-jack pushover apparatus. [Nonika Antonaki, 2012]

4.3.3. Pushover Apparatus

The pushover apparatus (**Fig.4.5.a**) consists of a servomotor which is controlled by a computer and attached to a screw-jack actuator and can apply the horizontal displacement which will be selected by the computer. Then a device which is connected at the edge of the actuator will measure the applied load. For the calibration of the beams and columns of our model, a load cell with loading capacity of 10 kg was used. [Nonika Antonaki, 2012]

4.3.4. Calibration of Artificial Plastic Hinges

The calibration of each beam-column or column-footing connections was done by utilizing pushover apparatus. Each member with its joint was fixed on a base and then the pushover apparatus applied controlled displacement in a way that the member be perpendicular to the load cell that had been attached to the pushover apparatus. Imposing displacement continued until the artificial plastic hinge started to turn. As the apparatus was applying the displacement, the reaction force of the member was measured and also the displacement was measured with a laser displacement transducer in order to plot a force-displacement diagram for each structural member. This diagram consists of two branches: In firs branch, the member deforms elastically by increasing the load and in the second branch, the join starts to rotate without any further increase of the reaction force. The joint was tightened or loosened until the required bending strength was achieved. One of these bending moment-displacement diagrams is showed in **Fig.4.5.b** while the others are shown in **Appendix B**.

4.3.5. Installation of the Structure

All structural members were connected together and aligned outside the fault rupture box and then the whole structure was placed at the accurate defined location on the soil without disturbing the soil surface by special crane (**Fig.4.6**). In order to prevent the significant deformation of structural members during their installation by the crane, specific aluminum bars with small thickness were used as clockwise connectors of opposite joints.

4.3.6. Measurement Instruments

For measurement of vertical and horizontal components of deformation of different structural elements, a number of channels were used. For measurement of horizontal in-plane displacement of each story, a wired displacement transducer is installed in each story in order to give data for calculation of each story drift (Ch.3, 4, and 5 in **Fig.4.7**). The second and sixth transducers which are installed on back frame are measuring the horizontal displacement of left footings and differential horizontal displacement of the left and right footings respectively. In addition, two wired transducers are used on each footing of the back frame for measurement of the vertical displacement of each side of the footing. Then, these measurements will be used for calculation of foundations rotation and settlement. **Fig.4.10** shows the installation of these transducers on different structural elements.

4.3.7. Fault Rupture Simulation

As for the free field experiment, the vertical displacement was applied to the base of the box gradually in order to simulate the fault rupture propagation. The rupture started from 5mm upward vertical displacement of left part of the soil and increased gradually with 5mm increment in each step until reaching the total vertical displacement of 0.1 m. **Fig.4.11** shows the whole idea of how the thrust fault rupture will hit the structure. **Fig.4.12** presents the model before and after applying the rupture. As the rupture hits the left footing of the structure, the left footing is on hangingwall and the right one is on footwall. **Fig.4.13** magnifies the left column of the structure which is on hangingwall before and after applying the rupture.

In **Fig.4.14** to **Fig.4.18**, the horizontal displacement of the both left and right deformed columns which are on hangingwall and footwall respectively are shown for different values of vertical displacement of rupture (h). These diagrams are based on the horizontal displacement measurements which the transducers of each story and the footings have given us. In these figures, the deformed shape of the columns compared to their original state is represented. We can see that the left columns have much bigger horizontal displacement than the right ones and also they have deformed in opposite directions.

4.4. Finite Element Model

4.4.1. Model Properties

The finite element model for the simulation of fault rupture with considering the presence of the structure is displayed in **Fig.4.19**. The foundation is modeled with octahedral infinitely stiff solid elements from concrete and the columns and beams are modeled as flexural beam elements from aluminum, while the possibility of sliding and detachment between the foundation and the underlying soil is considered through the use of special interface elements. The beam-column and column-footing connections are modeled as elements consist of rigid and plastic elements as shown in **Fig.4.20.** The moment capacities of plastic elements which were determined in pushover analysis were defined in the material properties of these elements in model in ABAQUS as ultimate plastic stress, F_{ult}, which is $F_{ult} = \frac{M_{ult}}{Z}$, in which M_{ult} is the ultimate plastic moment of the elements and Z is the plastic section modulus which is $Z = \frac{a \times b^2}{4}$ for a rectangular cross section.

The soil properties are the same as what were defined for the free field motion in the numerical analysis.

4.4.2. Fault Rupture Simulation

As in the free field motion, the differential displacement is applied to the left part of the model (until $x = 0.90$ m) in small constitutive steps of 5mm until reaching the total vertical displacement of 0.1mm.

The undeformed and deformed model with plastic strain magnitude (PEMAG) before and after applying the rupture is presenting in **Fig.4.21**.

4.5. Verification of Model

In order to verify our model in ABAQUS, the results from the experiment and numerical analysis should be compared. This has been done in **Fig.4.22** to **Fig.4.27**.

In **Fig.4.22**, the horizontal displacement of the foundations of back frame in experiment and in numerical analysis are compared until $h/H = 10\%$. We just compare the results of one frame because their displacements are the same due to the symmetry. Since the left foundation is on hangingwall, it has much larger horizontal displacement than the right one which is on footwall (about 10 times larger). We can see that this is true for both experiment and numerical analysis. For both foundations, there is sufficient agreement between the experimental and numerical results.

In **Fig.4.23**, the horizontal displacement of each story is presented which is calculated at center of mass of each roof for the model in ABAQUS and by transducers in model in experiment. These outputs were used to calculate the drift ratio of each story which is shown in **Fig.4.24** and **Fig.4.25** in percentage. For the drift ratio of first story, we should calculate it separately for the left column which is on hangingwall and for the right column which is on footwall because their bases displace completely differently. However, for the second and third story, as the floors are rigid, we can calculate the drift ratio for the whole story. These figures show that by increasing the fault amplitude, *h*, the numerical and experimental results become more close to each other.

In **Fig.4.26**, the counterclockwise rotation of both foundations of the back frame is displayed for the base vertical displacement until 75mm ($h/H = 10\%$). Again, the both results in experiment and in numerical analysis show much more rotation for the footing which is on hangingwall rather than the one on footwall (about 10 times larger).

In **Fig.4.27**, the rigid body rotation and rigid body settlement in base level are demonstrated. These figures also show that as the base vertical displacement, *h*, increases, the numerical and experimental results become more close to each other.

4.6. Conclusion

The comparison between the numerical and experimental outputs which were presented in previous section shows sort of good agreement between the results especially by increasing the base displacement. Maybe one reason is that in large rupture offsets, the elements have become plastic but in low values of base vertical displacement, some elements have become plastic while others are in elastic limit. Therefore we can see discrepancy between the numerical and experimental results. However, the structure and foundation general behavior are the same in both numerical and experimental analysis and this small discrepancy which we can see among the results is acceptable for the verification of our model because there are lots of parameters that should be considered for numerical modeling and it is always impossible to simulate the experiment conditions completely in the model. Therefore, we can neglect this difference between the results and we can verify that our numerical model can simulate the reality condition of Fault Rupture-Soil-Foundation-Structure interaction very well.

Figures of **Chapter 4**

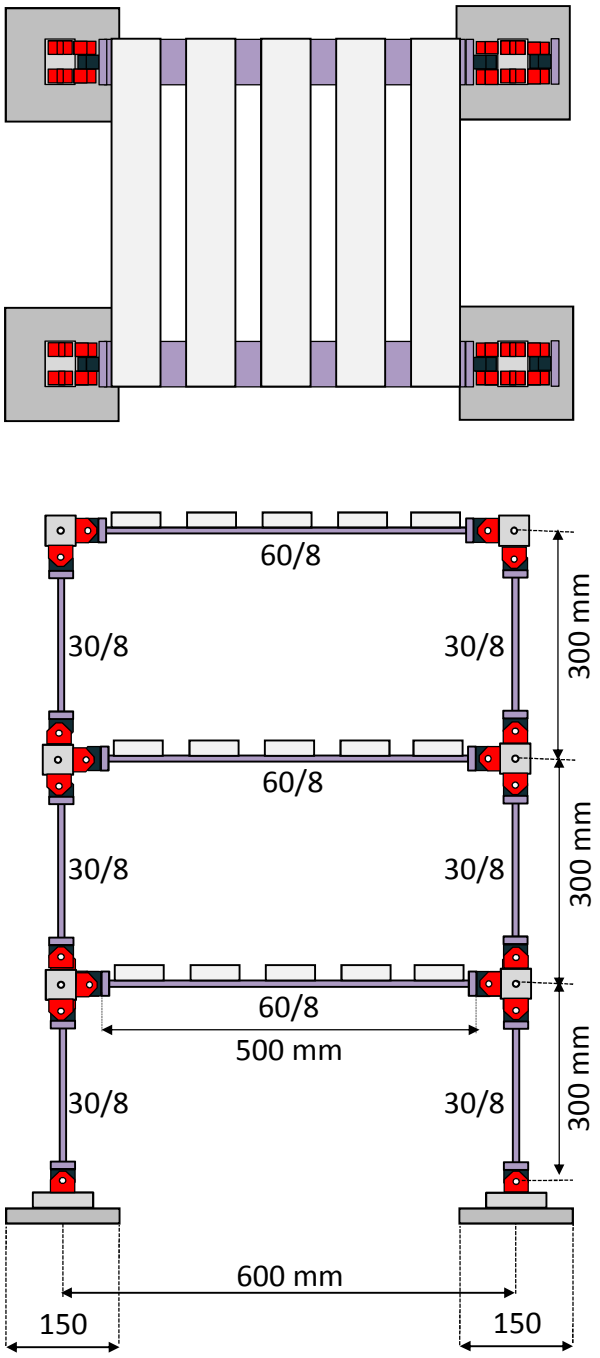

Figure 4.1 Schematic illustration of the 3-storey building which was used in experiment

Figure 4.2 Photograph of physical model which was used for the experiment in Laboratory of Soil Mechanics of N.T.U.A

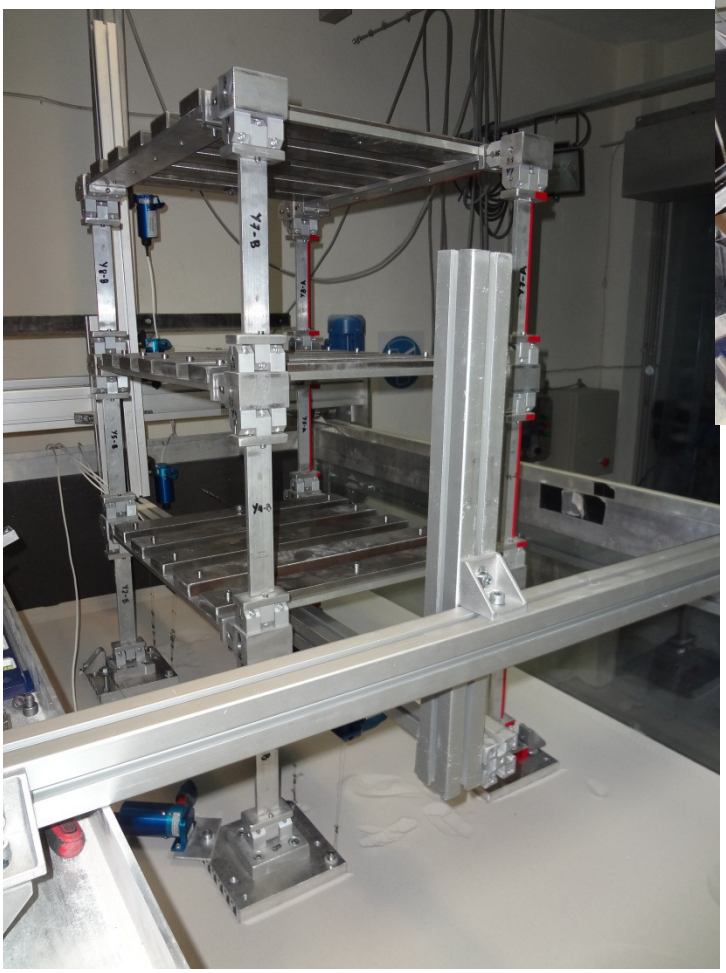

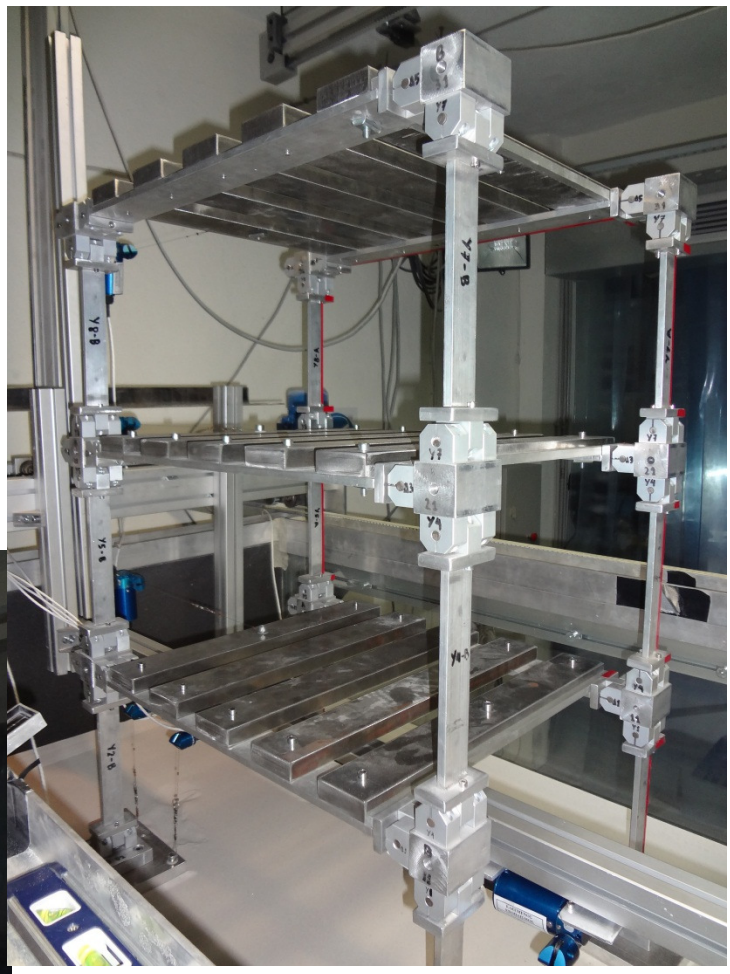

Figure 4.3 Photograph of physical model which was used for the experiment in Laboratory of Soil Mechanics of N.T.U.A

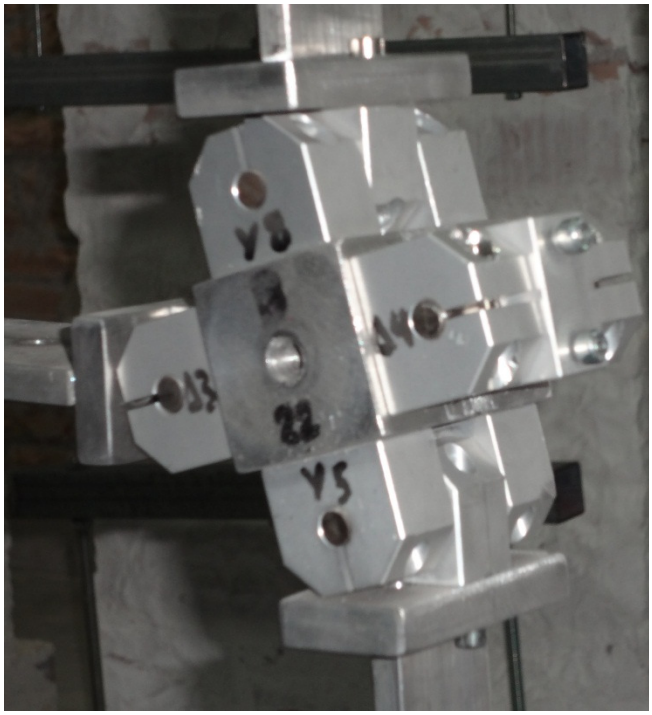

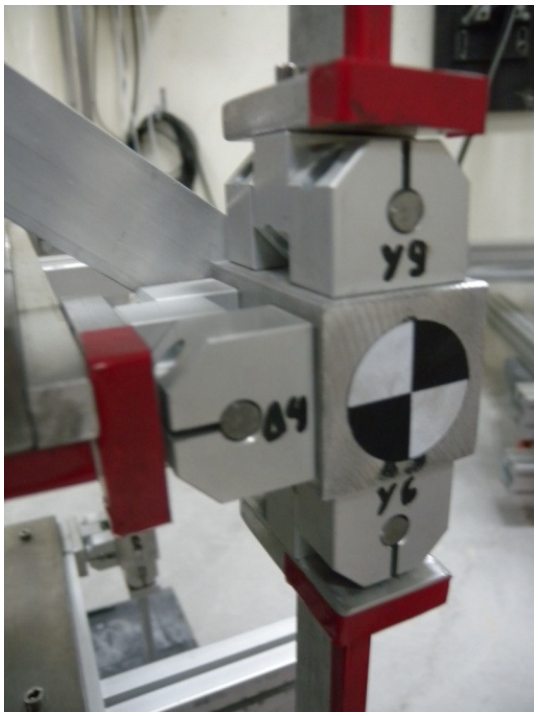

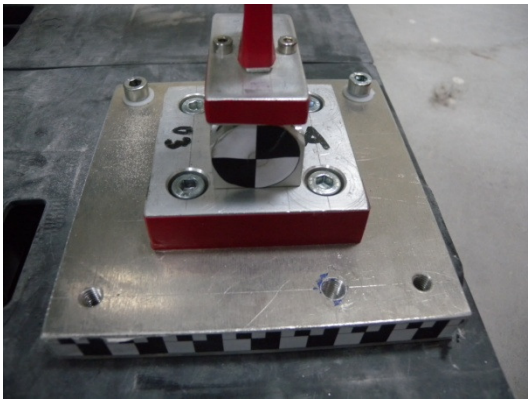

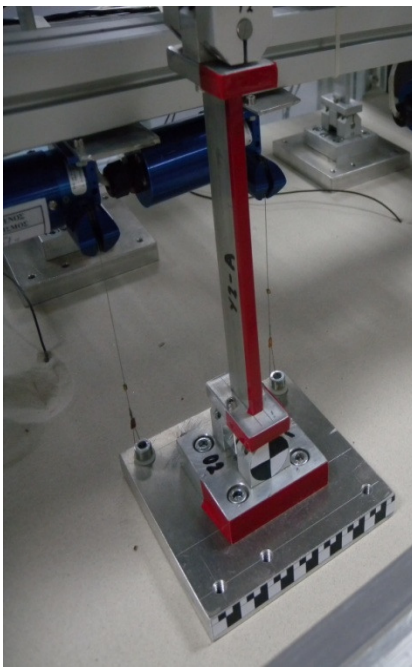

Figure 4.4 Photograph of details of the artificial plastic hinges of the structure

(a)

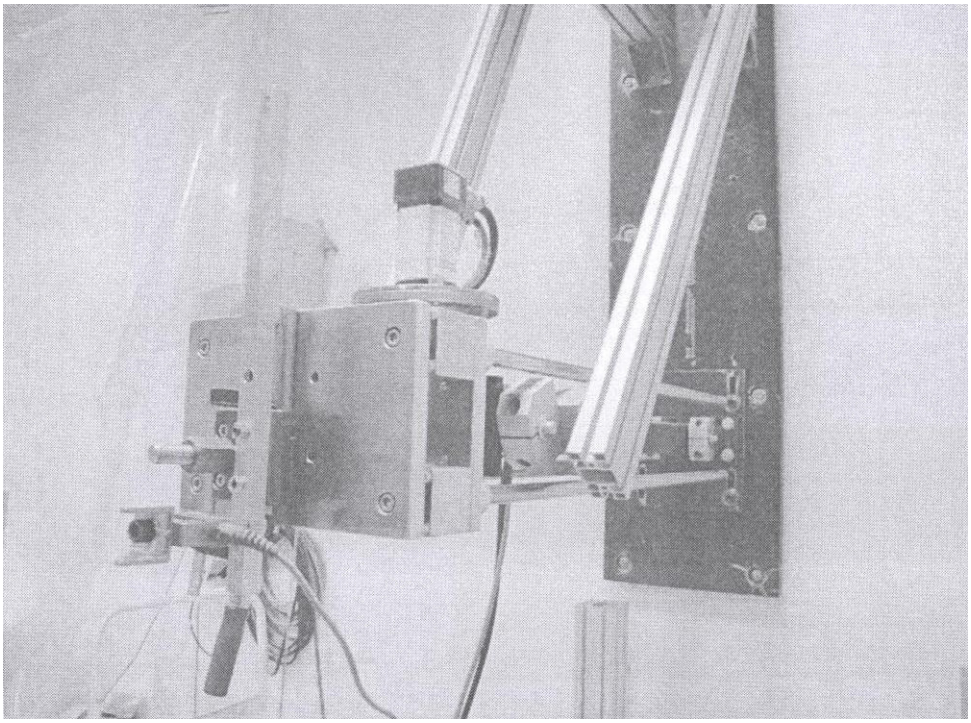

(b)

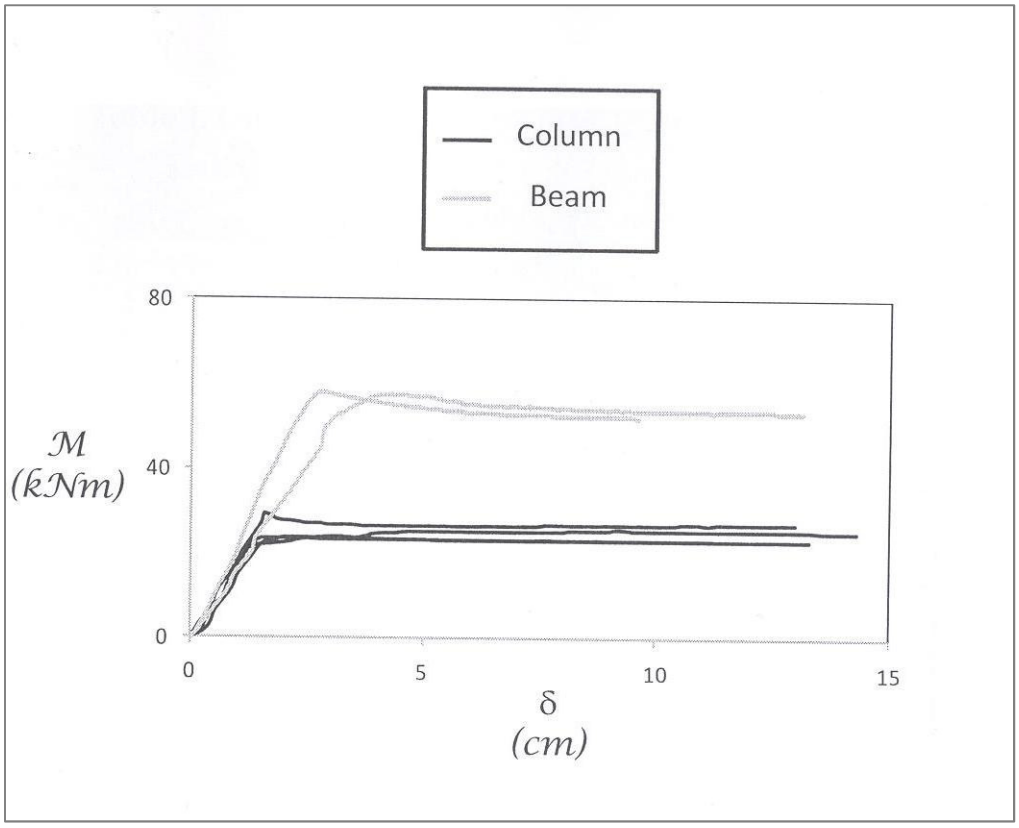

Figure 4.5 (a) Photograph of the pushover apparatus with (b) indicative diagram of calibration of an artificial plastic hinge. [Nonika Antonaki 2012]

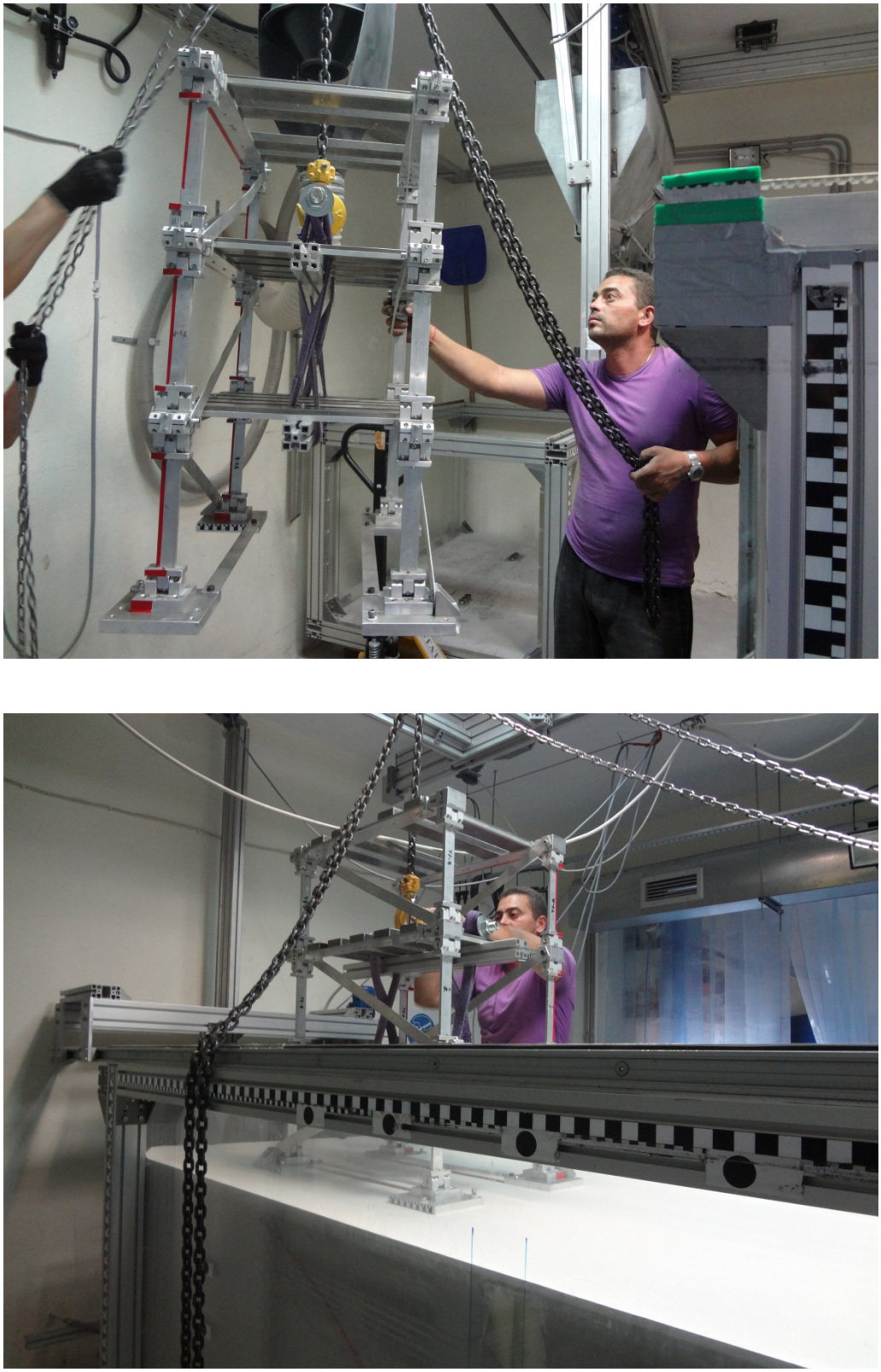

Figure 4.6 Installation of the structure on the sand box for the experiment

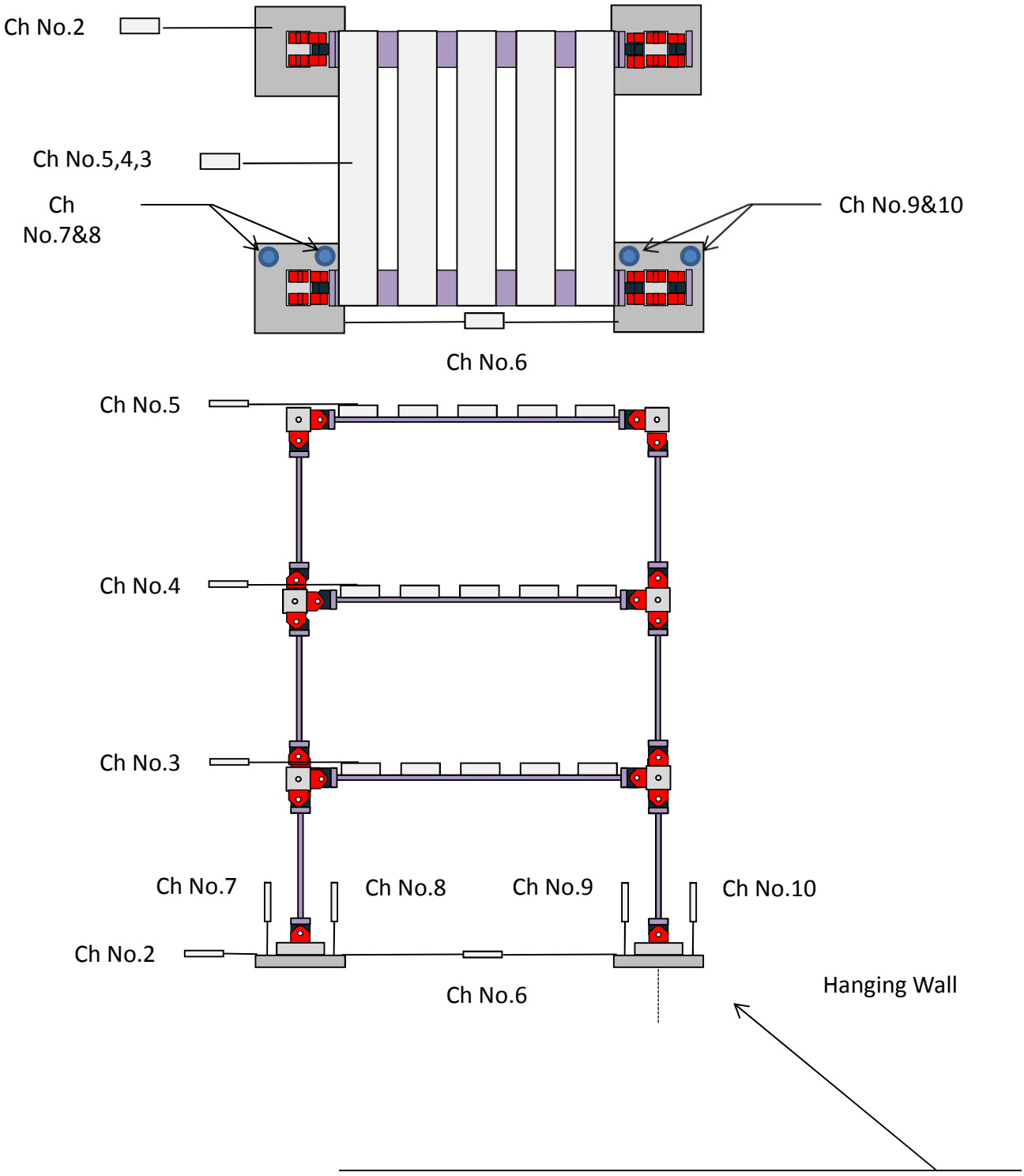

Figure 4.7 Schematic illustration of the channels which were used for measurement of vertical and horizontal components of deformation of different parts of the structure during the experiment

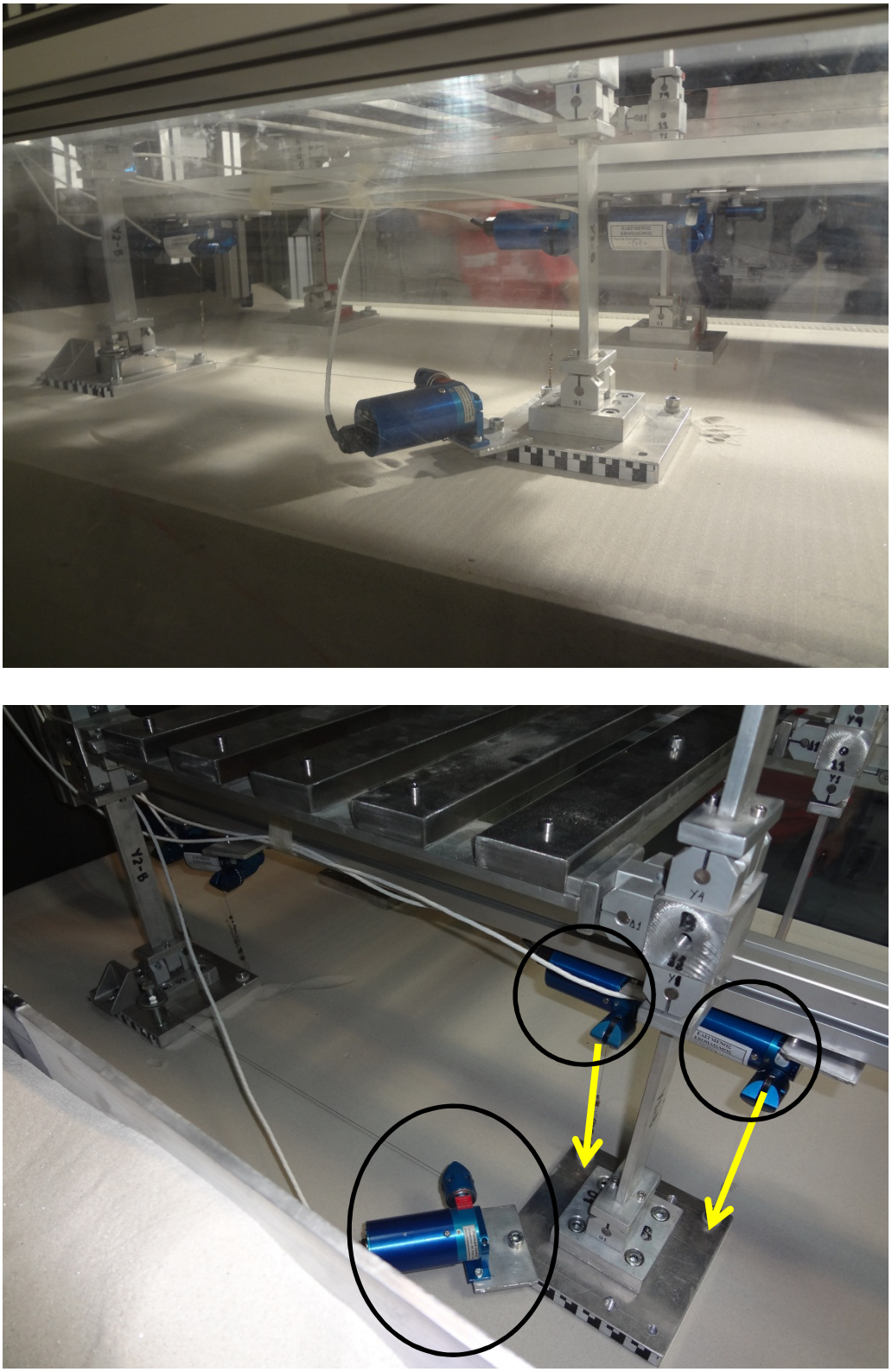

Figure 4.8 Photograph of the channels which were set up for measurement of the horizontal and vertical displacement of the foundations

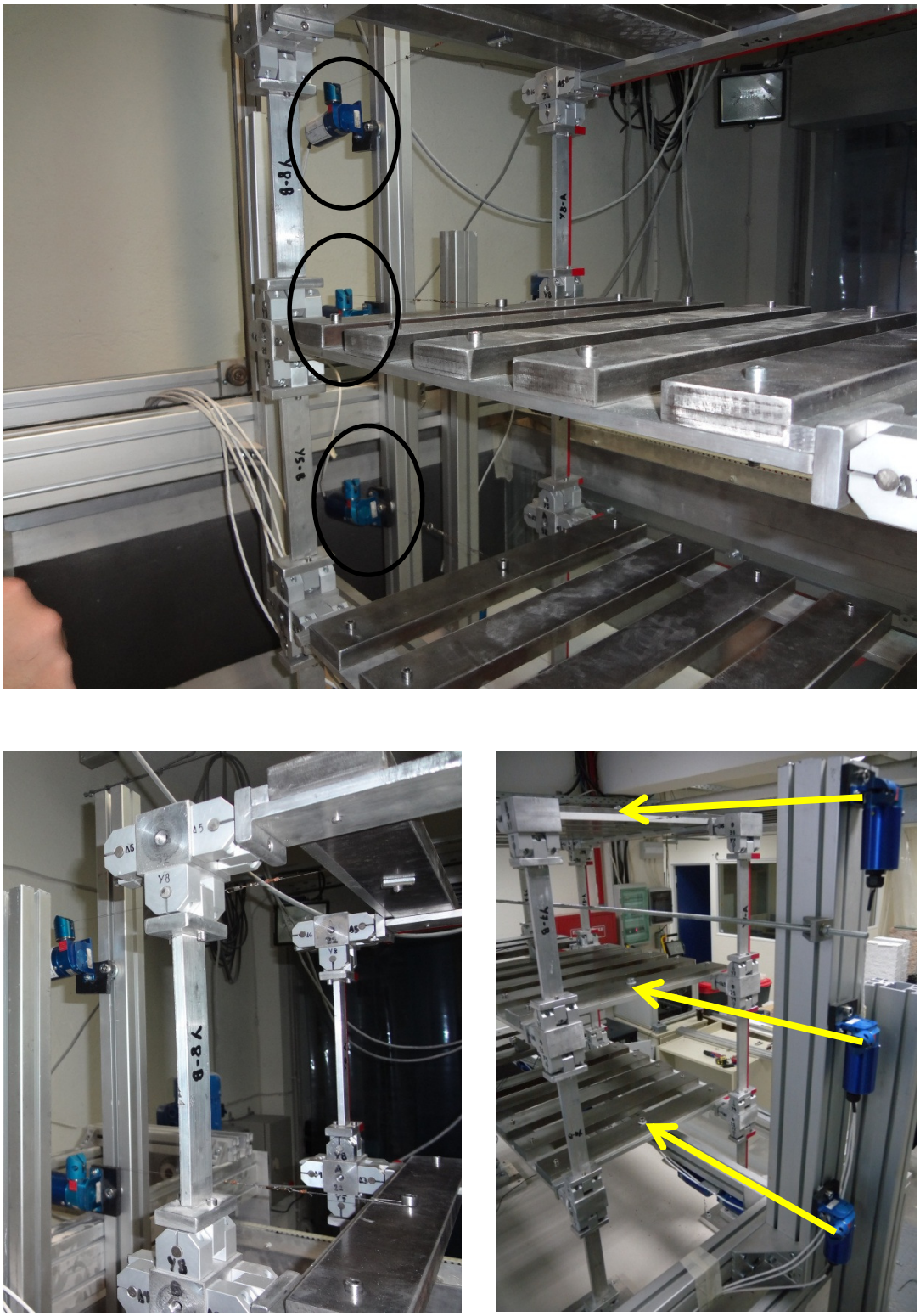

Figure 4.9 Photograph of the channels which were set up for measurement of the horizontal and displacement of the floors

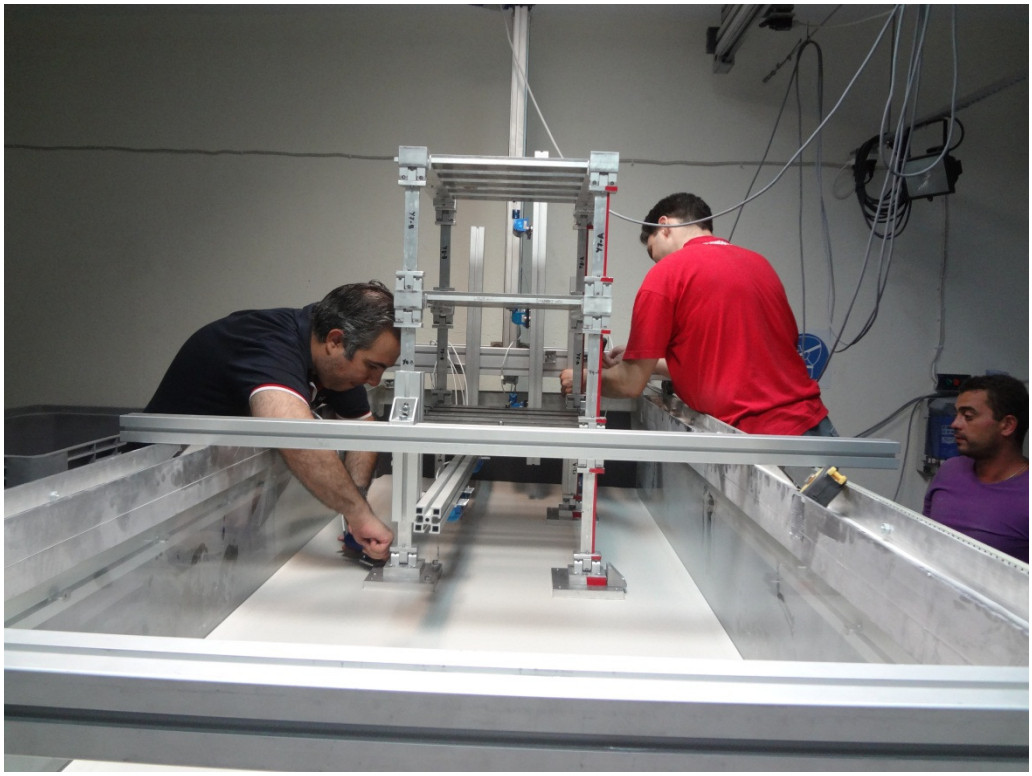

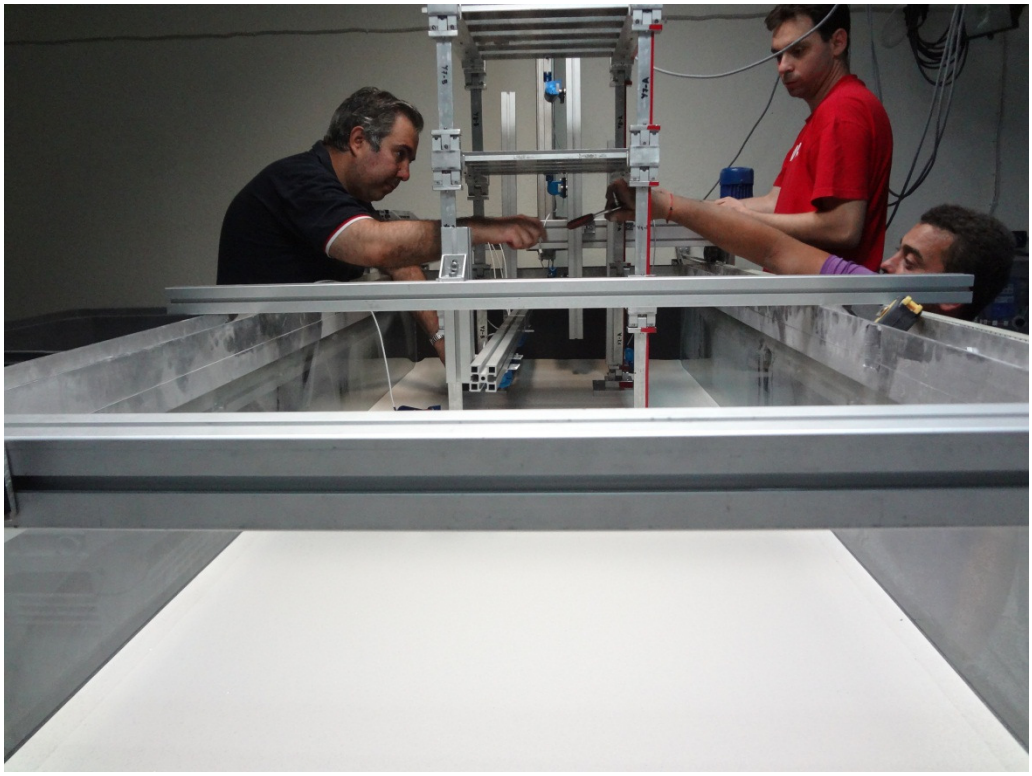

Figure 4.10 Fixing up the channels on the structure for measurement of horizontal and vertical components of displacement of the structure

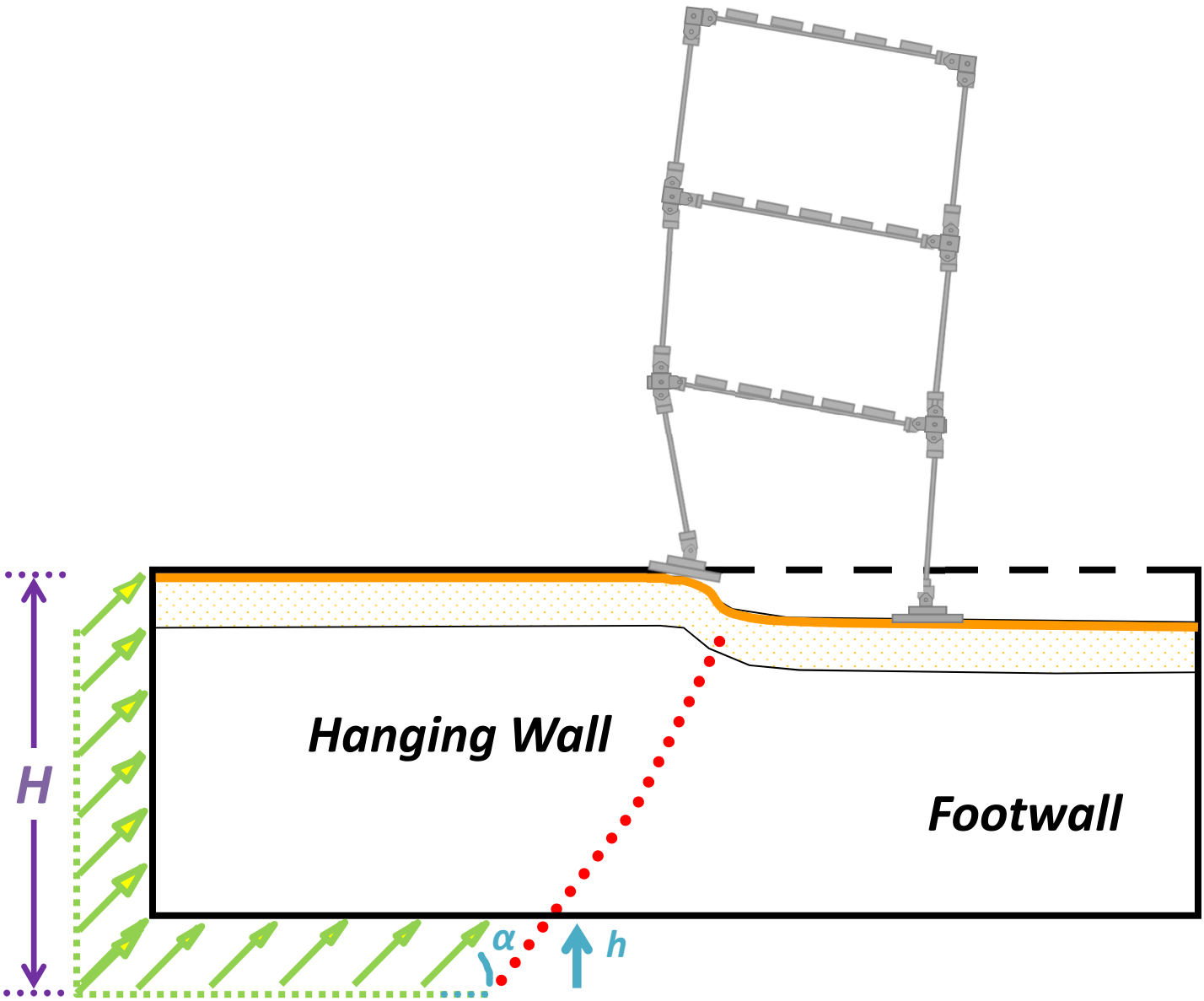

Figure 4.11 Schematic illustration of thrust fault rupture with amplitude h which hits the structure

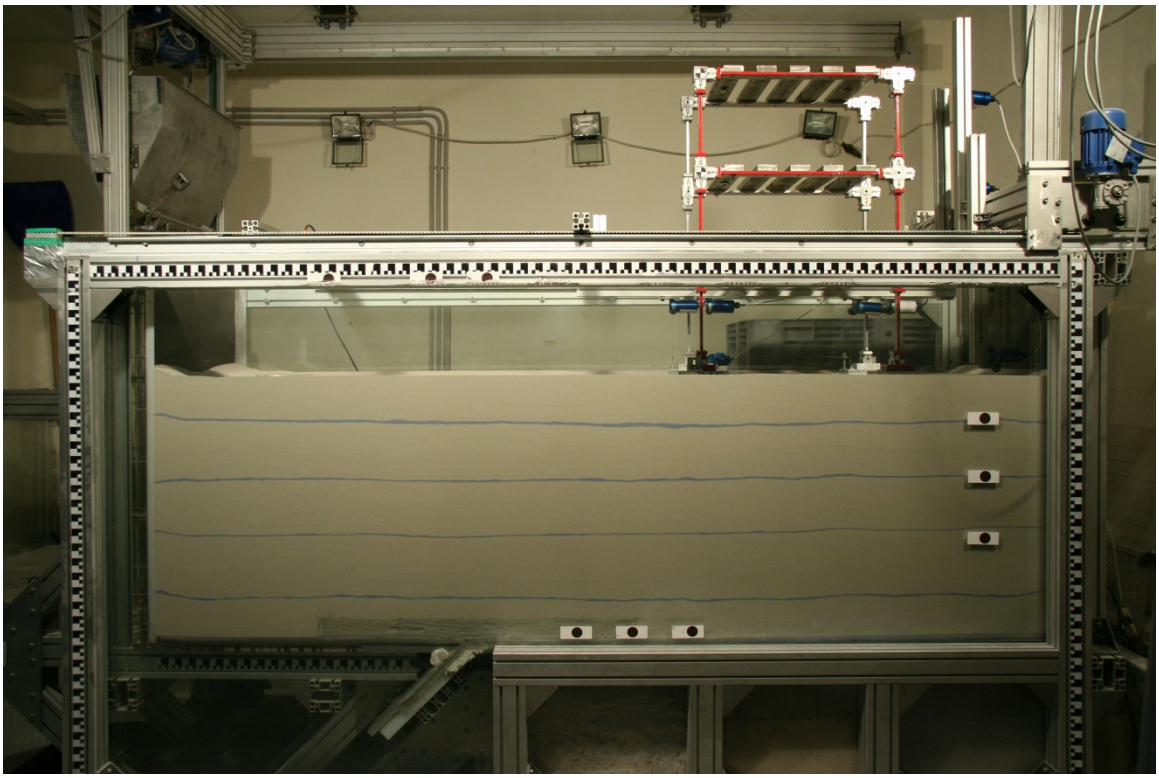

(a)

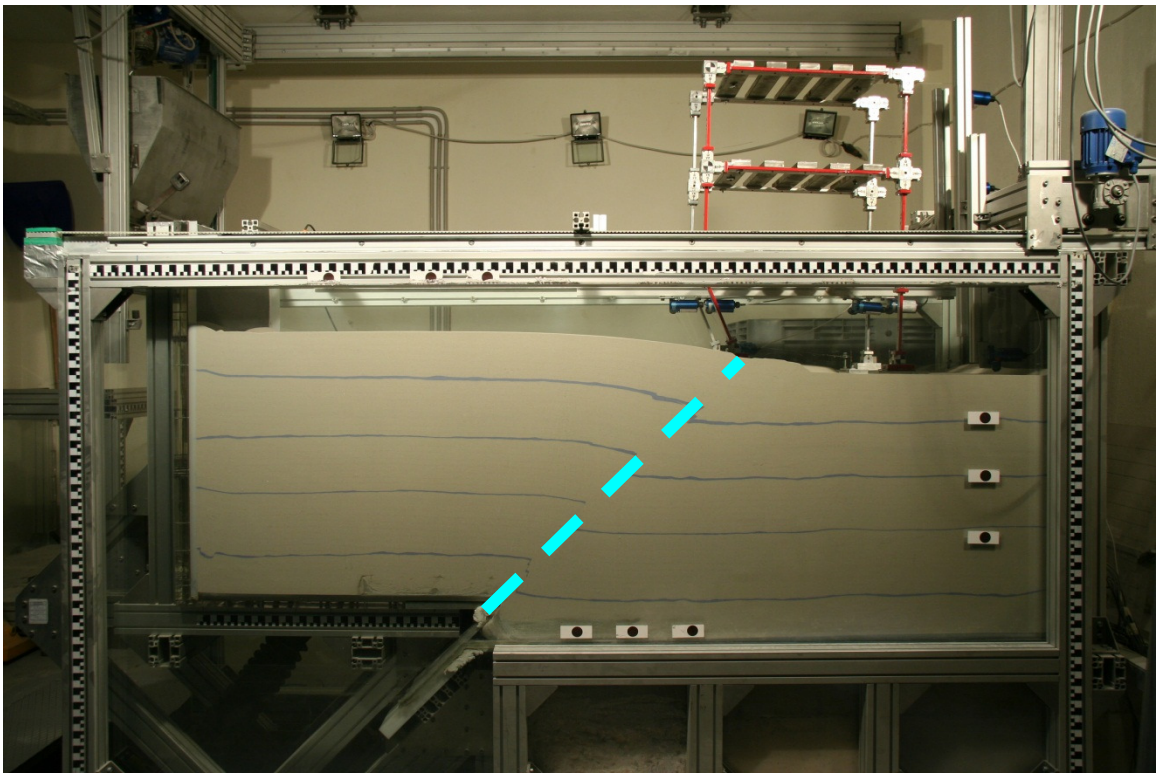

(b)

Figure 4.12 Soil-Structure interaction experiment during fault rupture in Soil Mechanic Laboratory of N.T.U.A: (a) Before applying the rupture, and (b) after applying rupture with final amplitude of 0.1m

(a) (b)

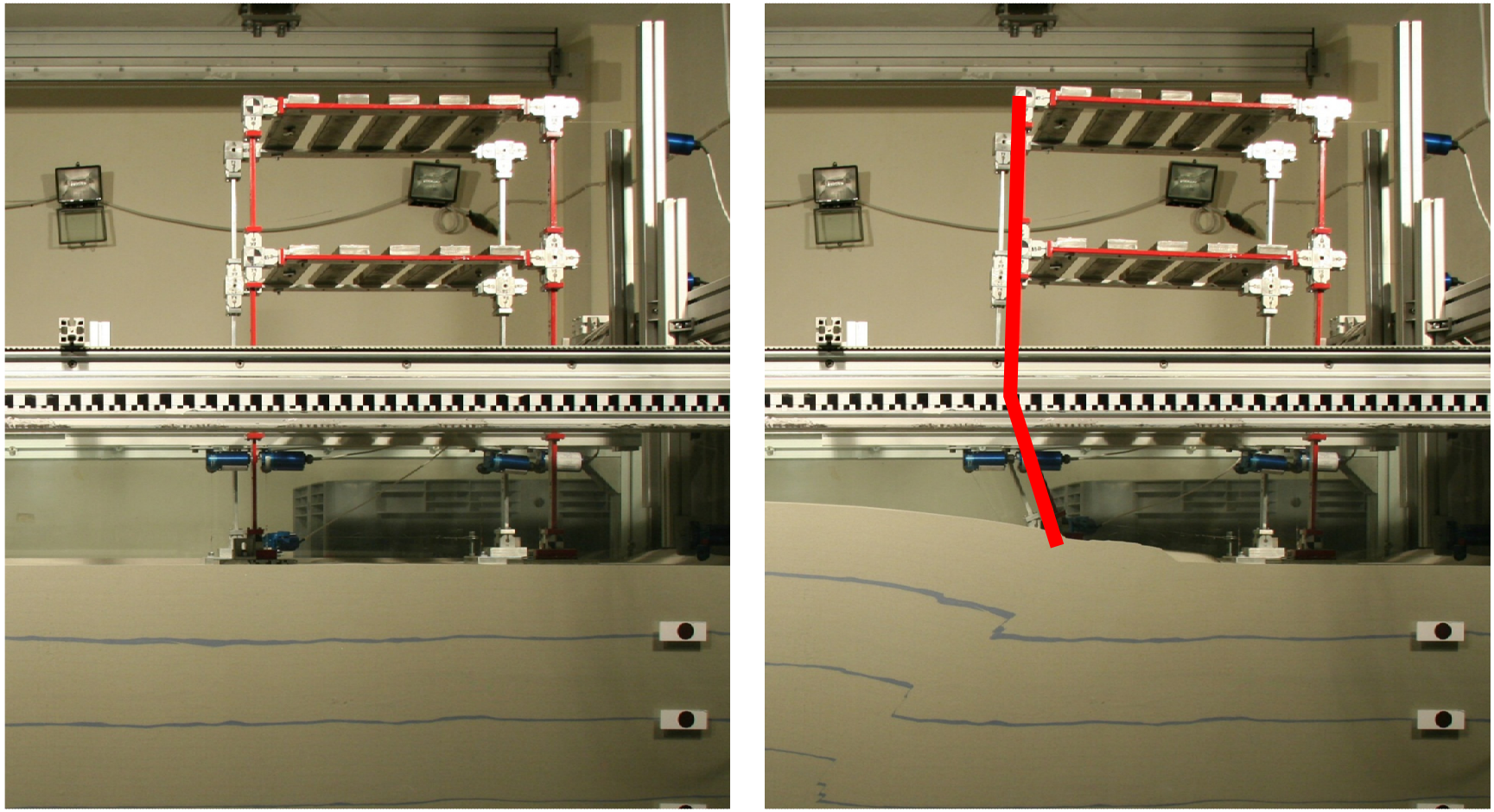

Figure 4.13 Soil-Structure interaction experiment during fault rupture in Soil Mechanic Laboratory of N.T.U.A: (a) Before applying the rupture, and (b) after applying rupture with final amplitude of 0.1m

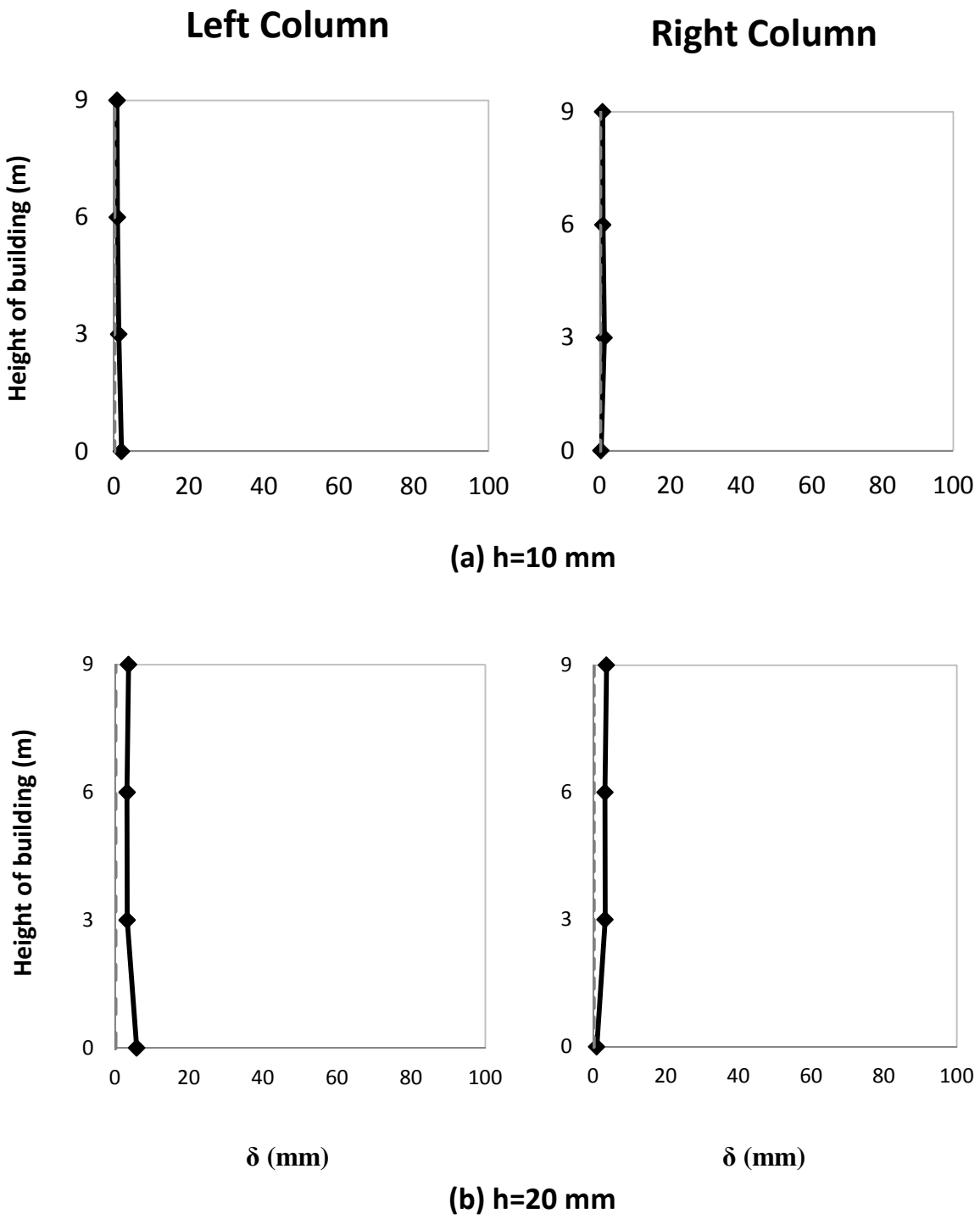

Figure 4.14 Horizontal displacement of columns for vertical displacement of (a) h=10mm, and (b) h=20mm

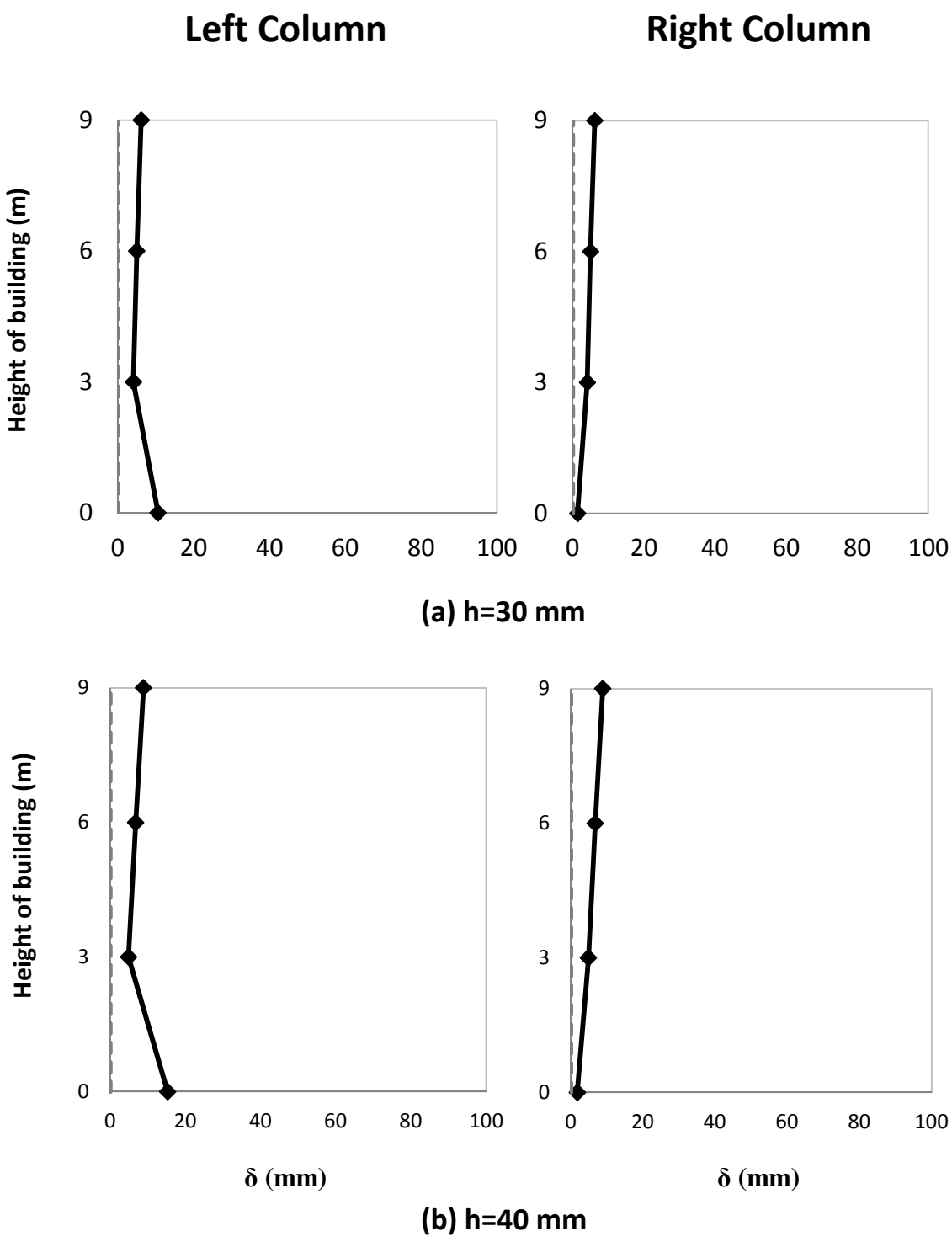

Figure 4.15 Horizontal displacement of columns for vertical displacement of (a) h=30mm, and (b) h=40mm

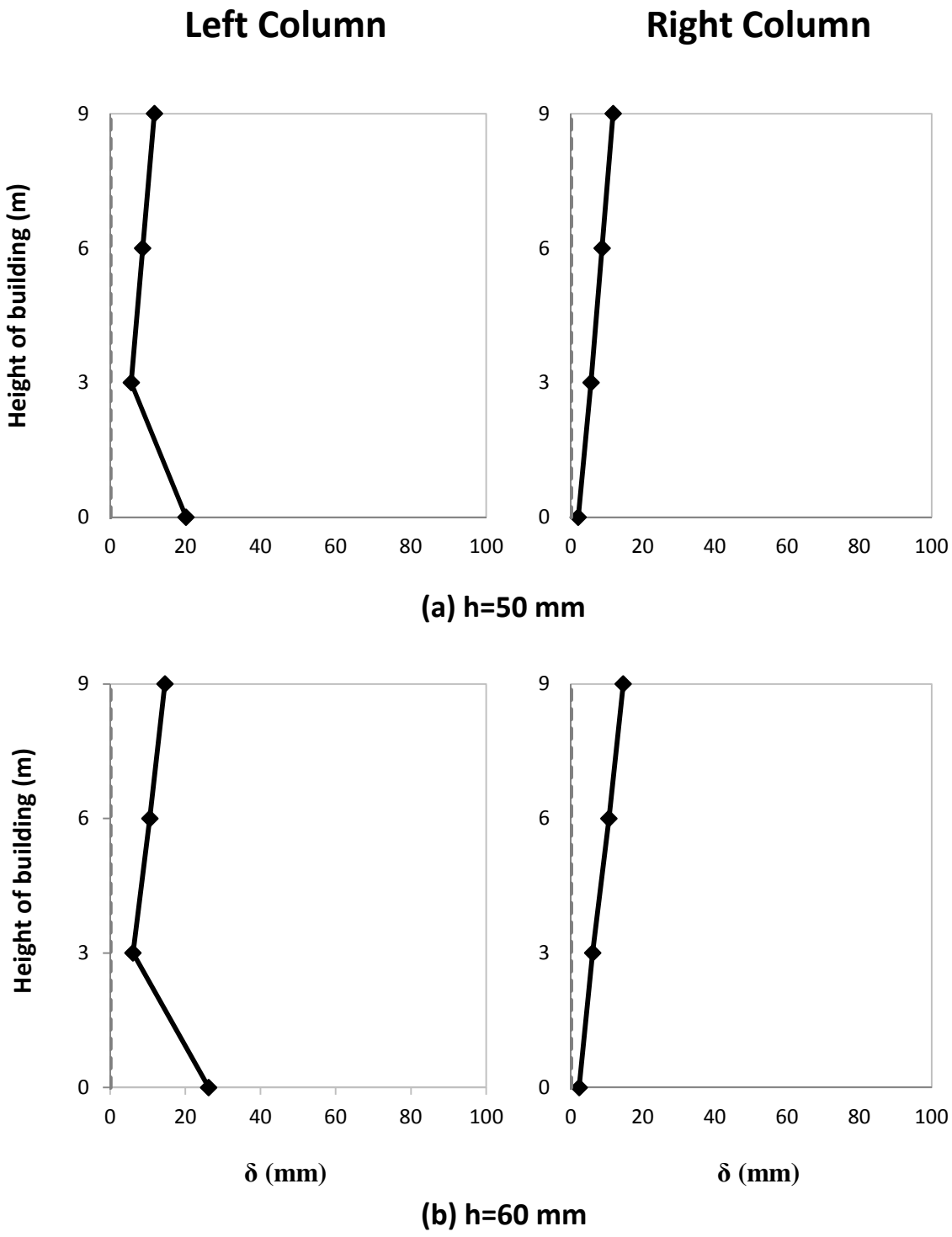

Figure 4.16 Horizontal displacement of columns for vertical displacement of (a) h=50mm, and (b) h=60mm

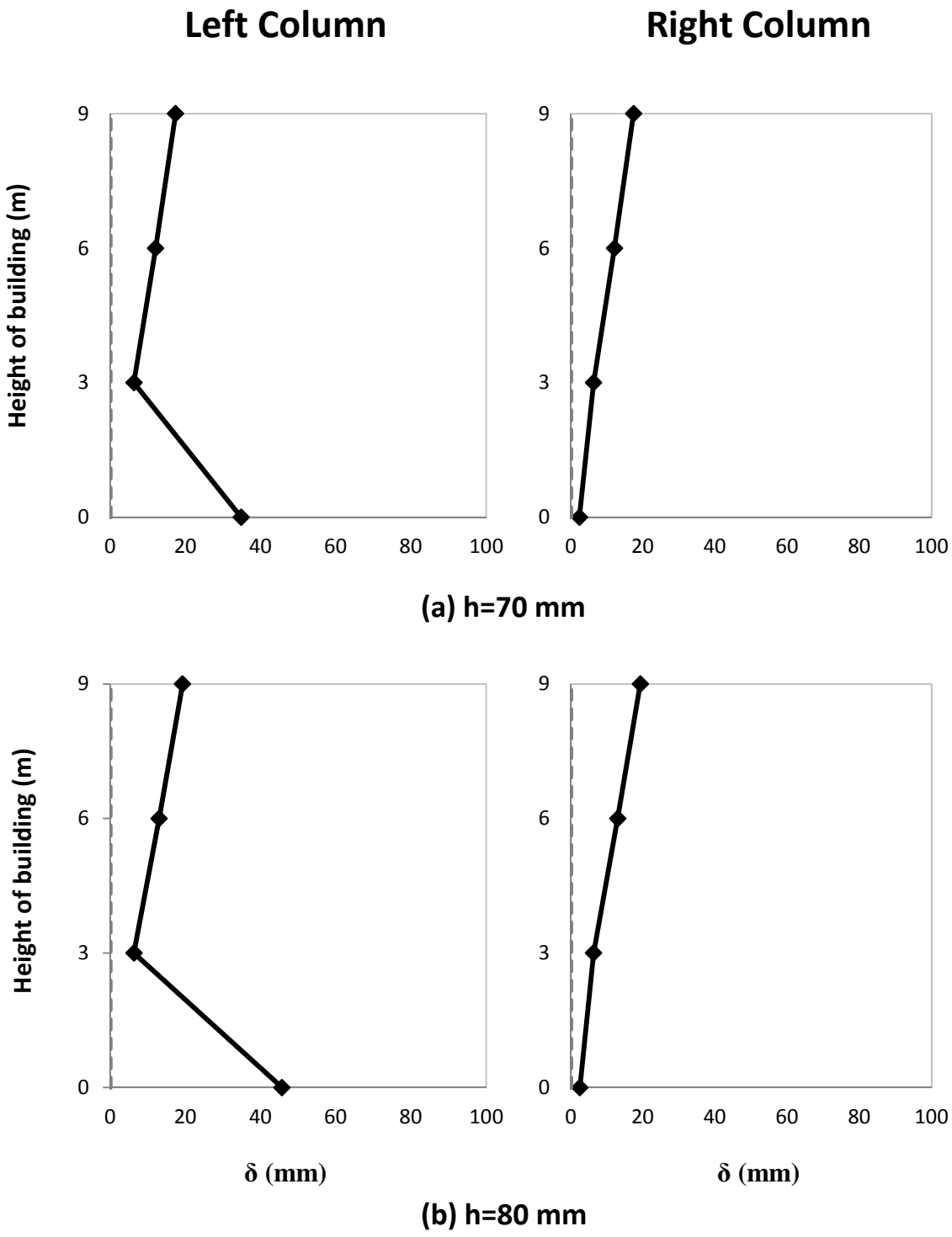

Figure 4.17 Horizontal displacement of columns for vertical displacement of (a) h=70mm, and (b) h=80mm

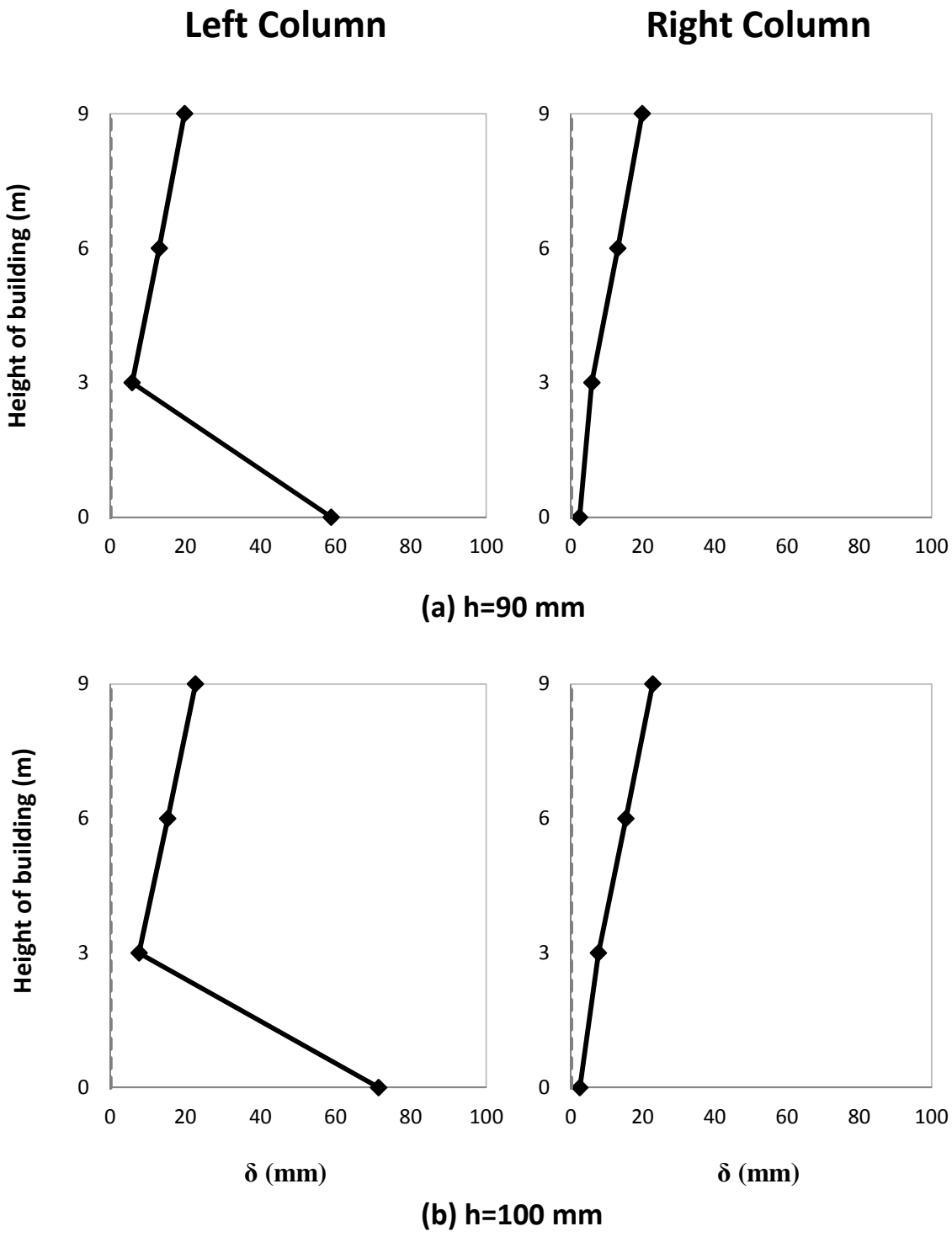

Figure 4.18 Horizontal displacement of columns for vertical displacement of (a) h=90mm, and (b) h=100mm

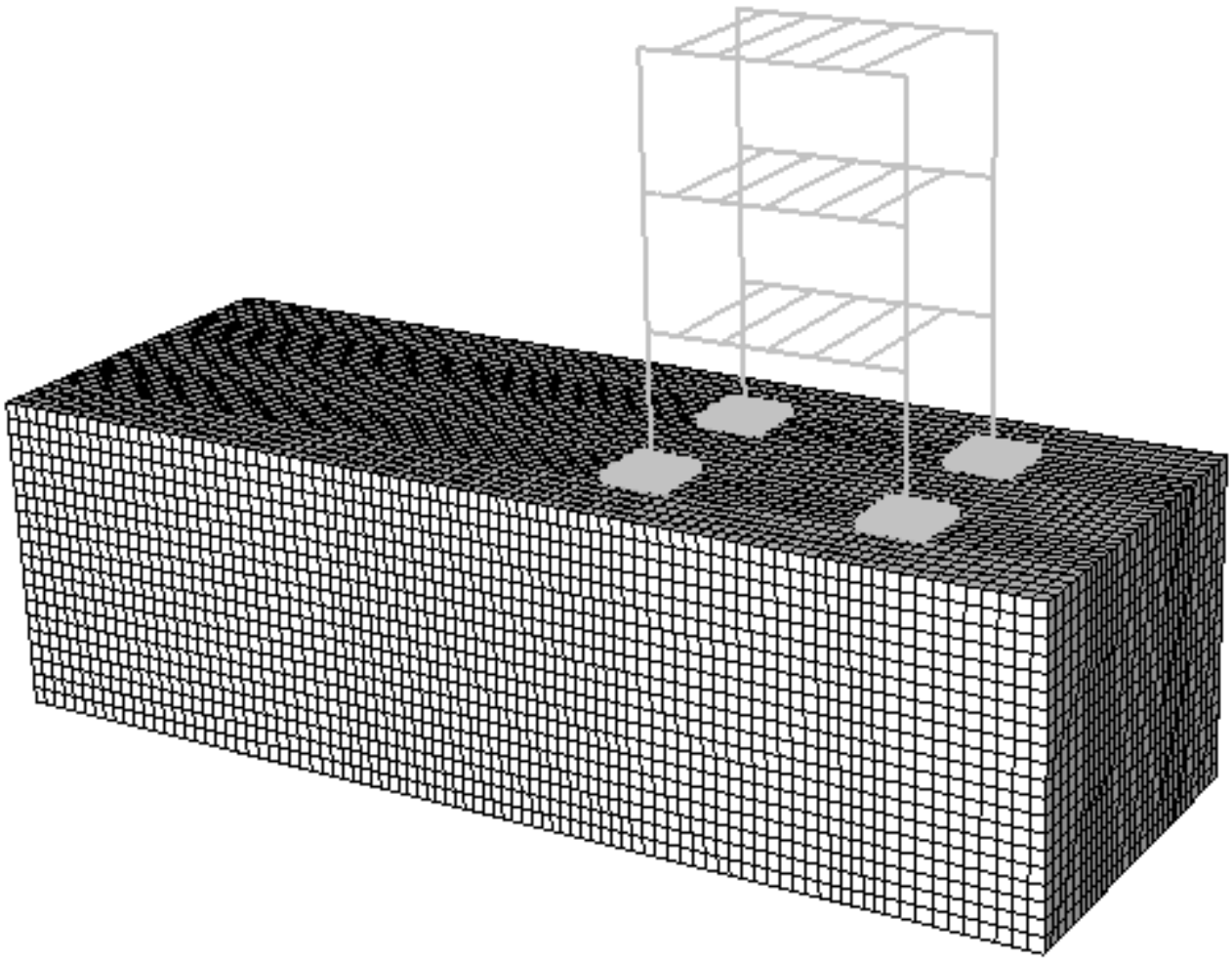

Figure 4.19 The model in ABAQUS

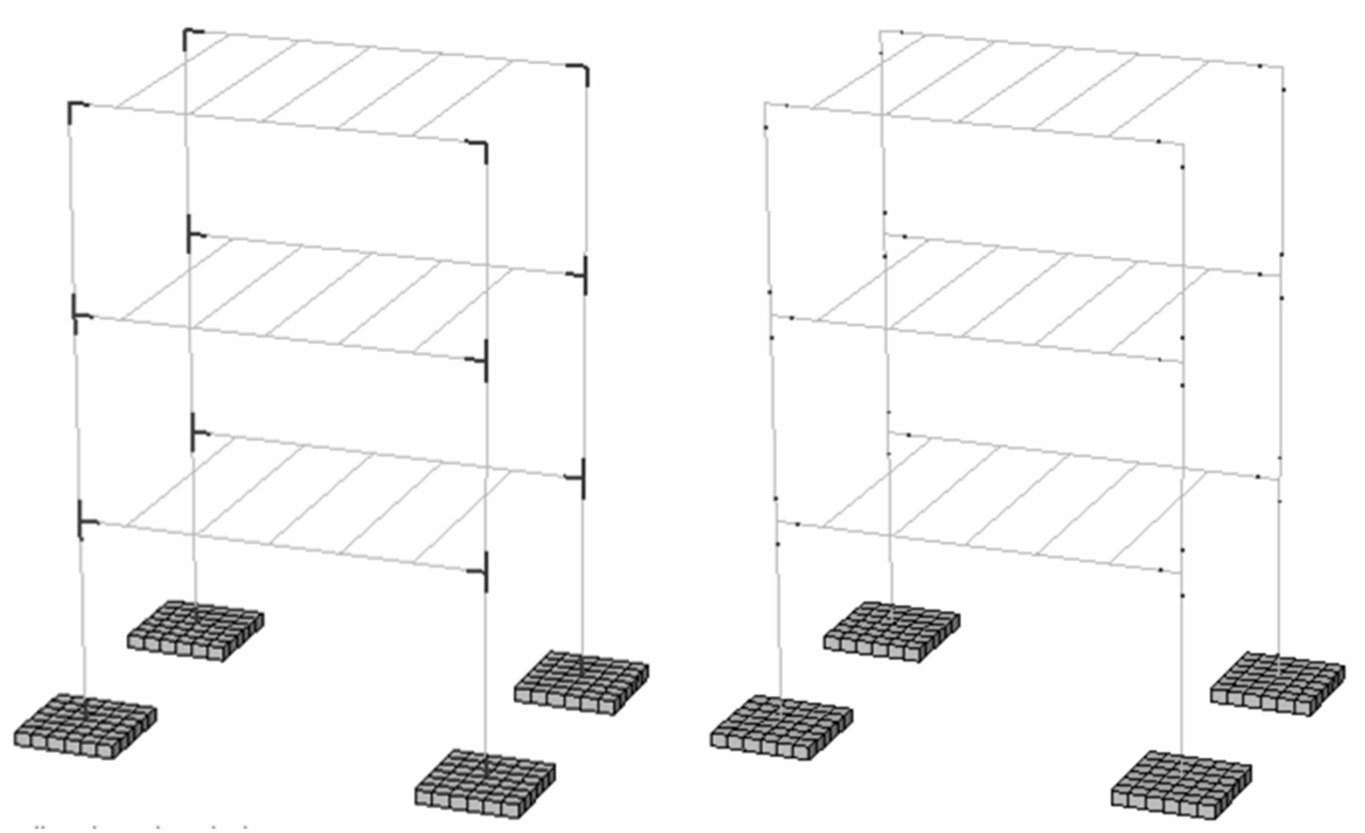

(a) (b)

Figure 4.20 (a) Rigid, and (b) plastic elements in the model in ABAQUS

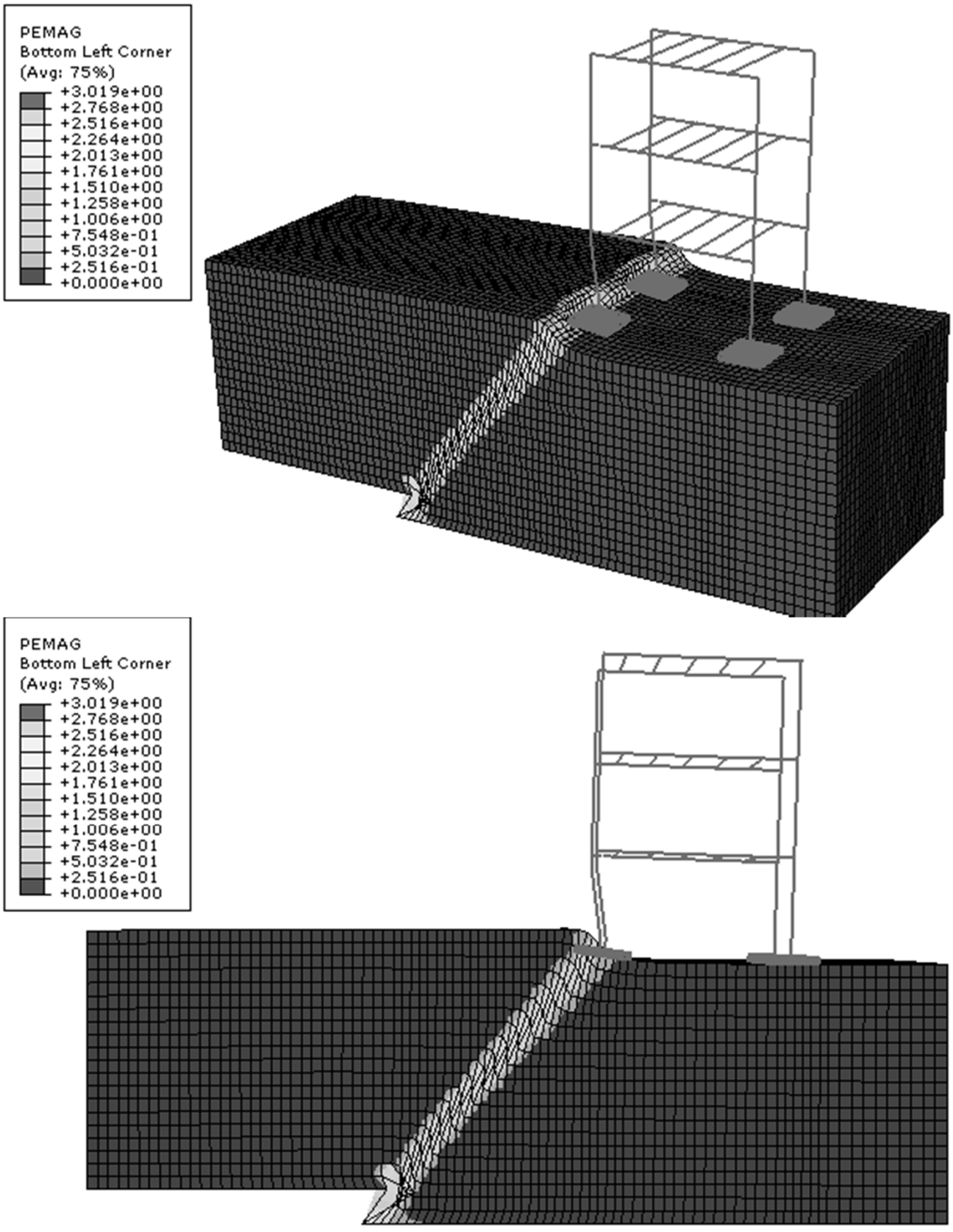

Figure 4.21 The deformed model in ABAQUS for fault rupture with amplitude of h=0.1 m

(a)

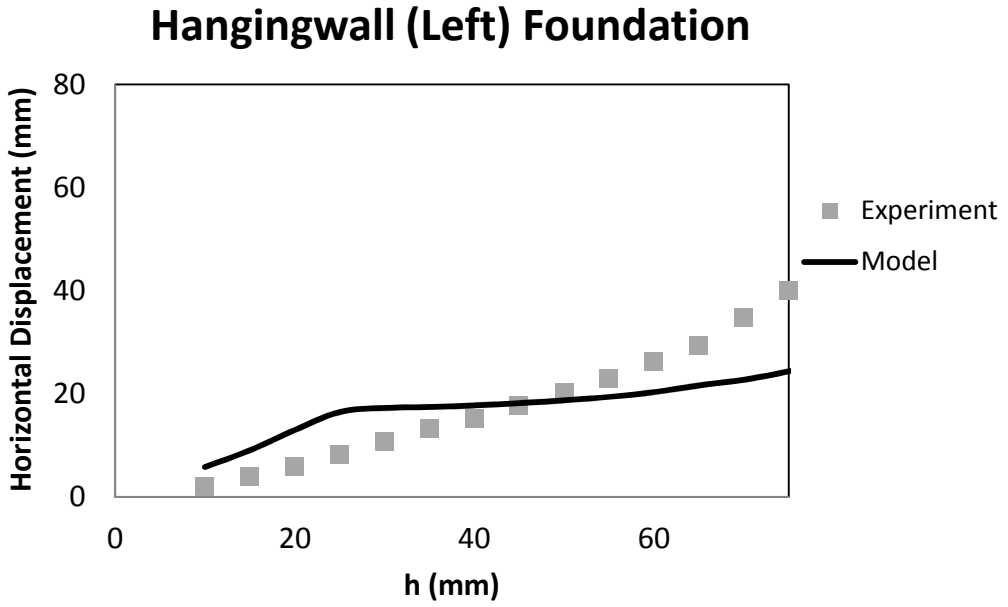

(b)

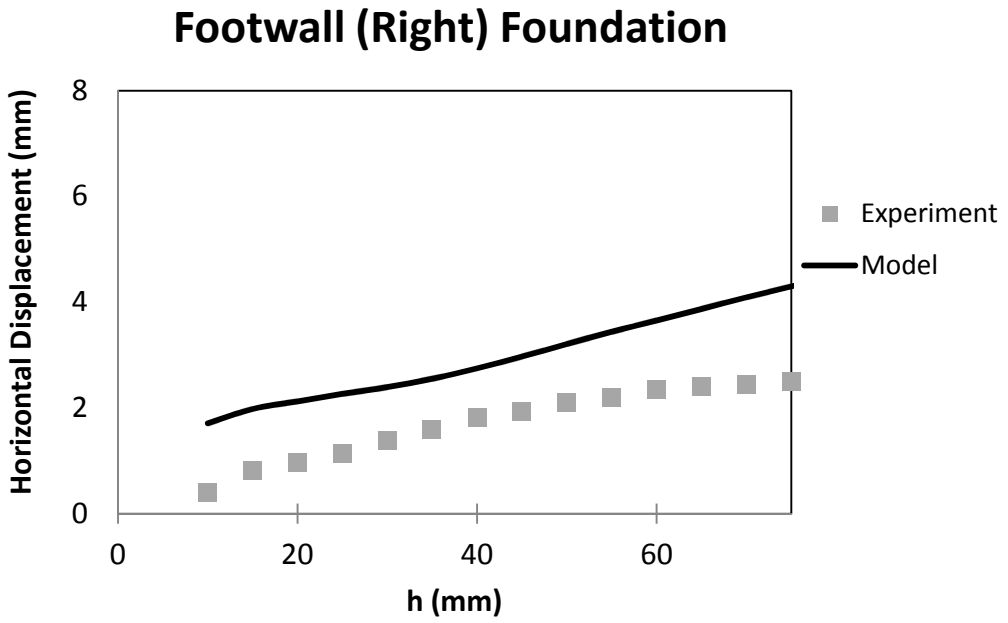

Figure 4.22 Comparison of the results of experiment and the model in ABAQUS for the horizontal displacement of (a) hangingwall (left), and (b) footwall (right) foundation

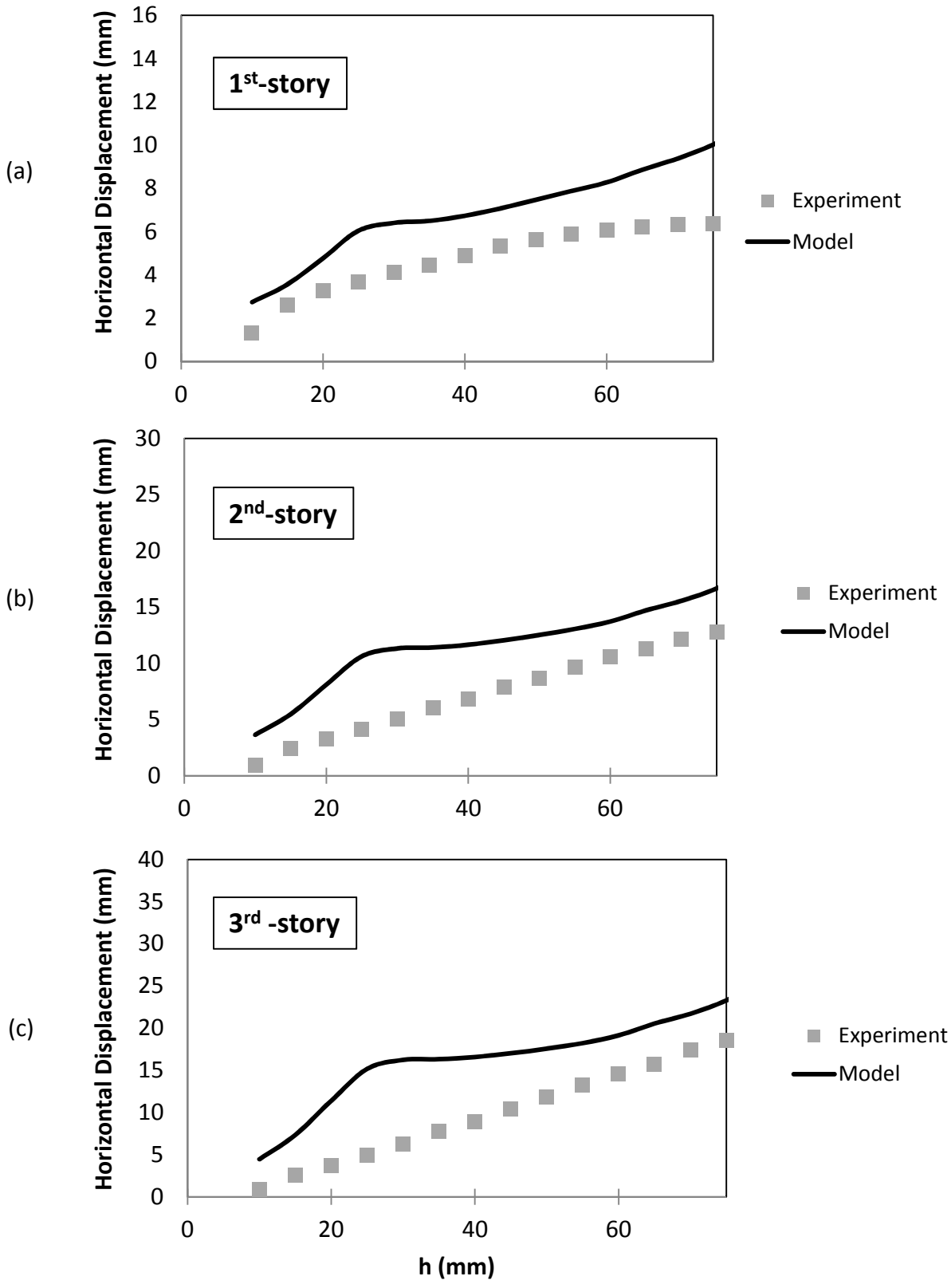

Figure 4.23 Comparison of the results of experiment and the model in ABAQUS for the horizontal displacement of (a) 1st story (b) 2nd story, and (c) 3rd story

(a)

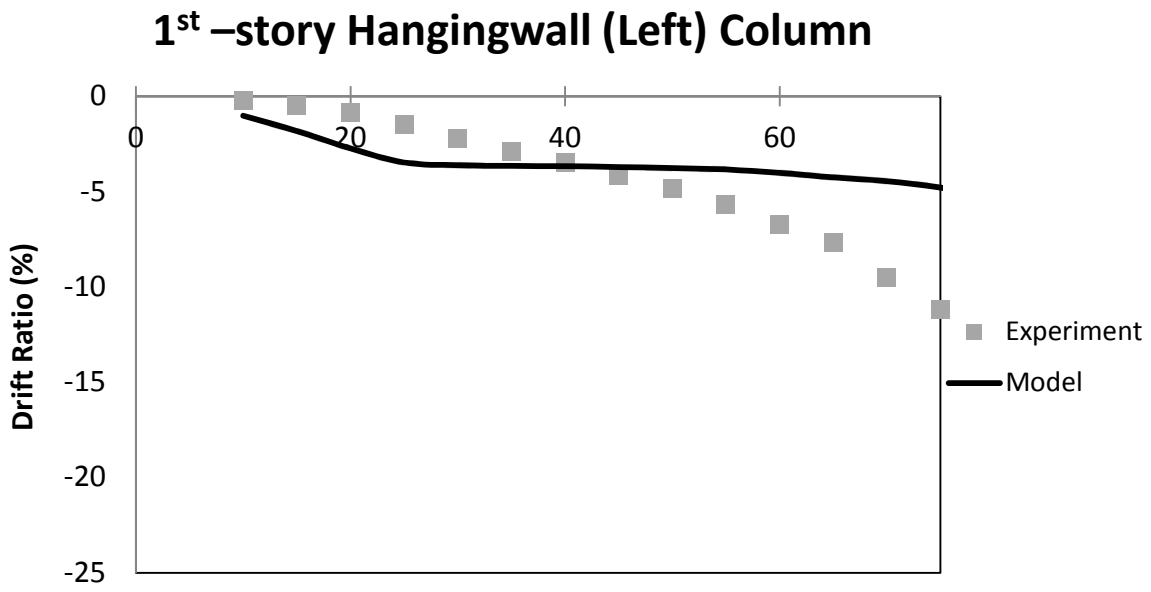

(b)

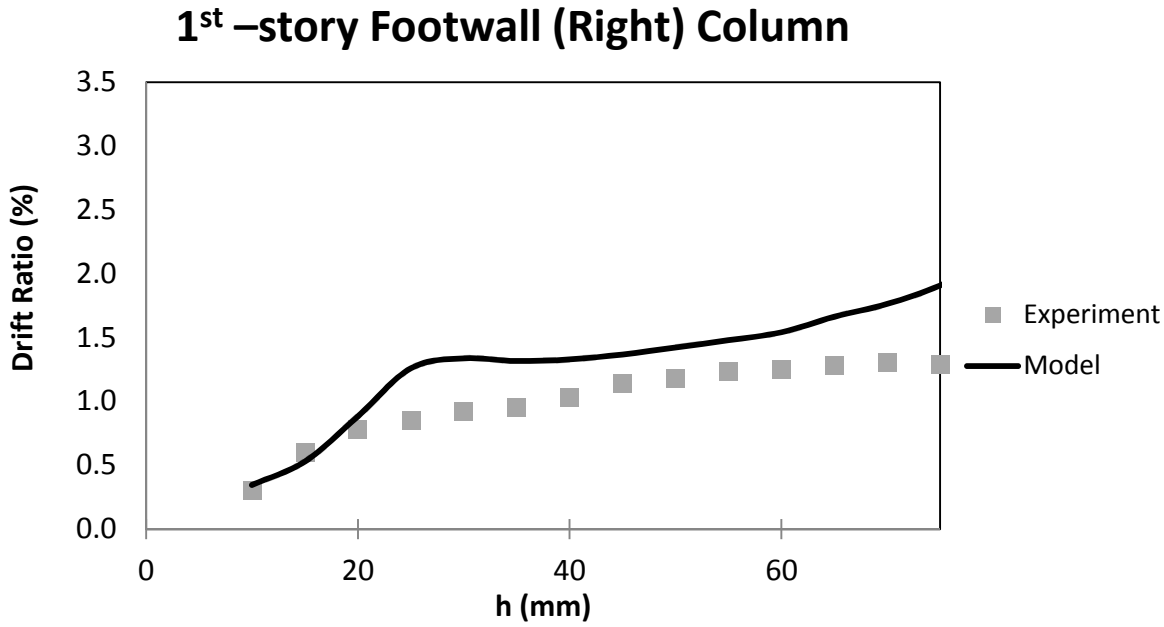

Figure 4.24 Comparison of the results of experiment and the model in ABAQUS for drift ratio of (a) 1st –story hangingwall (left) column, and (b) 1st –story footwall (right) column

(a)

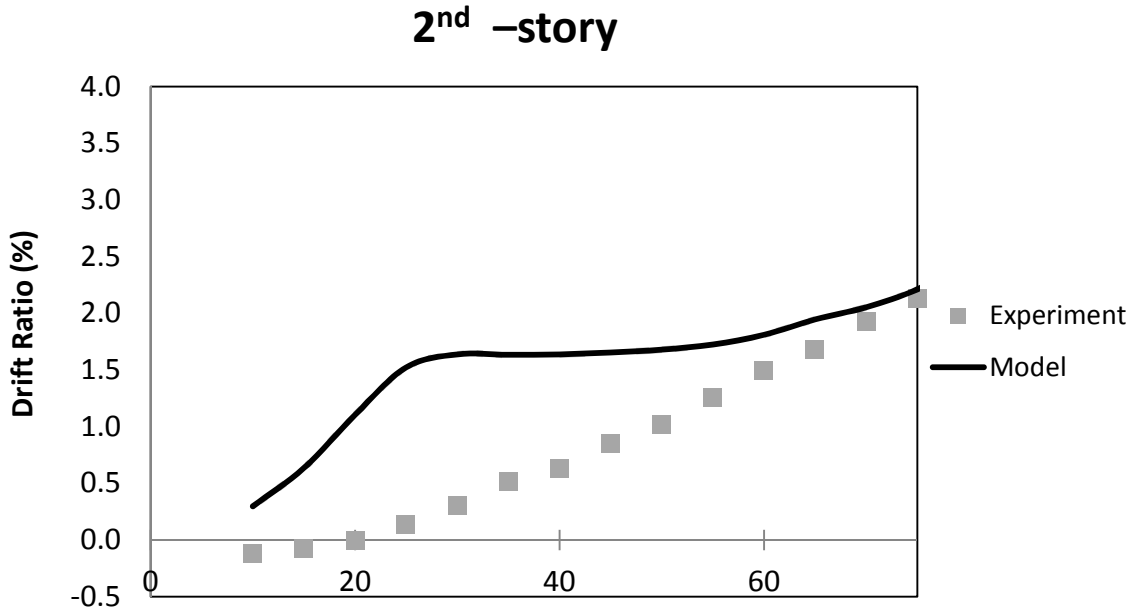

(b)

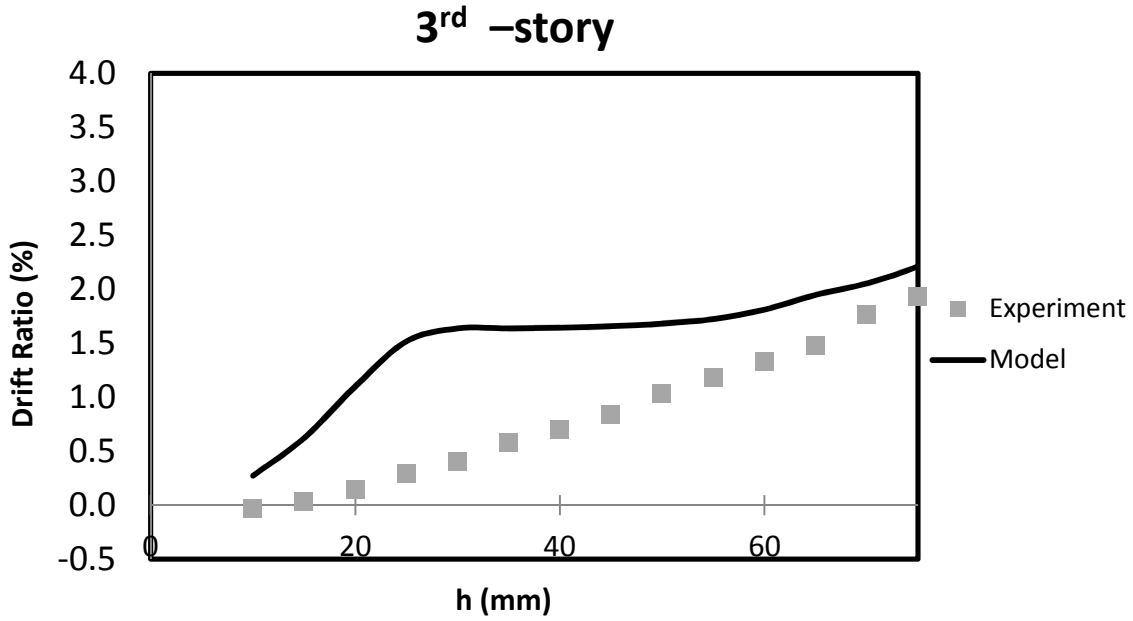

Figure 4.25 Comparison of the results of experiment and the model in ABAQUS for drift ratio of (a) 2nd story, and (b) 3rd story

(a)

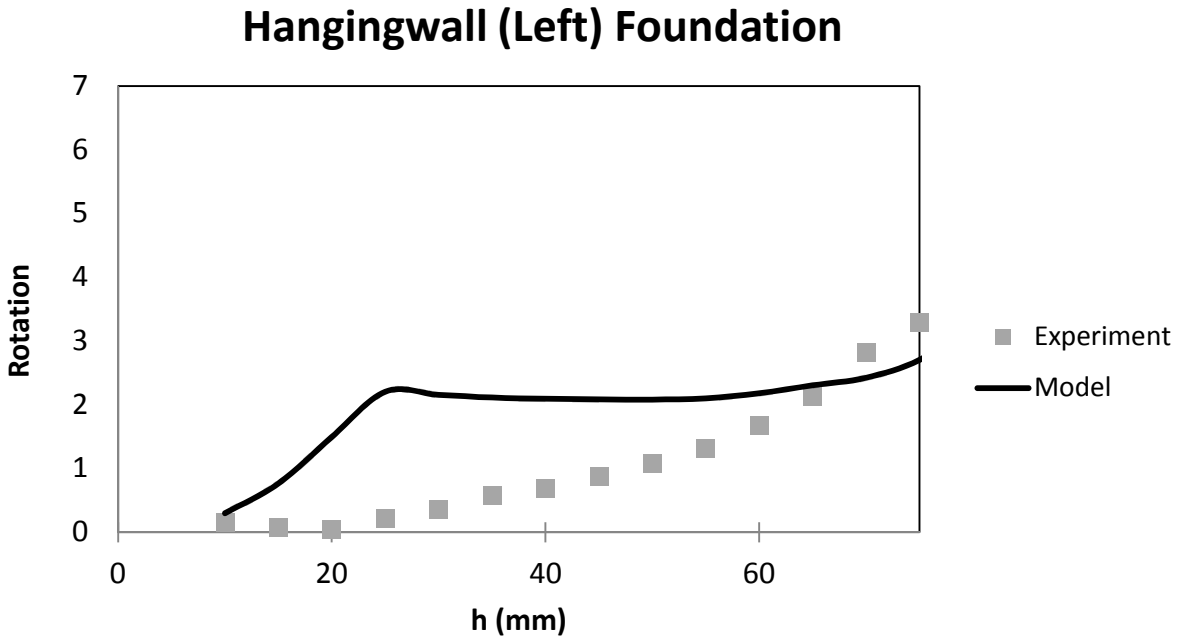

(b)

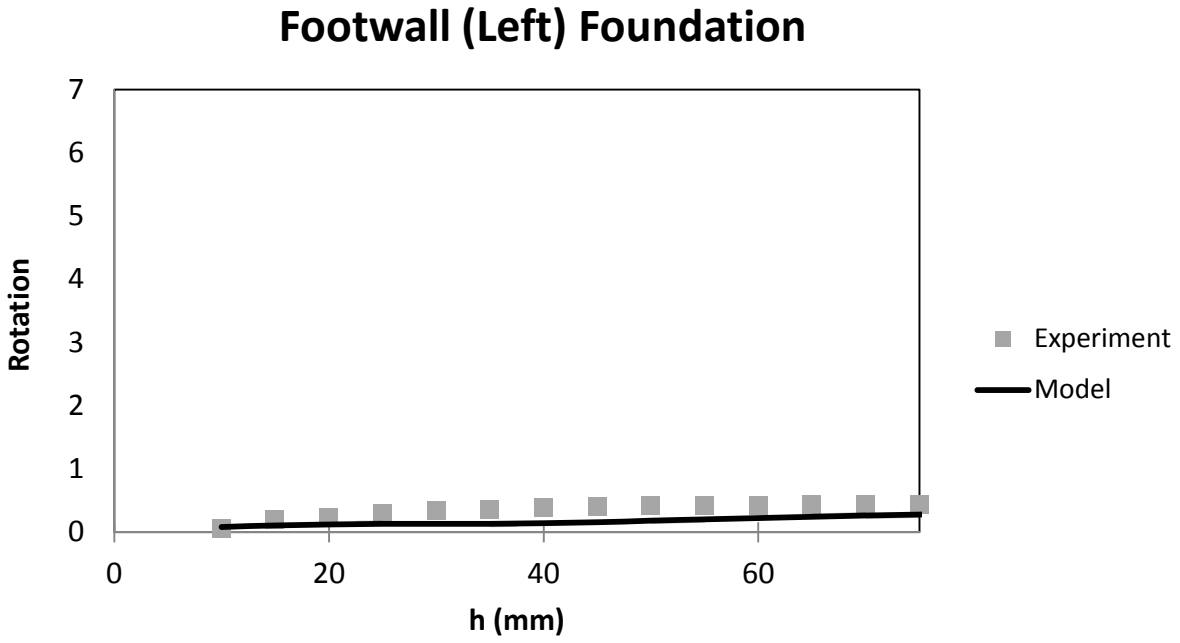

Figure 4.26 Comparison of the results of experiment and the model in ABAQUS for rotation of (a) hangingwall (left) foundation, and (b) footwall (right) foundation

(a)

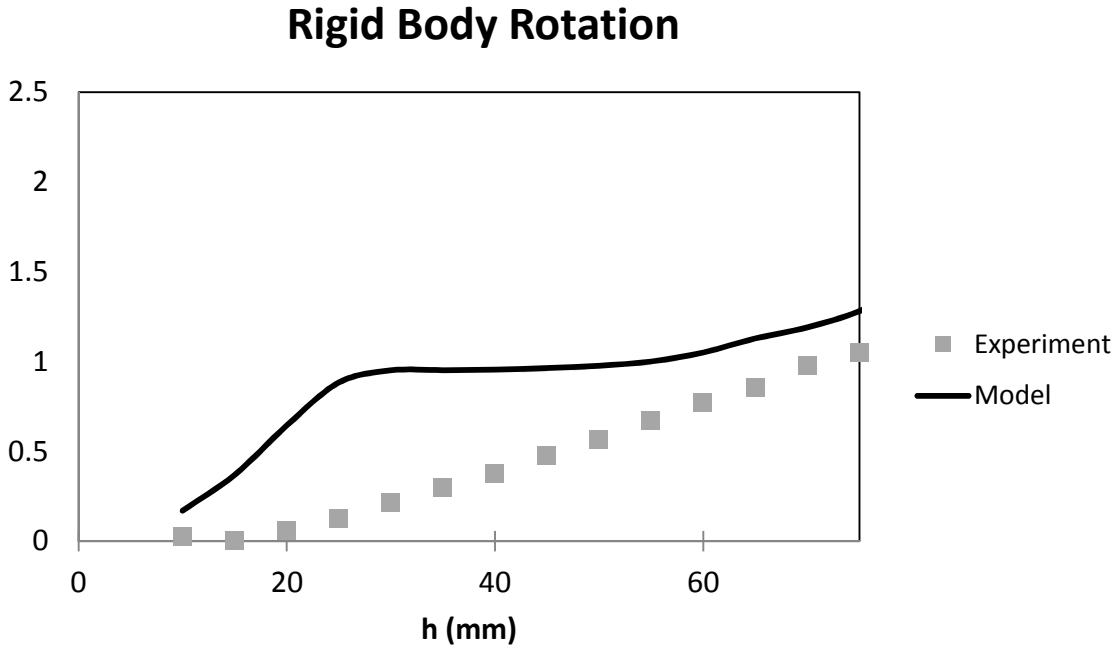

(b)

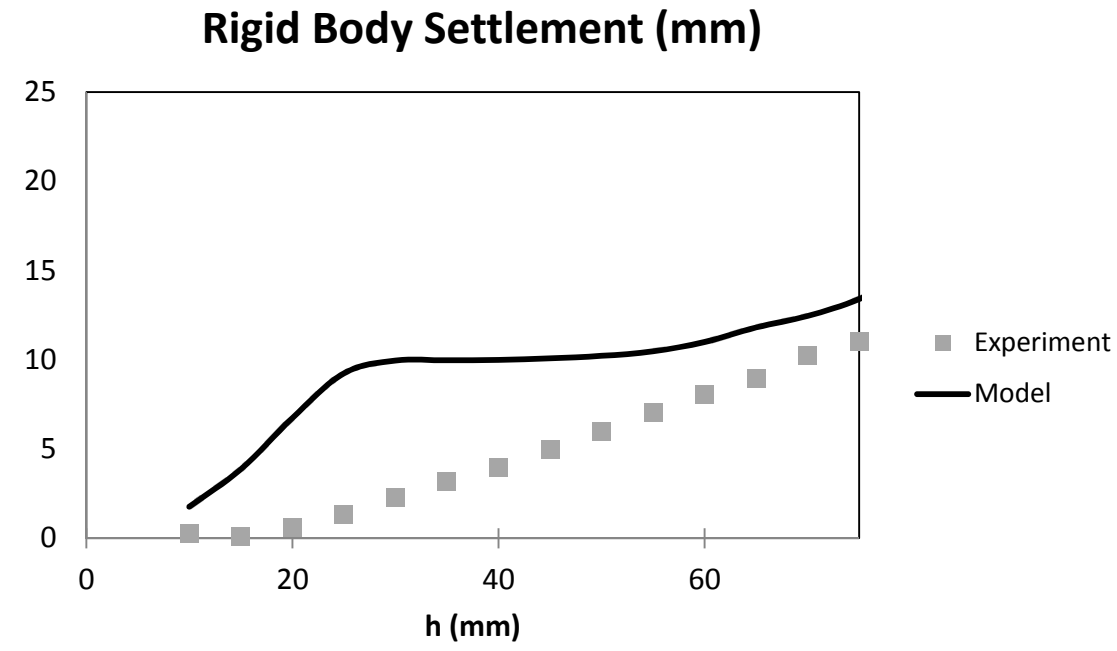

Figure 4.27 Comparison of the results of experiment and the model in ABAQUS for (a) rigid body rotation, and (b) rigid body settlement (mm)

Chapter 5

5. Parametric Investigation

5.1. Introduction

In previous chapter, nonlinear finite element model were utilized to analyze the performance of 3-storey structure with isolated footings on top of the outcropping reverse fault rupture and this method was verified by the reduced-scale experiment which has taken place in Laboratory of Soil Mechanics of N.T.U.A. This chapter uses this model to undertake a parametric study on the interaction of the building structure founded on isolated foundations with thrust fault rupture. In this parametric analysis, the influence of relative outcropping position of the rupture as well its amplitude will become investigated.

5.2. Analysis Methodology

This chapter undertakes a deep analysis of foundation and structure behavior sitting directly on a rupture which propagates from the base rock to the ground surface. In order to investigate the interaction between the thrust fault and the structure sitting on top of it, the finite element model which was verified in previous chapter is used herein and three dimensional (3D) plane-strain analyses are performed. As the previous chapter, an elastoplastic constitutive model includes Mohr-Coulomb failure criterion with an isotropic strain softening characteristics will be used. Also as the previous chapter, a very refined mesh in the neighborhood of potential rupture and under the foundations will be used for the betterment of the finite element modeling and achieving more accurate results.

In this chapter, the role of Fault Rupture-Soil-Foundation-Structure interaction is parametrically investigated by using the same finite element model. For investigation of the effect of amplitude of the rupture, *h*, the numerical analysis will be undertaken on a rupture starting from $x = 0.9\,m$ and different parameters like structural moment, foundation horizontal displacement, structural drift ratio in percentage, foundation

rotation and rigid body rotation and settlement will be evaluated with respect to vertical base displacement (h).

For analysis of the influence of location of rupture, the above mentioned parameters are investigated for different relative outcropping positions of the rupture. Then the maximum value of each parameter for a specific location of rupture is calculated in order to plot an envelope of each parameter for different values of x.

5.3. The Finite Element Model

For parametric investigation of soil-foundation-structure interaction during fault rupture, the verified finite element model of previous chapter is going to be used. As in the previous chapter, the structural model is consisting of beam elements and it is placed on top of soil layers with using special interface elements which are infinitely stiff in compression but show no resistance in tension and they obey Coulomb friction law in shear. Therefore, it is possible to model the structure not bonding to the soil and both uplifting and slippage would occur like in reality.

In order to analyze the effect of different locations of outcropping rupture, a soil box of $42 \times 90 \times 75$ cm should be added to the end of the previous model with elements with same dimensions. The complete 3D model and its 2D view are displayed in **Fig.5.1**.

For investigation of the effects of magnitude of rupture offset, the finite element model is used for a rupture starting from point $x = 0.9$ m and for the evaluation of the influence of location of rupture, the same model is utilized for about 18 locations of outcropping rupture.

5.4. Results

The main results for our fault rupture soil-foundation-structure interaction analysis are discussed in terms of the distribution of plastic strains, the vertical displacement profile Δy, the foundation horizontal displacement, the structural drift ratio, structural moment, the foundation and structure rotation, the rigid body rotation in foundation and structure level and the rigid body settlement.

5.4.1. Effect of Magnitude of Rupture Offset

For investigation of the effect of increasing the vertical base movement, the results for the base rupture location of x = 0.9 m are analyzed. **Fig.5.2** to **Fig.5.8** show the above mentioned parameters variation with respect to *h*. As it is illustrated in these figures, the foundation and structure displacement is increasing by the increase of fault rupture amplitude. However, these diagrams have two branches with different slopes. These diagrams show the intense increase of structural movement until the base vertical displacement of 20 mm and afterwards, they have milder slopes which show less increase of structure deformation. This is due to the change of mechanism of fault rupture propagation through the soil. When the rupture has not outcropped yet (until h = 20 mm), the increase of base vertical displacement causes the horizontal displacement of whole masses of the soil on the slip surface to increase. However, after outcropping of the rupture, more increase of the base vertical displacement doesn't lead to more increase of horizontal displacement of the footings because the rupture outcrops just before the left foundations due to presence of the structure and its load.

5.4.2. Effect of Location of Rupture

For analysis of the influence of location of rupture, among the 18 locations which were analyzed, five of them which are the best representatives for other locations have been chosen. Then, the maximum value of each above mentioned parameters was calculated for each location in order to plot an envelope of each parameter for different values of *x*.

The results for different locations of rupture are presented in **Fig.5.9** to **Fig.5.43**.

Fault Rupture initiating at distance of $x = 0.80\ m$

The distribution of plastic strains is showing in **Fig.5.9** in both 3D and 2D views. As illustrated in this figure, the rupture outcrops about 5 cm before the foundations which also can be seen in ground surface profile as it's displayed in **Fig.5.10** for both mid points and edge nodes of the surface.

Fig.5.11.a shows the horizontal displacement of footings of back frame. As it is illustrated in this figure, the foundation which is more near to rupture has much larger horizontal displacement (about two times) than the other one. The horizontal displacement of the left foundation has 2 branches: first branch with steeper slope and the second one with milder slope. This occurred because of change of the mechanism of rupture propagation and diversion of rupture path due to presence of the structure.

As displayed in **Fig.5.11.b**, the drift ratio of the first story right column and the second and third stories are approximately the same and are about 1% while the drift ratio of the first story left column is larger and it is about 2% and also occurs in opposite direction.

In **Fig.5.12**, the rotation of both foundations and both columns of the back frame are illustrated. Also we can see that the rotation of the left footing is increasing by increasing the vertical displacement of the bedrock until 20 mm and then it decreases while the right footing rotation increases continuously. That's again because of the

diversion of rupture path due to structure loads. Therefore the rupture outcrops just before the footings and the left footing rotation decreases. For the rotation of left column, the first story column has the maximum rotation value of about $-1°$ while the second and third story columns has the maximum value of about $0.42°$. It should be mentioned that, the positive rotation is considered to be the counterclockwise rotation. For the right columns, all three stories columns have an approximately the same value of about $0.42°$ and also they rotate in same direction. The same rotation of left and right columns of second and third stories is in the agreement with the assumption of having rigid floors. Therefore it is right to calculate just one drift ratio for each second and third stories while we should calculate separate drift ratios for the left and right columns of first story because of different movement of their bases.

The rigid body rotation of the whole structure has been calculated both in foundation and structure level as illustrated in **Fig.5.13**. For the structure level, the rigid body rotation has been calculated in third story level. From this figure, we can see that the rigid body rotation in foundation level which is $0.56°$ is more than the rotation in roof of the structure which is $0.33°$. Also as we can see, the rigid body settlement of the structure is about $6\ mm$.

As it is presented in the figures for this location of the rupture, since it outcrops about 5 cm before the structure footings, it doesn't cause significant deformation to the structure and its foundation.

Fault Rupture initiating at distance of $x = 1.00\ m$

The plastic strains distribution is showing in **Fig.5.16** in 3D and 2D views. As represented in this figure, the rupture outcrops under the middle of the left footing. The ground vertical displacement is displayed in **Fig.5.17** for both mid points of the surface and edge nodes.

As illustrated in **Fig.5.18.a**, the horizontal displacement of the footings increases linearly with increasing the base vertical displacement. Also the left foundation has much larger horizontal displacement than the right one which located on the footwall (about 77 mm compared to 7 mm). That happens because the rupture hits directly the left footing and causes it to displace more.

The drift ratio of the structure is displayed in **Fig.5.18.b**. We can observe that the drift ratio of the structure increases linearly with increasing the amplitude of the rupture. It shows that the drift ratio of the first story column which is on footwall and the second and third stories are approximately the same and are about 9% while the drift ratio of the first column which is on hangingwall is much larger and it is about 15% and also occurs in opposite direction. Also it is obvious that, for rupture initiating from $\mathrm{x} = 0.95\ \mathrm{m}$ which outcrops exactly under the middle of the left footing, the structure drift ratio is much larger than the previous location of rupture. This large drift ratio will cause the structure to collapse surely if the connections were designed more according to reality!

As it is shown in **Fig.5.19**, the rotation of left foundation is much more than the right one (8.6° compared to 0.3°). For the rotation of left column which is on hangingwall, the first story column has the maximum rotation value of about $-8.7°$ while the second and third story columns have the maximum value of about 5°. For the right column on the footwall, all three stories columns have an approximately the same value of about 5° and also they rotate in same direction. For foundations and column rotations also we can see much bigger rotation for this outcropping rupture than for the previous one which outcrops before the left foundation.

The rigid body rotation of the whole structure in foundation level is about 5.2° and larger than the rigid body rotation in third story level which is about 3.2° as it is

illustrated in **Fig.5.20**. Also as we can see, the rigid body settlement of the structure is about 54 mm which is about 10 times more than the previous position of rupture.

Fault Rupture initiating at distance of $x = 1.20\ m$

The plastic strains distribution is displayed in **Fig.5.23** in 3D and 2D views. As demonstrated in **Fig.5.24**, the rupture which initiates from $x = 1.175$ m, outcrops between two footings and therefore it causes large displacements of left footing and large differential displacement (**Fig.5.25.a**) of the foundations, but small value of rotation (**Fig.5.26.a**). That's because the rupture outcrops between the two footings and one footing is completely on hangingwall while the other is entirely on footwall. Also, as illustrated in **Fig.5.25.b** and **Fig.5.26.b**, the structural drift ratio and columns rotations are so large because of large relative displacement of the base of the columns.

Also it seems that for this location of rupture, the requested parameters increase linearly with increase of base displacement. That's because the rupture propagation doesn't change its mechanism and it doesn't divert due to presence of any foundation on location of rupture outcropping.

The rigid body rotation of the whole structure in both foundation level and 3rd story level and rigid body settlement of the structure are also large again due to the large differential movement of the structure columns in their bases as illustrated in **Fig.5.27**.

Fault Rupture initiating at distance of $x = 1.60\ m$

The rupture which initiates from point $x = 1.55$ m outcrops under midpoint of the right footing as it is shown in **Fig.5.30** in 3D and 2D views and in **Fig.5.31** by displaying the ground vertical displacement of mid and edge nodes of the surface.

In this case, both left and right footings are on hangingwall and therefore they have large horizontal displacements which are close to each other as it is indicated in **Fig.5.32.a**. Thus, they have small relative displacement which is become even negative in higher steps due to larger horizontal displacement of the right footing.

As it is represented in **Fig5.32.b**, the stories of the structure undertake nearly same drift ratio due to positioning of both columns on hangingwall. However, we can see that the drift ratio of right column of first story and second and third stories has two branches which shows the altering of the mechanism of fault rupture propagation through the right footing while the left column drift ratio increases linearly as it is far from the rupture path.

As it is shown in **Fig.5.33**, the rotation of right foundation is much more than the right one due outcropping of the rupture under the middle of right foundation. However, for column rotation, since both were located on hangingwall, they have approximately the same rotation. Here also we can again observe slight change of the rupture path for the right column which causes the rotation diagram of this column to have two branches.

The rigid body rotation of the structure which is calculated in both foundation level and third story level and also rigid body settlement of the whole structure are illustrated in **Fig5.34**. As it is indicated in this figure, again the diagrams have two branches due to change of the mechanism of the rupture propagating through the left footing. Also, as both footings located almost on the hangingwall (but not exactly), the whole structure has less value of rigid body rotation and settlement compared to the previous case.

Fault Rupture initiating at distance of $x = 1.70\ m$

The plastic strains distribution for the rupture which initiates at the distance of $x = 1.71$ m is showed in **Fig.5.37** in 3D and 2D views. As it is presented in this figure and also the surface profile of mid and edge nodes of the soils in **Fig.5.38**, the rupture outcrops after the structure footings and therefore both footings are exactly in same location relative to rupture and therefore the structure deformation is not so significant while it has horizontal displacement. Thus, both left and right footings have equally large horizontal displacements with the same value as the base vertical uplifting as it is indicated in **Fig.5.39.a**. Since both footings move in same way, there isn't any differential displacement between two footings.

The drift ratio of first, second and third stories, are presented in **Fig.5.39.b**. As it is illustrated, all the stories have nearly equal drift ratios which increase with increasing the base vertical displacement intensely until $h = 15$ mm and after that they have milder slope which shows the change of the mechanism of the fault rupture propagation. That's because until vertical displacement of 15 mm, the rupture propagates through the soil and after that by increasing *h*, its path diverts and cause much less deformation and drift to the structure. However, these drift ratios do not have large values since the rupture completely outcrops about 35 cm after the right foundation.

Fig.5.40 represents small values of rotation for footings and columns and also for rigid body rotation and settlement because of outcropping of the rupture far from the structure. For these parameters also we can see two branches of the diagrams with different slope due to reasons which mentioned above.

Envelope Diagrams

The maximum values of the above calculated parameters for each location have been determined and envelope diagrams have been plotted for these parameters as it is represented in **Fig.5.44** to **Fig.5.50**.

In **Fig.5.44.a**, maximum value of footings rotation is displayed with respect to *x* and as it indicates, the left footing undertake large rotation in smaller *x* while the right footing is being faced with large rotation when rupture initiates from the points more to right of the box. For the left footing, the maximum rotation is occurred in $x = 0.92$ m while for right footing, it occurs in $x = 1.60$ m. However, for the rigid body rotation of the structure, the maximum value occurs for the rupture initiation location of between about $x = 1.00$ m to $x = 1.60$. The reason is that it is the range of the locations where the rupture outcrops under the structure and therefore causes rigid body rotation of the whole structure.

In **Fig.5.44.b**, maximum value of rotation of columns for each value of *x* represented. As it is illustrated, the rotation of firs story left column is increasing by increase of *x* until reaching its maximum value when the rupture starts from $x = 1.00$ m because of outcropping directly under the left footing and then decreases although it has larger value than the other columns until $x = 1.10$ m where it is the upper point of the range for rupture to hit the left foundation. After this point, the first story left column rotation decreases while the other columns maintain their maximum values because of rigid deformation of the second and third stories and approximately the same displacement of the first story right column as the second and third stories columns in these locations where the rupture outcrops under the structure.

Finally the columns and beams moment envelopes with their ultimate moment capacities (maximum and minimum) are demonstrated in **Fig.5.45** to **Fig.5.50**. As it is concluded from these diagrams, the columns reach their ultimate capacities while the beam elements never exceed their elastic limit. One reason for that is the wrong design of the structure to have weak columns rather than weak beams. The other reason may be the presence of the transverse beams which cause greater loads on beams and not allow them

to rotate significantly. Therefore the columns of this structure rotate considerably more than the beams during fault rupture.

Maximum value of rotation for both foundations of back frame through all these locations of rupture is represented in **Fig.5.51**. For the left foundations which are on hangingwall, the maximum rotation occurs for rupture initiation at $x = 0.92$ m while for the right foundations which are on footwall, maximum rotation occurs at $x = 1.60$ m. The maximum rigid body rotation and rigid body settlement happens in $x = 1.30$ m.

Maximum rotation of columns through all these locations of rupture is showed in **Fig.5.52**. Maximum rotation of left column of first story occurs at fault rupture location of $x = 1.00$ m while maximum rotation of right column of first story, columns of second and third stories and also rigid body rotation of the whole structure occurs at $x = 1.30$ m.

Minimum and maximum values of bending moment in column and beam elements for all of the locations of rupture which were analyzed are presented in **Fig.5.53** and **Fig5.54**. Among all the columns, just two elements did not reach their ultimate bending moment capacities and all others have reached their plastic limit while none of the beam elements exceed their elastic limits. Therefore, we observe plastic hinges in columns rather than beams which is not according capacity design principles.

5.5. Conclusion

The main conclusions of this parametric study are:

[1] The structural and foundation deformation increases by increasing the base vertical displacement.

[2] When the rupture location is somewhere that it will outcrop very near to the footings, the structure and foundation displacement increases much intensely with respect to *h* until the rupture outcrops at the surface and after that by increasing the base vertical displacement, the structure deformation has less increase because of diversion of the rupture path due to presence of the structure.

[3] When the rupture outcrops before the structure but so near (about 5 cm before the first footings), the structure and its foundations will have small deformation. Also the bending moment in different elements won't reach their capacities.

[4] When the fault rupture directly hits the left footing, the left footing undertakes much larger horizontal displacement and rotation than the right one while the stories and both columns have large drift ratios and rotations due to rigid displacement of the stories.

[5] When the rupture outcrops between two footings, it causes larger horizontal displacement of the footing which is on the hangingwall than the one on the footwall but both without significant rotation because it doesn't directly hit any of the footings. However it causes large value of structural drift and rotation due to the different displacement of the footings which causes the structure to collapse.

[6] When the rupture hits the right footing directly, both footings go under large horizontal displacement because of both being positioned somehow on hangingwall but the right one has much larger rotation than the left one because of being hit directly by the rupture. However the structure has much less deformation than the previous cases because the both footings are somehow on same places related to the rupture. Therefore we observe less drift ratio or rigid body rotations for the structure.

[7] When the rupture passes the structure entirely, we can again observe large horizontal displacement for both footings approximately equal to base vertical displacement but small value of rotation. Also the structure deformations and rigid body rotation and settlement also decreases substantially compared to the previous cases.

[8] When the rupture outcrops under the structure or even after that and causes large displacement of the structure, the structure columns reach their bending moment capacities while the beams never reach their ultimate capacities. This has occurs because of being designed to have weak columns rather that weak beams and also because of presence of larger loads on beams which prevents them from rotating.

Figures of **Chapter 5**

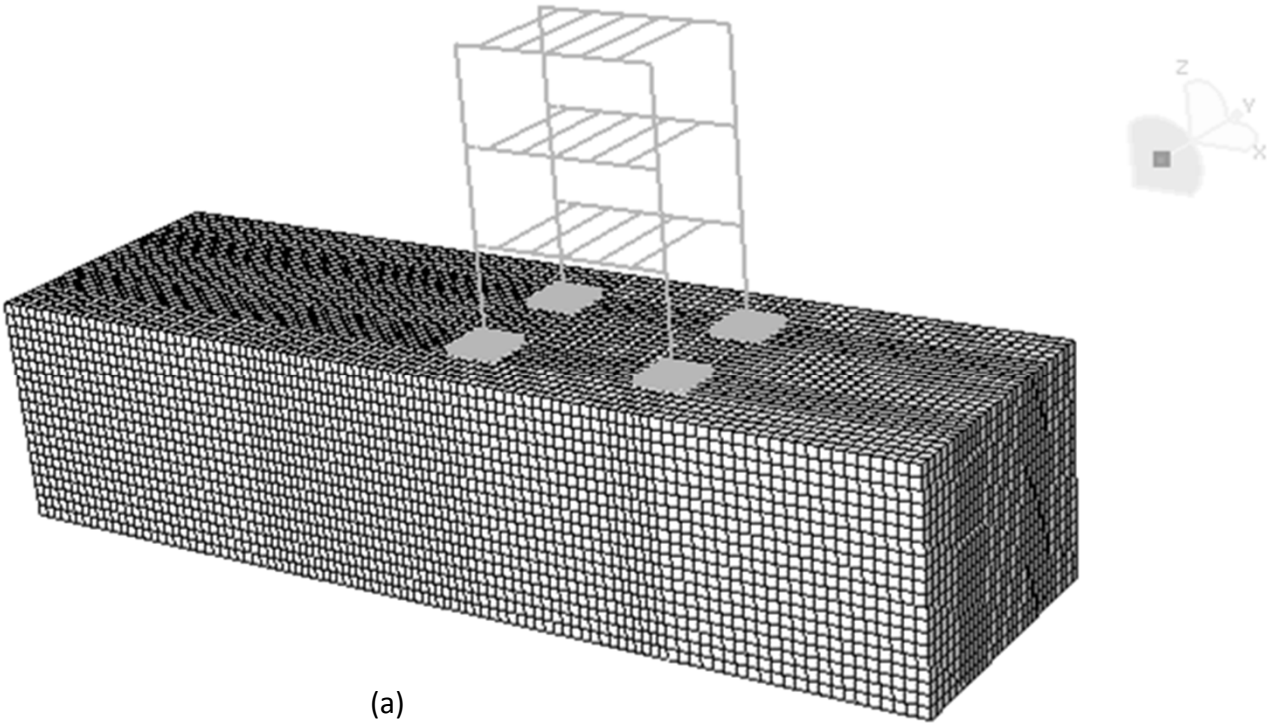

(a)

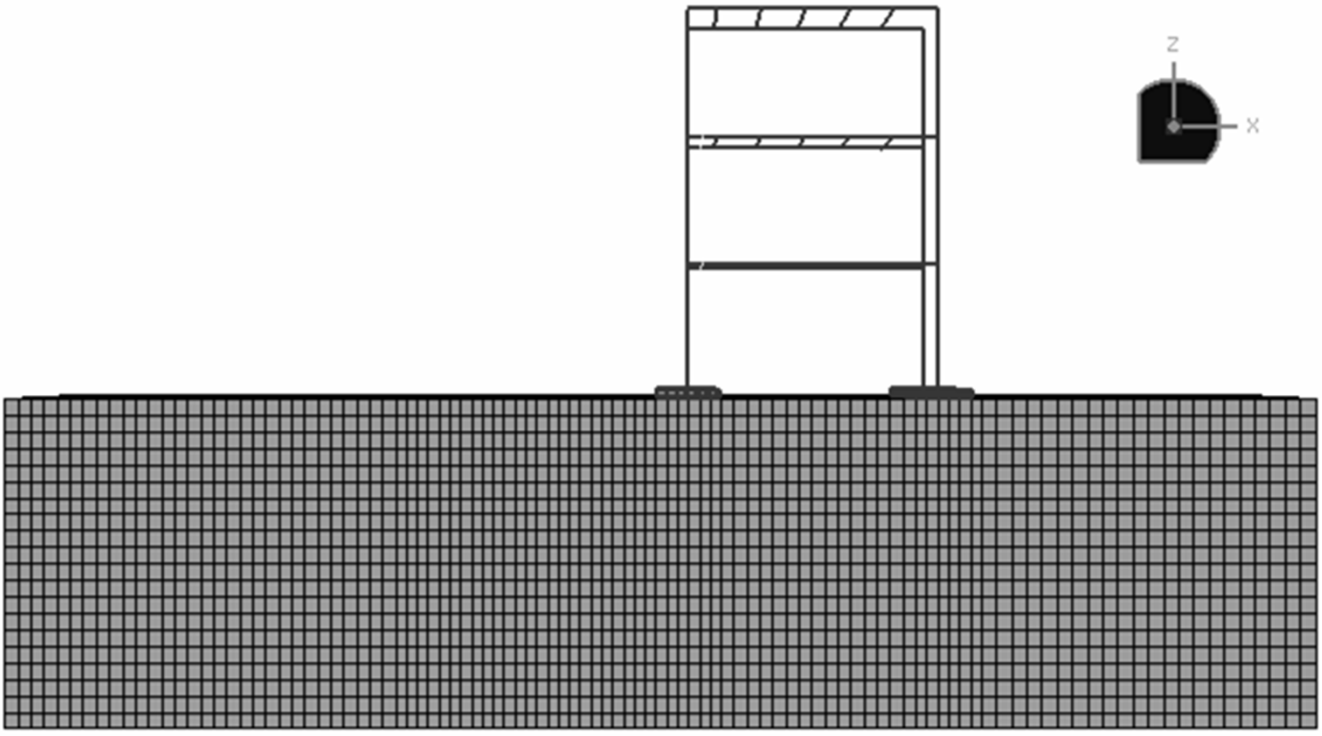

(b)

Figure 5.1 The model in ABAQUS for rupture location of x=0.75 m : (a) 3D, and (b) 2D view

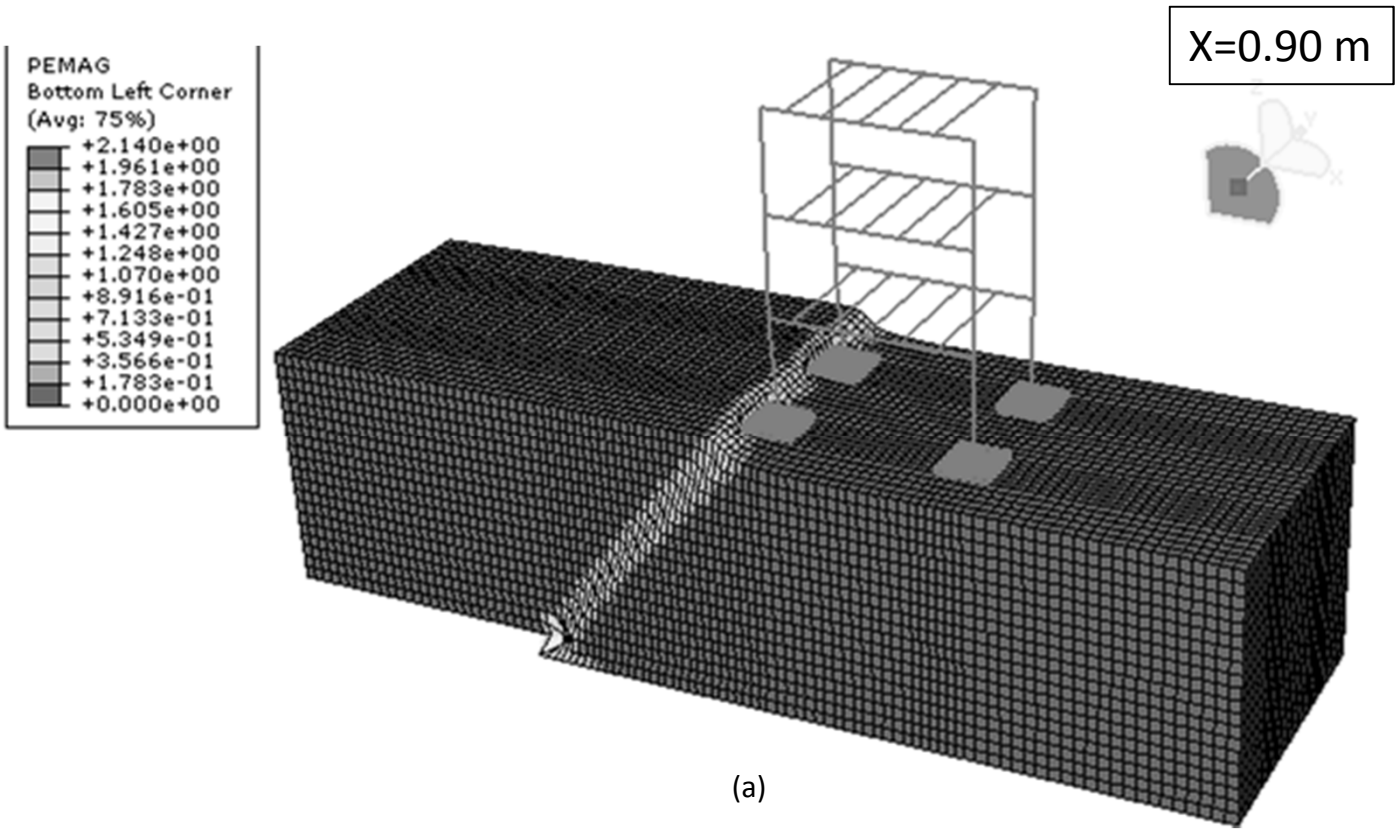

(a)

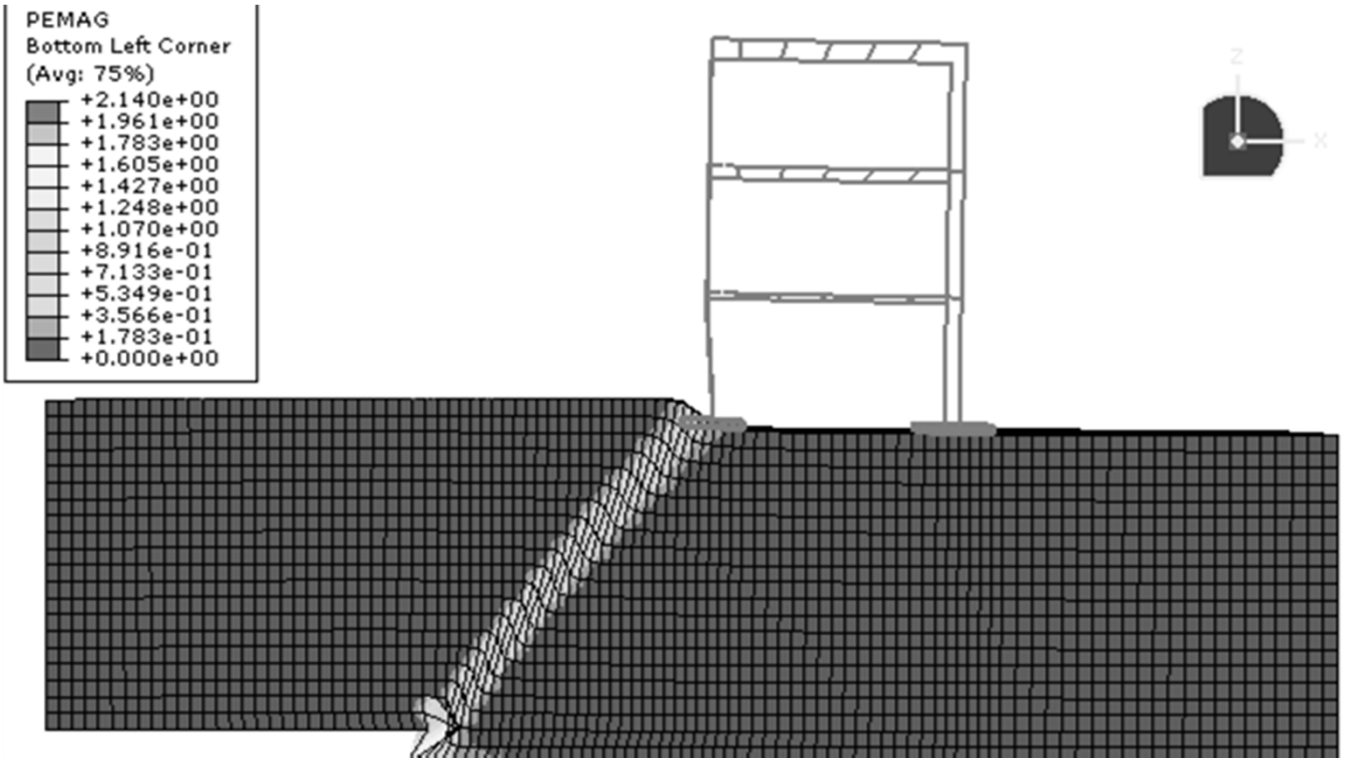

(b)

Figure 5.2 The model in ABAQUS for rupture location of x=0.90 m : (a) 3D, and (b) 2D view

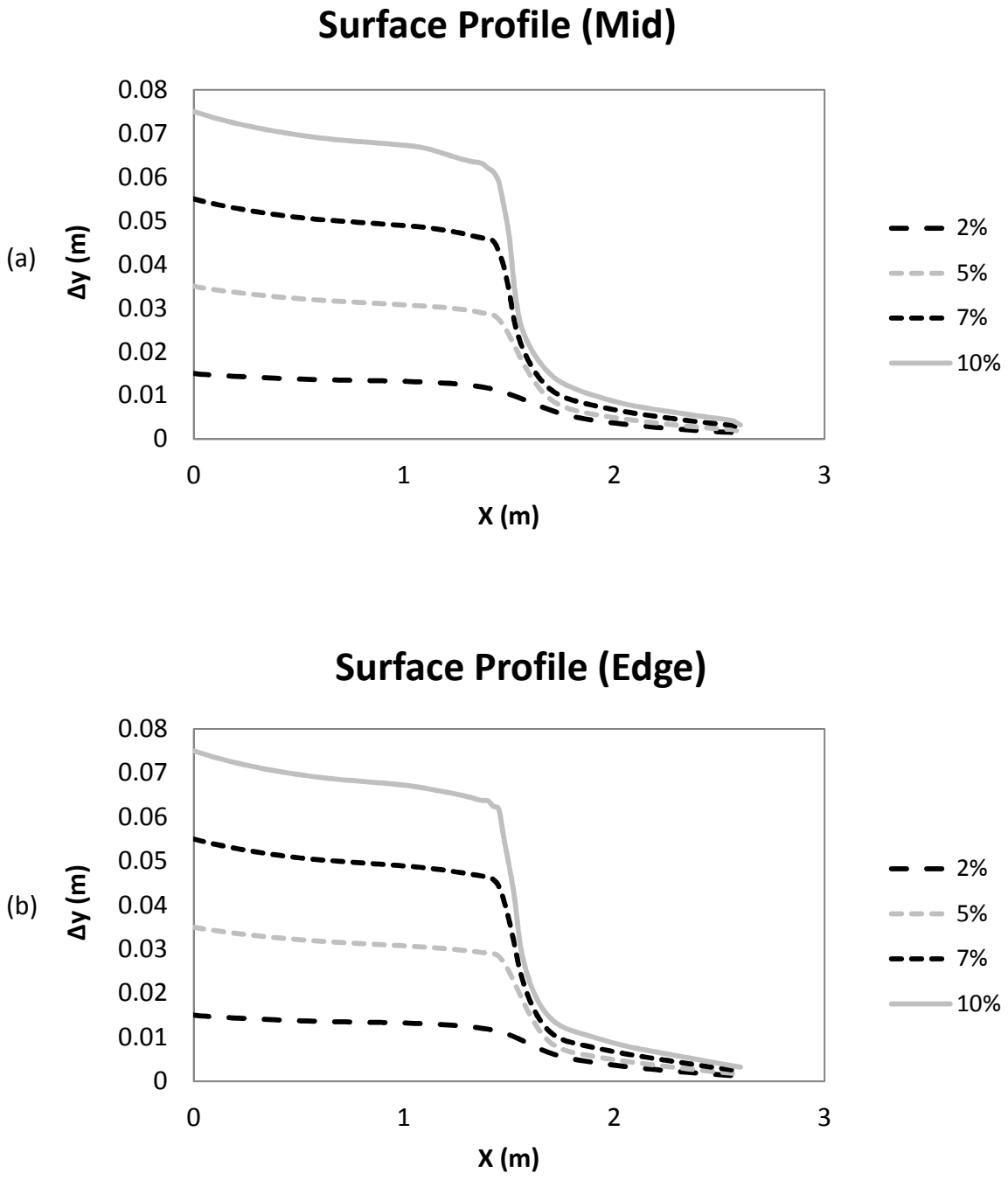

Figure 5.3 Vertical displacement at the surface for normalized bedrock displacement ranging from h/H=2% to 10% at (a) middle, and (b) edge of the soil surface

(a)

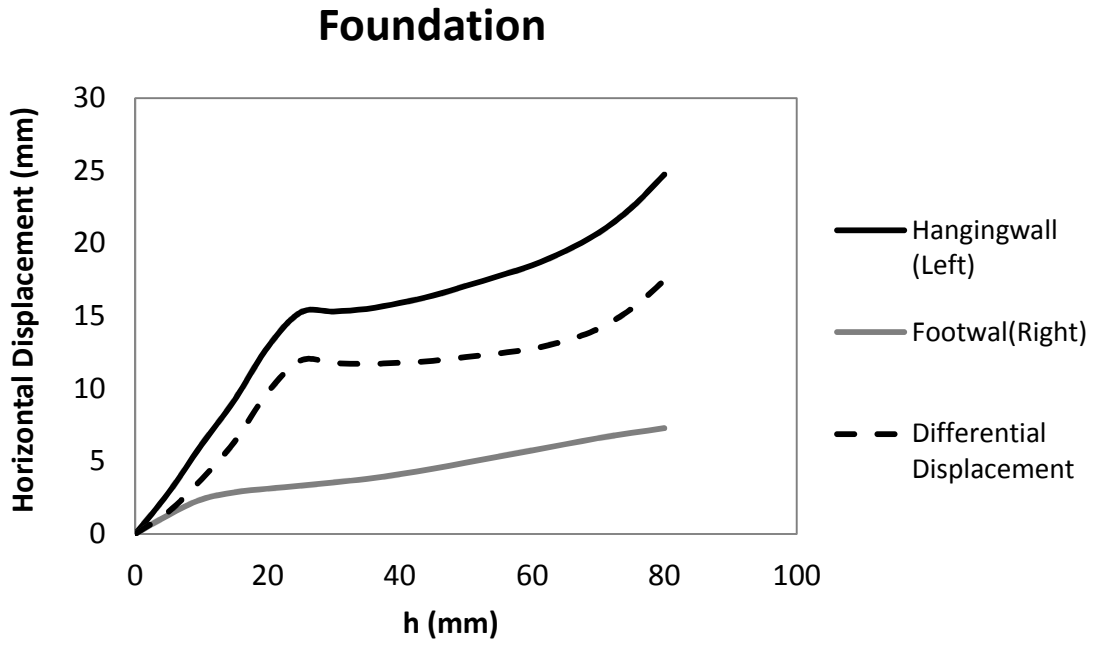

(b)

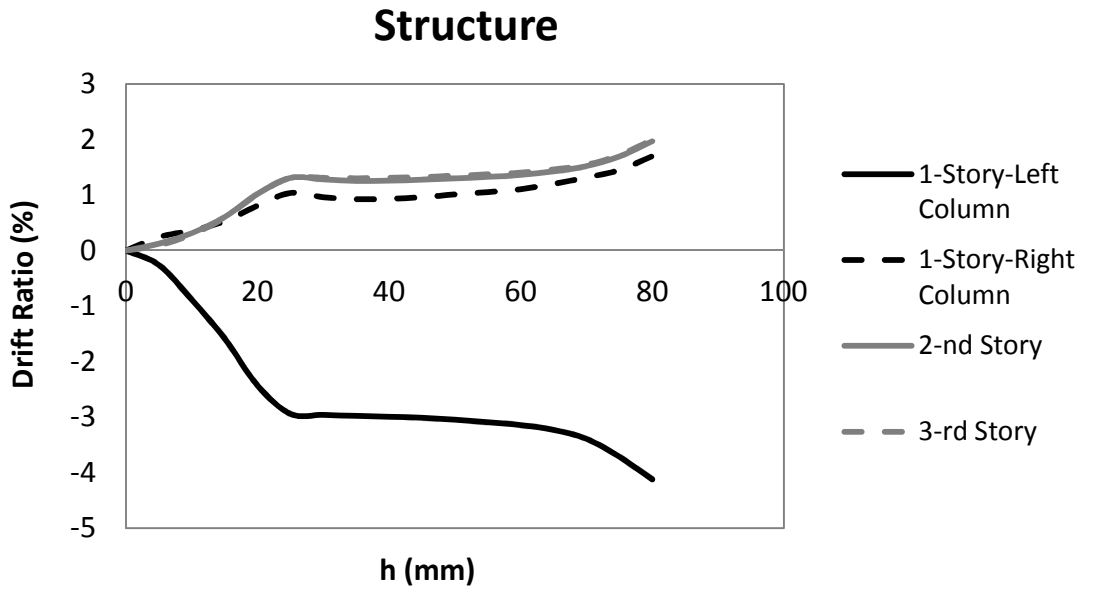

Figure 5.4 (a) foundation horizontal displacement, and (b) structural drift ratio

(a)

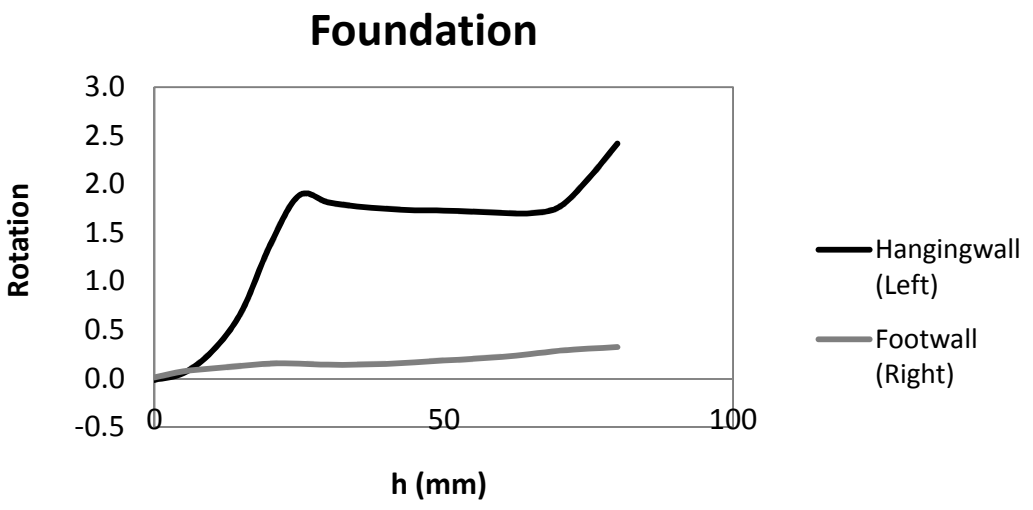

(b)

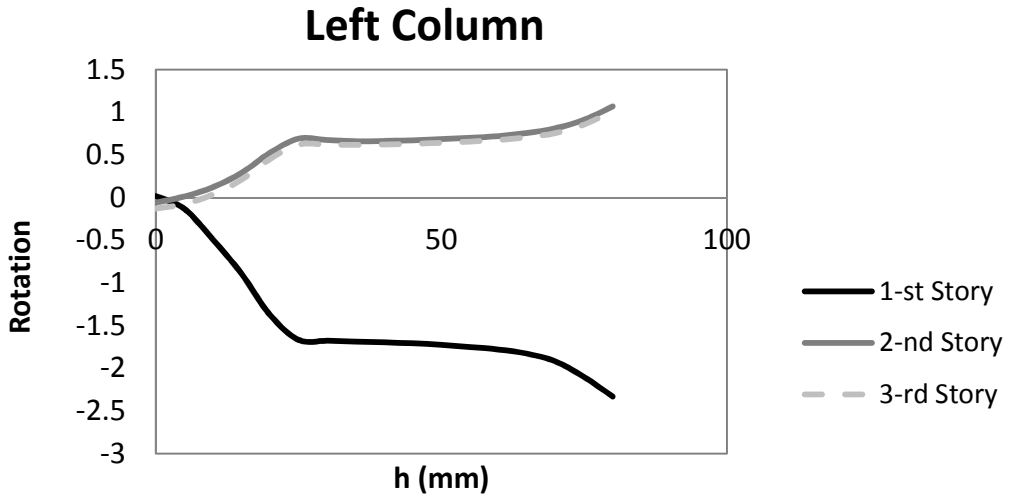

(c)

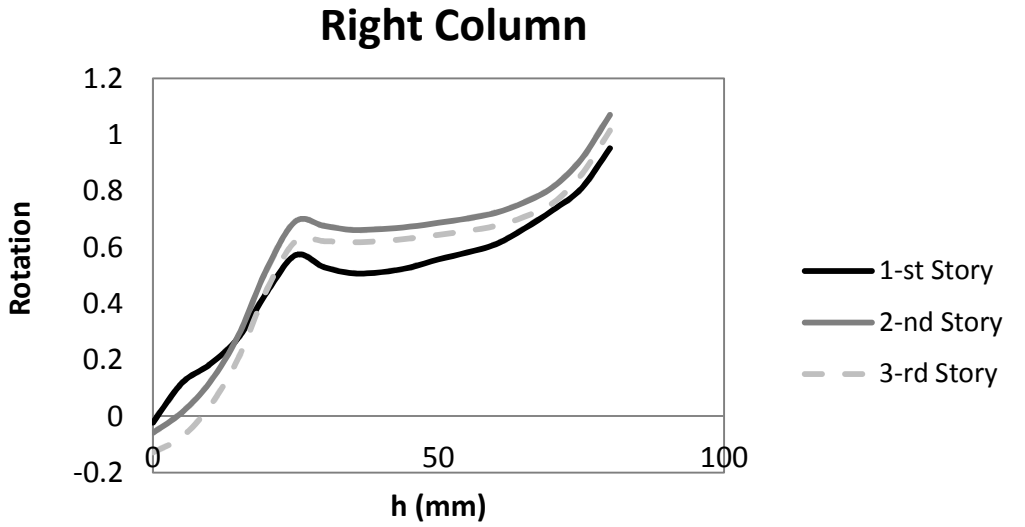

Figure 5.5 Diagrams of rotation of (a) foundation, (b) left, and (c) right columns with respect to the amplitude of rupture (h)

(a)

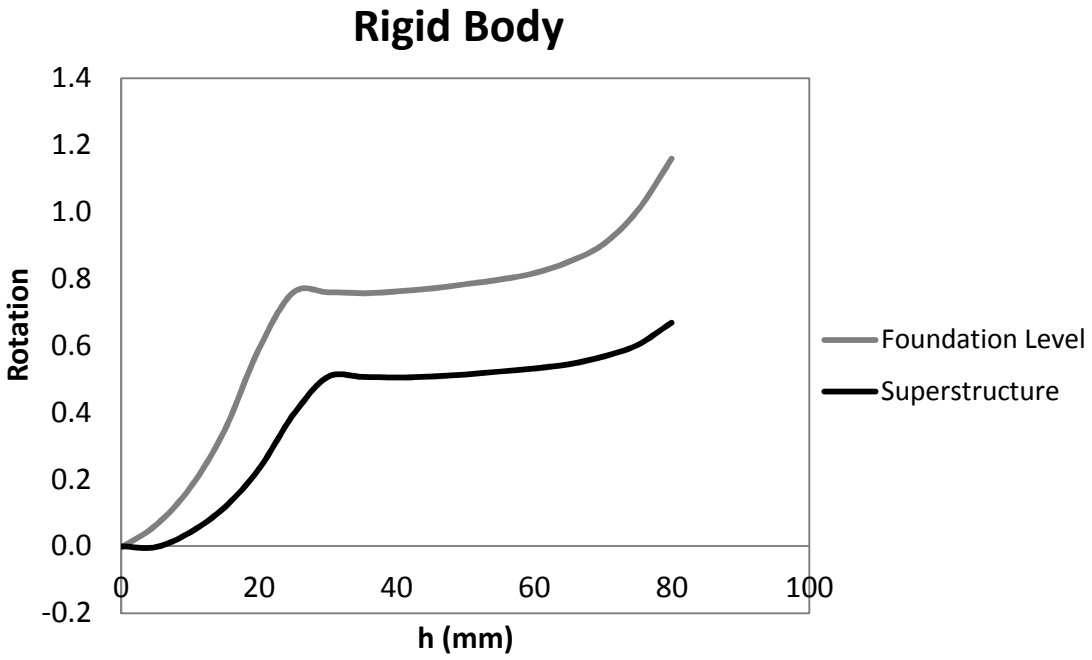

(b)

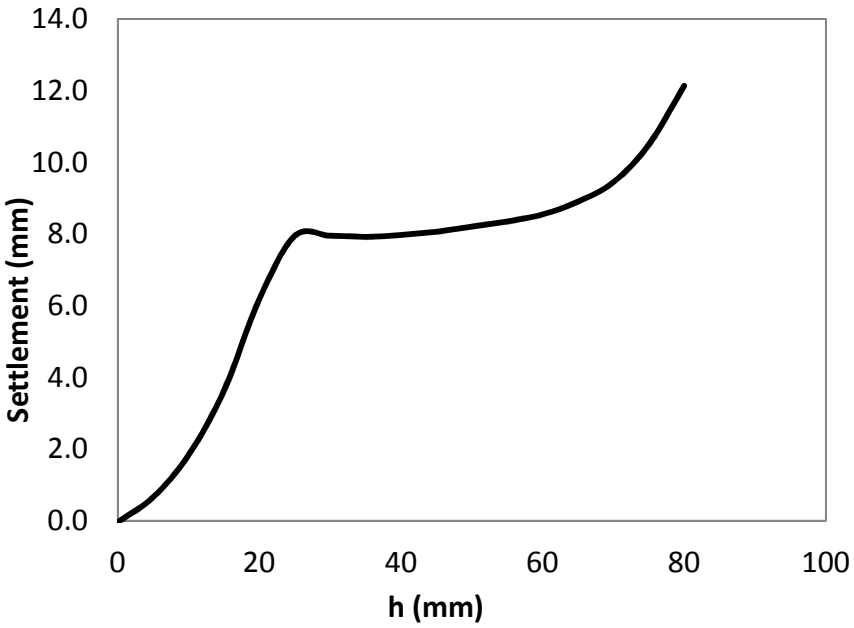

Figure 5.6 Diagrams of rigid body (a) rotation, and (b) settlement with respect to the amplitude of rupture (h)

(a)

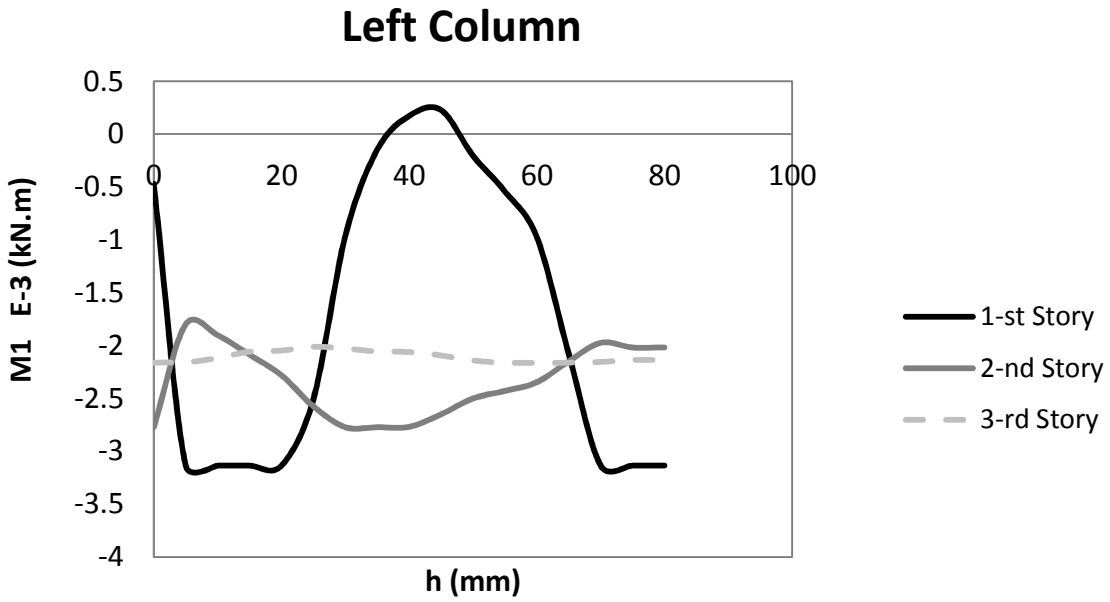

(b)

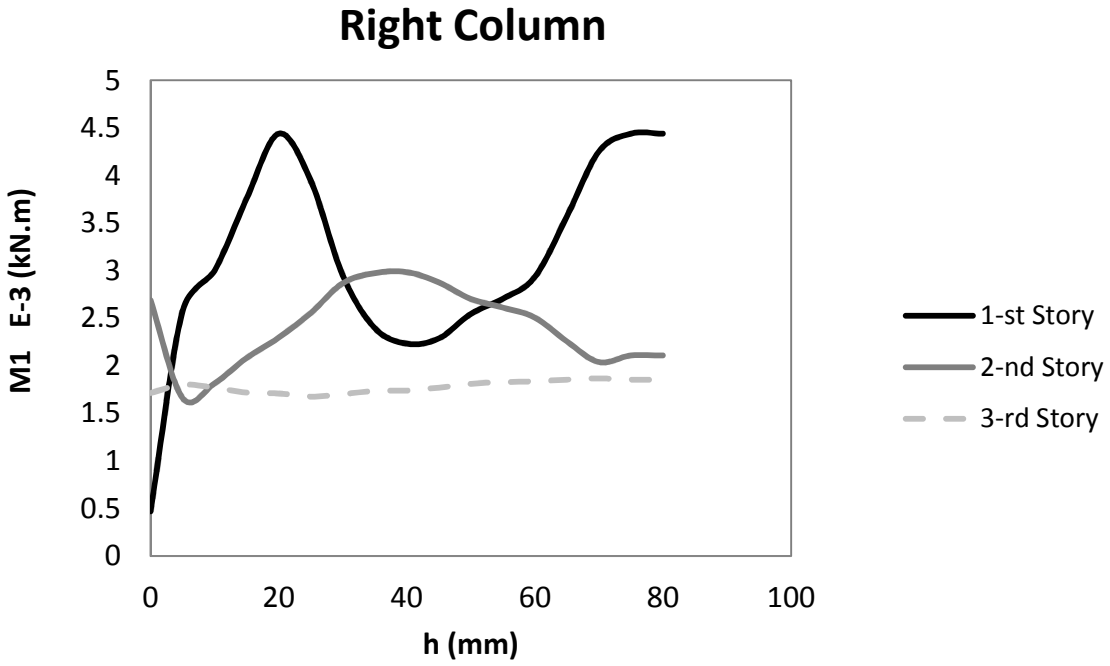

Figure 5.7 Diagrams of (a) left, and (b) right column moment (M1) with respect to the amplitude of rupture (h)

(a)

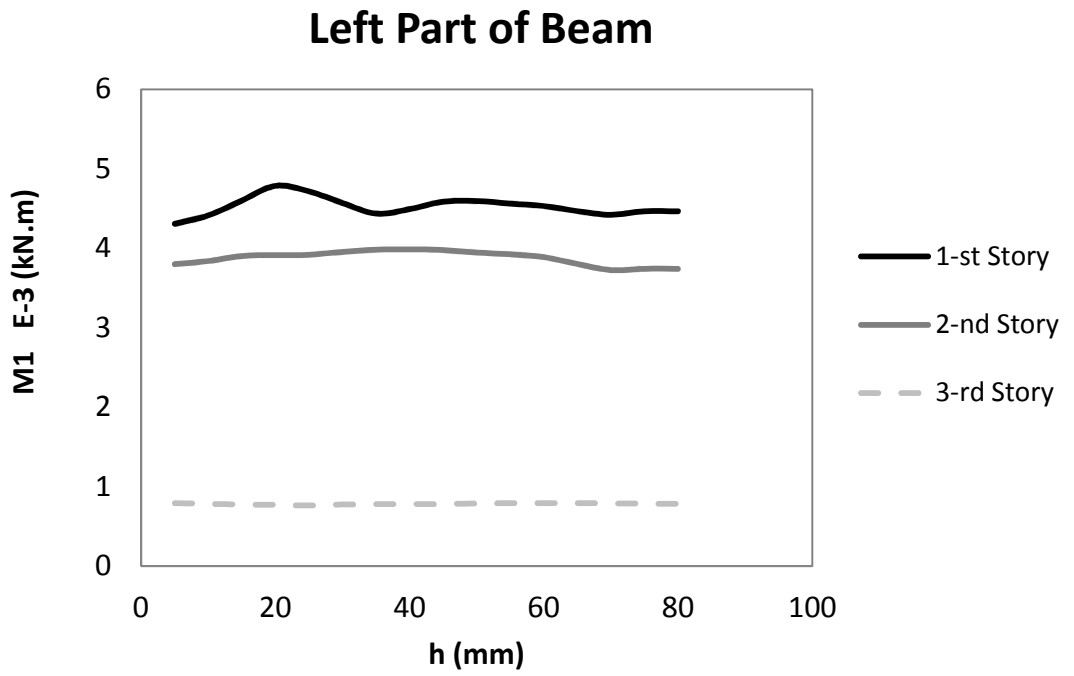

(b)

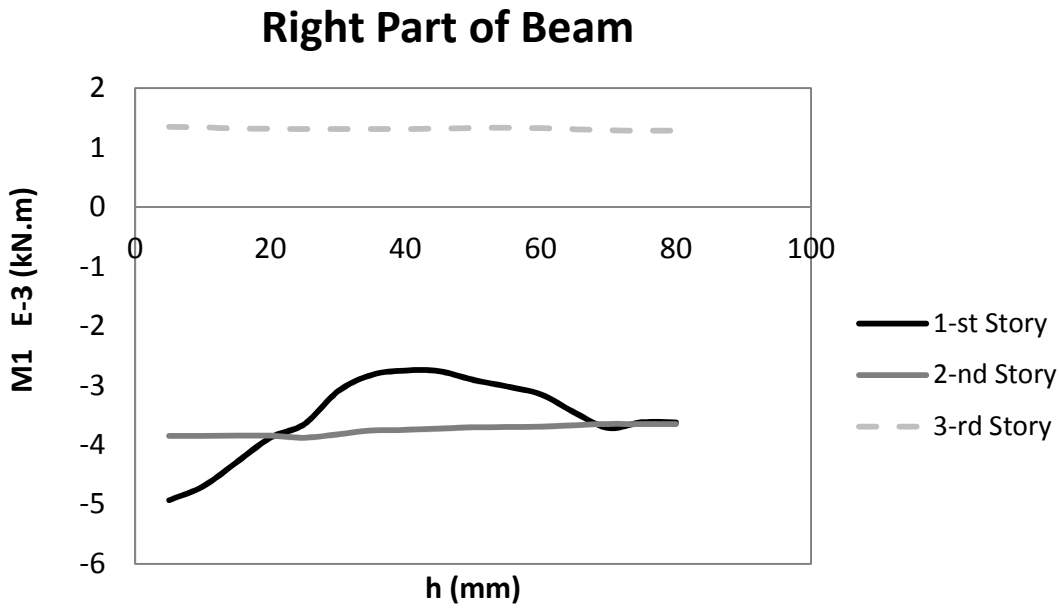

Figure 5.8 Diagrams of moment (M1) of (a) left, and (b) right part of beams with respect to the amplitude of rupture (h)

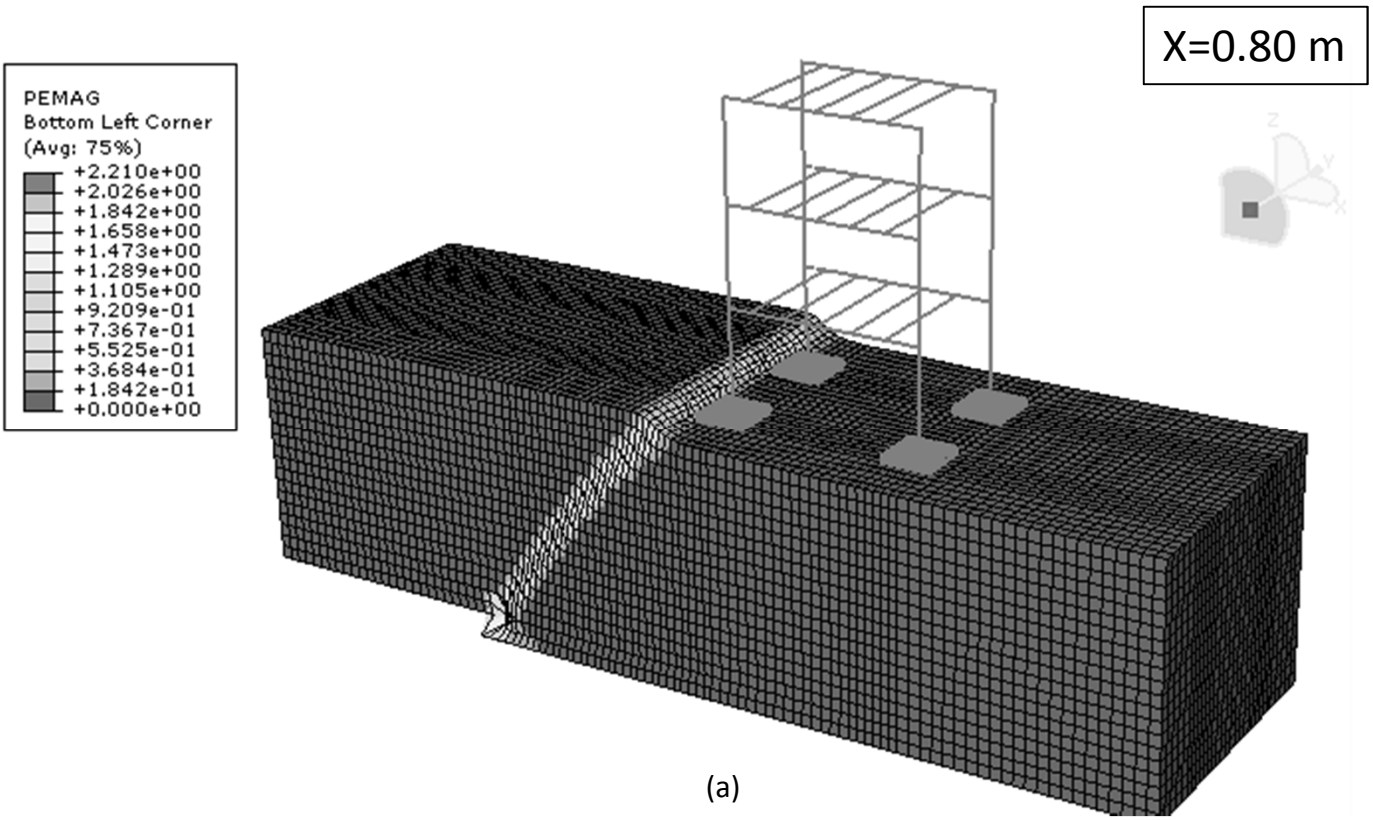

(a)

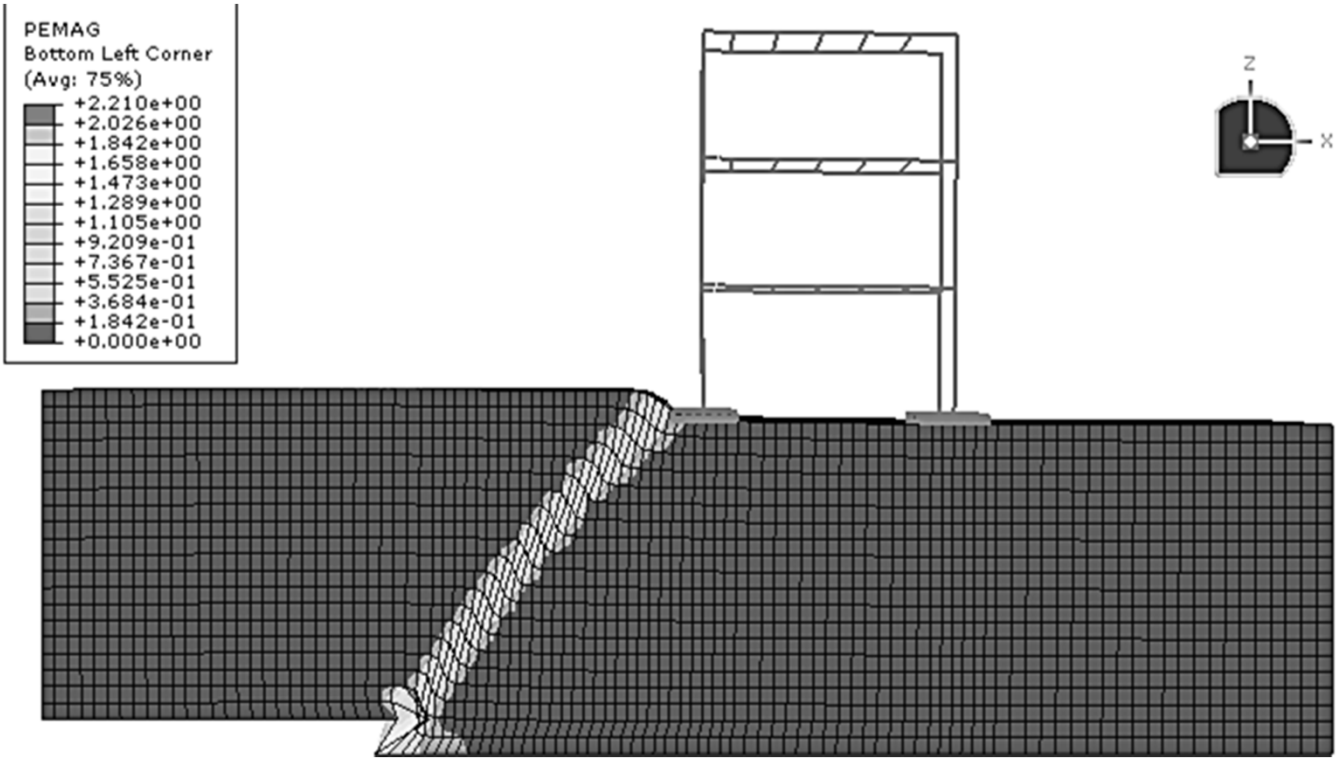

(b)

Figure 5.9 The model in ABAQUS for rupture location of x=0.80 m : (a) 3D, and (b) 2D view

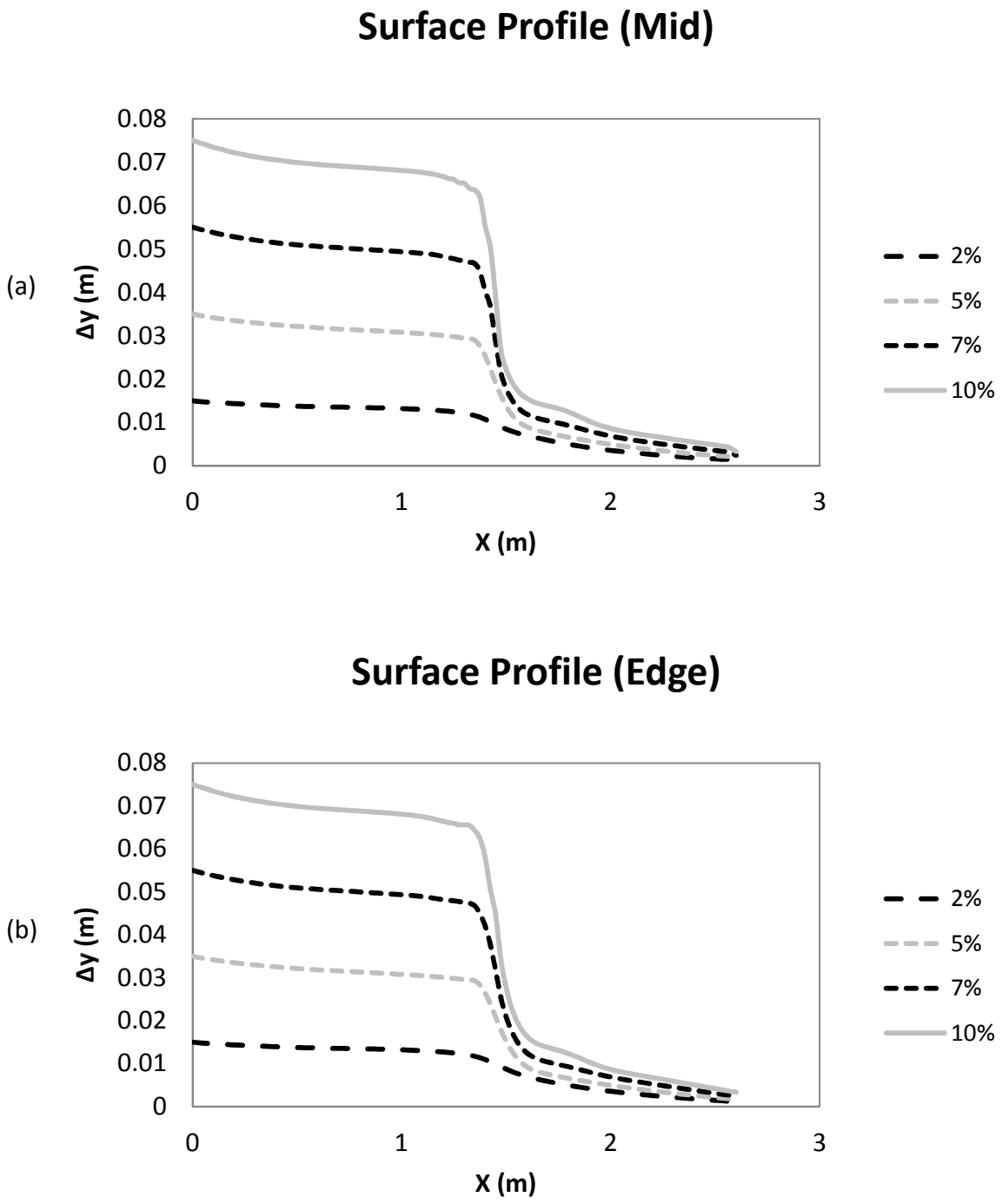

Figure 5.10 Vertical displacement at the surface for normalized bedrock displacement ranging from h/H=2% to 10% for the fault rupture location of x=0.80 m in (a) middle, and (b) edge of the soil surface

(a)

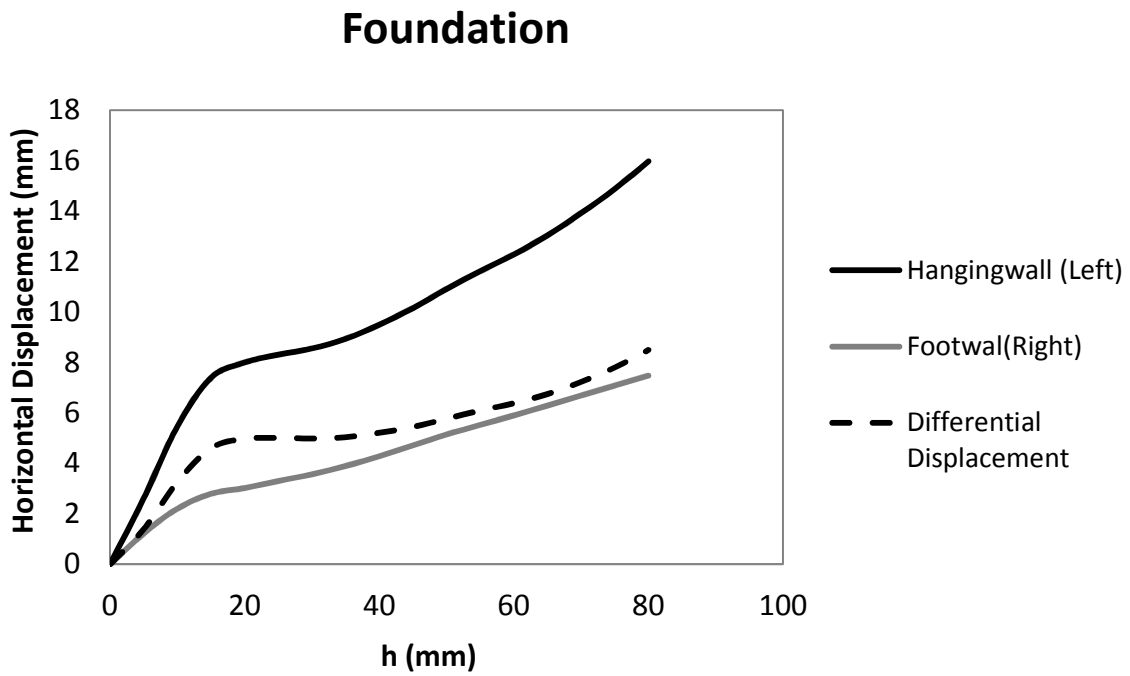

(b)

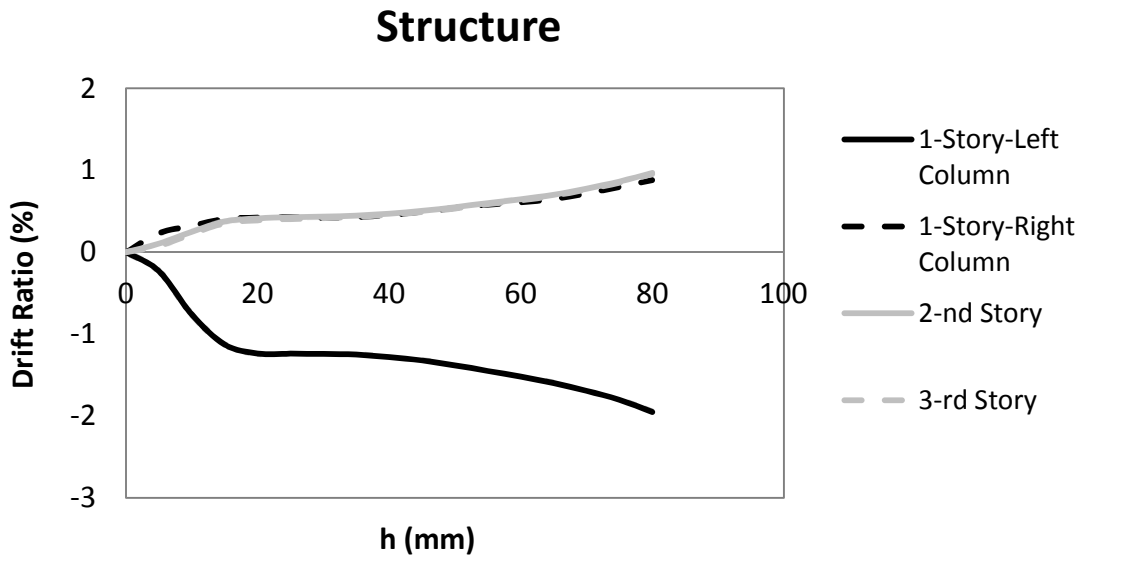

Figure 5.11 (a) foundation horizontal displacement, and (b) structural drift ratio for fault rupture location of x=0.80 m

(a)

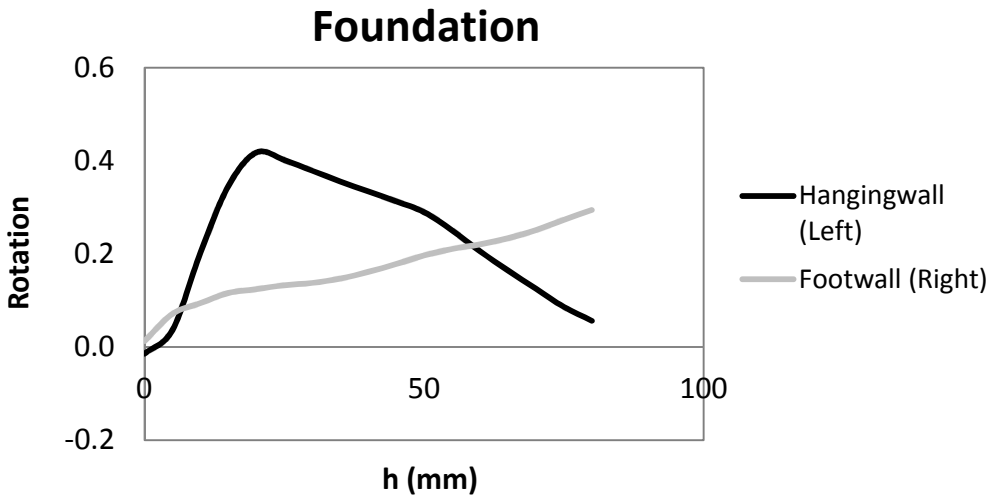

(b)

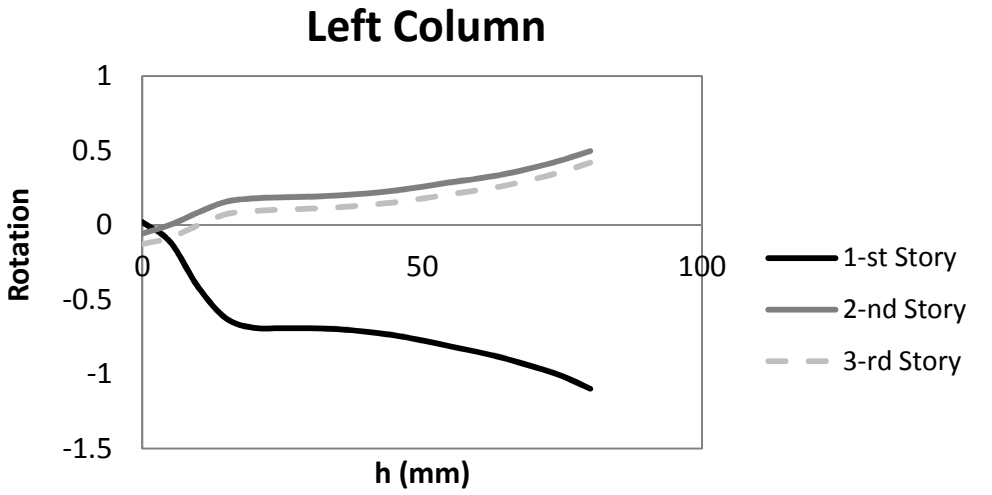

(c)

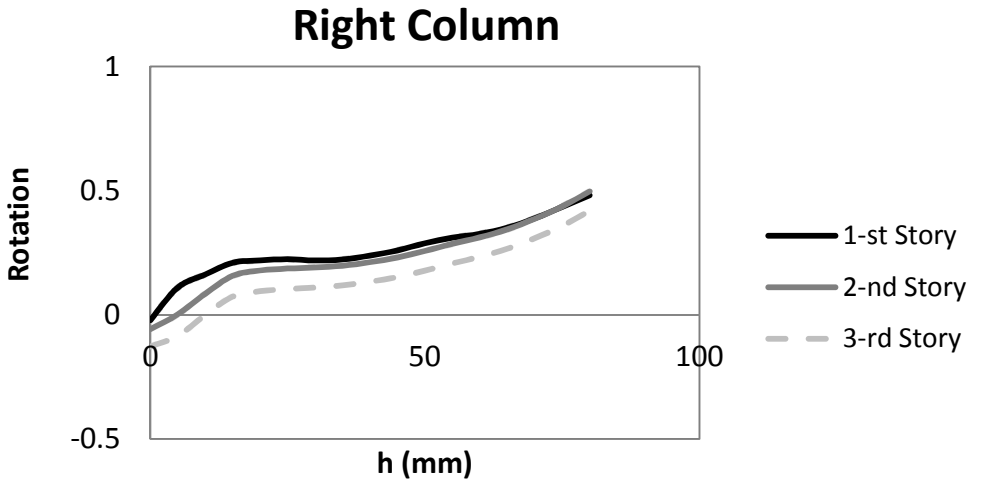

Figure 5.12 Diagrams of rotation of (a) foundation, (b) left, and (c) right columns with respect to the amplitude of rupture (h) for fault rupture with location of x=0.80 m

(a)

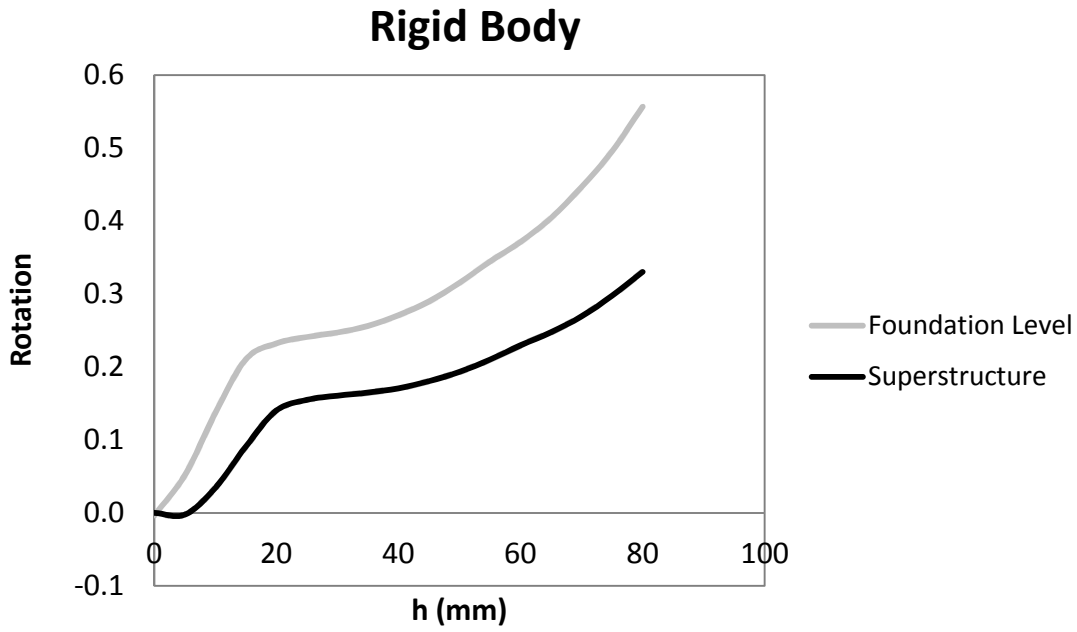

(b)

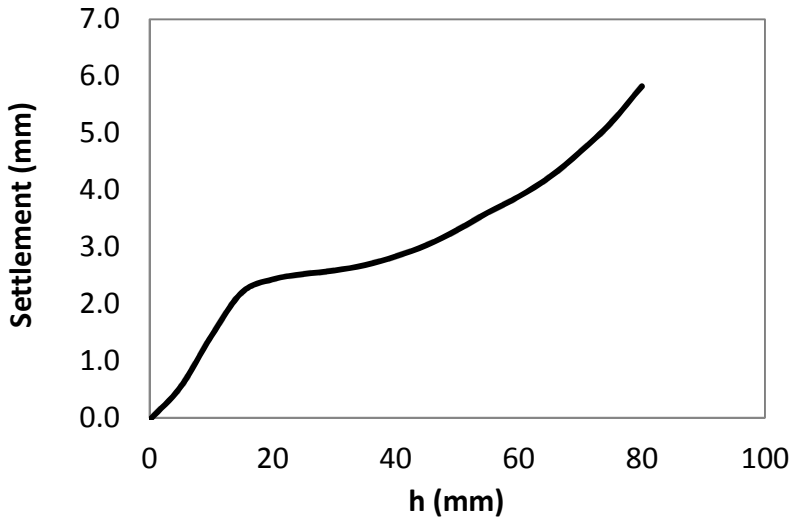

Figure 5.13 Diagrams of (a) left, and (b) right column moment (M1) with respect to the amplitude of rupture (h) for fault rupture with location of x=0.80 m

(a)

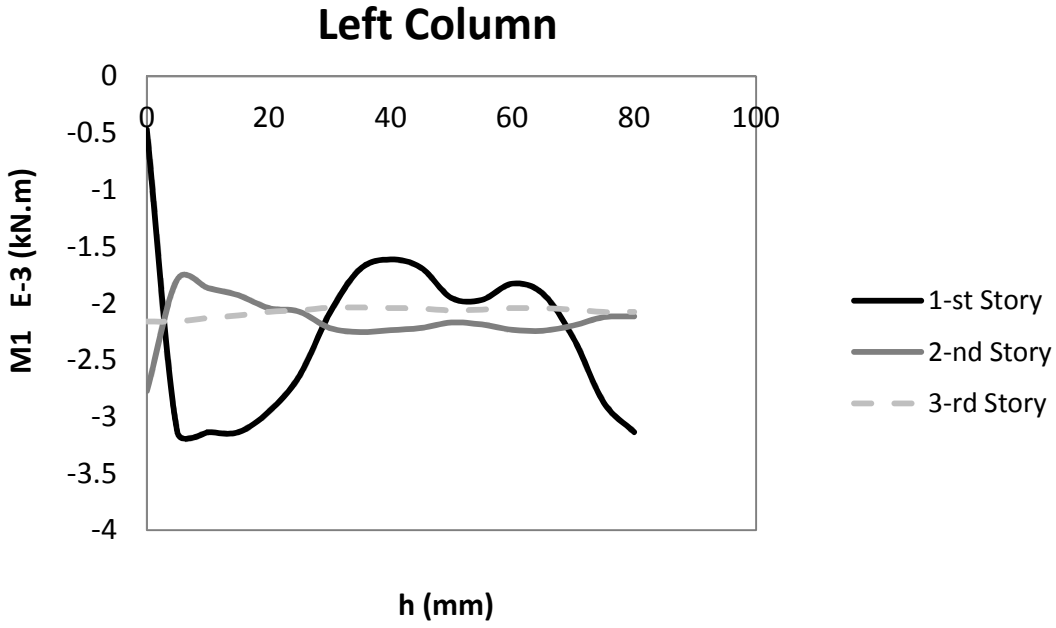

(b)

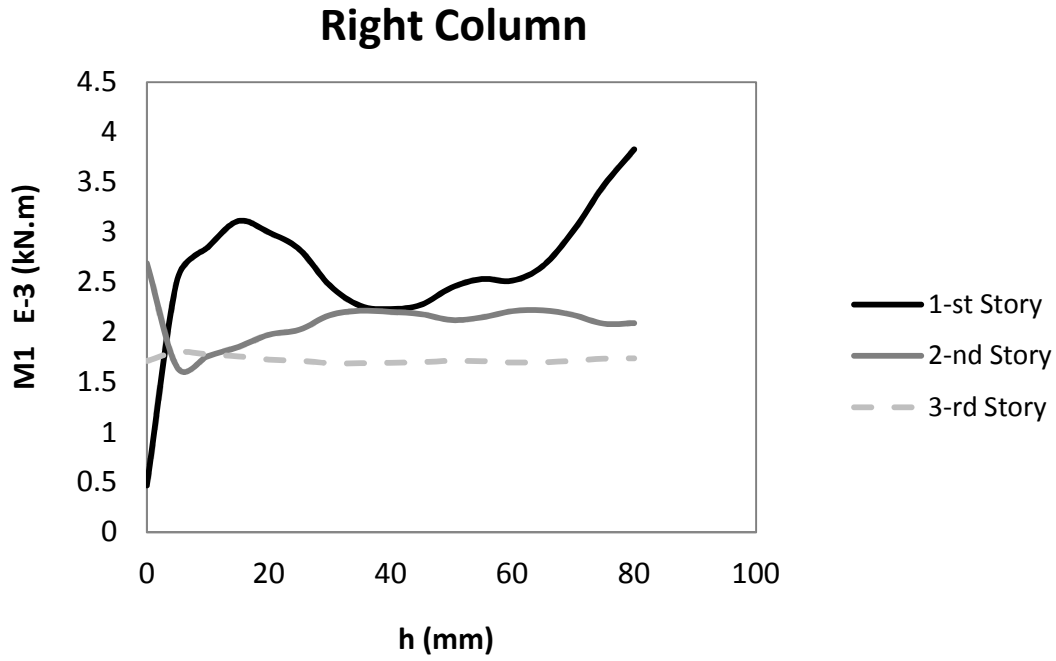

Figure 5.14 Diagrams of (a) left, and (b) right column moment (M1) with respect to the amplitude of rupture (h) for fault rupture with location of x=0.80 m

(a)

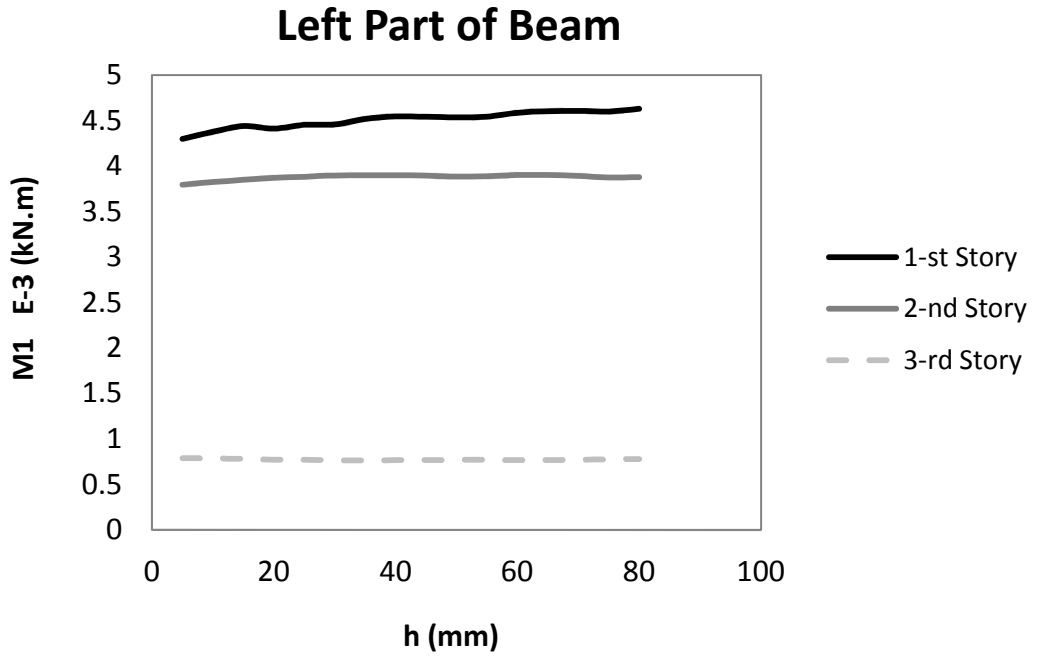

(b)

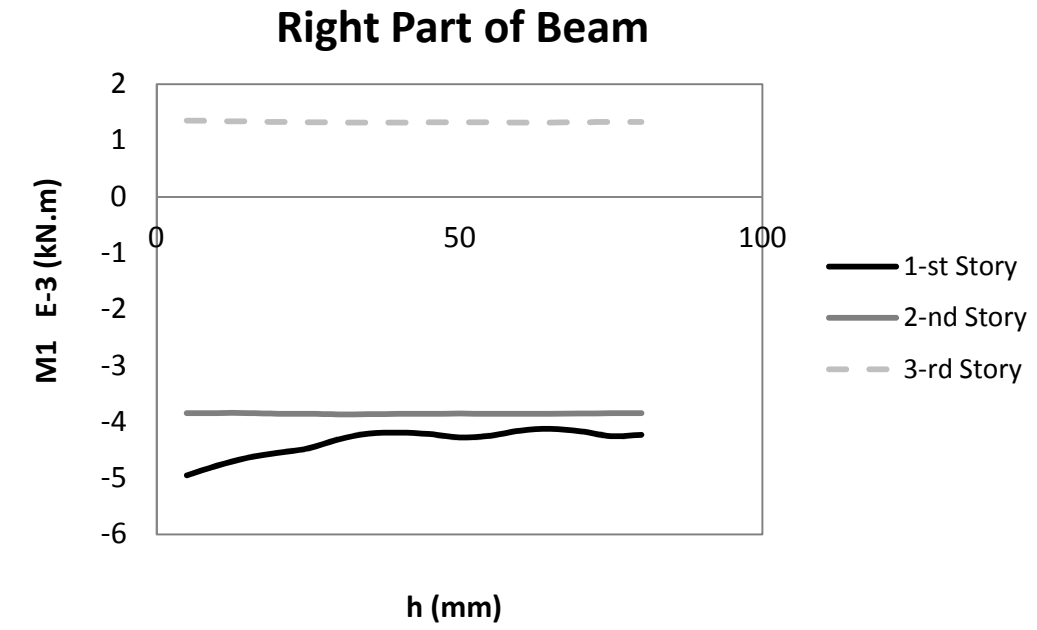

Figure 5.15 Diagrams of moment (M1) of (a) left, and (b) right part of beams with respect to the amplitude of rupture (h) for fault rupture with location of x=0.80 m

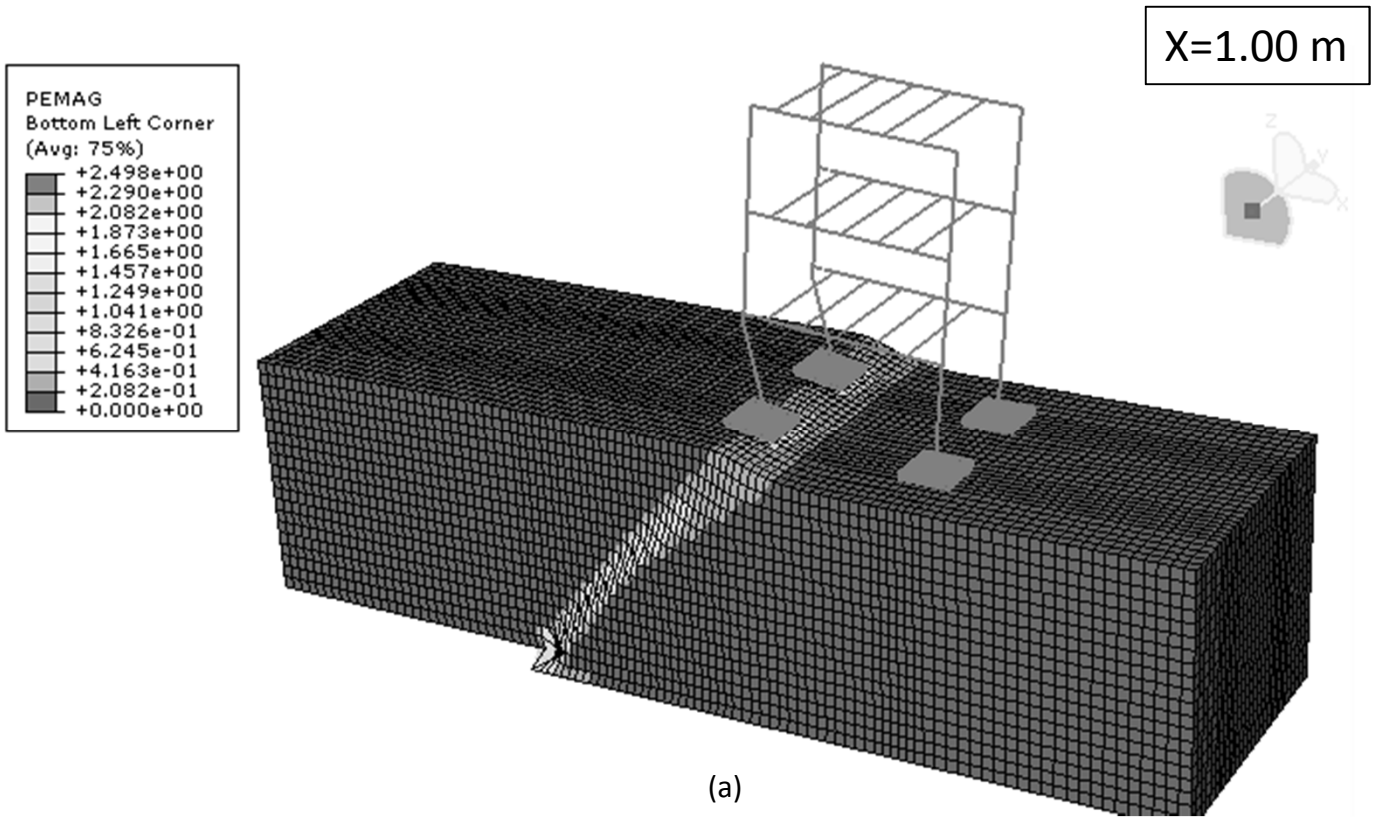

(a)

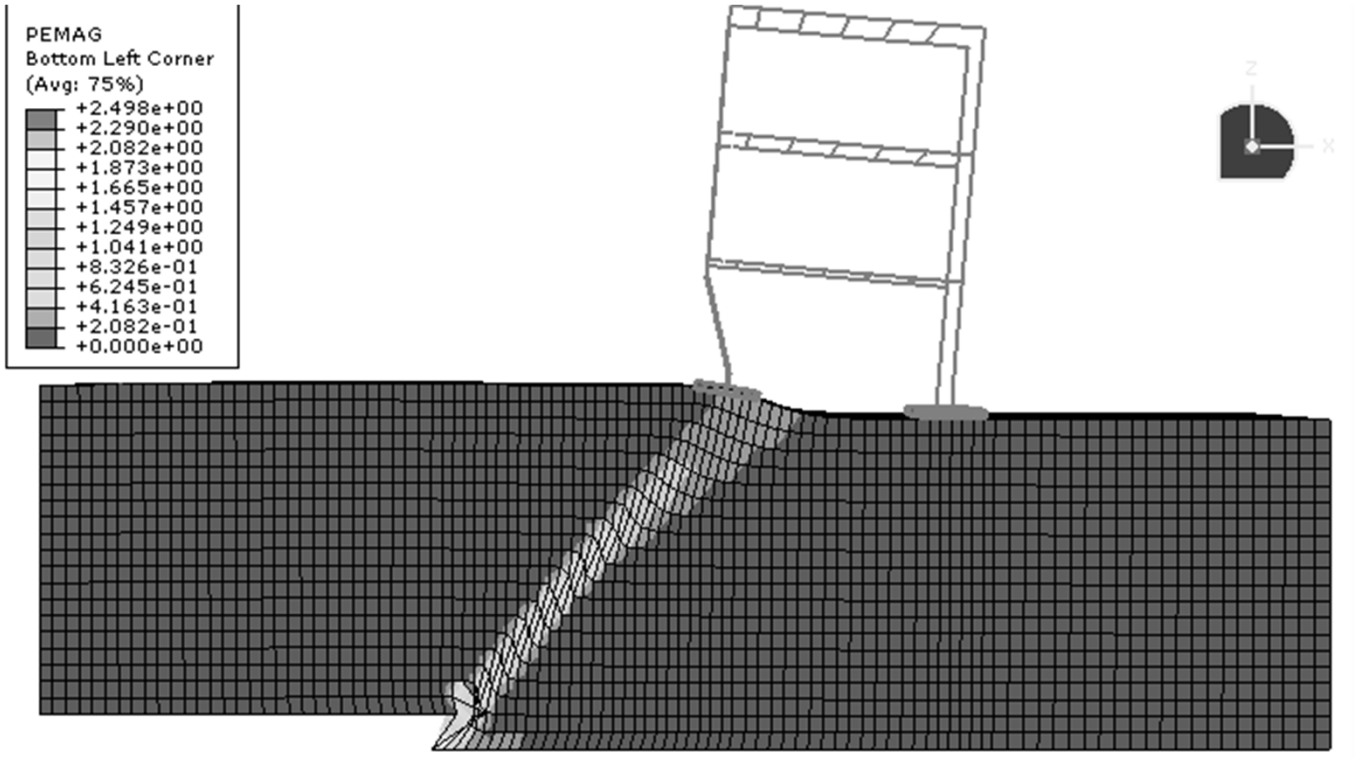

(b)

Figure 5.16 The model in ABAQUS for rupture location of x=1.00 m : (a) 3D, and (b) 2D view

(a)

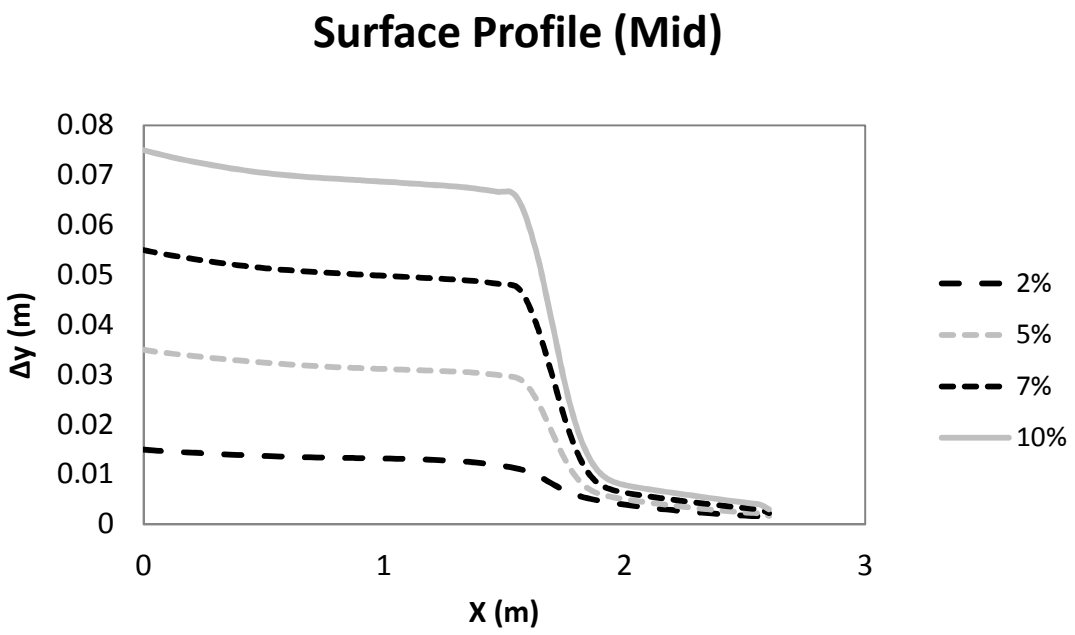

(b)

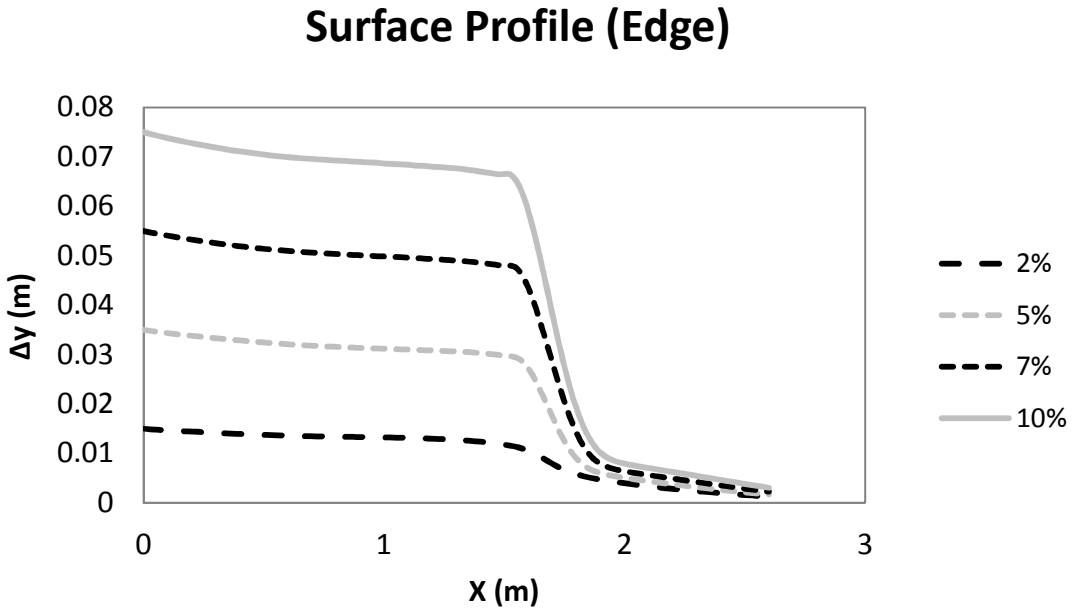

Figure 5.17 Vertical displacement at the surface for normalized bedrock displacement ranging from h/H=2% to 10% for the fault rupture location of x=1.00 m in (a) middle, and (b) edge of the soil surface

(a)

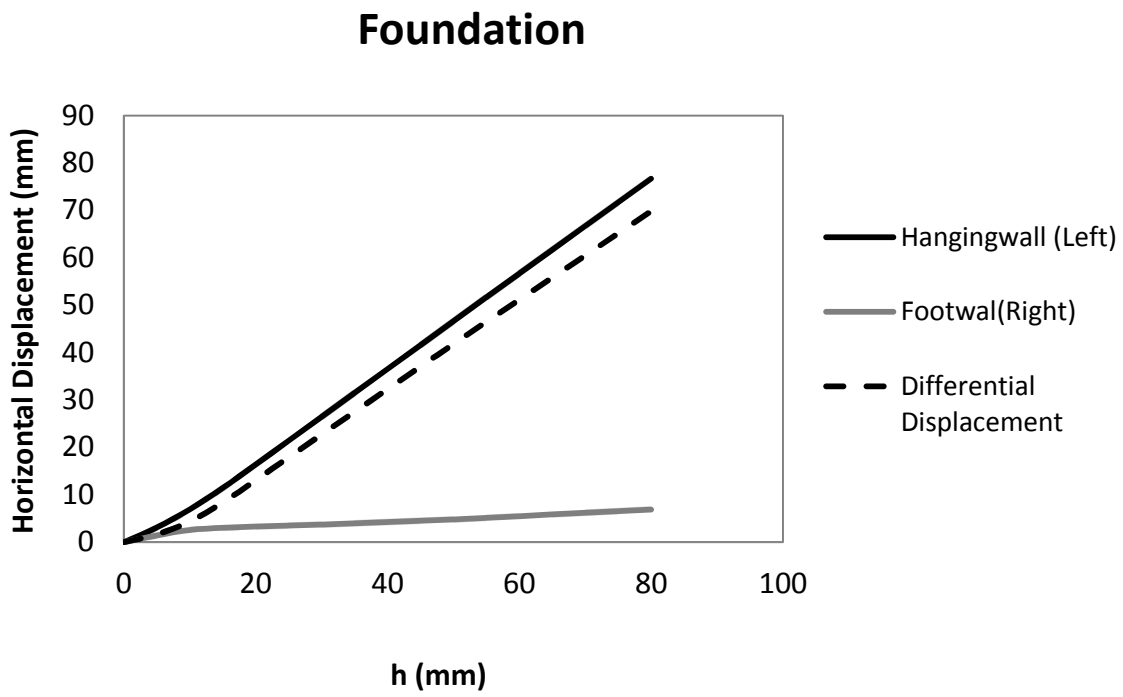

(b)

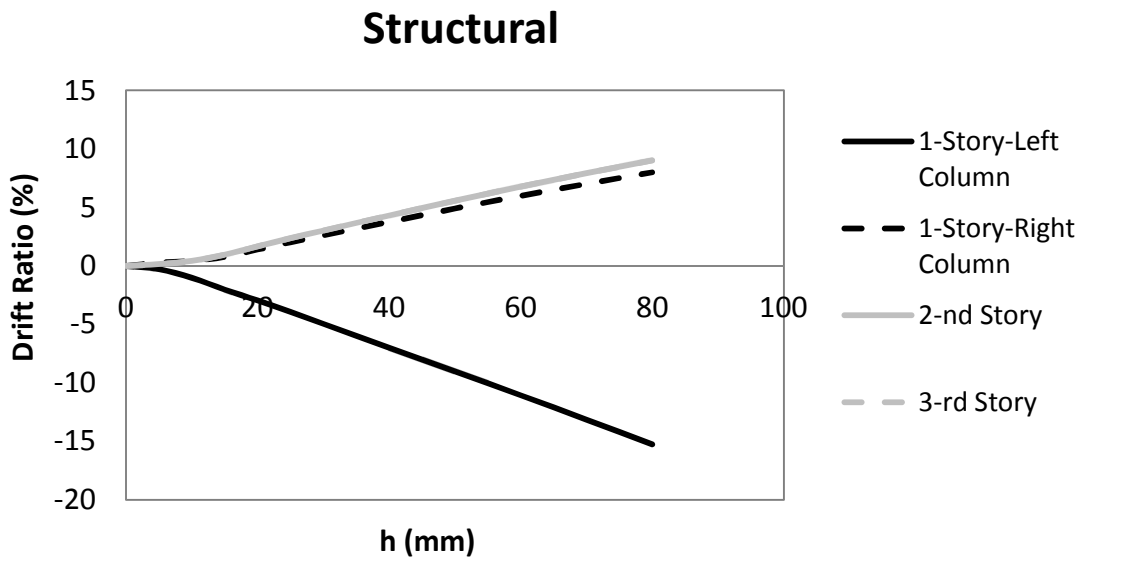

Figure 5.18 (a) foundation horizontal displacement, and (b) structural drift ratio for fault rupture location of x=1.00 m

(a)

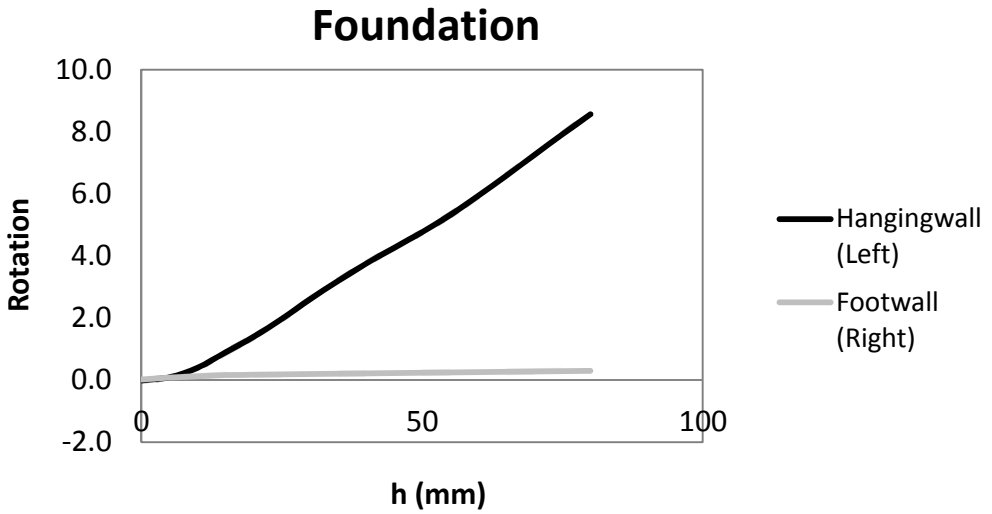

(b)

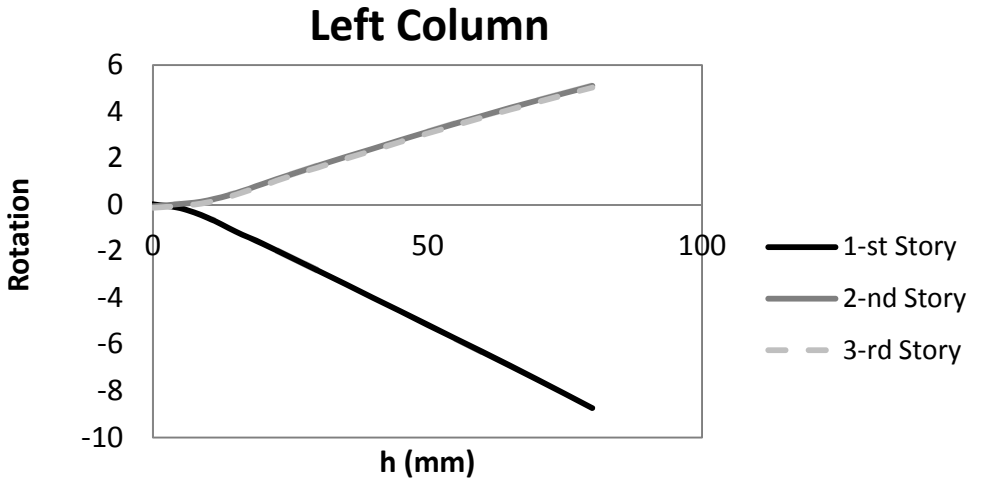

(c)

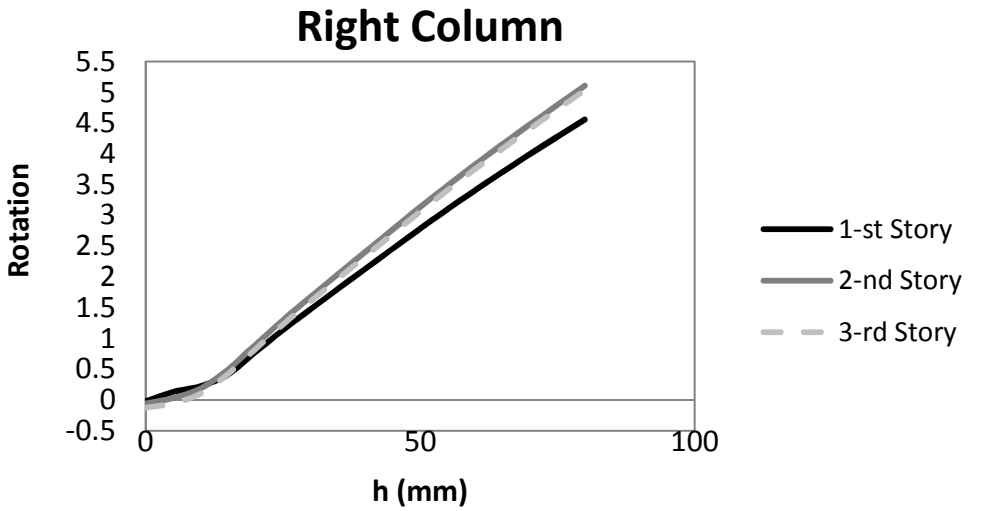

Figure 5.19 Diagrams of rotation of (a) foundation, (b) left, and (c) right columns with respect to the amplitude of rupture (h) for fault rupture with location of x=1.00 m

(a)

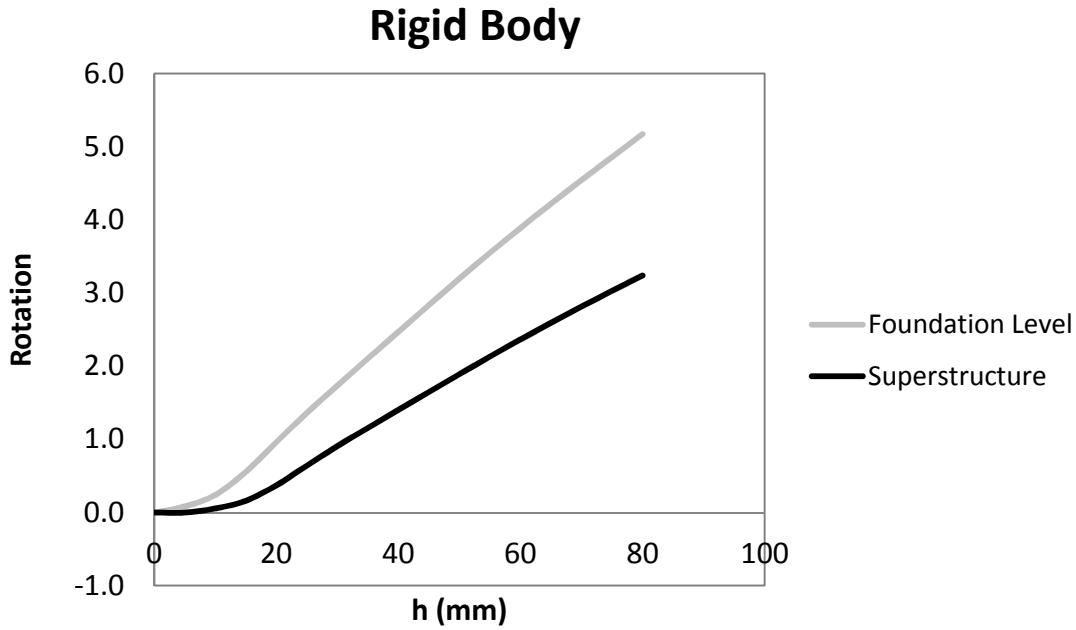

(b)

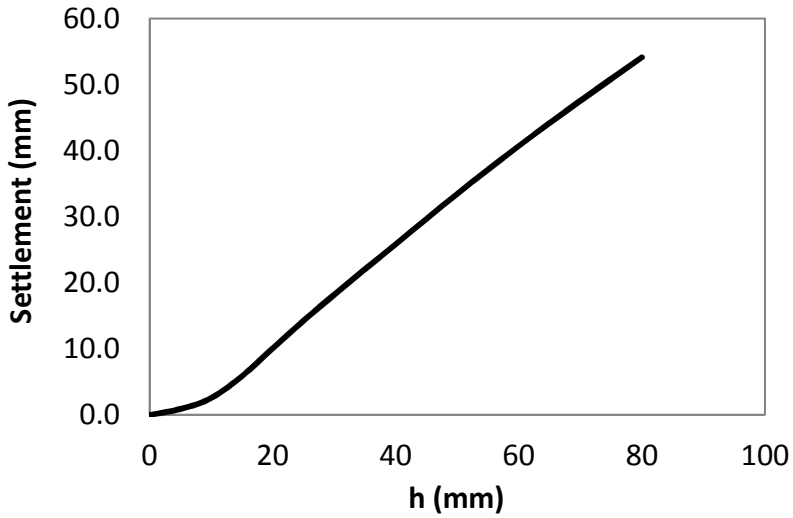

Figure 5.20 Diagrams of (a) left, and (b) right column moment (M1) with respect to the amplitude of rupture (h) for fault rupture with location of x=1.00 m

(a)

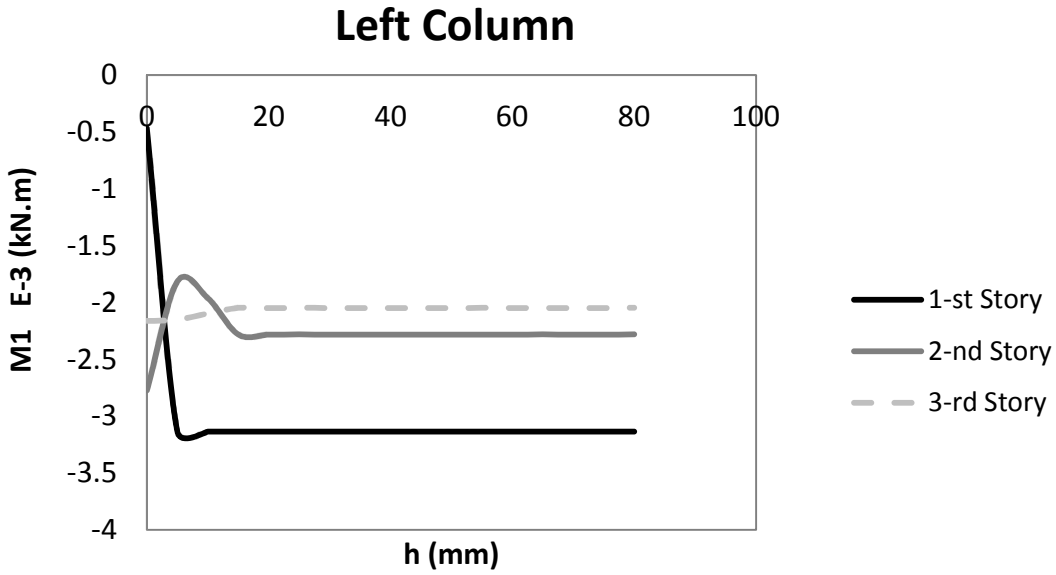

(b)

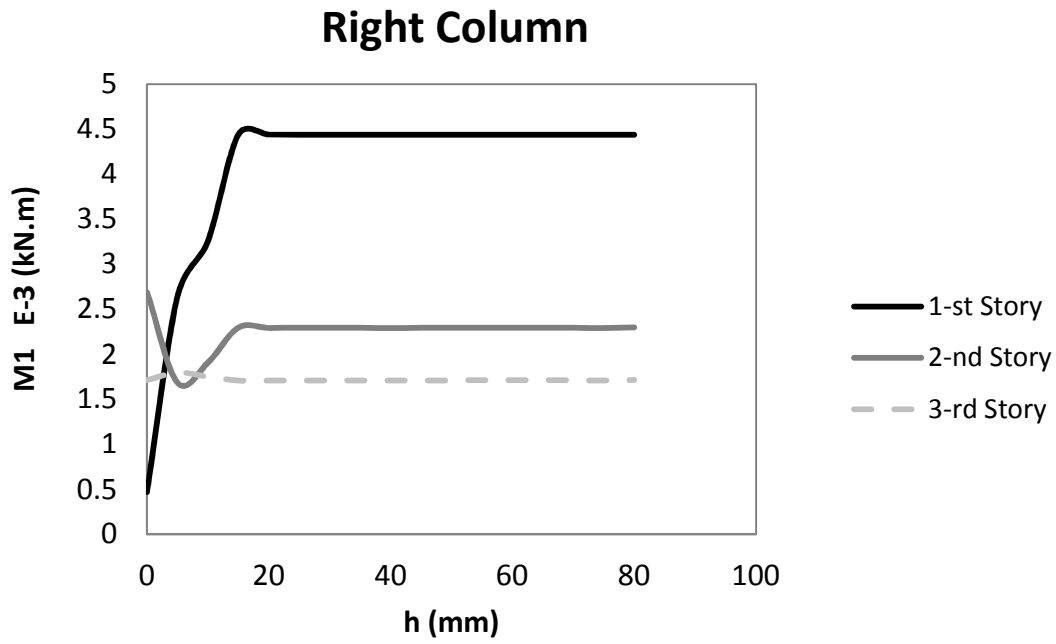

Figure 5.21 Diagrams of moment (M1) of (a) left, and (b) right part of beams with respect to the amplitude of rupture (h) for fault rupture with location of x=1.00 m

(a)

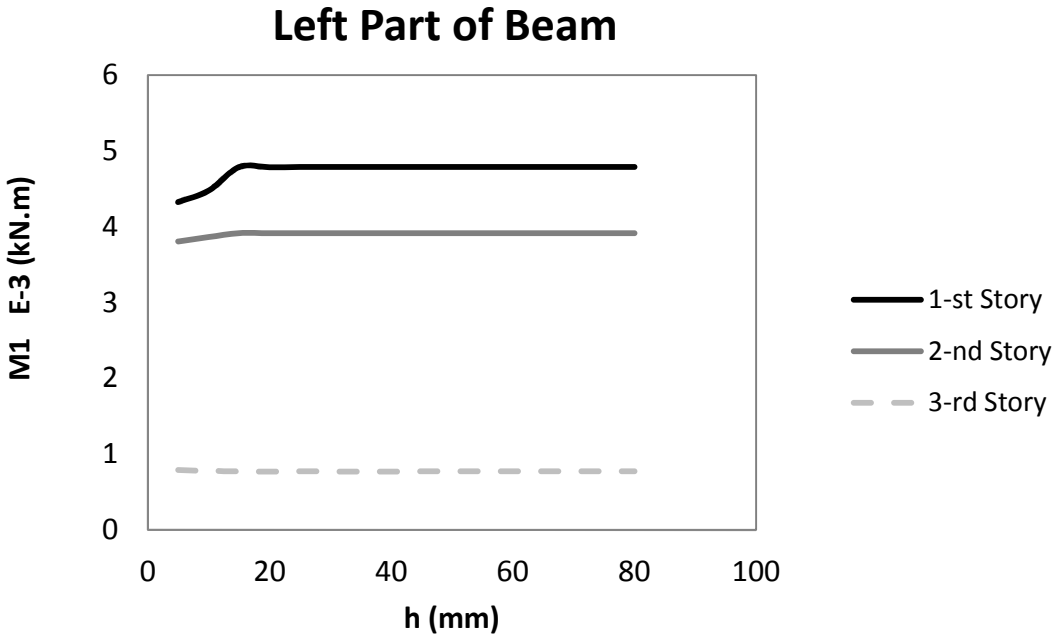

(b)

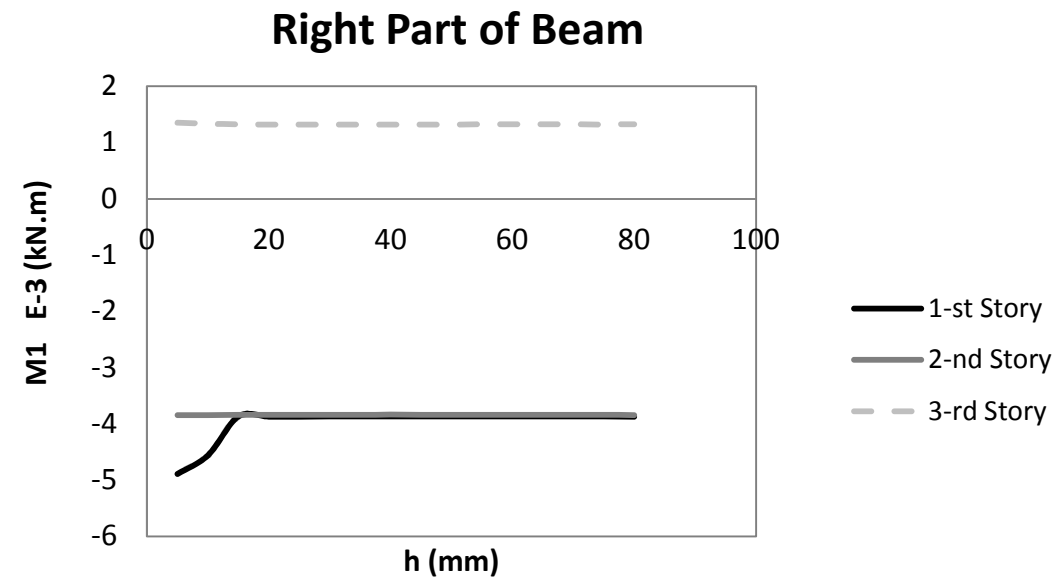

Figure 5.22 Diagrams of moment (M1) of (a) left, and (b) right part of beams with respect to the amplitude of rupture (h) for fault rupture with location of x=1.00 m

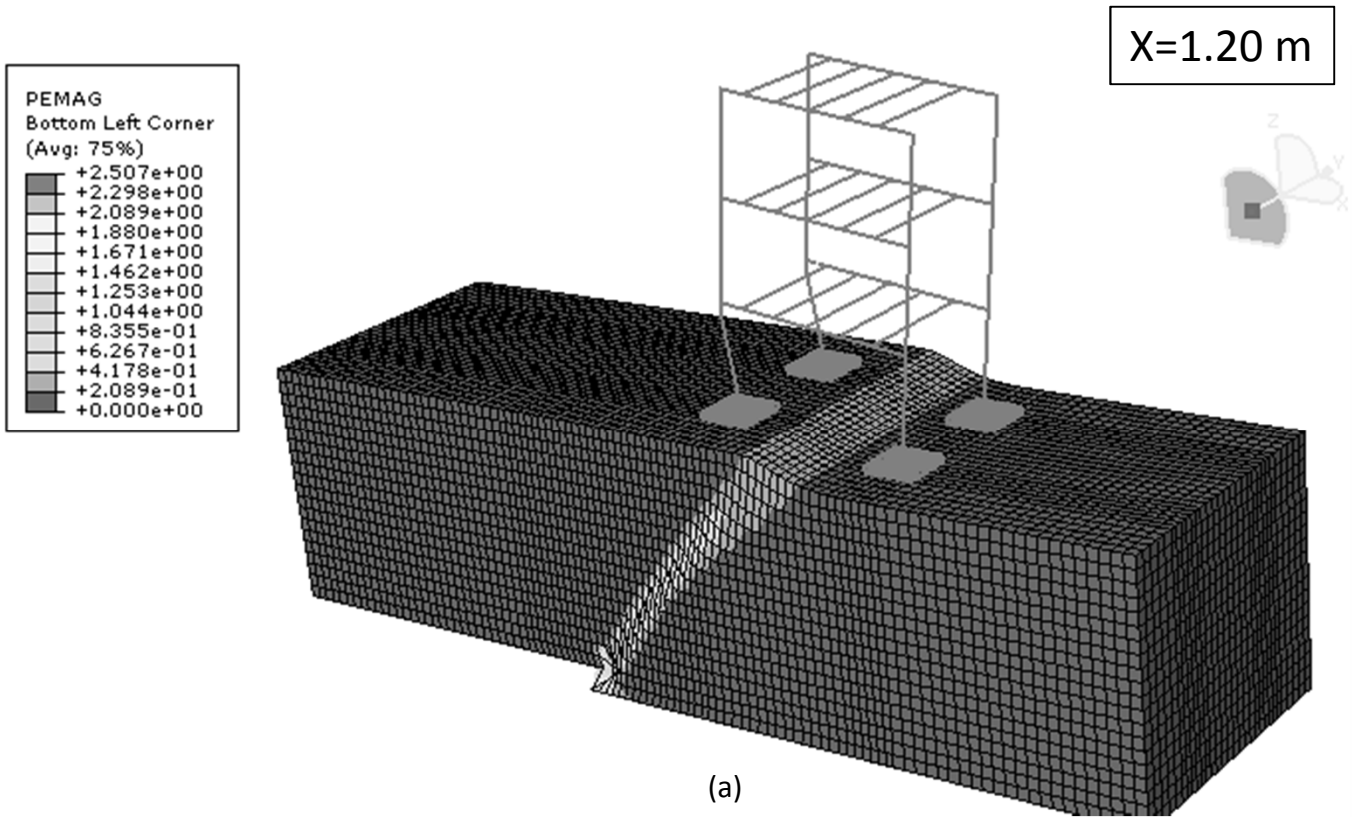

(a)

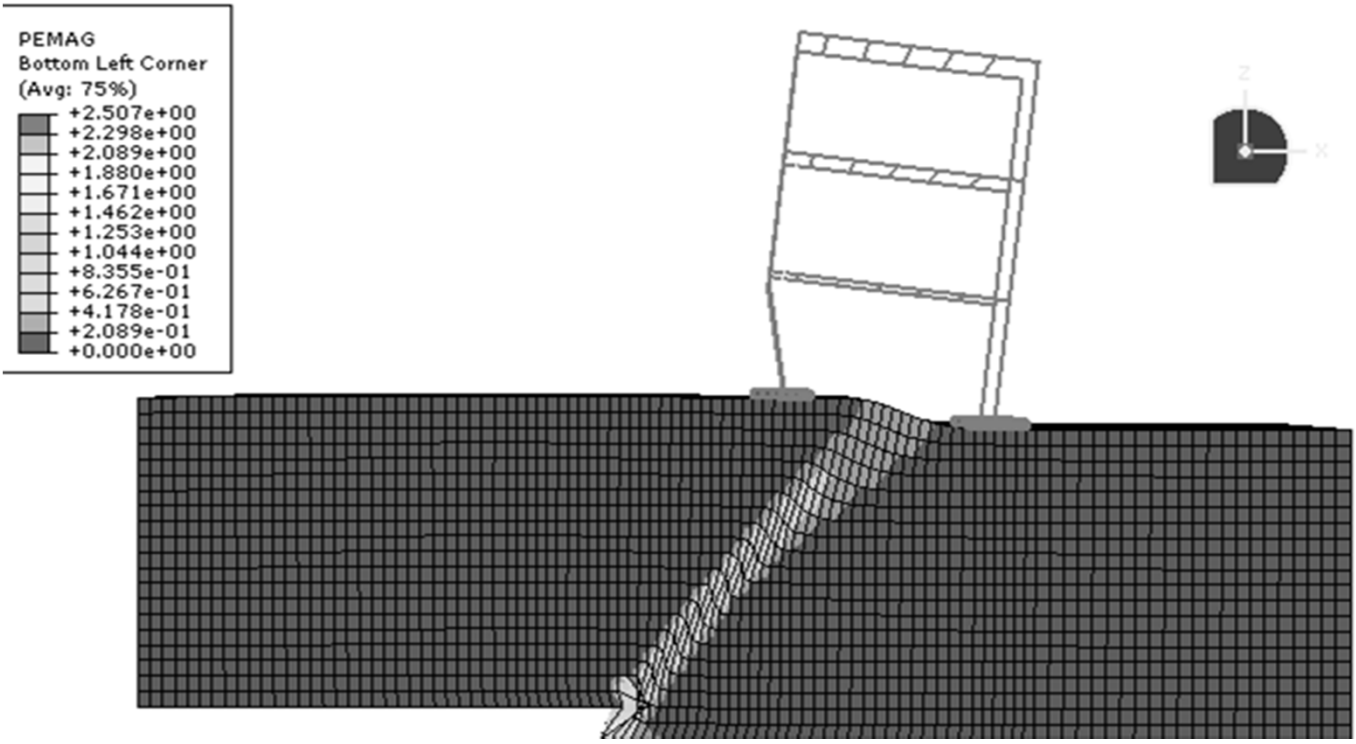

(b)

Figure 5.23 The model in ABAQUS for rupture location of x=1.20 m : (a) 3D, and (b) 2D view

(a)

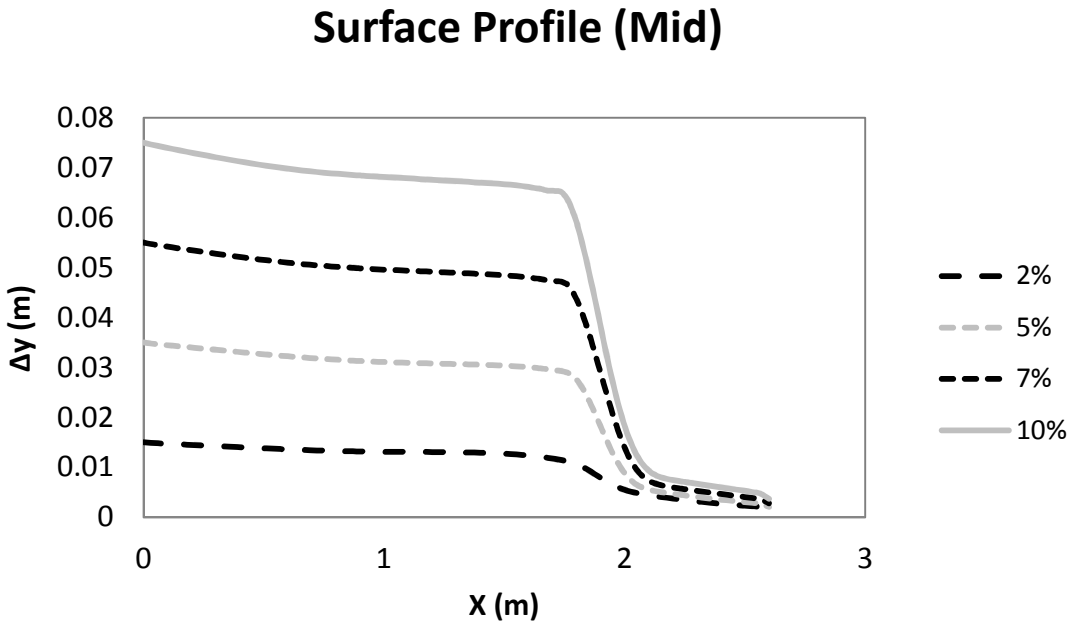

(b)

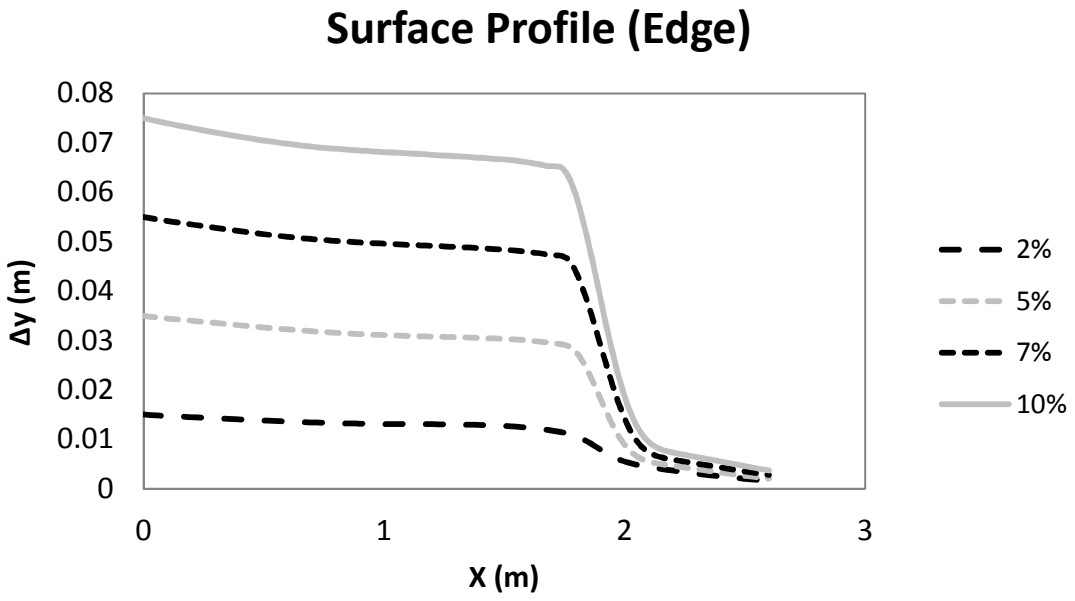

Figure 5.24 Vertical displacement at the surface for normalized bedrock displacement ranging from h/H=2% to 10% for the fault rupture location of x=1.20 m in (a) middle, and (b) edge of the soil surface

(a)

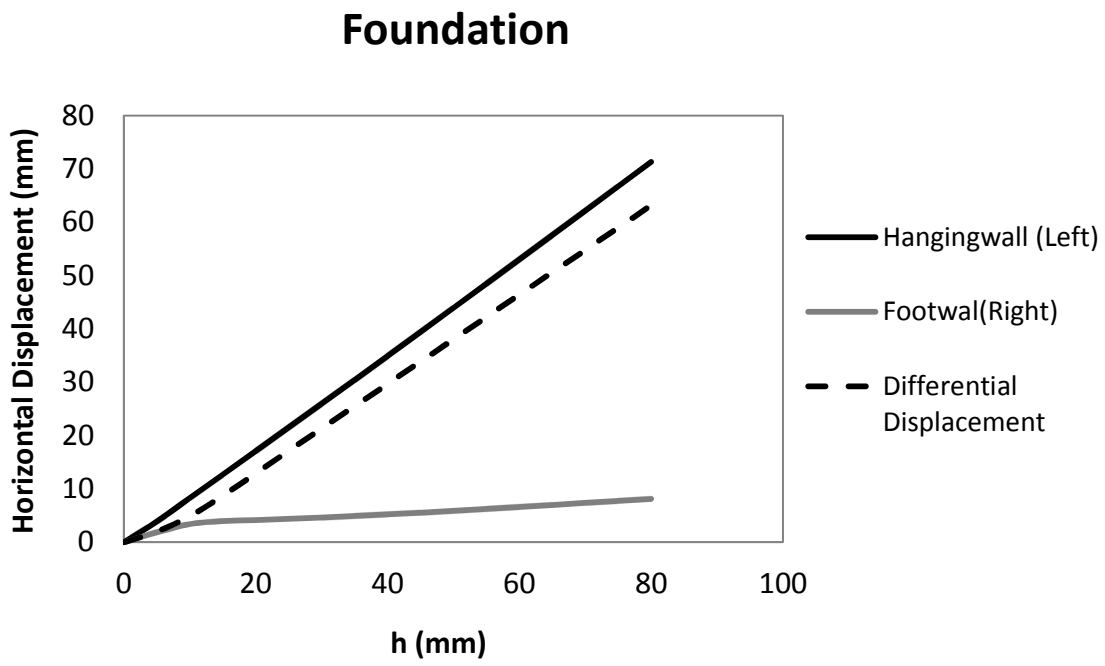

(b)

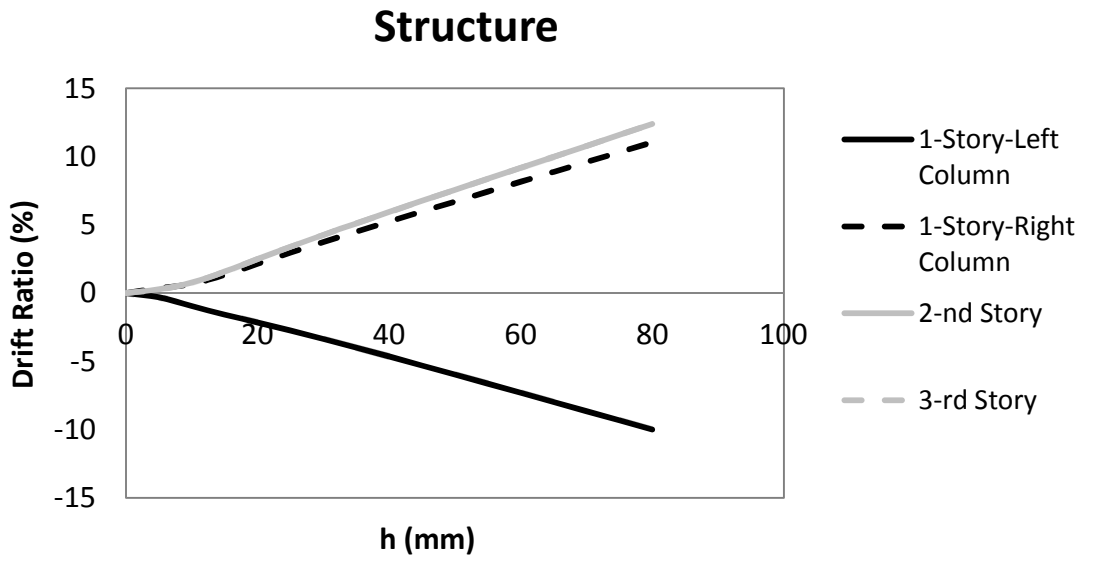

Figure 5.25 (a) foundation horizontal displacement, and (b) structural drift ratio for fault rupture location of x=1.20 m

(a)

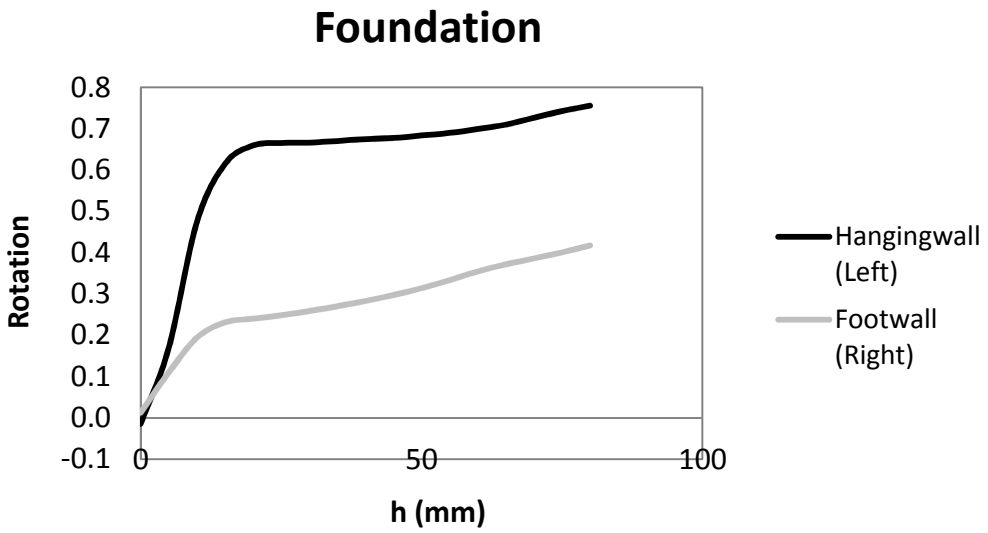

(b)

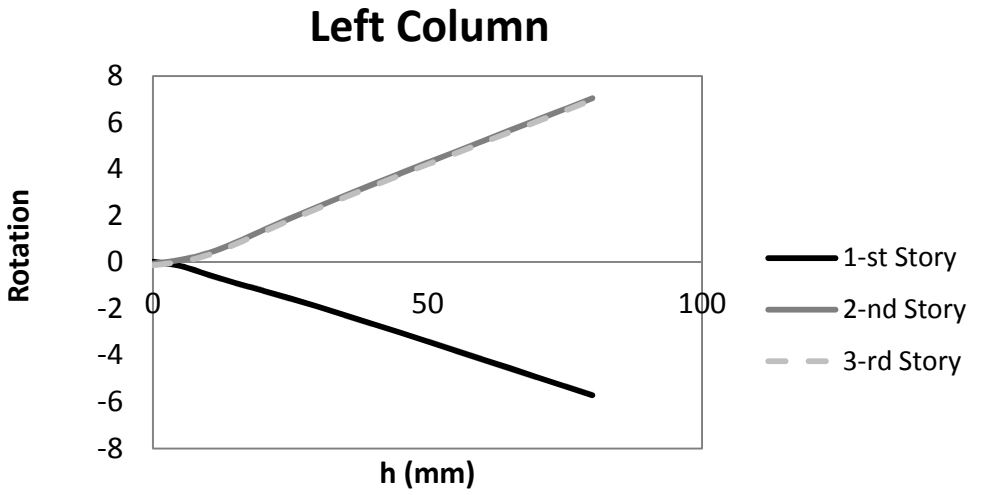

(c)

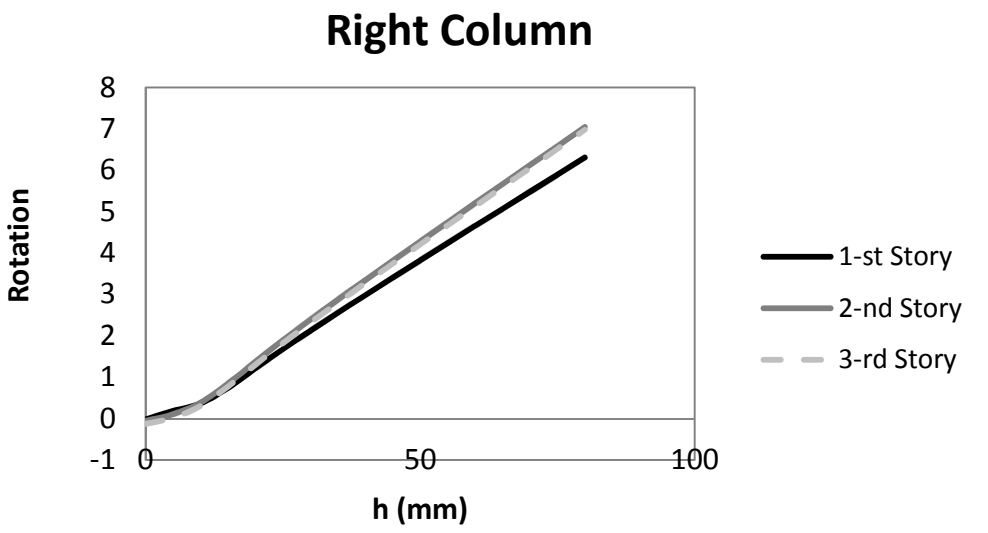

Figure 5.26 Diagrams of rotation of (a) foundation, (b) left, and (c) right columns with respect to the amplitude of rupture (h) for fault rupture with location of x=1.20 m

(a)

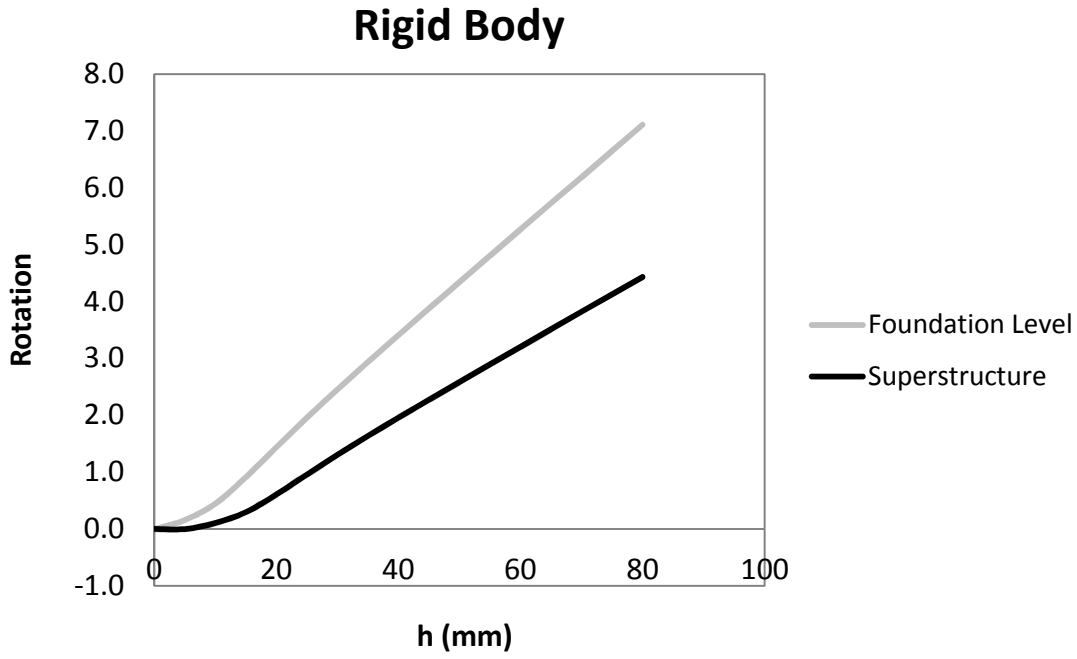

(b)

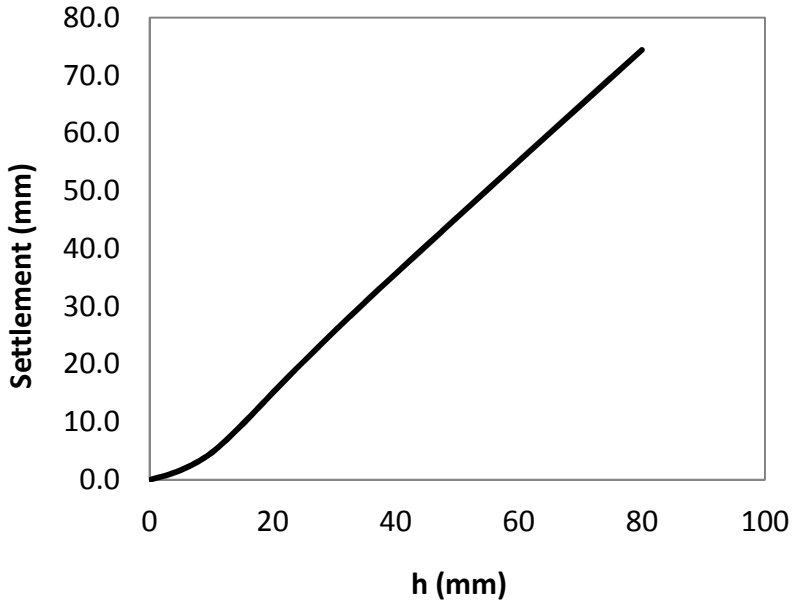

Figure 5.27 Diagrams of (a) left, and (b) right column moment (M1) with respect to the amplitude of rupture (h) for fault rupture with location of x=1.20 m

(a)

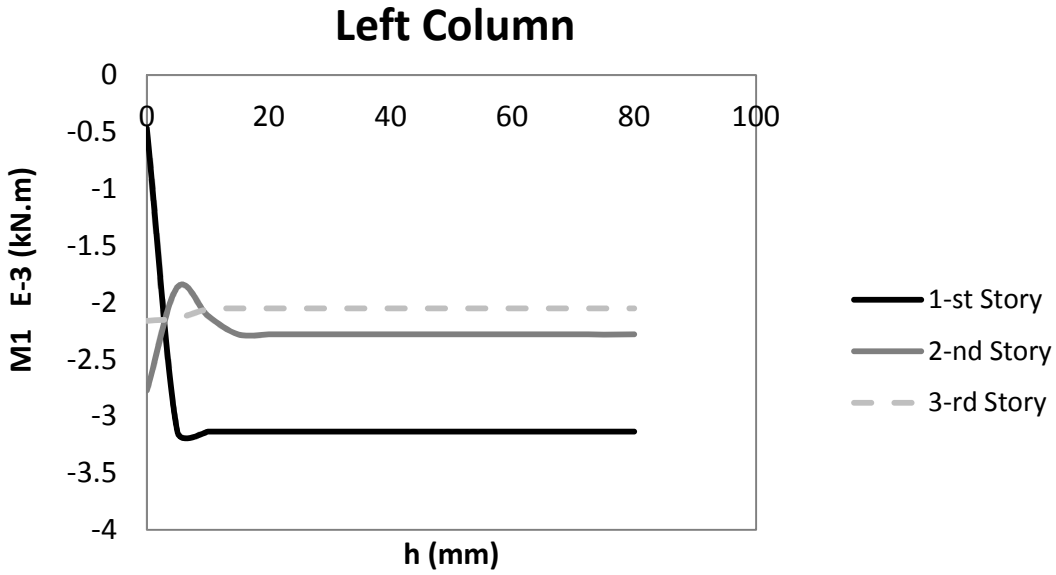

(b)

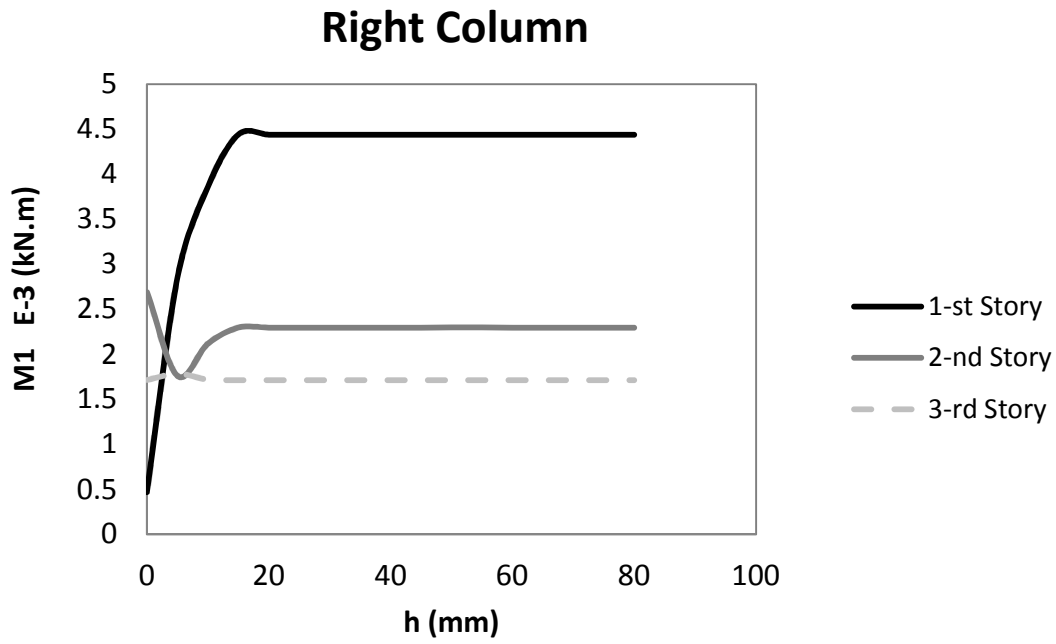

Figure 5.28 Diagrams of moment (M1) of (a) left, and (b) right part of beams with respect to the amplitude of rupture (h) for fault rupture with location of x=1.20 m

(a)

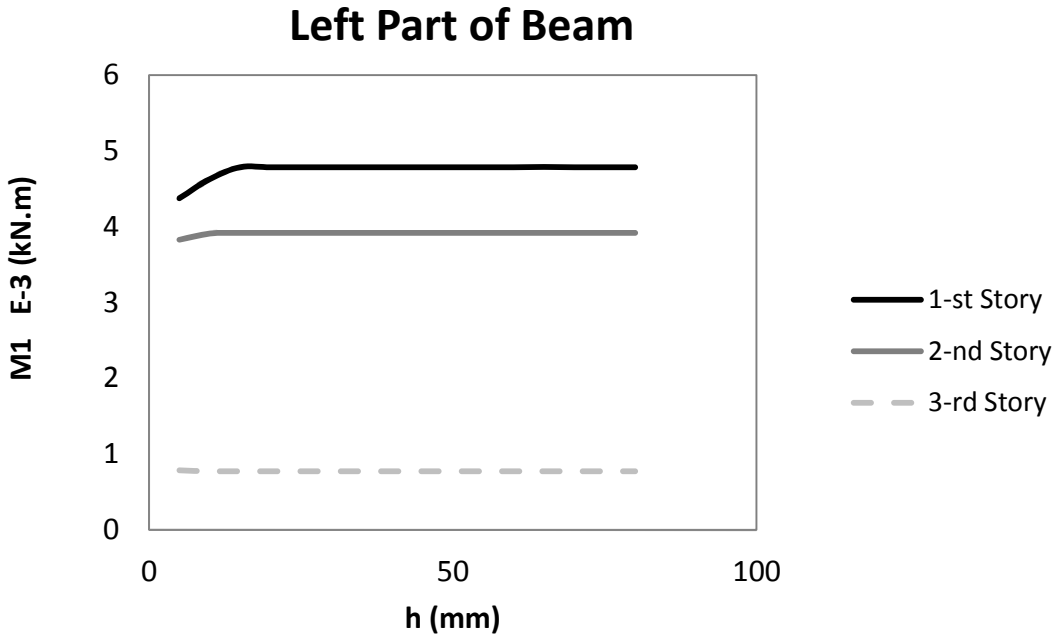

(b)

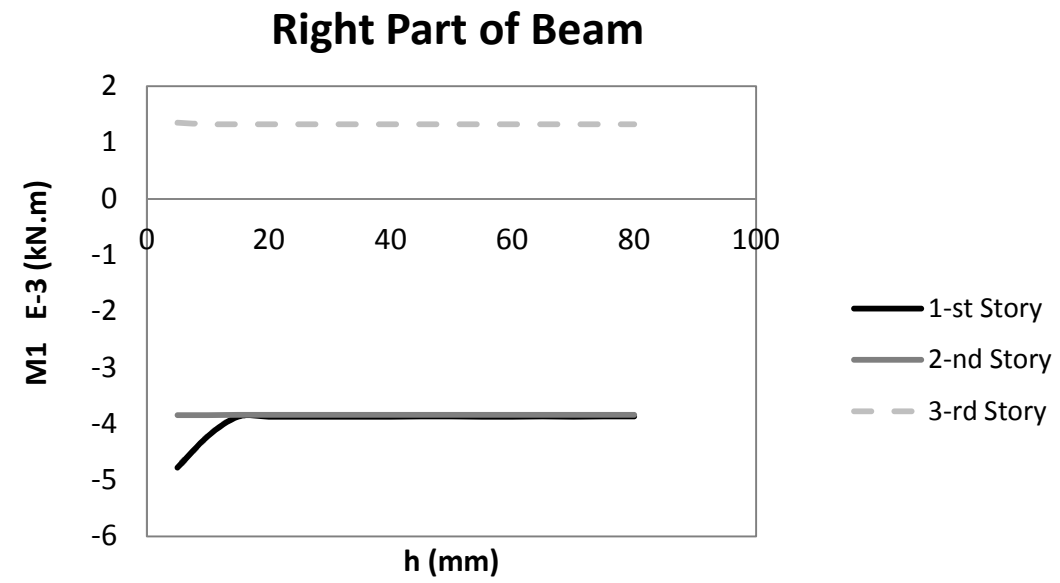

Figure 5.29 Diagrams of moment (M1) of (a) left, and (b) right part of beams with respect to the amplitude of rupture (h) for fault rupture with location of x=1.20 m

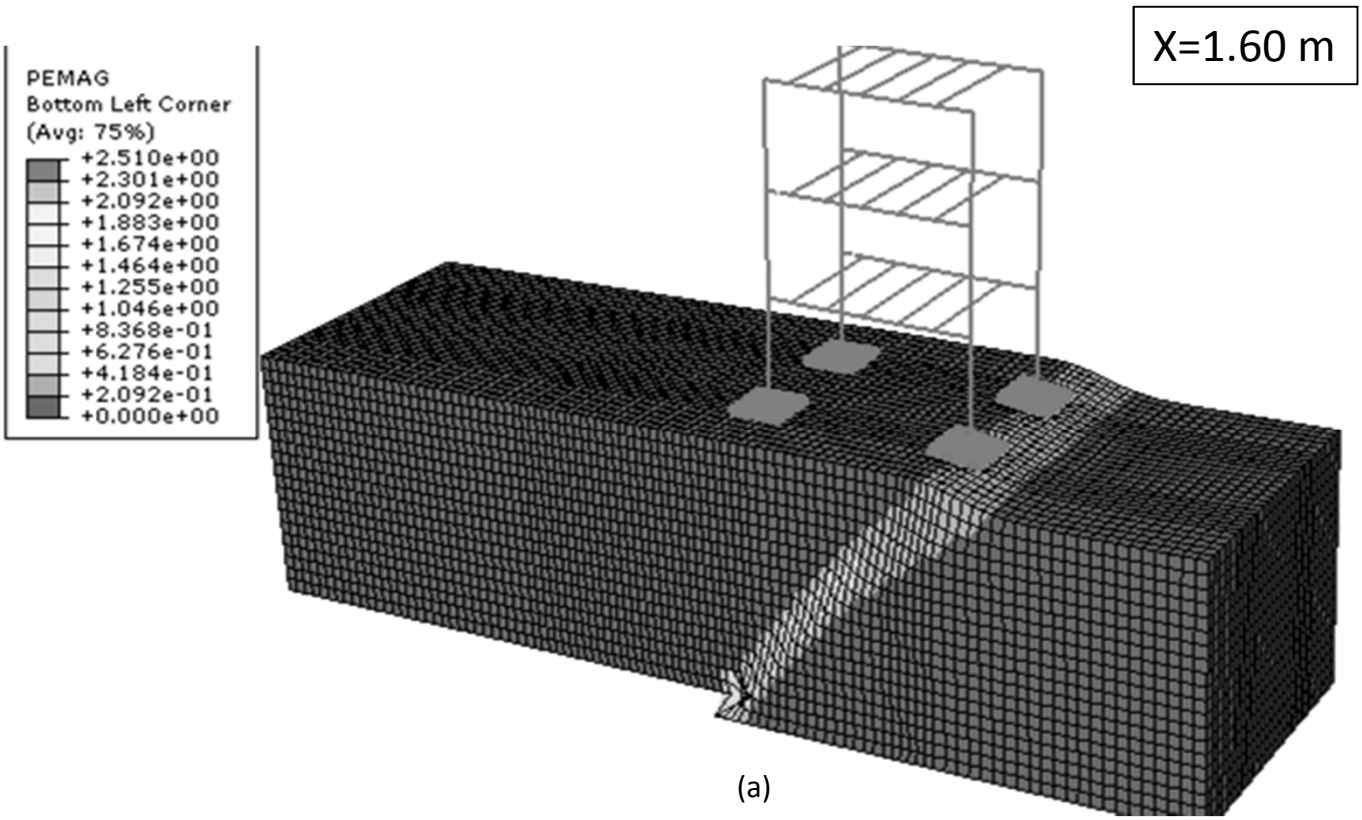

(a)

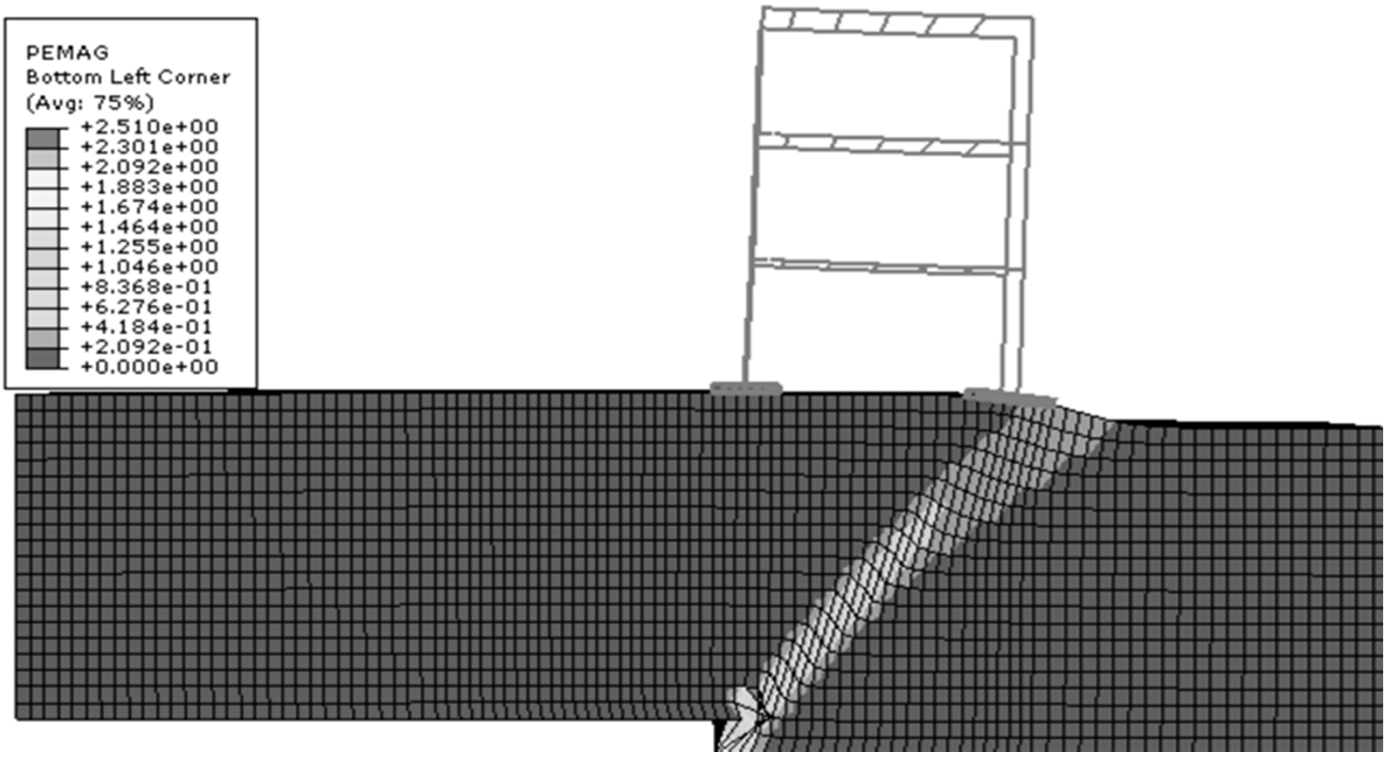

(b)

Figure 5.30 The model in ABAQUS for rupture location of x=1.60 m : (a) 3D, and (b) 2D view

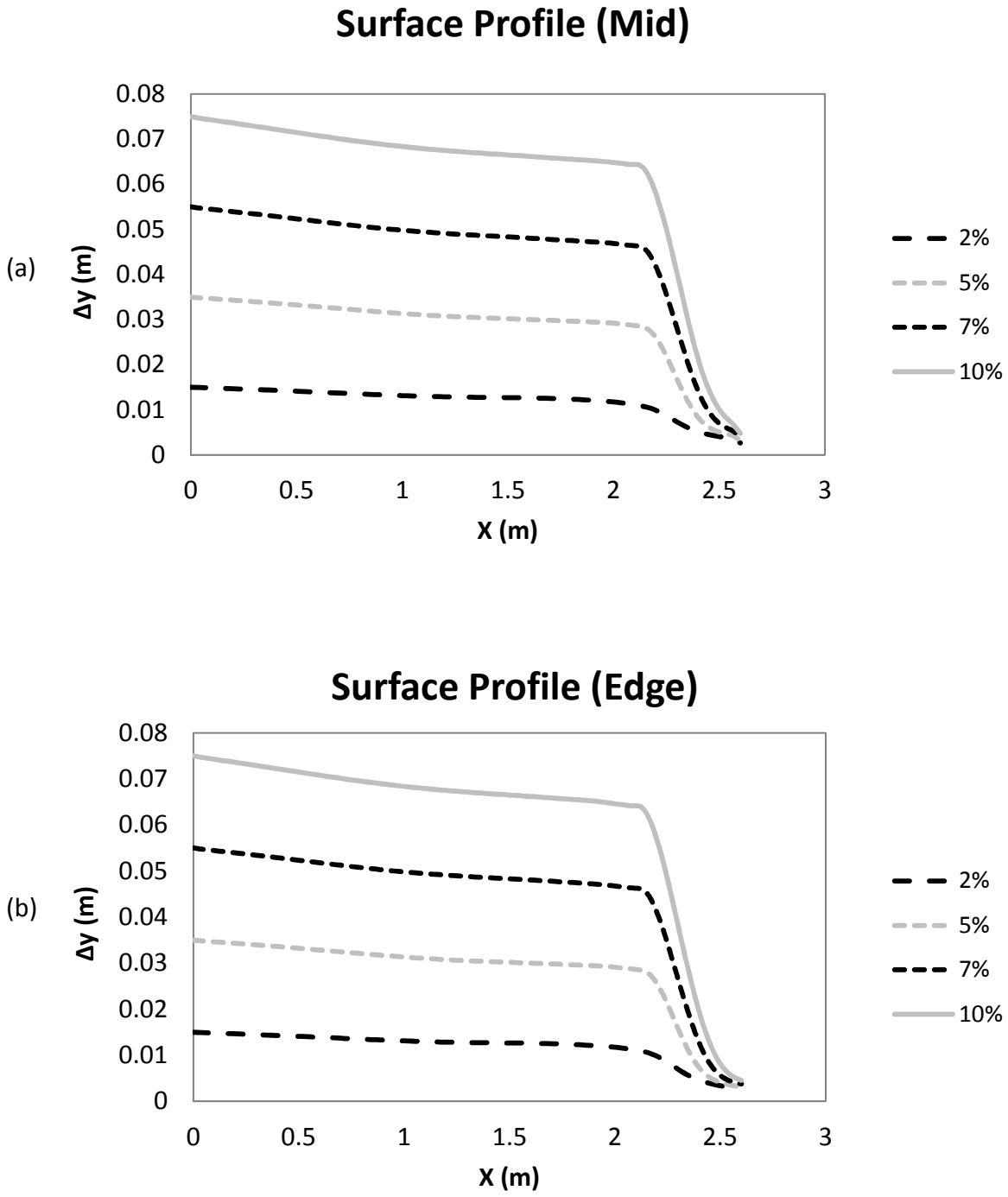

Figure 5.31 Vertical displacement at the surface for normalized bedrock displacement ranging from h/H=2% to 10% for the fault rupture location of x=1.60 m in (a) middle, and (b) edge of the soil surface

(a)

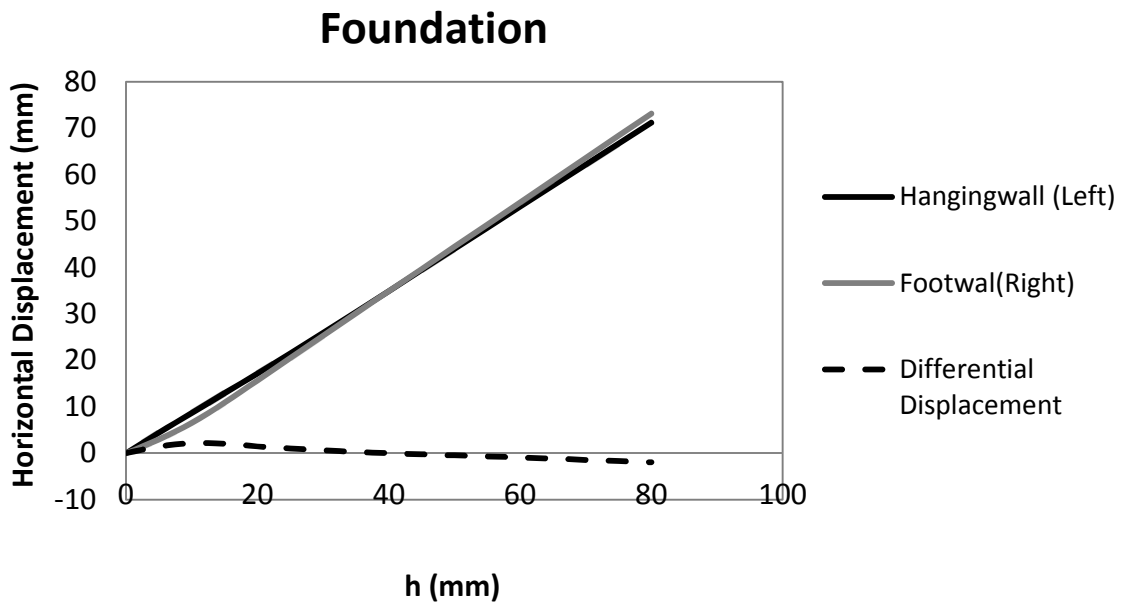

(b)

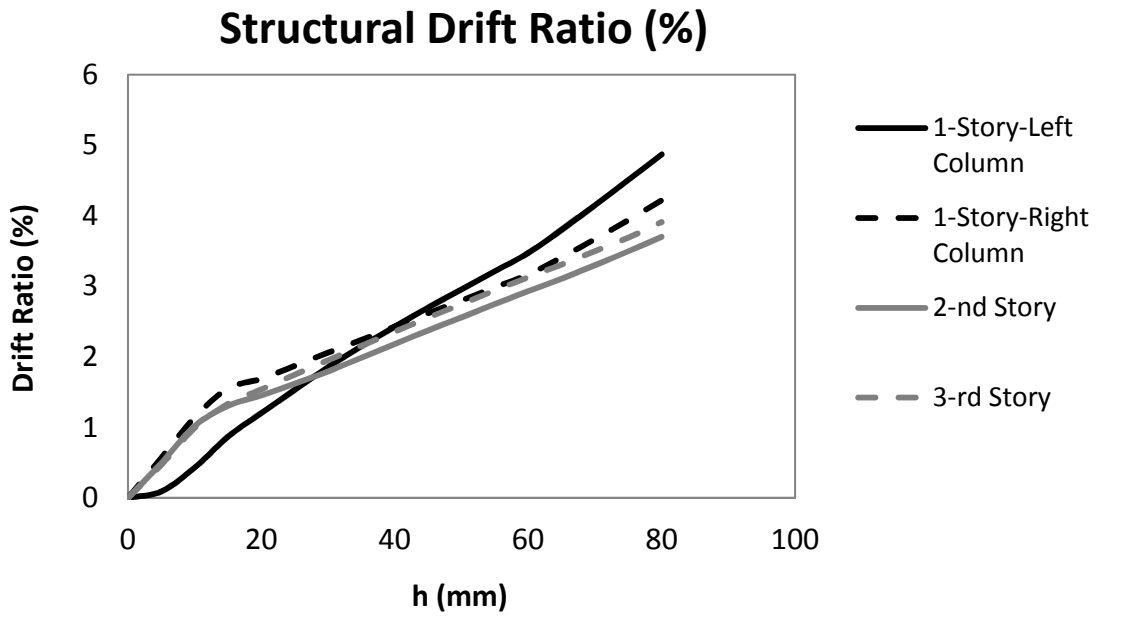

Figure 5.32 (a) foundation horizontal displacement, and (b) structural drift ratio for fault rupture location of x=1.60 m

(a)

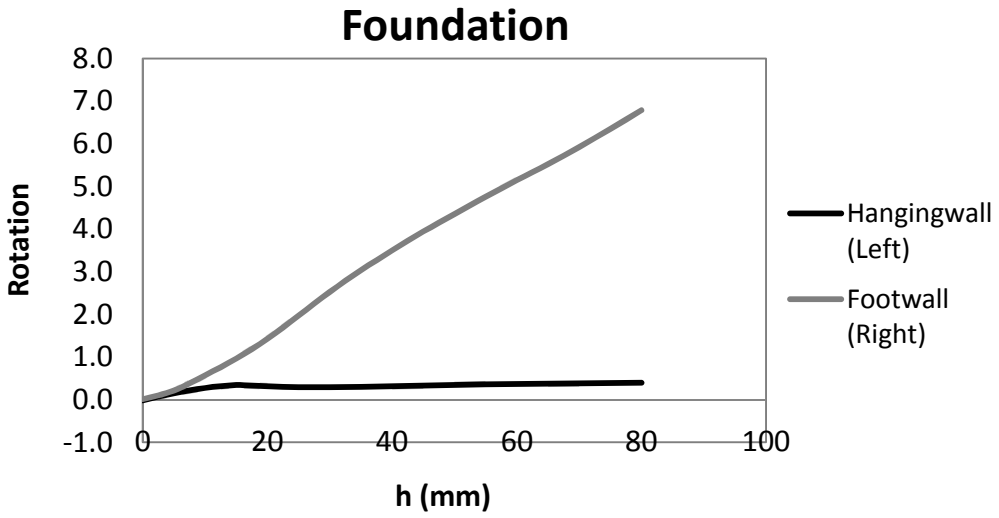

(b)

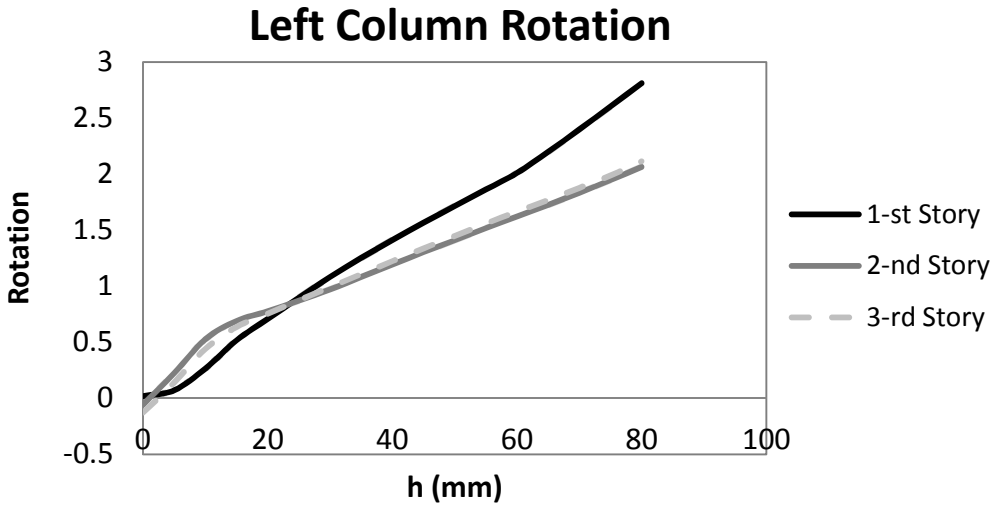

(c)

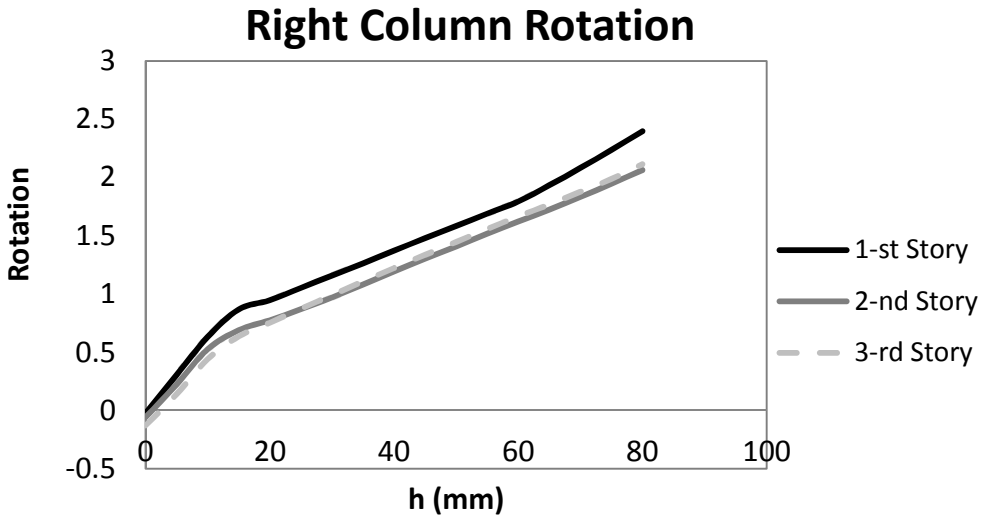

Figure 5.33 Diagrams of rotation with respect to the amplitude of rupture (h) for fault rupture with location of x=1.60 m of (a) foundation, (b) left, and (c) right columns

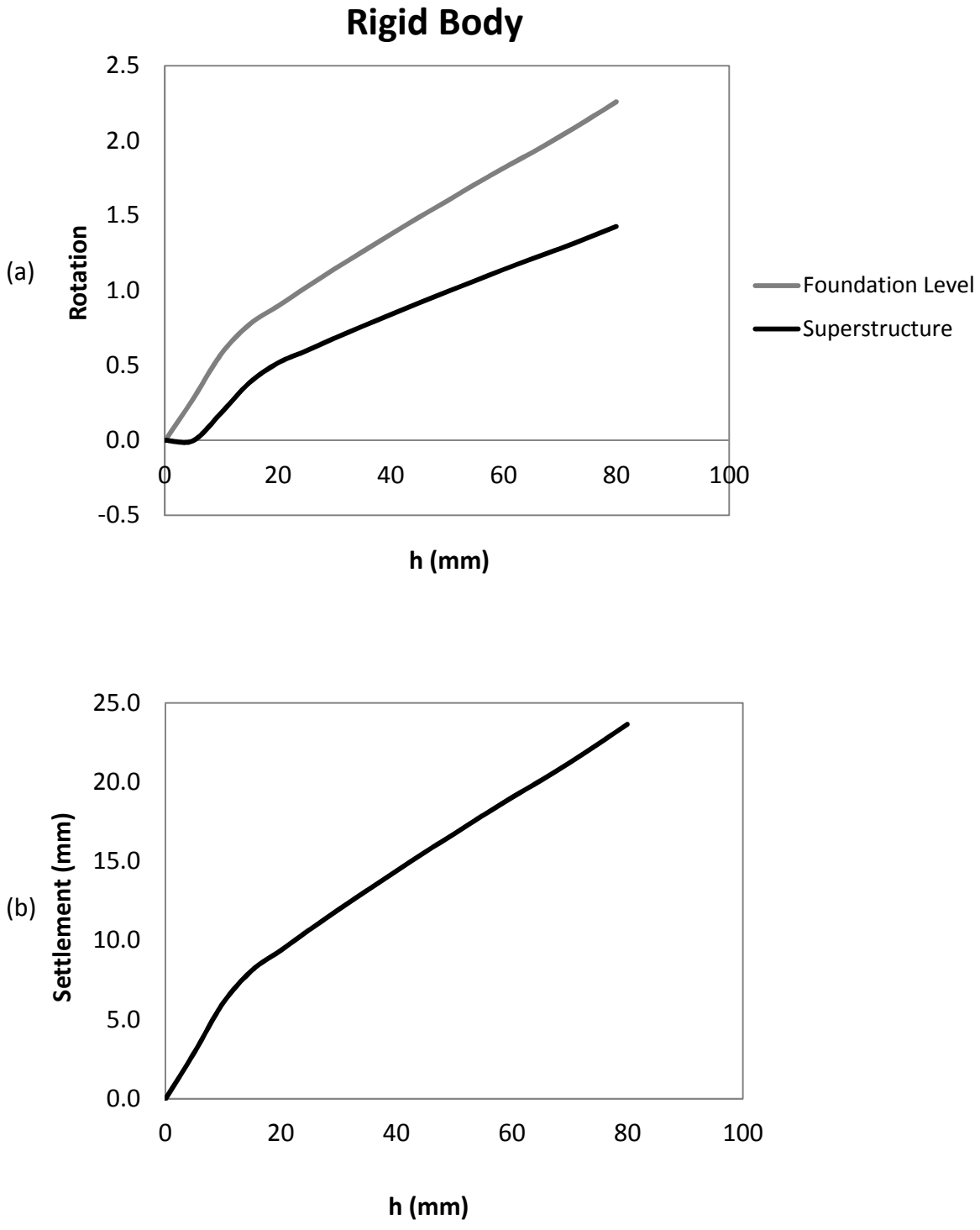

Figure 5.34 Diagrams of (a) left, and (b) right column moment (M1) with respect to the amplitude of rupture (h) for fault rupture with location of x=1.60 m

(a)

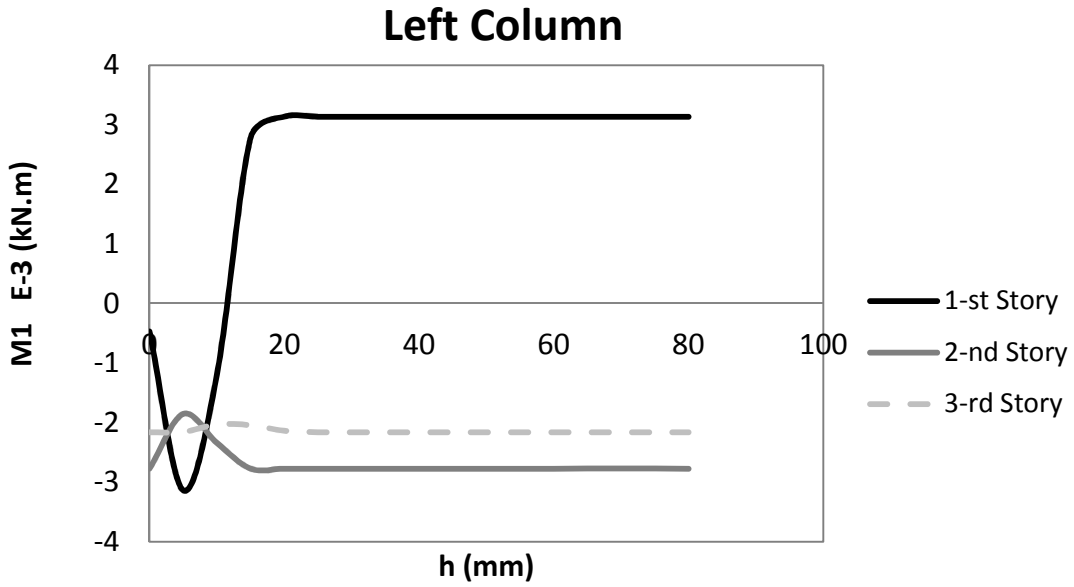

(b)

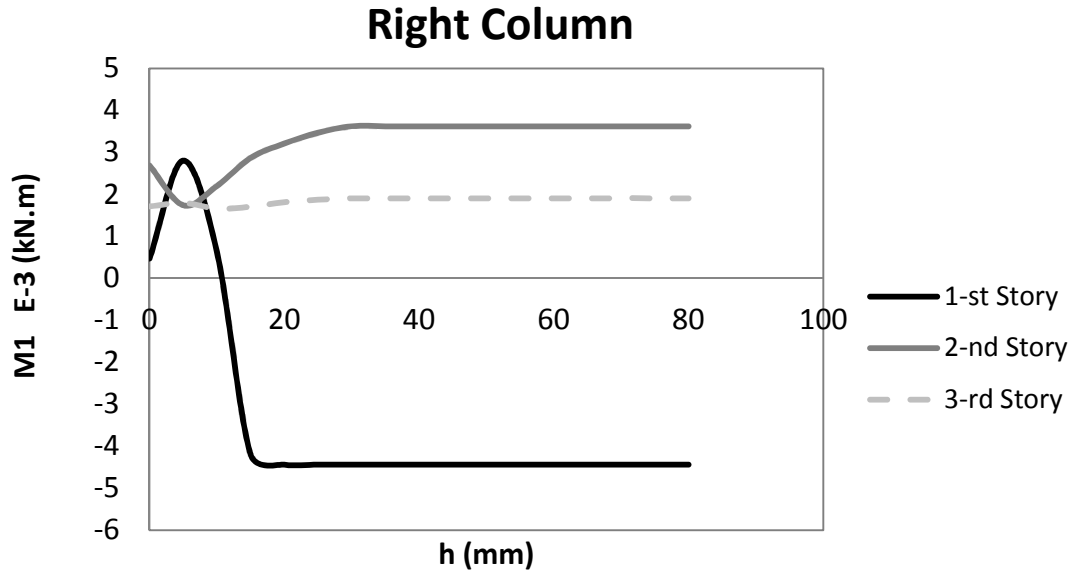

Figure 5.35 Diagrams of moment (M1) of (a) left, and (b) right part of beams with respect to the amplitude of rupture (h) for fault rupture with location of x=1.60 m

(a)

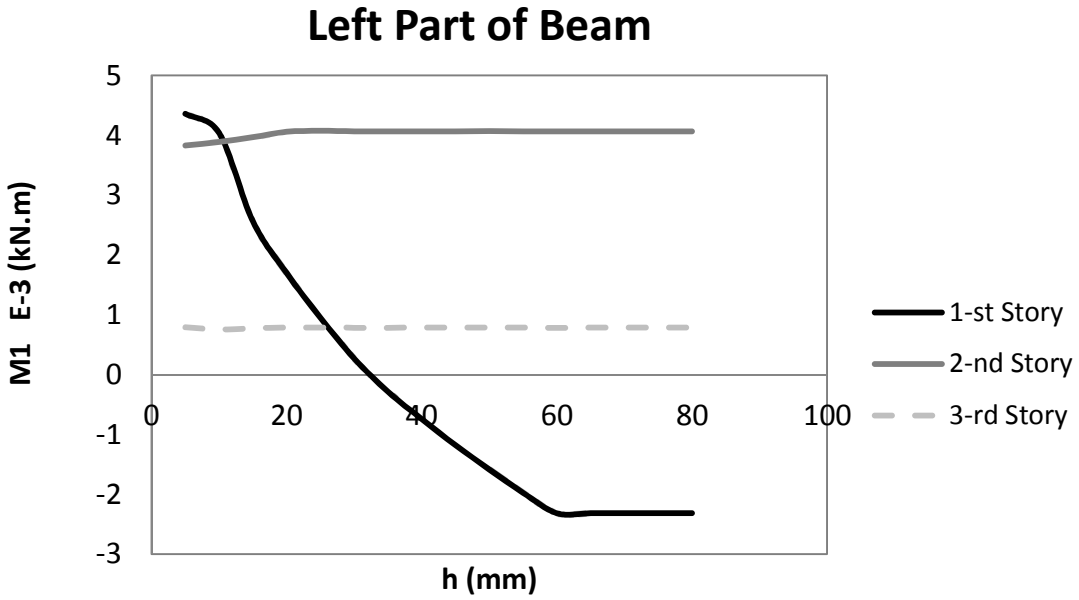

(b)

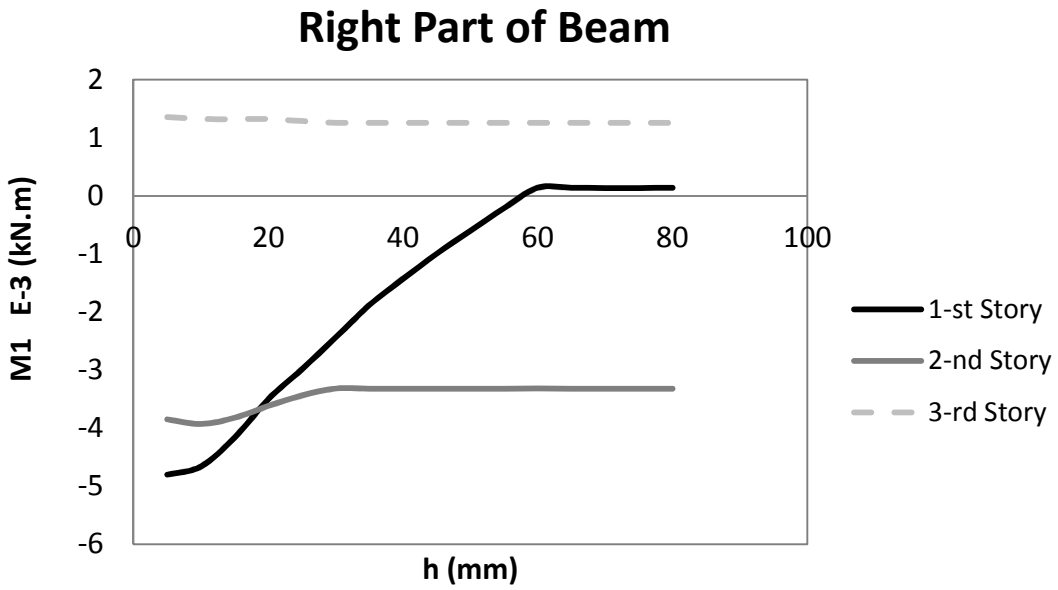

Figure 5.36 Diagrams of moment (M1) of (a) left, and (b) right part of beams with respect to the amplitude of rupture (h) for fault rupture with location of x=1.60 m

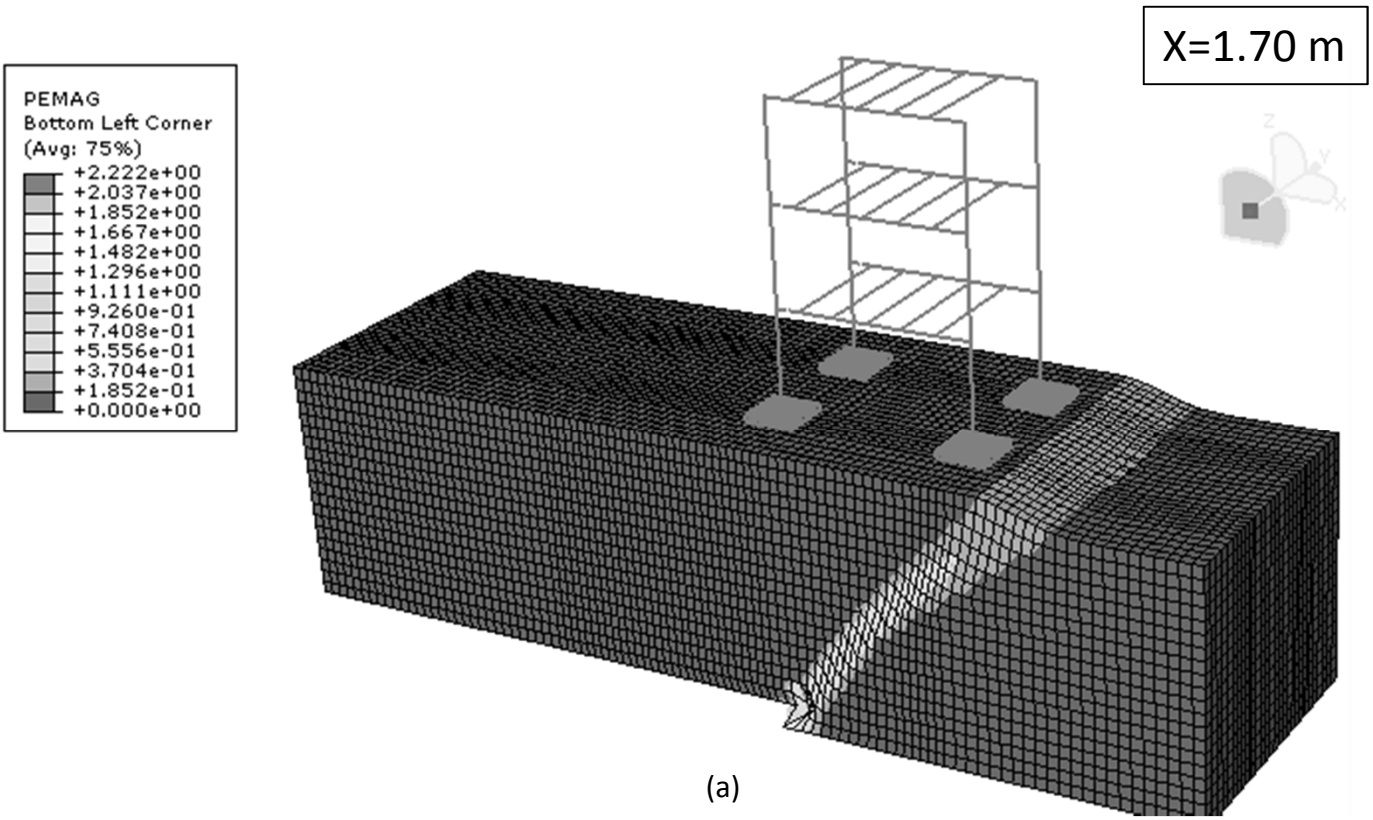

(a)

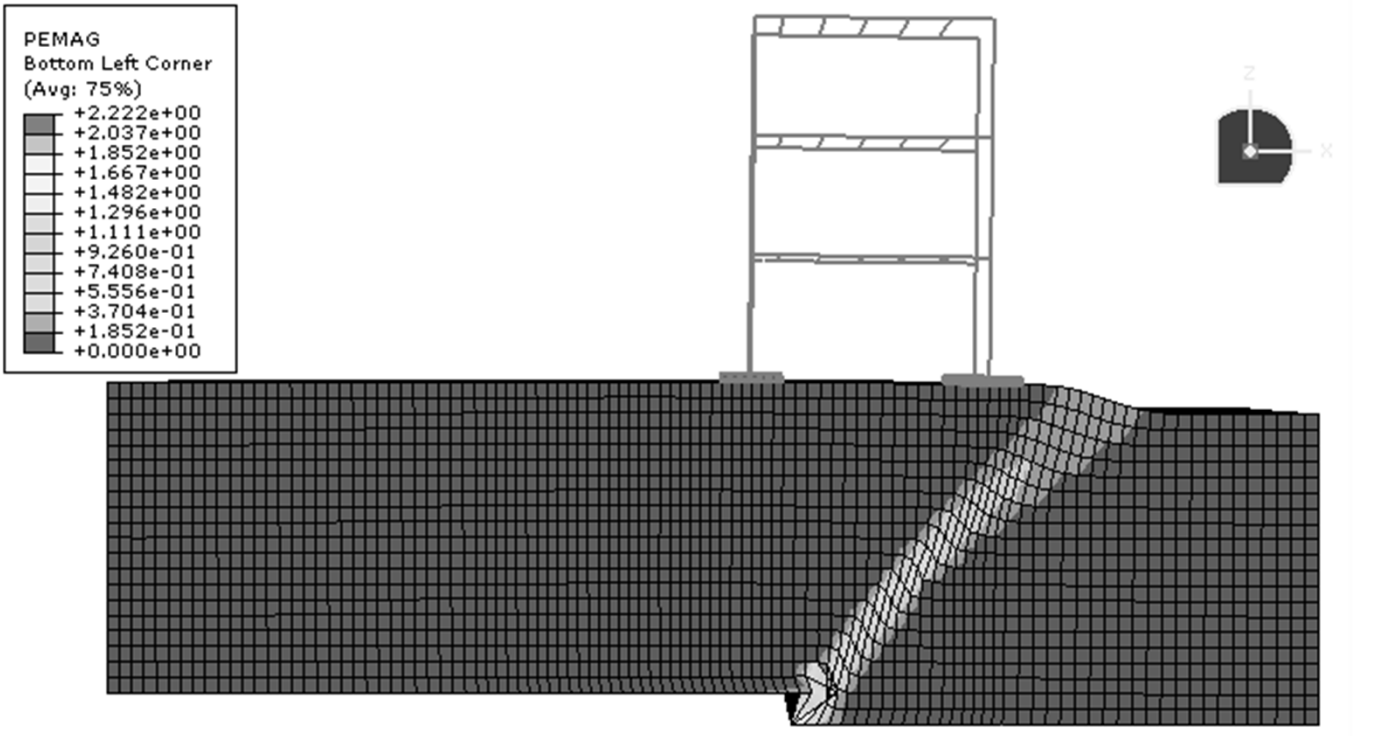

(b)

Figure 5.37 The model in ABAQUS for rupture location of x=1.7 m : (a) 3D, and (b) 2D view

(a)

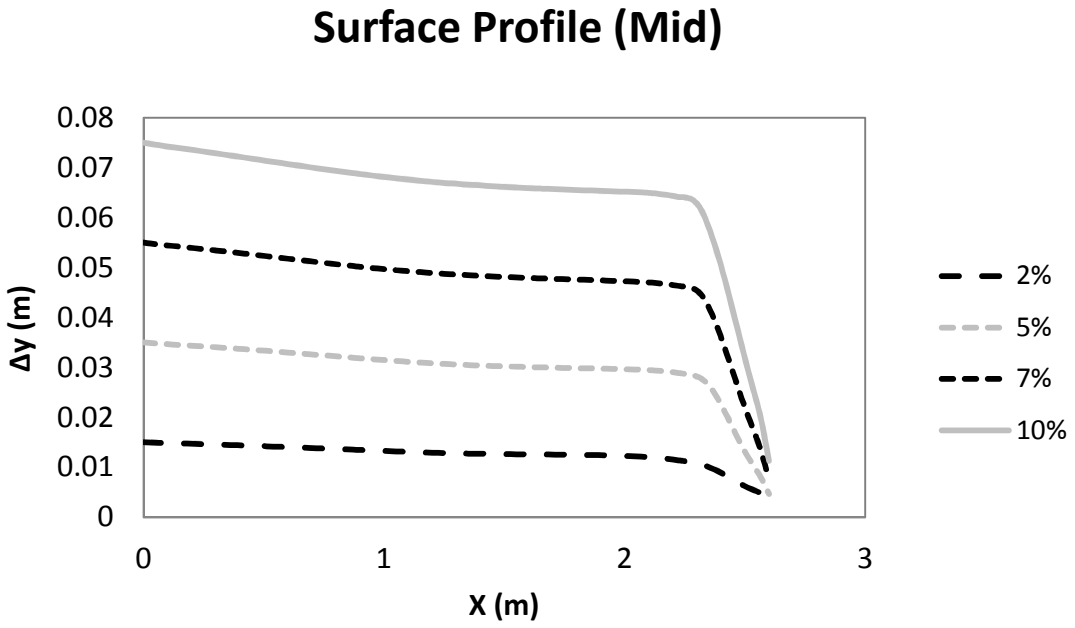

(b)

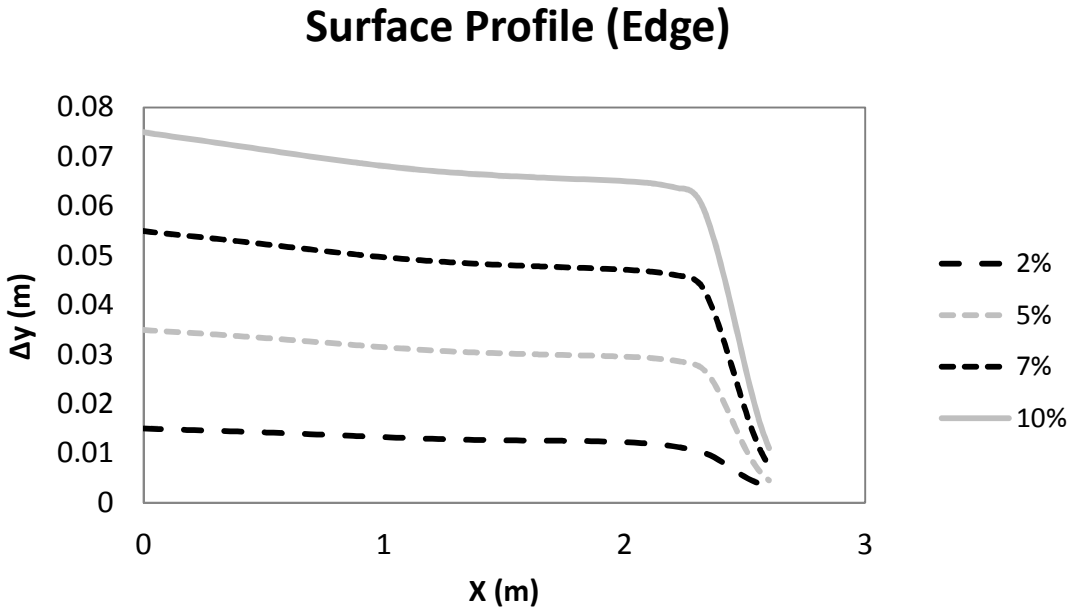

Figure 5.38 Vertical displacement at the surface for normalized bedrock displacement ranging from h/H=2% to 10% for the fault rupture location of x=1.70 m in (a) middle, and (b) edge of the soil surface

(a)

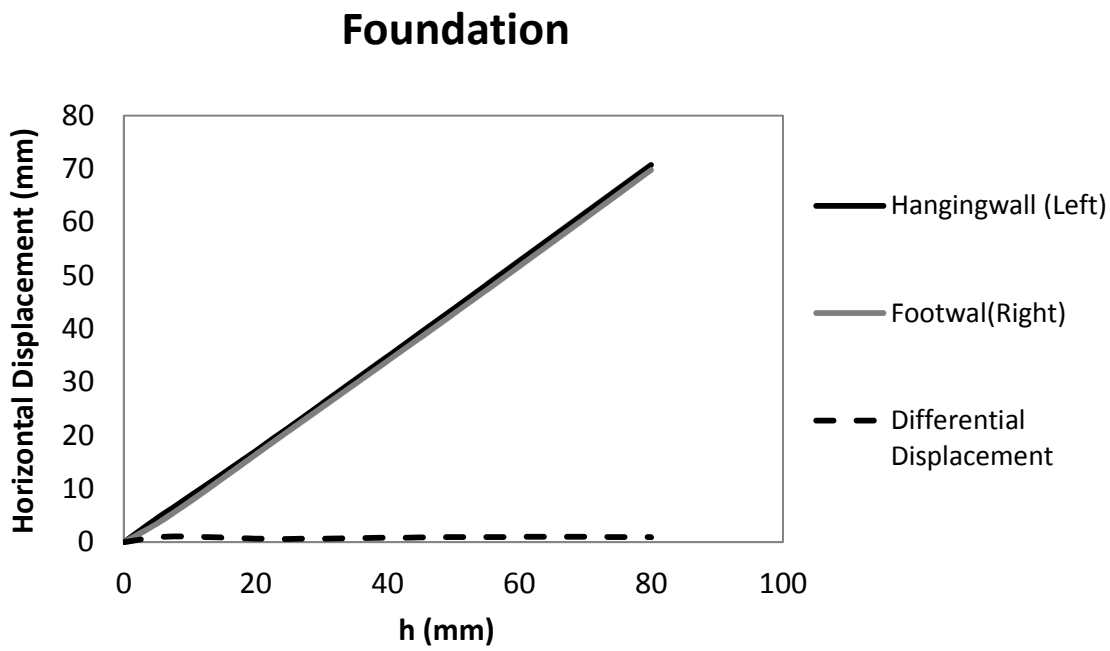

(b)

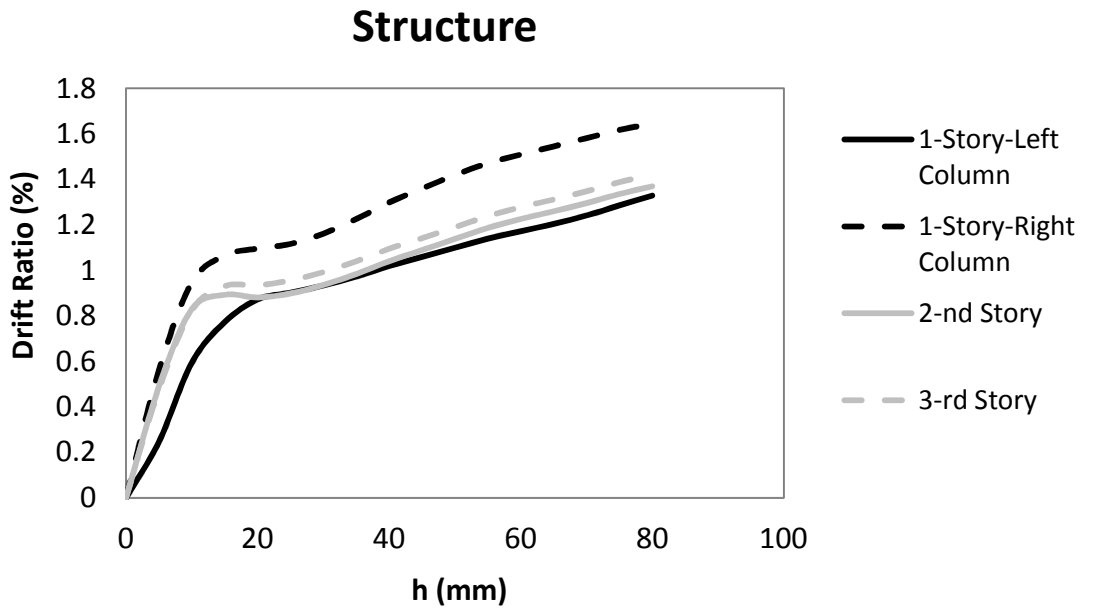

Figure 5.39 (a) foundation horizontal displacement, and (b) structural drift ratio for fault rupture location of x=1.70 m

(a)

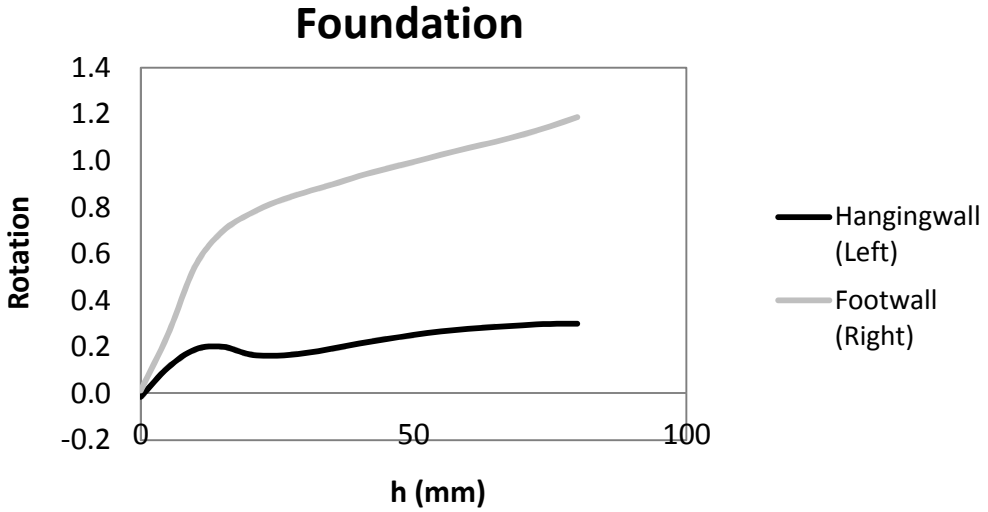

(b)

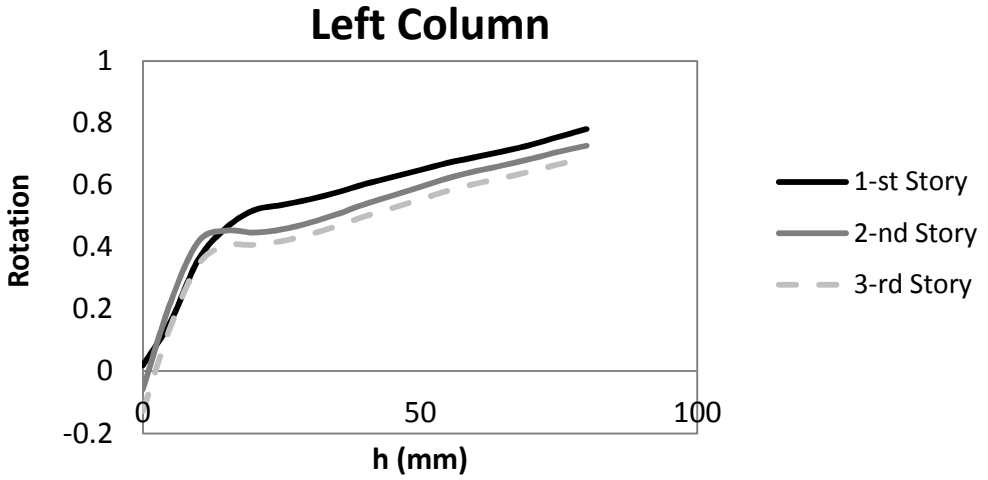

(c)

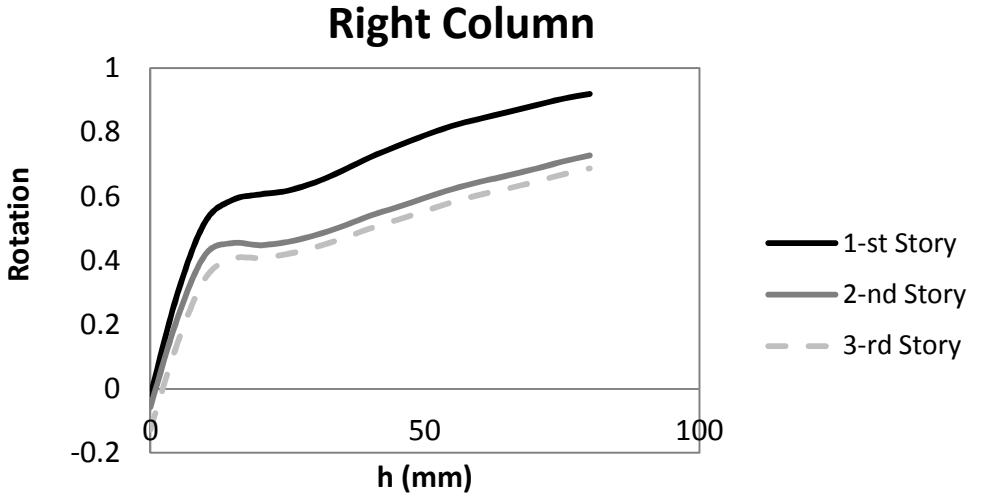

Figure 5.40 Diagrams of rotation with respect to the amplitude of rupture (h) for fault rupture with location of x=1.70 m of (a) foundation, (b) left, and (c) right columns

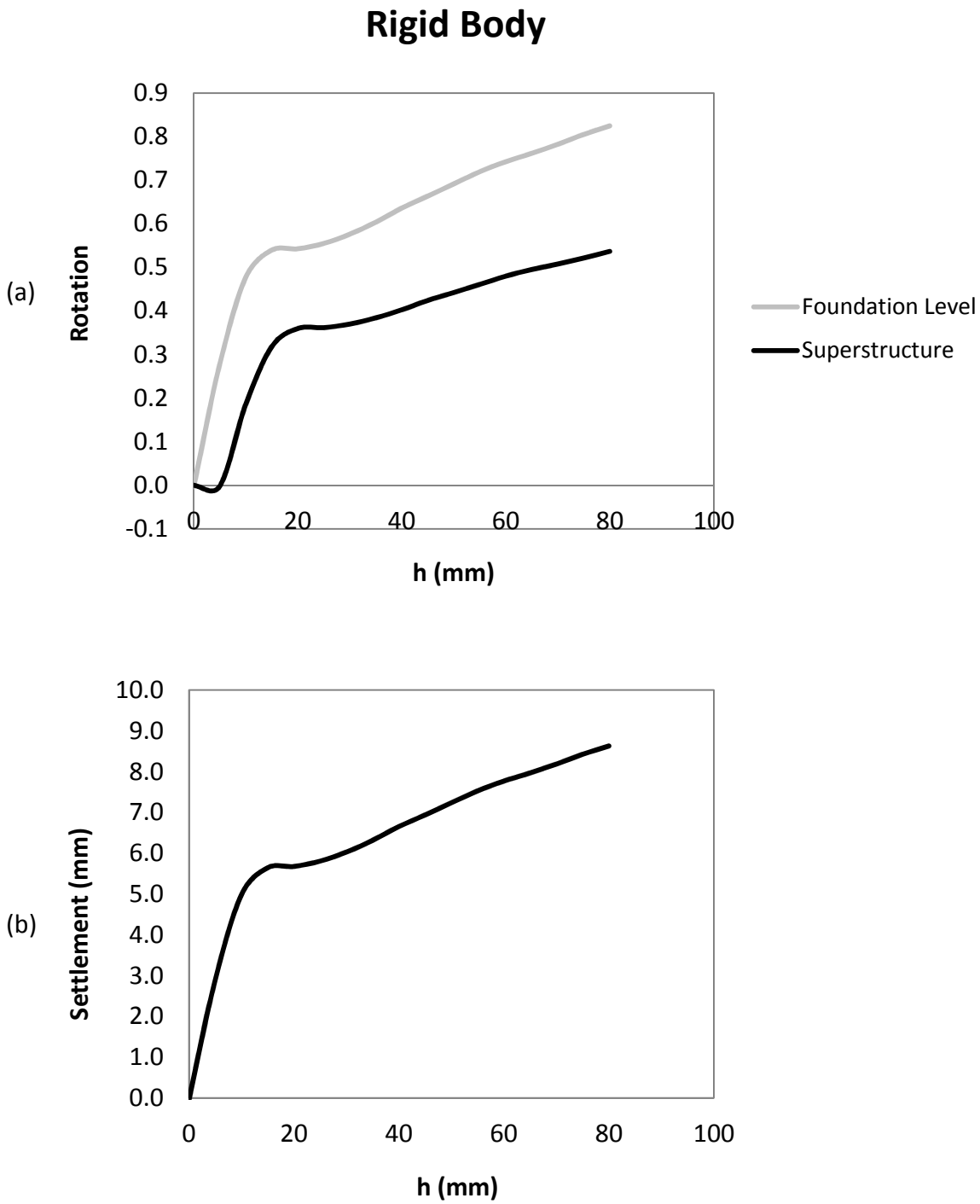

Figure 5.41 Diagrams of (a) left, and (b) right column moment (M1) with respect to the amplitude of rupture (h) for fault rupture with location of x=1.70 m

(a)

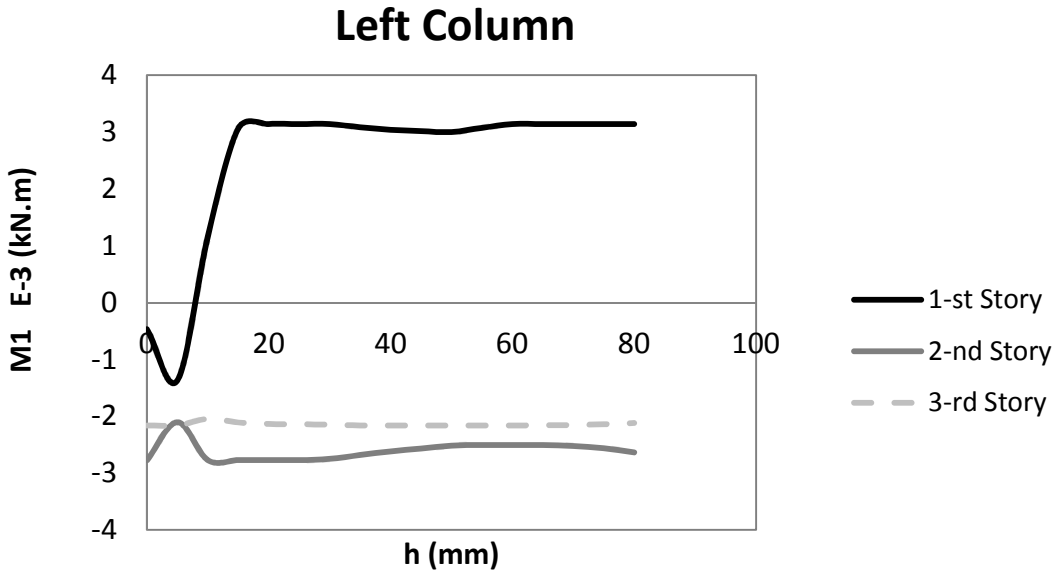

(b)

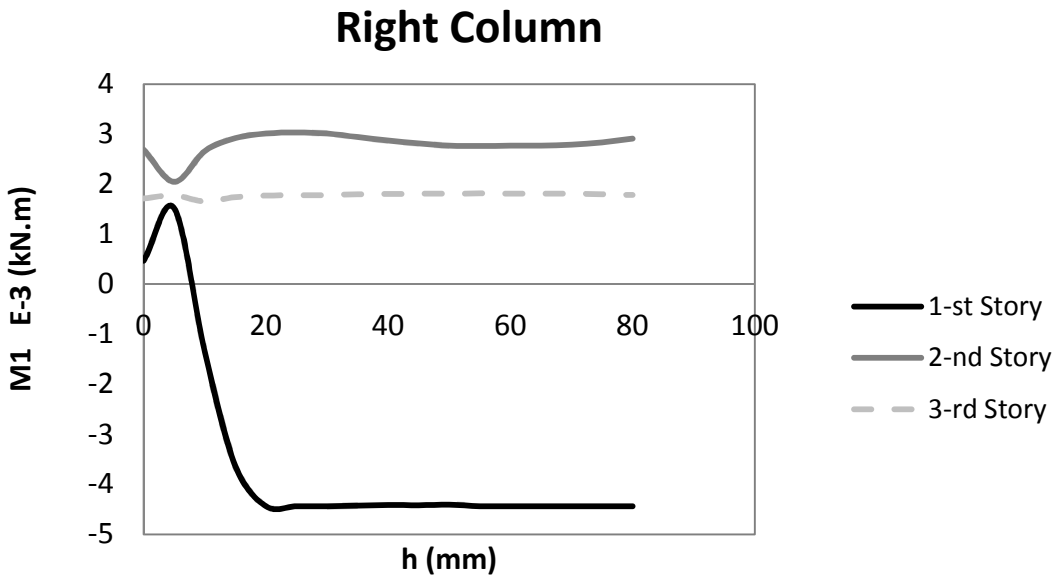

Figure 5.42 Diagrams of moment (M1) of (a) left, and (b) right part of beams with respect to the amplitude of rupture (h) for fault rupture with location of x=1.70 m

(a)

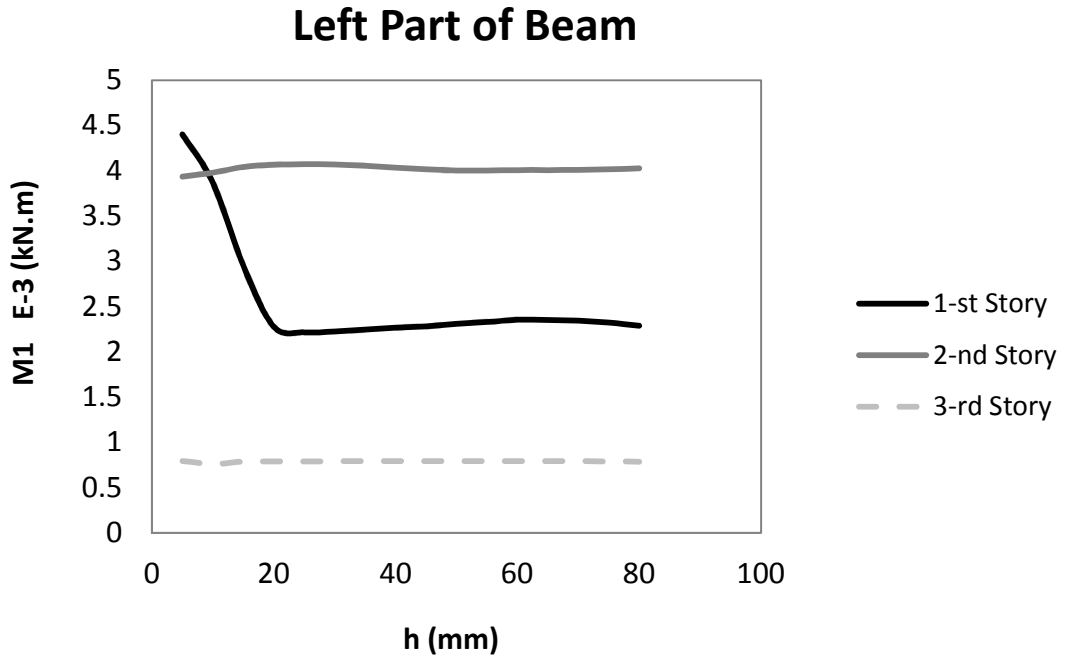

(b)

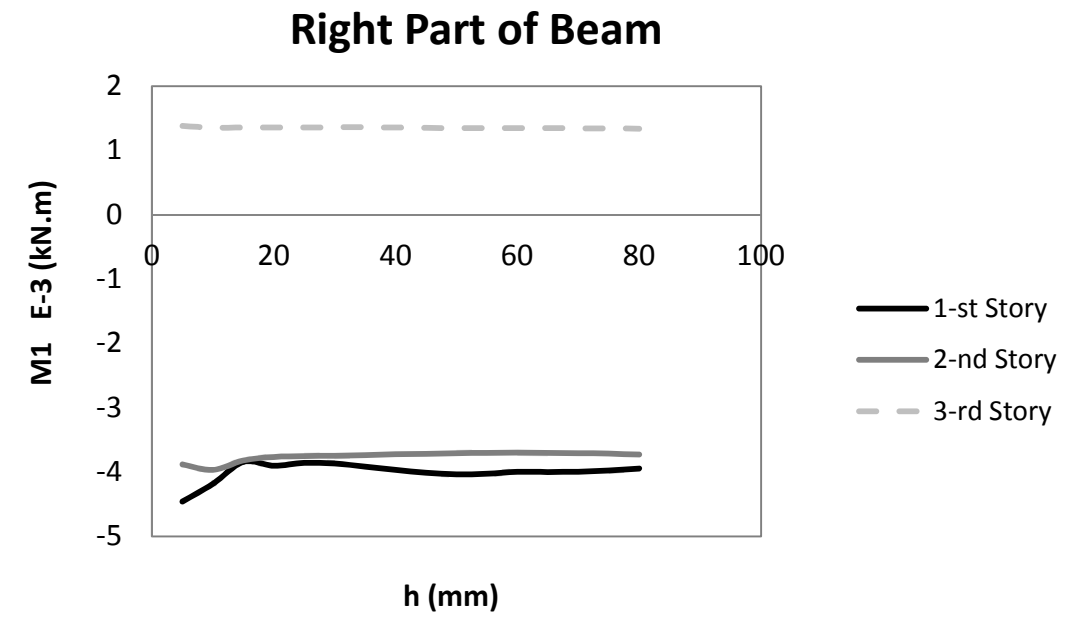

Figure 5.43 Diagrams of moment (M1) of (a) left, and (b) right part of beams with respect to the amplitude of rupture (h) for fault rupture with location of x=1.70 m

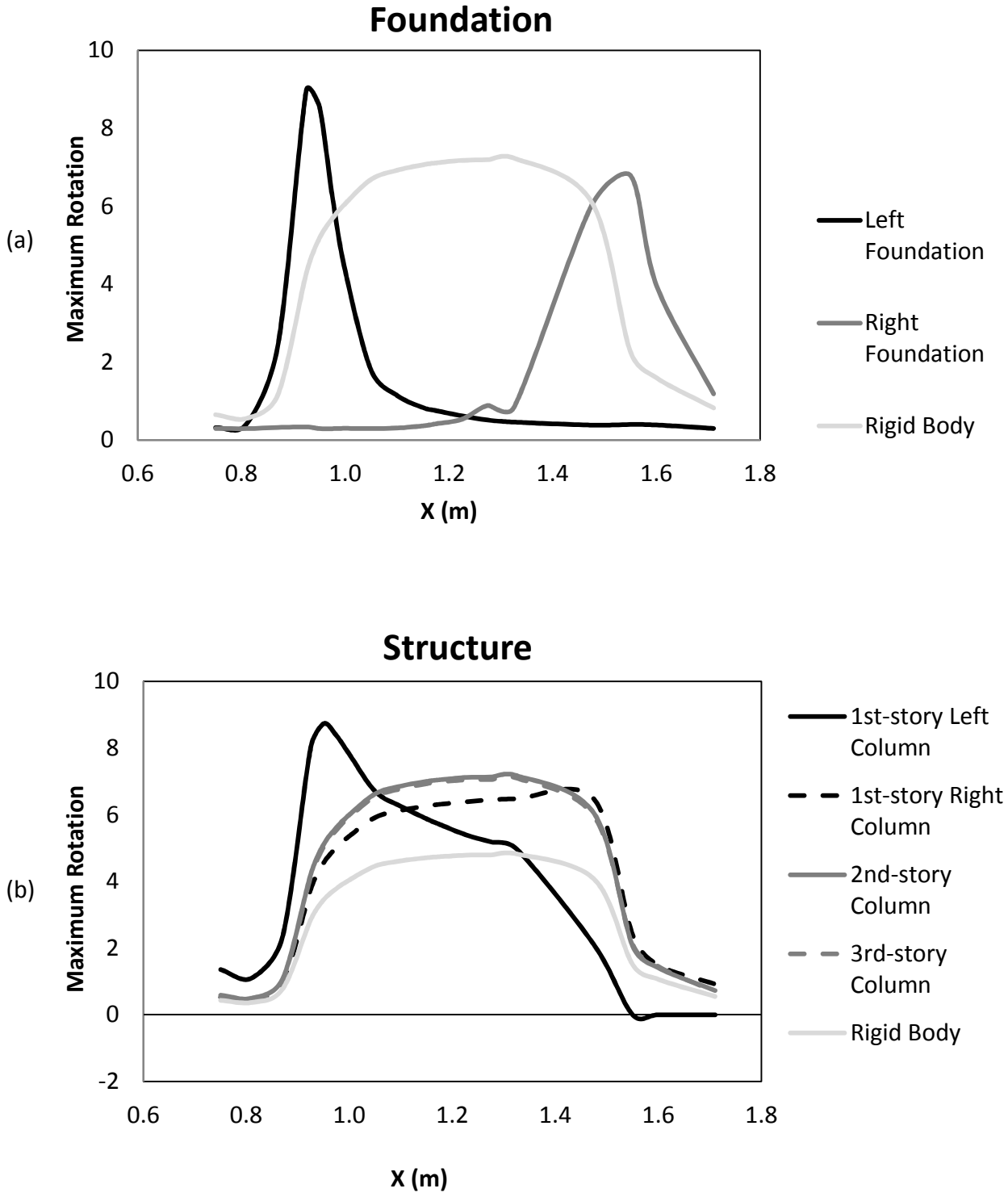

Figure 5.44 Envelope of maximum of (a) foundation, and (b) structural rotation for different locations of rupture

(a)

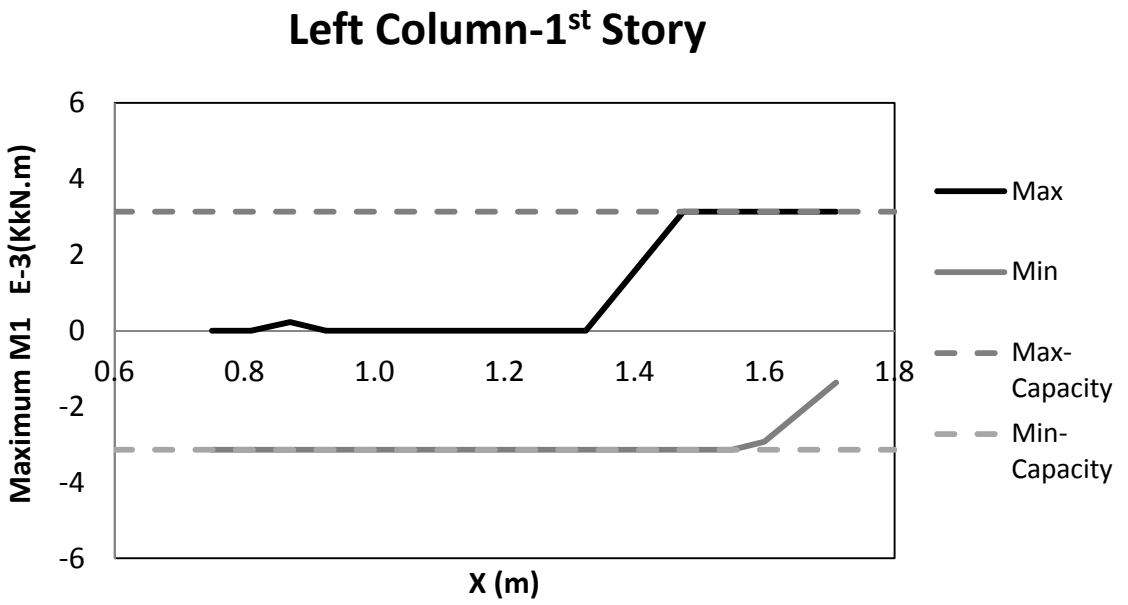

(b)

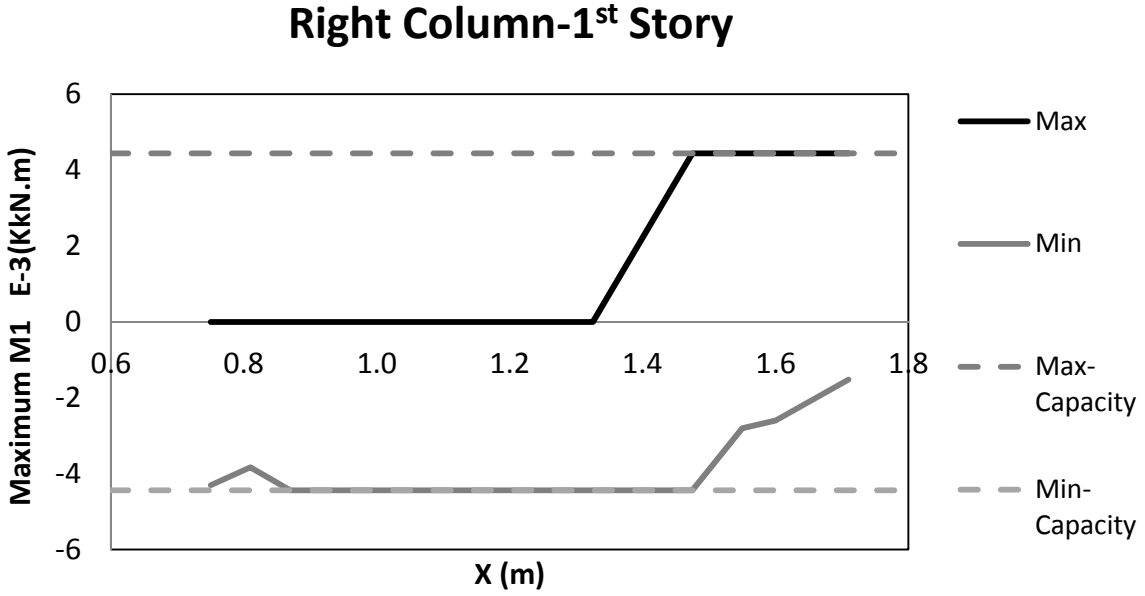

Figure 5.45 Envelope of maximum moment (M1) of (a) left, and (b) right column of 1st story for different locations of rupture

(a)

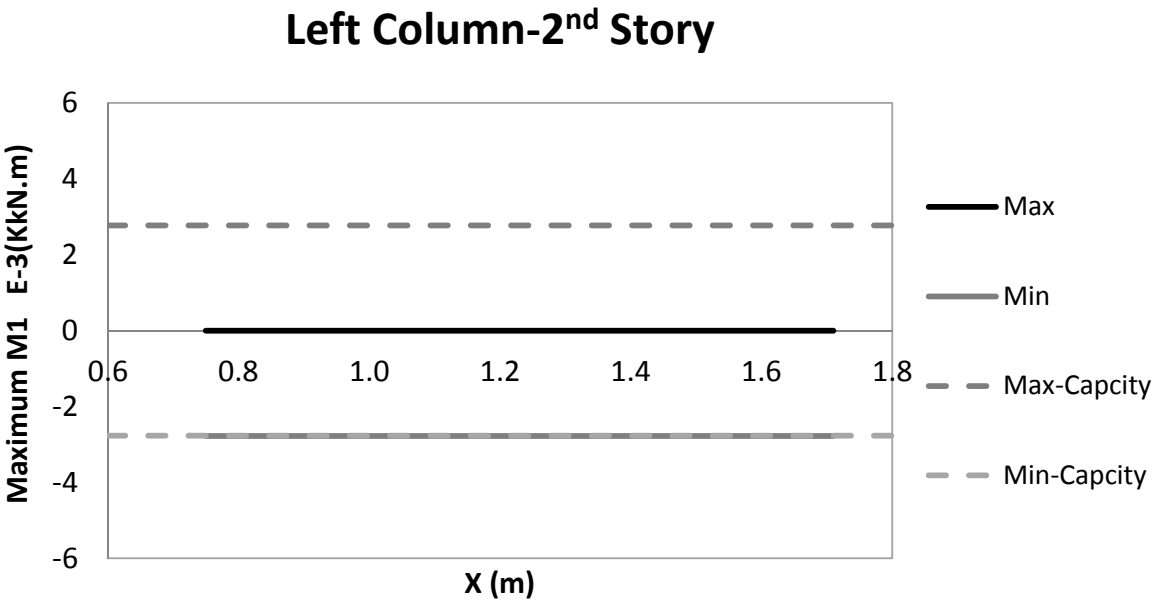

(b)

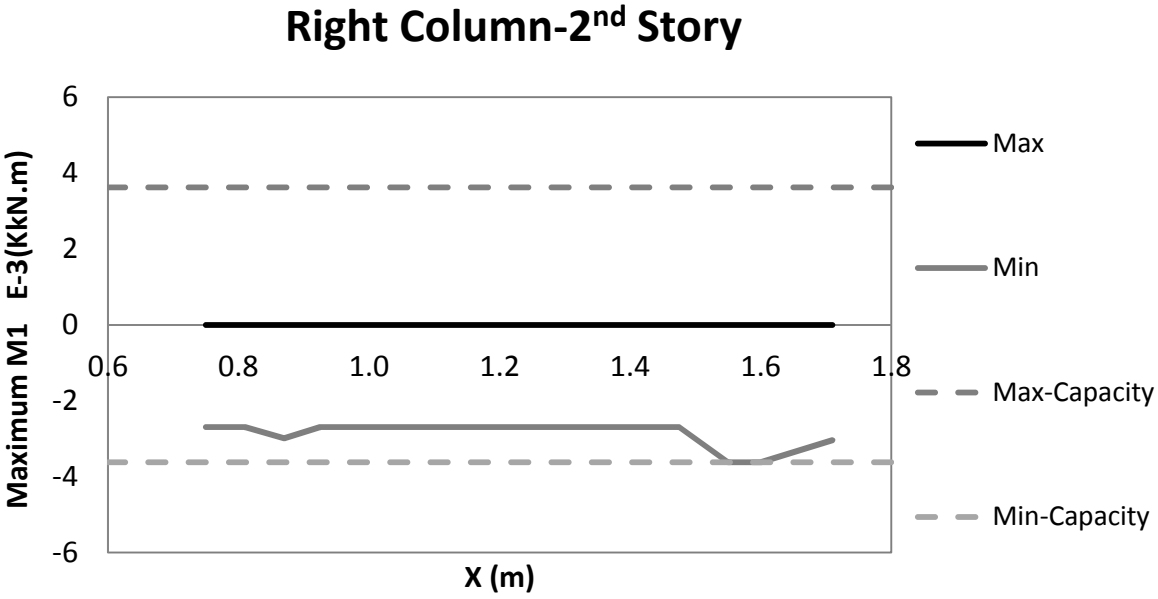

Figure 5.46 Envelope of maximum moment (M1) of (a) left, and (b) right column of **2nd** story for different locations of rupture

(a)

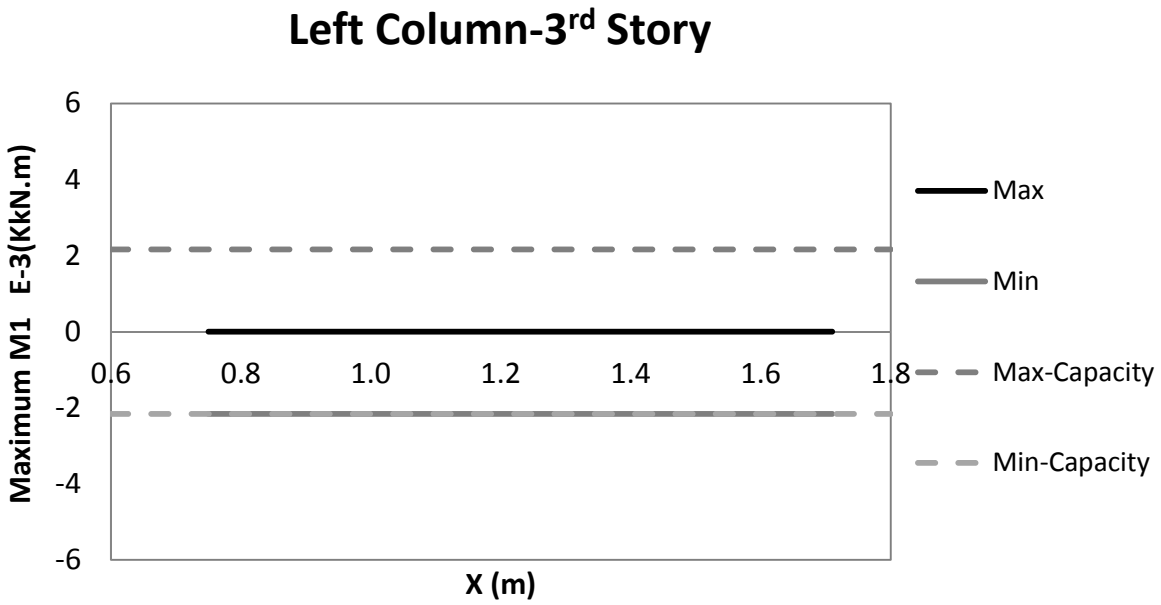

(b)

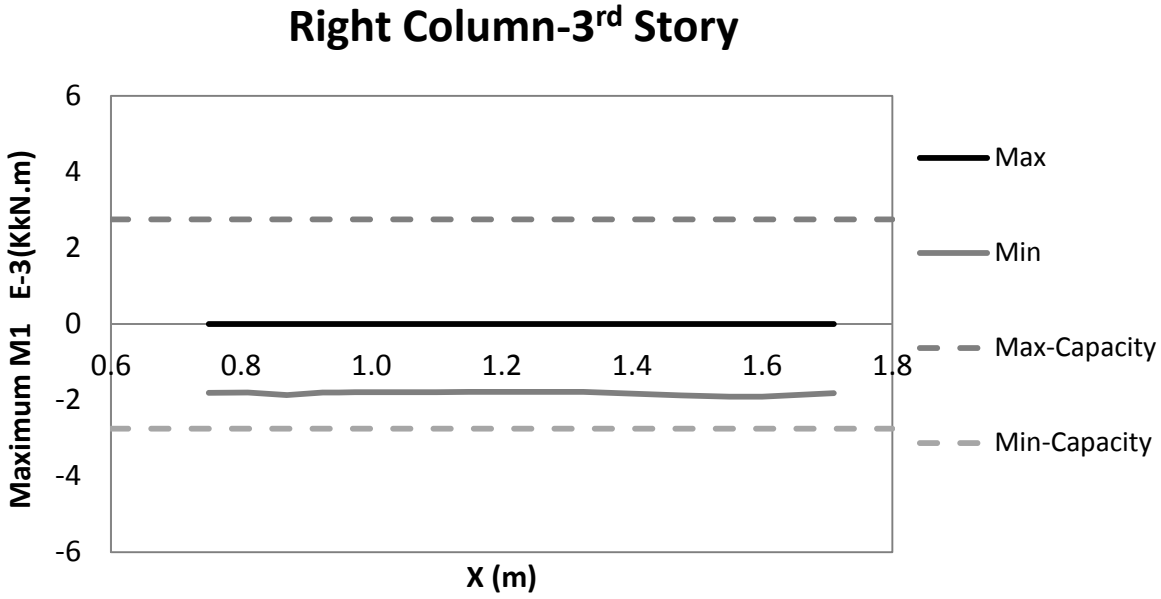

Figure 5.47 Envelope of maximum moment (M1) of (a) left, and (b) right column of **3rd** story for different locations of rupture

(a)

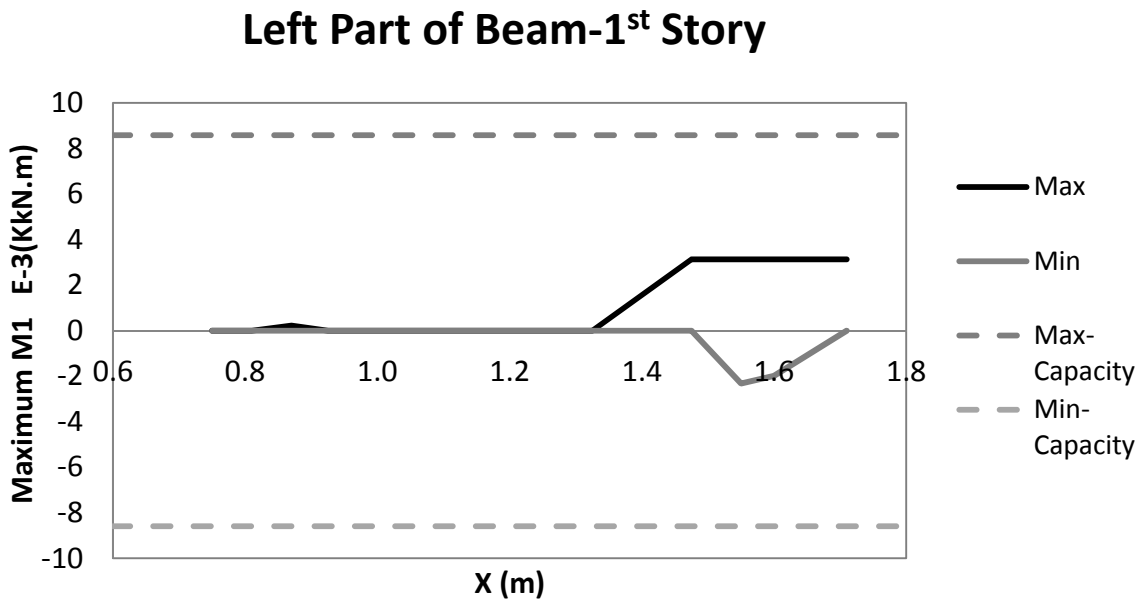

(b)

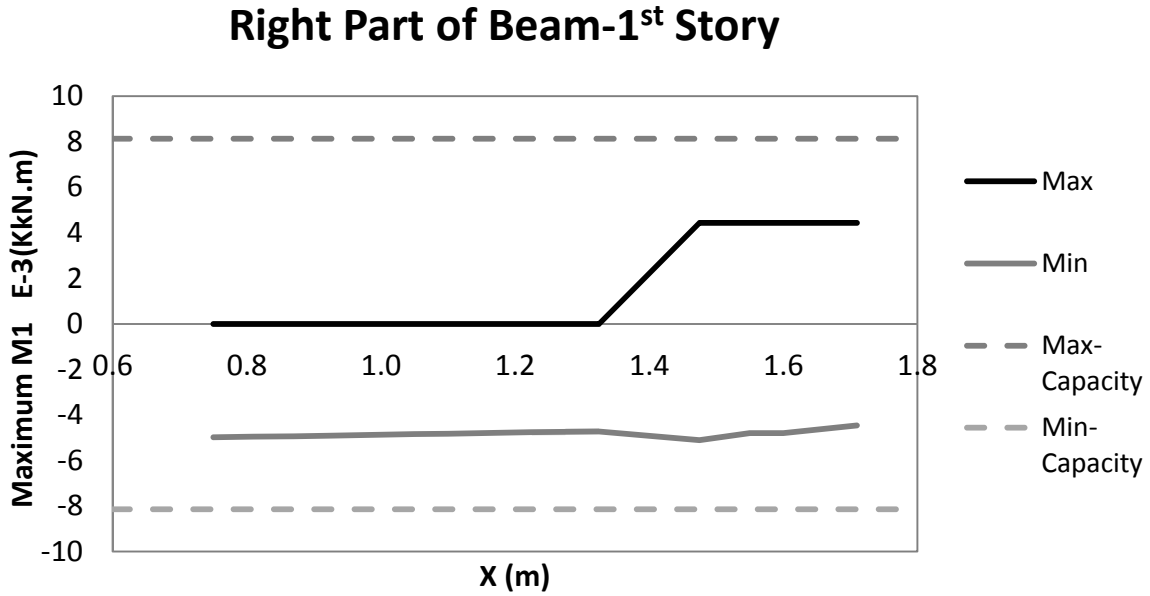

Figure 5.48 Envelope of maximum moment (M1) of (a) left, and (b) right part of beam of 1st story for different locations of rupture

(a)

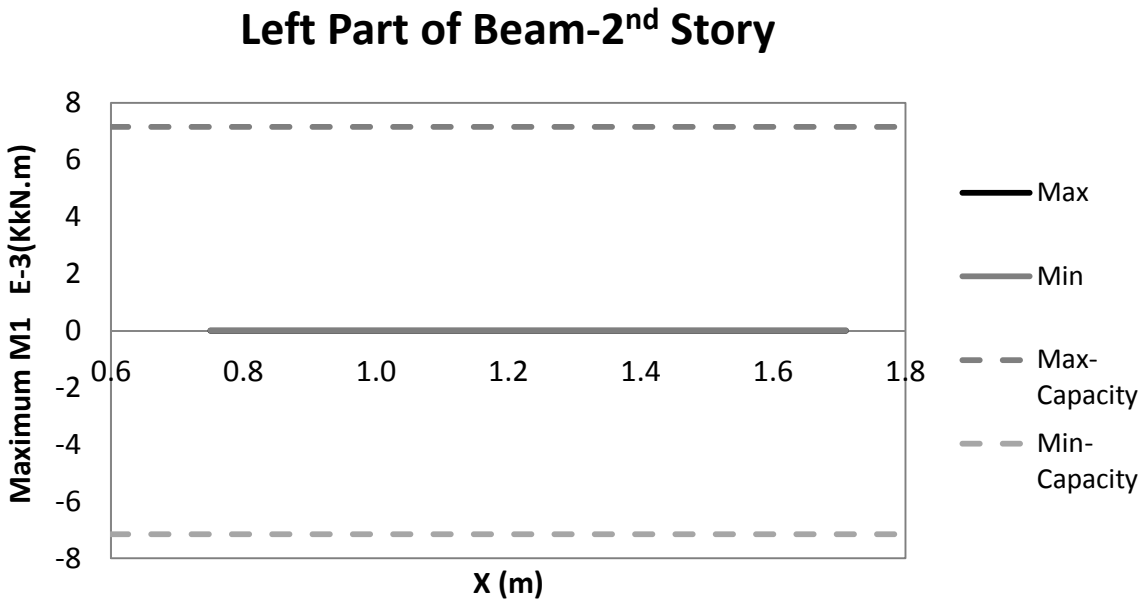

(b)

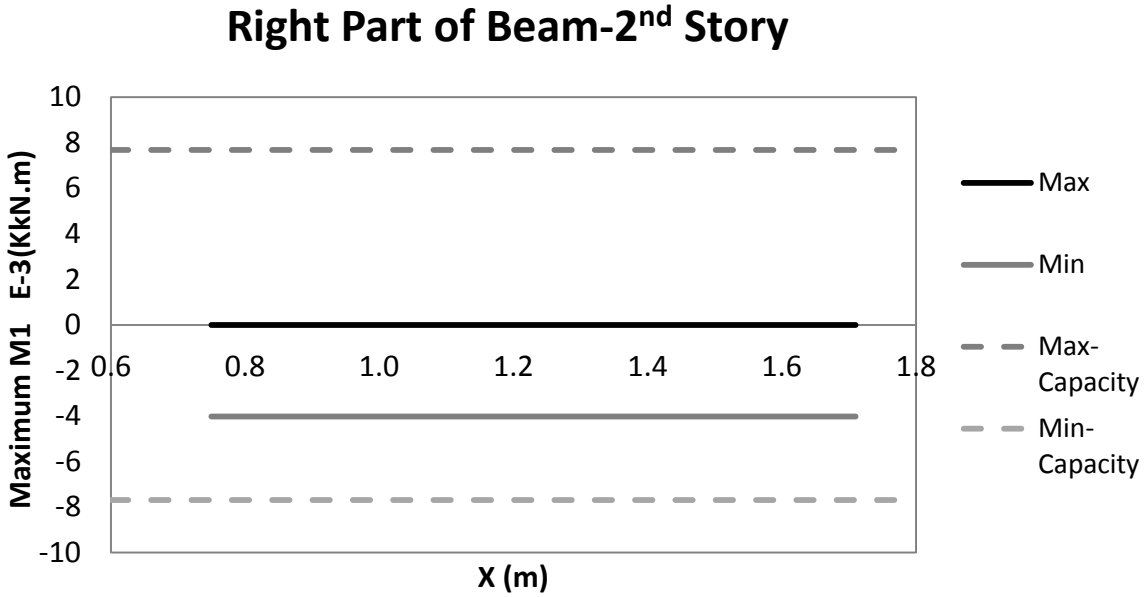

Figure 5.49 Envelope of maximum moment (M1) of (a) left, and (b) right part of beam of 2nd story for different locations of rupture

(a)

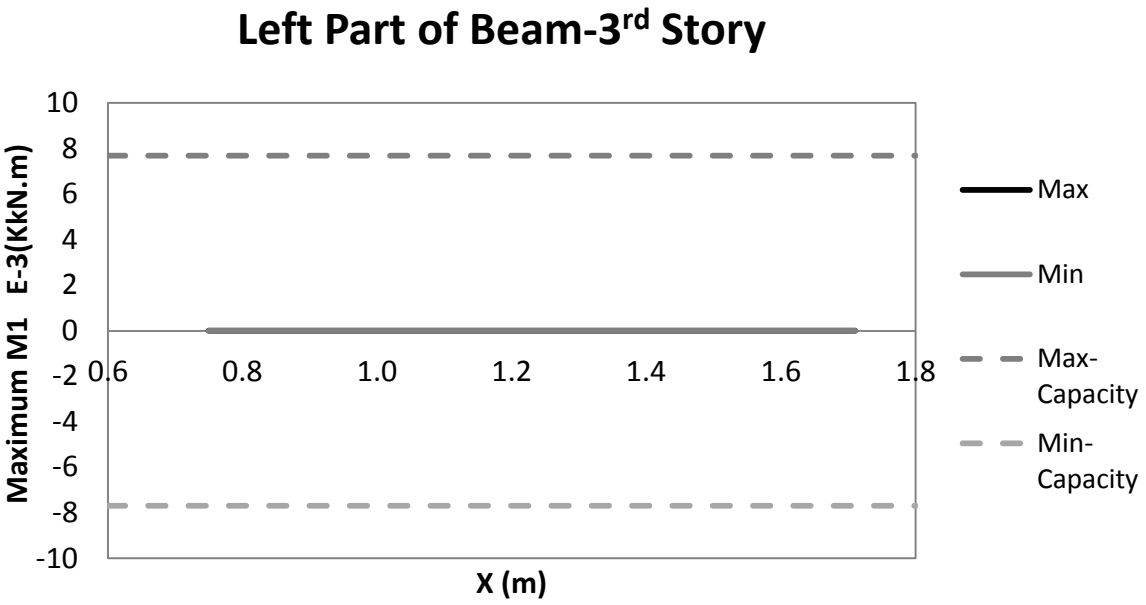

(b)

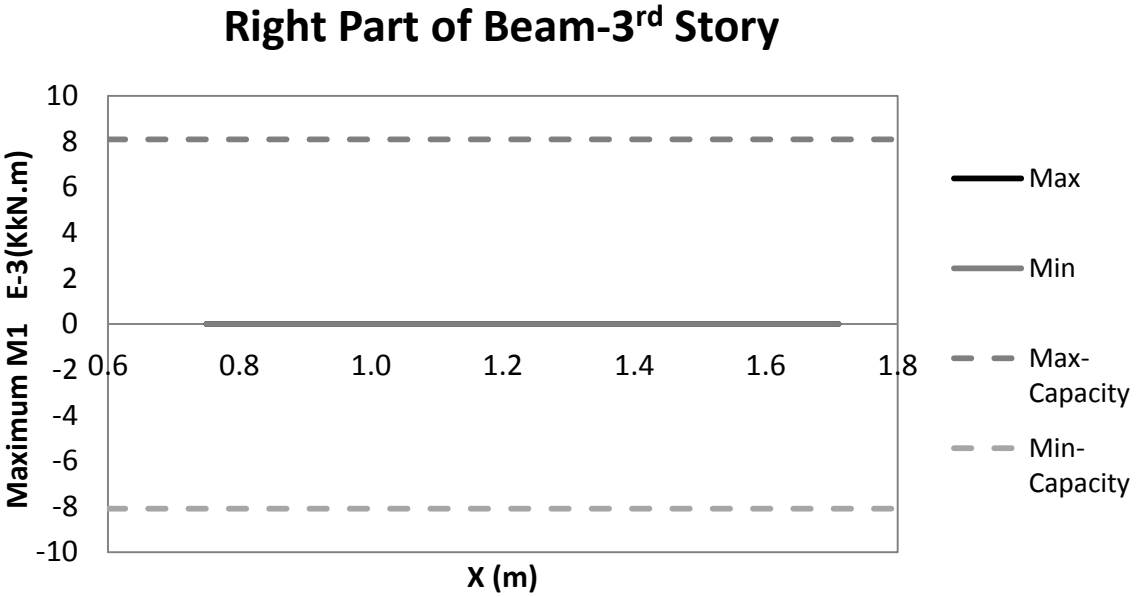

Figure 5.50 Envelope of maximum moment (M1) of (a) left, and (b) right part of beam of 3rd story for different locations of rupture

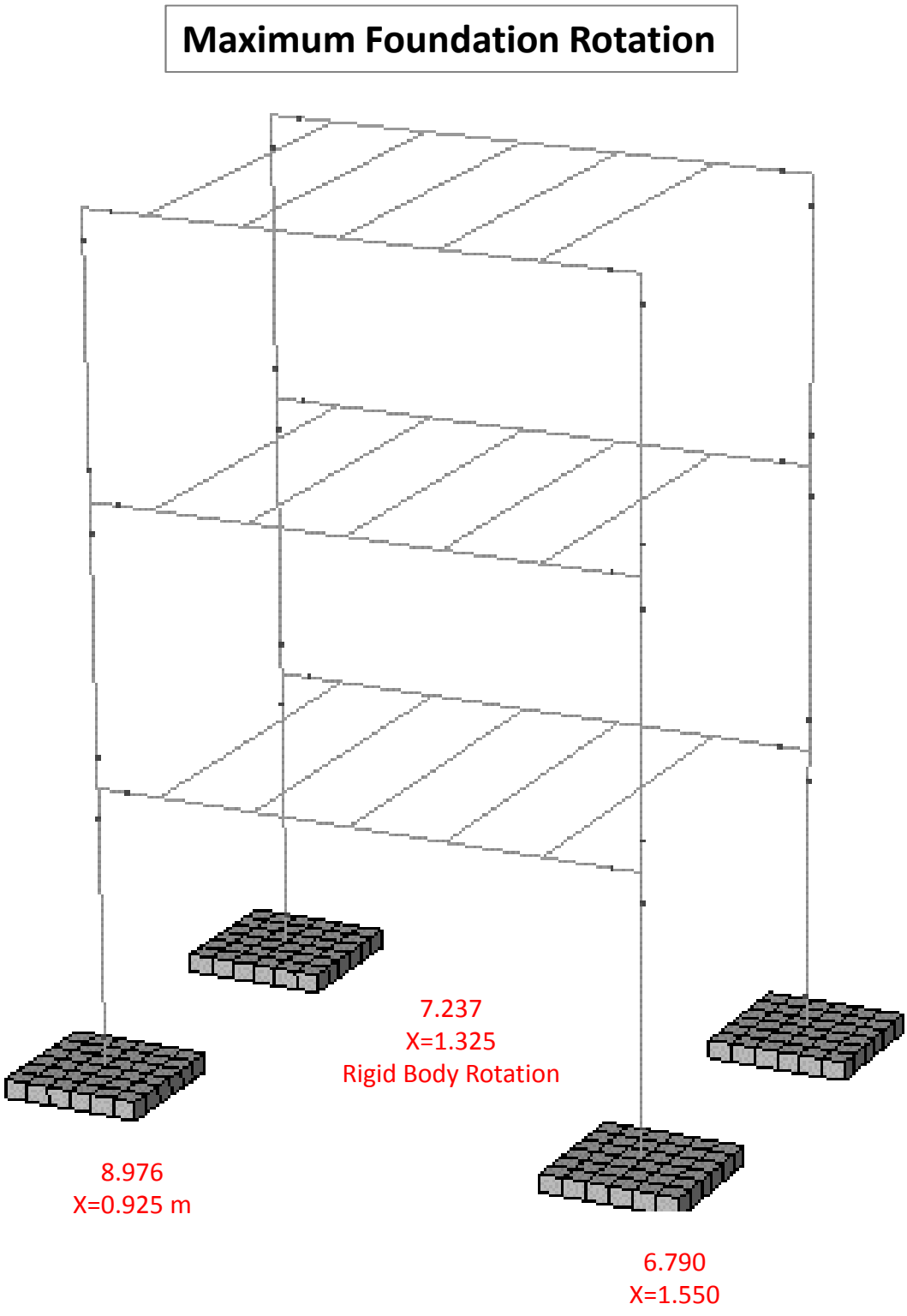

Figure 5.51 Maximum value of foundation rotation

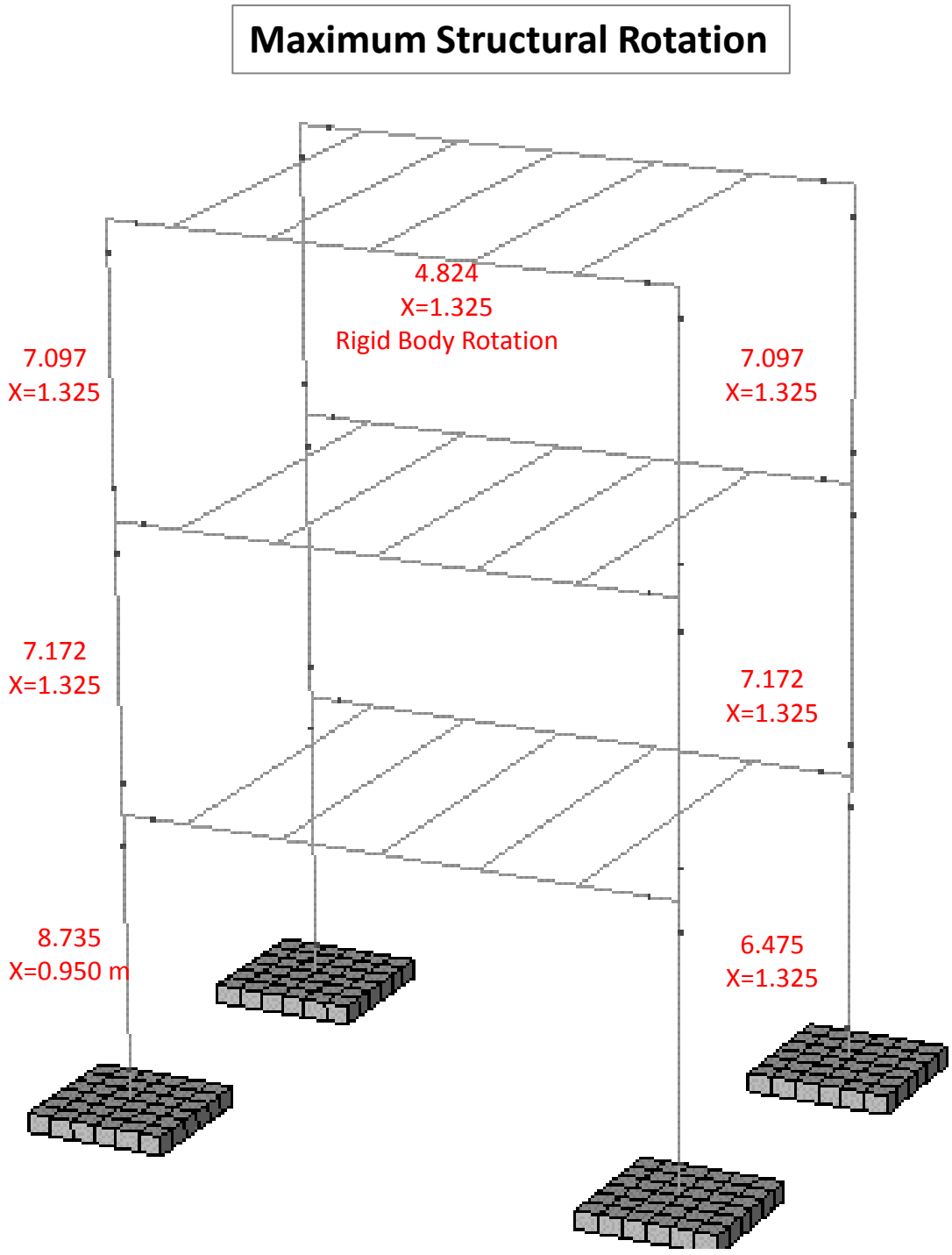

Figure 5.52 Maximum value of structural rotation

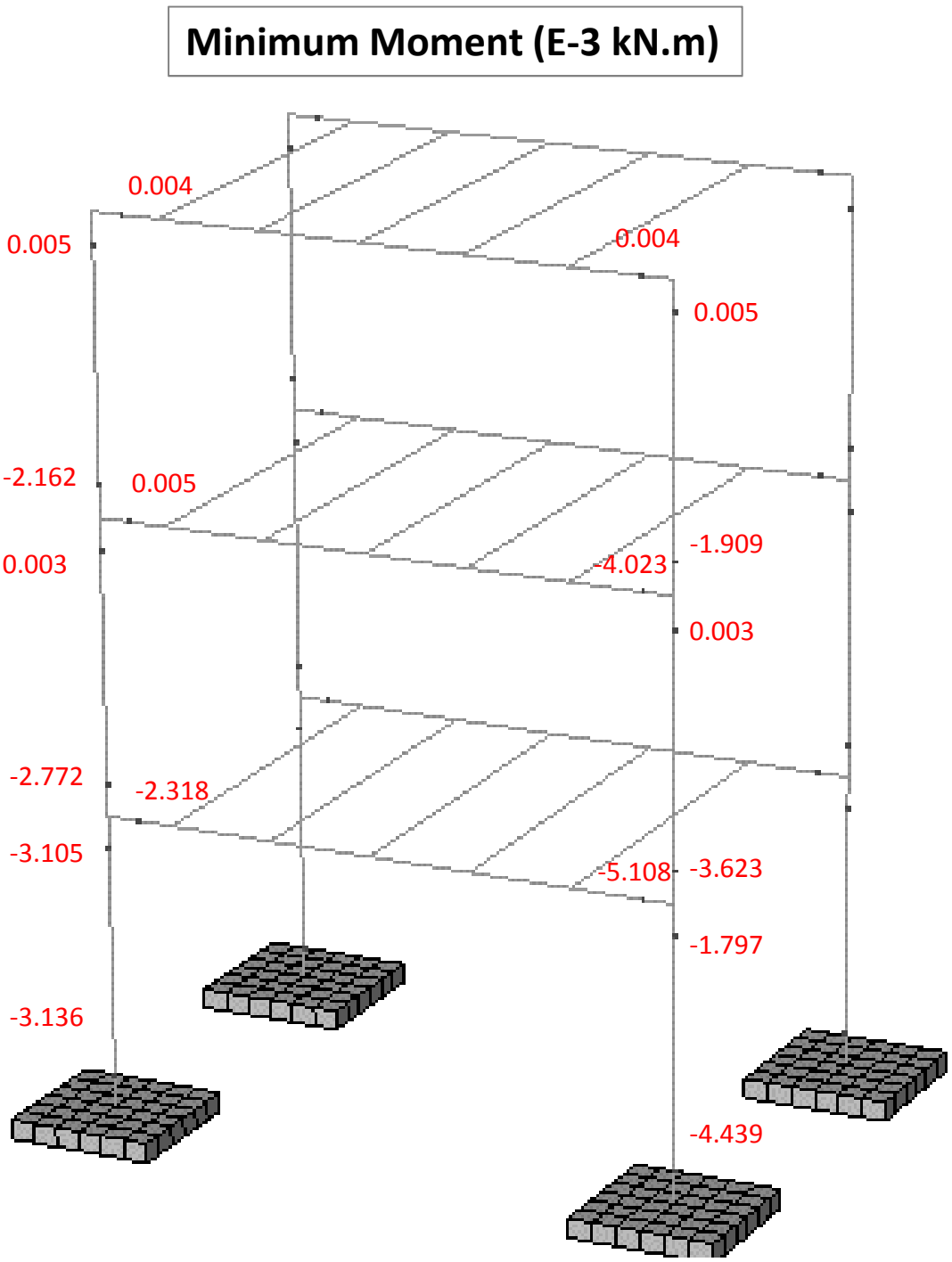

Figure 5.53 Minimum value of moment (M1) for structural elements

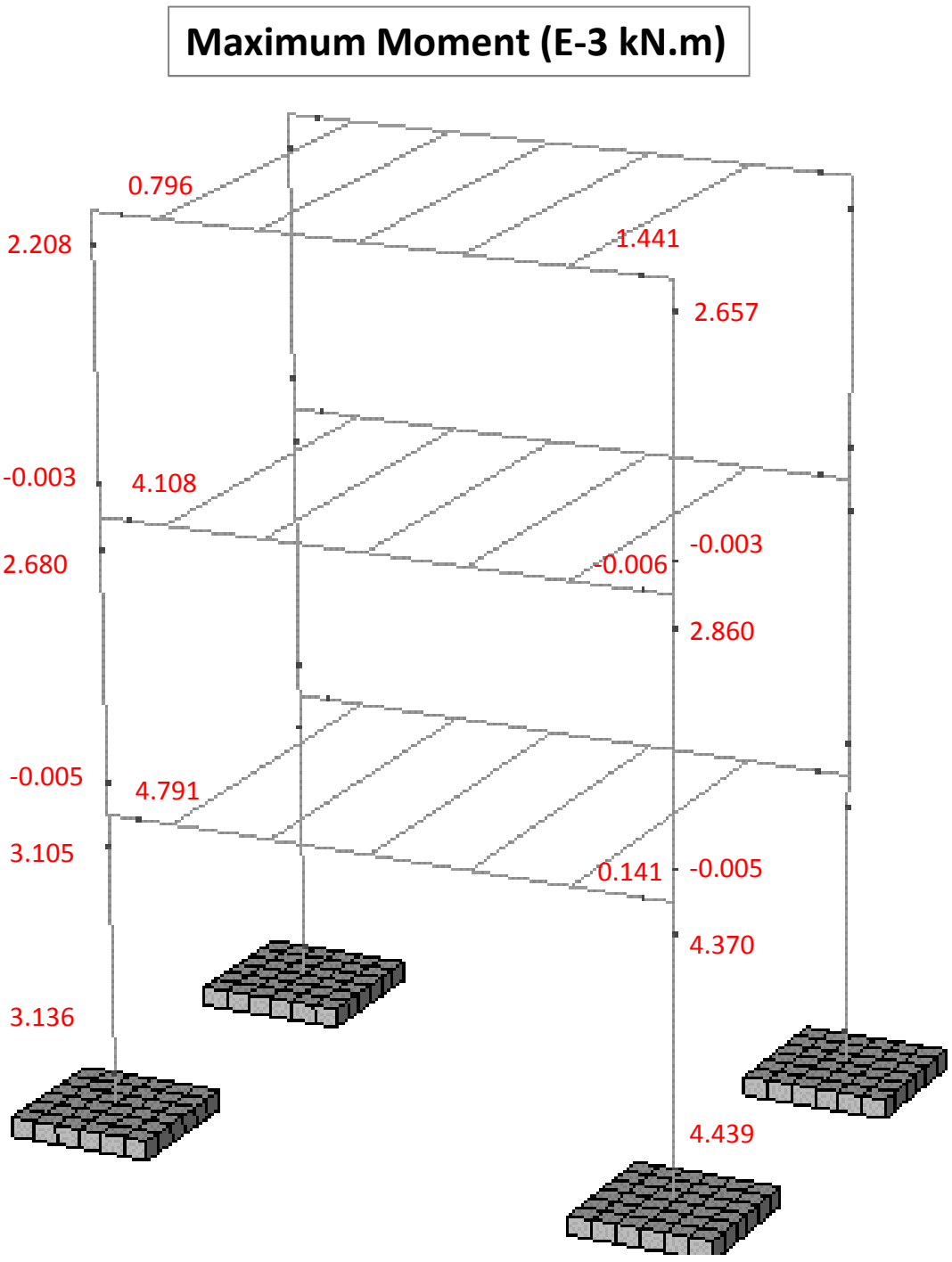

Figure 5.54 Maximum value of moment (M1) for structural elements

Chapter 6

6. Conclusion

The main conclusions of this research are as follows:

[1] Our numerical model can simulate the free field motion experiment very well.

[2] Achieving good agreement between numerical and experimental results with the presence of the structure especially for higher values of *h*

[3] The fault avoids rupturing directly underneath the footings.

[4] Like in the prototype structure which wasn't comply with capacity design principles and was prone to soft-story collapse mechanism, our reduced-scale model in ABAQUS also shows this soft-story failure and having plastic hinges in columns.

[5] Buildings on isolated footings are unable to avoid the direct hit of an underneath outcropping surface rupture. Consequently, the dislocation emerges within the structure causing significant deformation and distress.

Chapter 7

7. List of References

[1] Anastasopoulos I. & Gazetas G. (2005), "Design Against Fault Rupture: Methodology and Applications in Greece", *Proceedings of the 1st Greece – Japan Workshop: Seismic Design, Observation and Retrofit of Foundations,* Athens, October 11−12, 2005, pp. 345−366.

[2] Anastasopoulos I. (2005), Fault rupture-soil-foundation-structure interaction (FR-SFSI), Doctoral Dissertation, School of Civil Engineering, National Technical University, Athens

[3] Anastasopoulos I., Gazetas G. (2007), "Foundation–structure systems over a rupturing normal fault: Part I. Observations after the Kocaeli 1999 earthquake", *Bulletin of Earthquake Engineering,* Vol. 7, No. 5, pp. 253–275.

[4] Anastasopoulos I., Gazetas G., M.ASCE, Bransby M. F., Davies M. C. R., El Nahas A.,(2007), "Fault Rupture Propagation through Sand: Finite-Element Analysis and Validation through Centrifuge Experiments", *Journal of Geotechnical and Geoenvironmental Engineering,* ASCE, Vol. 133, No. 8, pp. 943-958.

[5] Anastasopoulos I., Callerio A., Bransby M. F., Davies M. C. R., El Nahas A., Faccioli E., Gazetas G., Masella A., Paolucci R., Pecker A., Rossignol E. (2008), "Numerical analyses of fault–foundation interaction", *Bulletin of Earthquake Engineerin,*

[6] Anastasopoulos I., Gazetas G., Drosos V., Georgarakos T., and Kourkoulis R. (2008a), "Design of bridges against large tectonic deformation", *Earthquake Engineering and Engineering Vibration*, Vol. 7, No. 4, pp. 345–368.

[7] Anastasopoulos, I., Gerolymos, N., Drossos, V., Kourkoulis, R., Georgarakos, P., Gazetas, G. (2008b), "Behaviour of Deep Immersed Tunnel under Combined Major Fault Rupture and Strong Seismic Shaking", *Bulletin of Earthquake Engineering*, Vol. 6, No.2, pp. 213–239.

[8] Anastasopoulos I., Gazetas G., Bransby M.F., Davies M.C.R., and El Nahas A. (2009), "Normal Fault Rupture Interaction with Strip Foundations", *Journal of Geotechnical and Geoenvironmental Engineering*, ASCE, Vol. 135, No. 3, pp. 359-370.

[9] Anastasopoulos I., Antonakos G., Gazetas G. (2010), "Slab Foundations subjected to Thrust Faulting: Parametric Analysis and Simplified Design Method", *Soil Dynamics & Earthquake Engineering*, Vol. 30, No. 10, pp. 912–924.

[10] Anastasopoulos I., Georgarakos T., Georgiannou V., Drosos V., Kourkoulis R. (2010), "Seismic performance of bar-mat reinforced-soil retaining wall: Shaking table testing versus numerical analysis with modified kinematic hardening constitutive model", *Bulletin of Soil Dynamics and Earthquake Engineering,* pp. 1089-1105.

[11] Antonaki N (2012), Experimental study of rocking isolation: Application to the retrofit of ax existing building. Master Thesis, School of Civil Engineering, National Technical University, Athens

[12] Bransby M.F., Davies M.C.R., El Nahas A., Nagaoka S. (2008), "Centrifuge modelling of reverse fault-foundation interaction", *Bulletin of Earthquake Engineering*, Vol. 6, No. 4, pp. 607-628.

[13] Bray JD (1990), The effects of tectonic movements on stresses and deformations in earth embankments. Ph.D. Dissertation, University of California, Berkeley

[14] Bray JD, Seed RB, Cluff LS, Seed HB (1994a). Earthquake fault rupture propagation through soil. J Geotech Eng ASCE 120(3):543–561

[15] Bray JD, Seed RB, Seed HB (1994b), Analysis of earthquake fault rupture propagation through cohesive soil. J Geotech Eng ASCE 120(3):562–580

[16] Bray J.D. (2001), "Developing mitigation measures for the hazards associated with earthquake surface fault rupture", *Seismic Fault-Induced Failures Workshop*, Japan Society for the Promotion of Science, University of Tokyo, Japan, pp. 55-79.

[17] Cole D.A. Jr., Lade P.V. (1984), "Influence Zones in Alluvium Over Dip-Slip Faults", J*ournal of Geotechnical Engineering*, ASCE, Vol. 110, No. GT5, pp. 599-615.

[18] Erickson SG, Staryer LM, Suppe J (2001), Initiation and reactivation of faults during movement over a thrust fault ramp: numerical mechanical models. J Struct Geol 23:11–23

[19] Faccioli E., Anastasopoulos I., Gazetas G., Callerio A., Paolucci R. (2008). Fault rupture–foundation interaction: selected case histories. *Bulletin of Earthquake Engineering.*

[20] Lade P.V., Cole D.A., Cummings D. (1984), "Multiple failure surfaces over dip-slip faults", *Journal of Geotechnical Engineering*, ASCE, Vol. 110, No. GT5, pp. 616–627.

[21] Loukidis D (1999), Active fault propagation through soil. Diploma Thesis, School of Civil Engineering, National Technical University, Athens

[22] Roth WH, Scott RF,Austin I (1981), Centrifuge modeling of fault propagation through alluvial soils. Geophys Res Lett 8(6):561–564

[23] Roth WH, Sweet J, Goodman RE (1982), Numerical and physical modeling of flexural Slip phenomena and potential for fault movement. Rock Mech 12:27–46 (Suppl.)

[24] Tuladhar, R. (2006). Seismic behavior of concrete pile foundation embedded in cohesive soil, Ph.D. Dissertation, Saitama University, Japan

[25] Ulusay, R., Aydan, O., Hamada, M. (2002), The Behavior of Structures Built on Active Fault Zones: Examples from the recent earthquakes of Turkey, *Structural Engineering & Earthquake Engineering*, JSCE, Vol. 19, No. 2, pp. 149–167.

[26] Yilmaz M.T., Paolucci R., (2007), "Earthquake Fault Rupture–Shallow Foundation Interaction in Undrained Soils: a Simplified Analytical Approach", *Earthquake Engineering and Structural Dynamics*, Vol. 36, No. 1, pp. 101–118.

Appendix A

12 x 200/30/8 aluminium

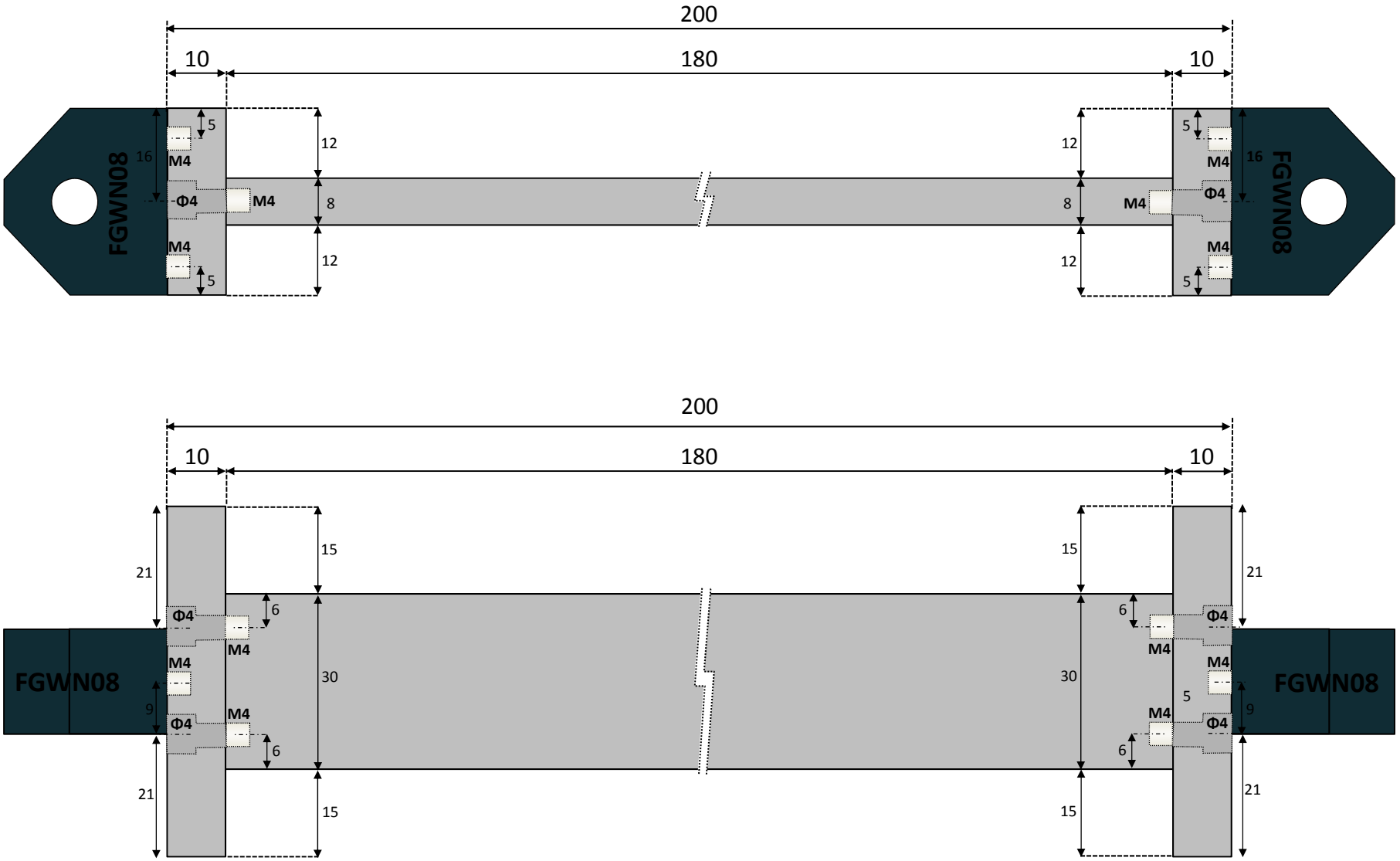

6 x 500/60/8 aluminium

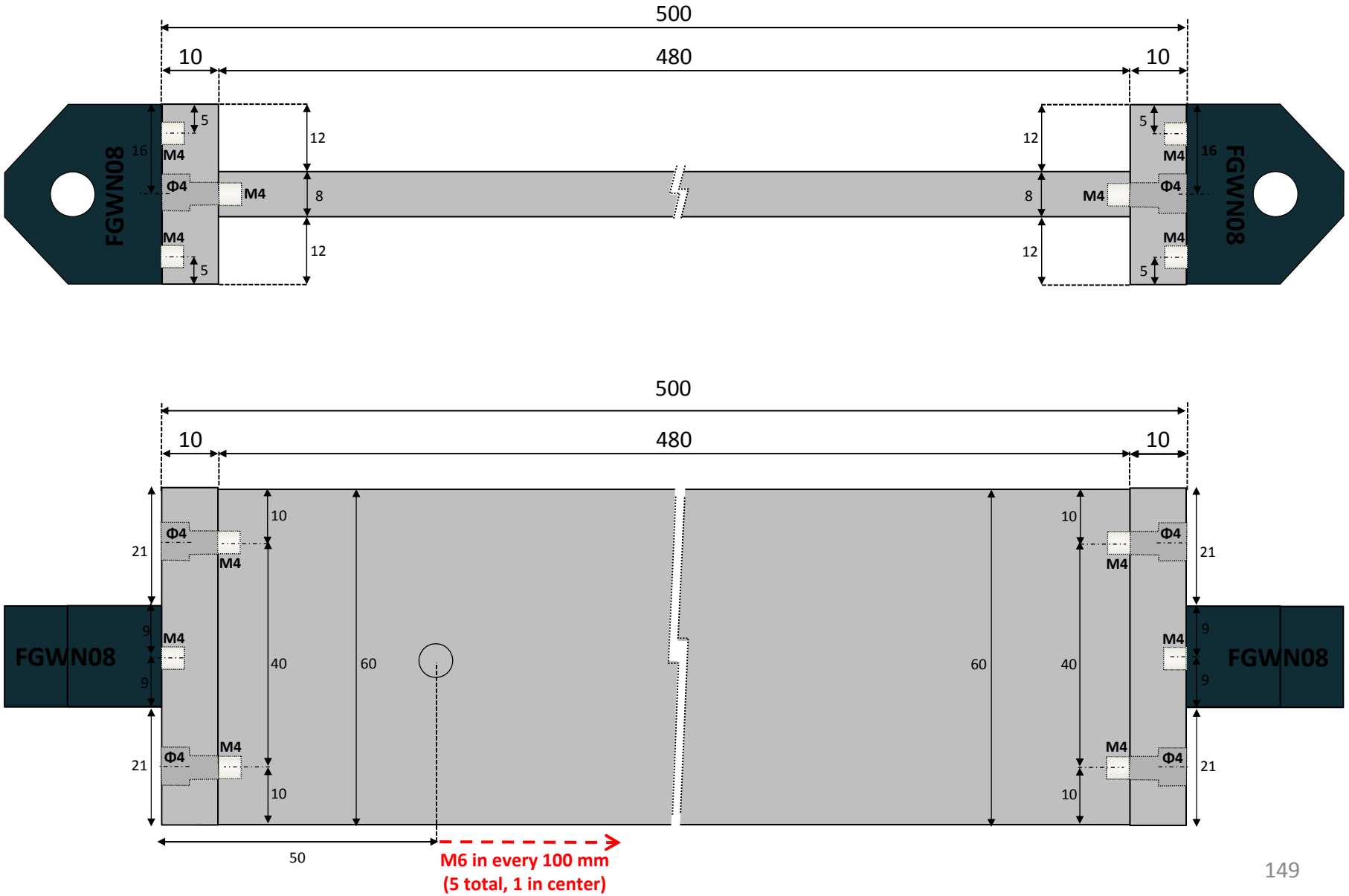

8 x

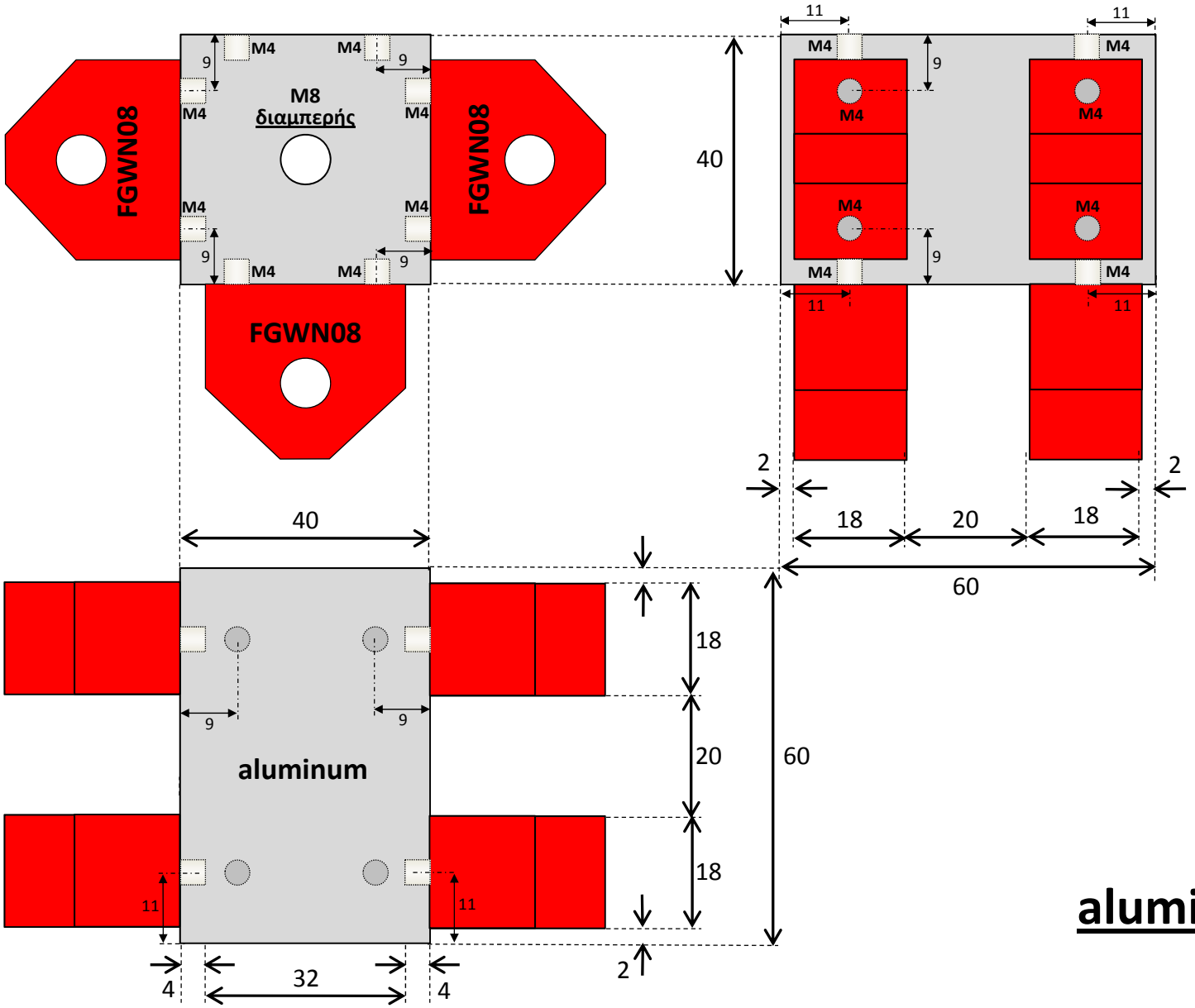
FGWN08
FGWN08
FGWN08
M8
διαμπερής
M4
9
40
11
2
18
20
60
aluminum
32
4

aluminum

4 x

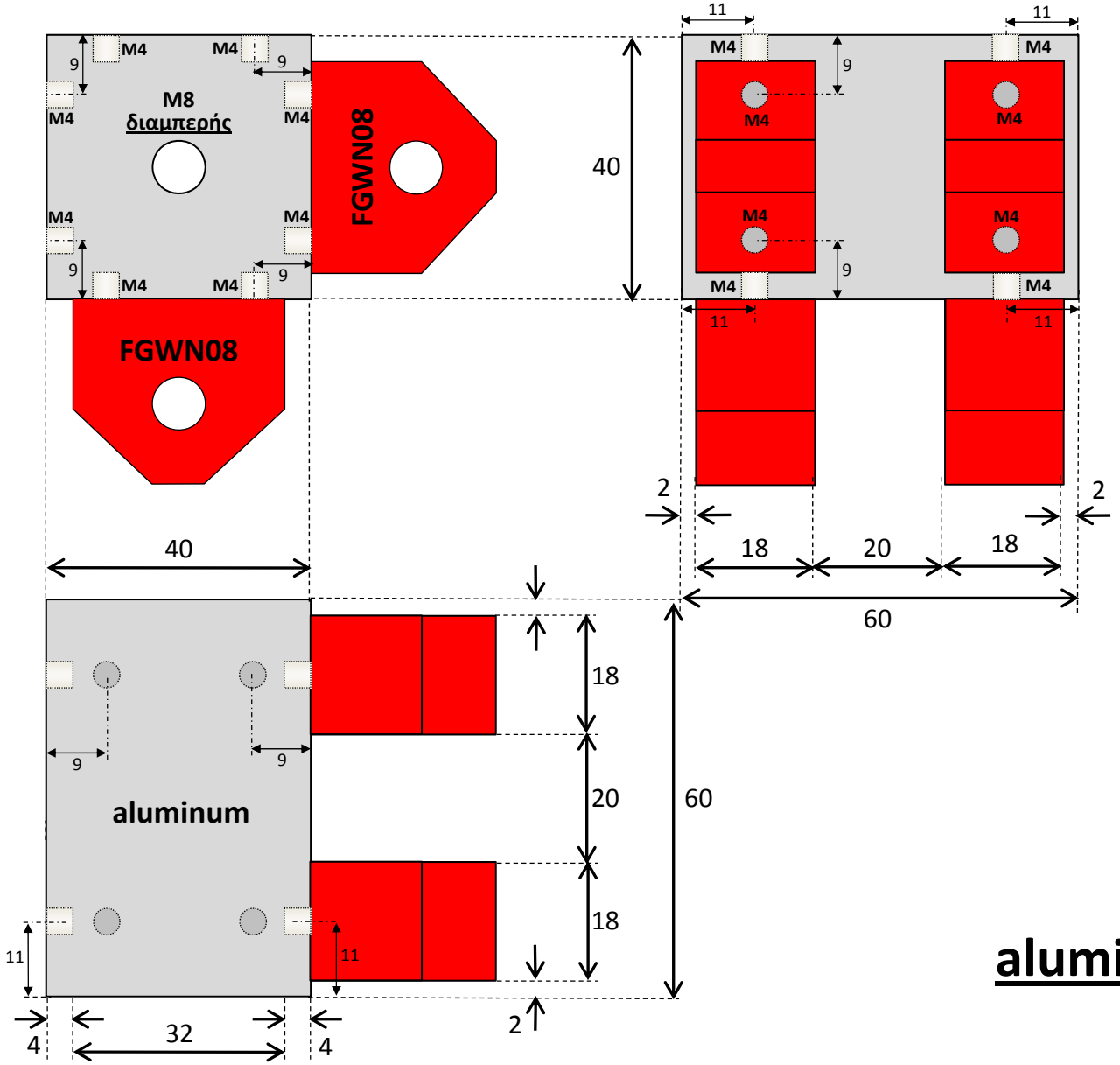

aluminum

4 x

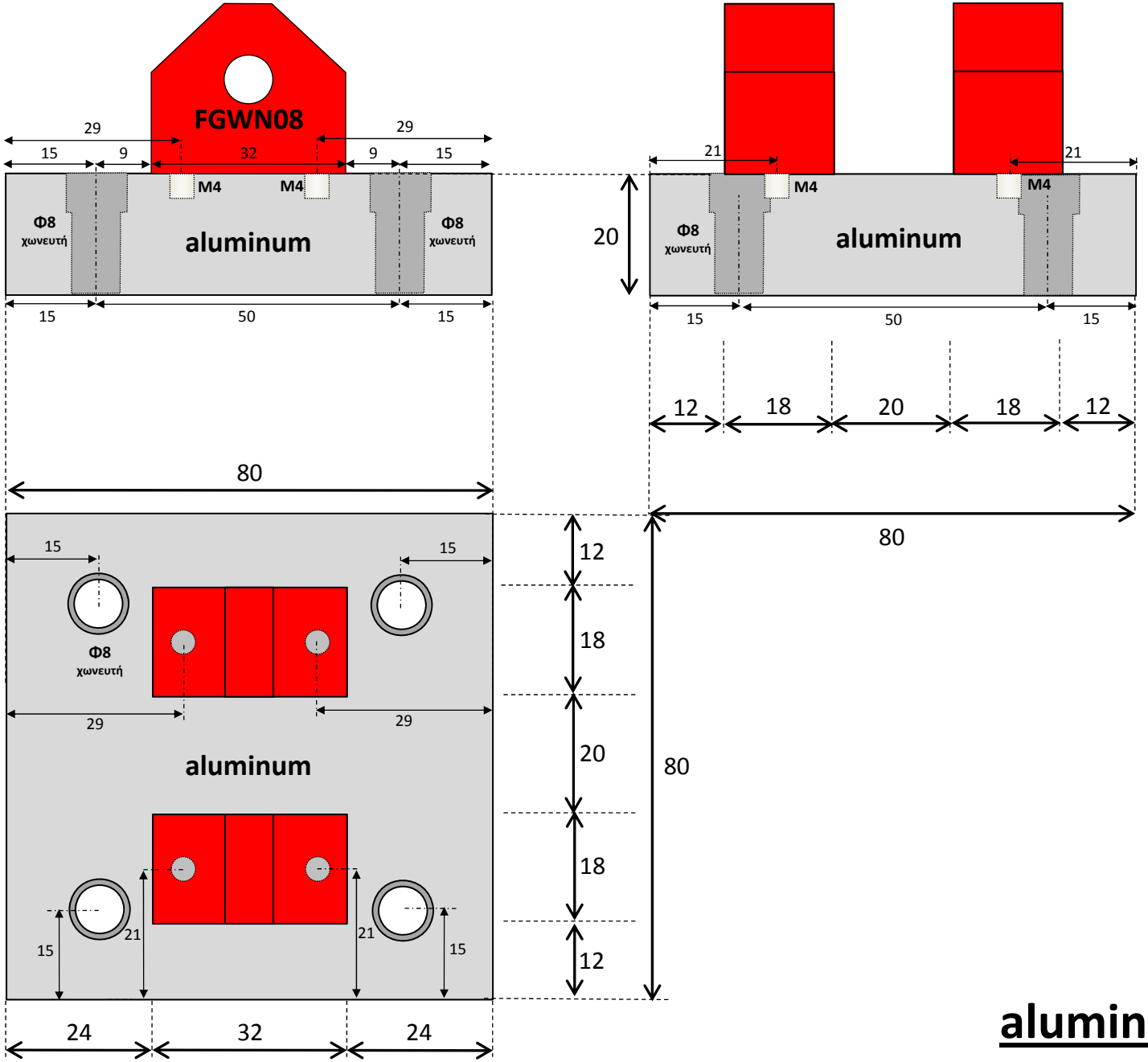
FGWN08
29
15
9
32
9
15
29
M4
M4
Φ8
χωνευτή
aluminum
Φ8
χωνευτή
15
50
15
20
21
21
M4
M4
Φ8
χωνευτή
aluminum
15
50
15
12
18
20
18
12
80
80
15
15
Φ8
χωνευτή
29
29
aluminum
21
21
15
15
12
18
20
18
12
80
24
32
24

aluminum

4 x

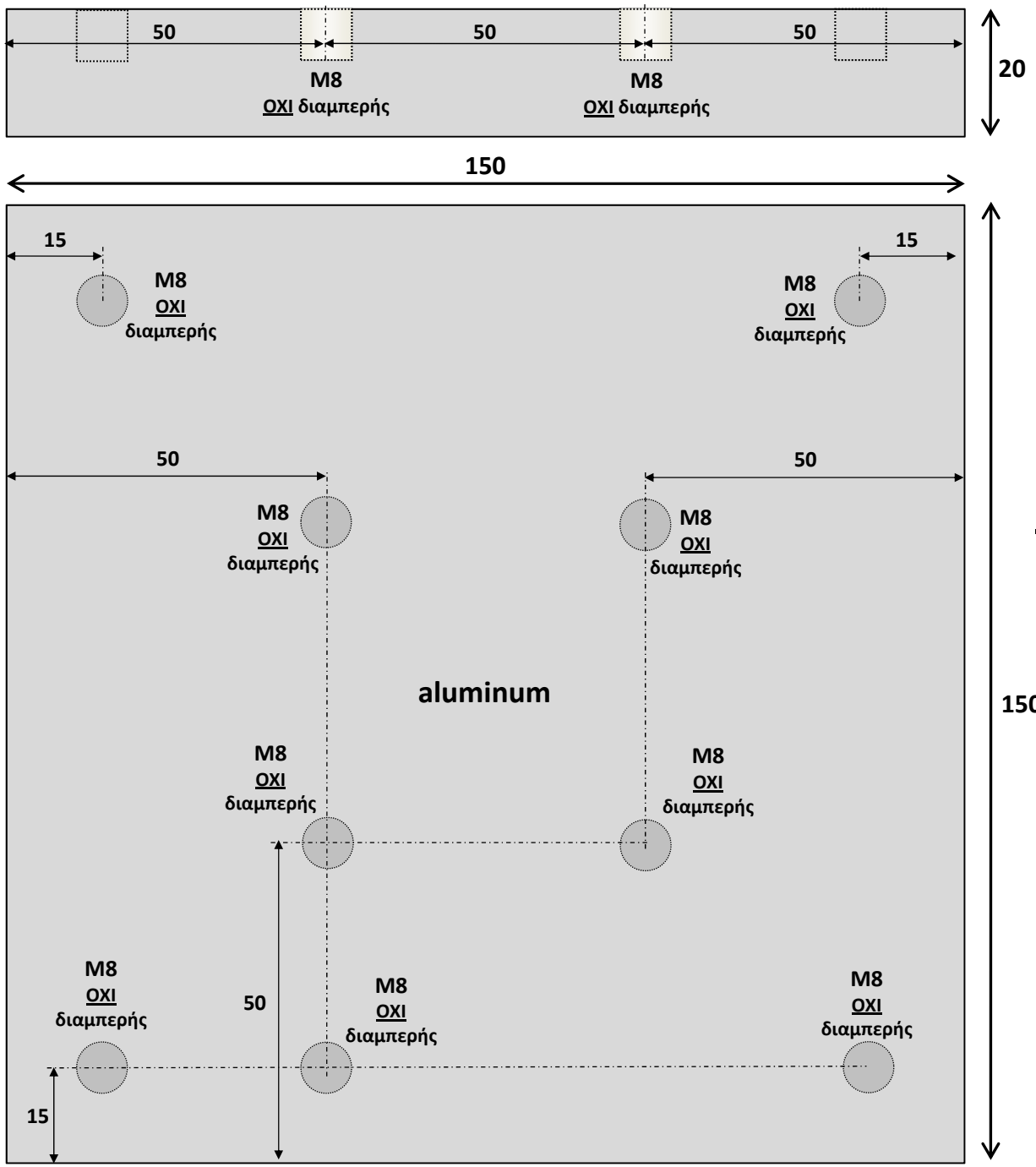
50
50
50
20
M8
OXI διαμπερής
M8
OXI διαμπερής
150
15
15
M8
OXI
διαμπερής
M8
OXI
διαμπερής
50
50
M8
OXI
διαμπερής
M8
OXI
διαμπερής
aluminum
M8
OXI
διαμπερής
M8
OXI
διαμπερής
M8
OXI
διαμπερής
M8
OXI
διαμπερής
M8
OXI
διαμπερής
50
15
150

aluminum

15 x

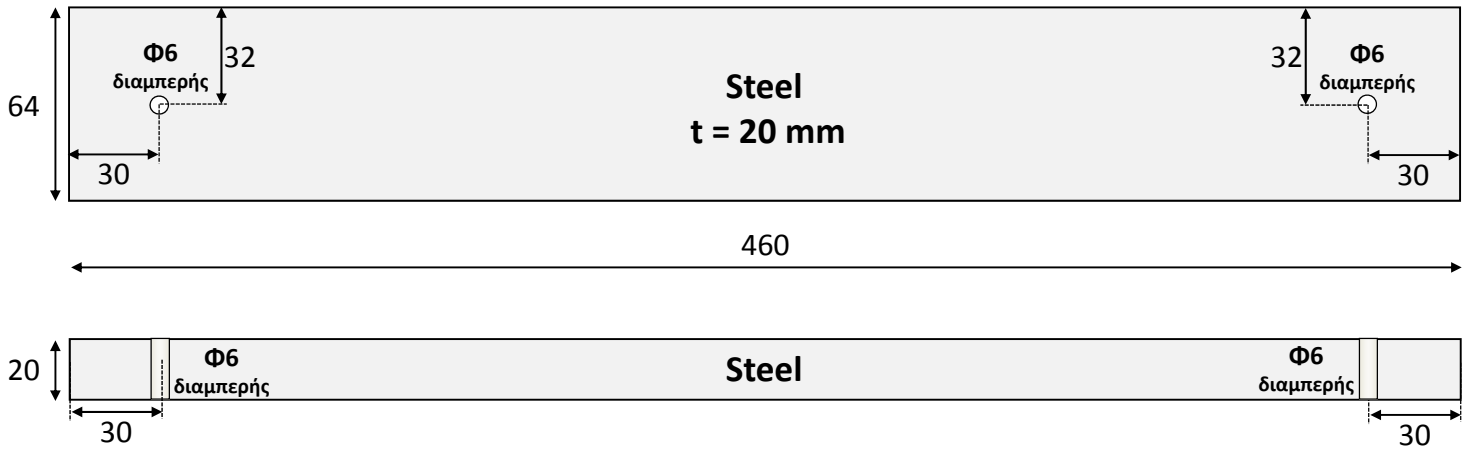
64
Φ6
διαμπερής
32
30
Steel
t = 20 mm
32
Φ6
διαμπερής
30
460
20
Φ6
διαμπερής
30
Steel
Φ6
διαμπερής
30

Appendix B

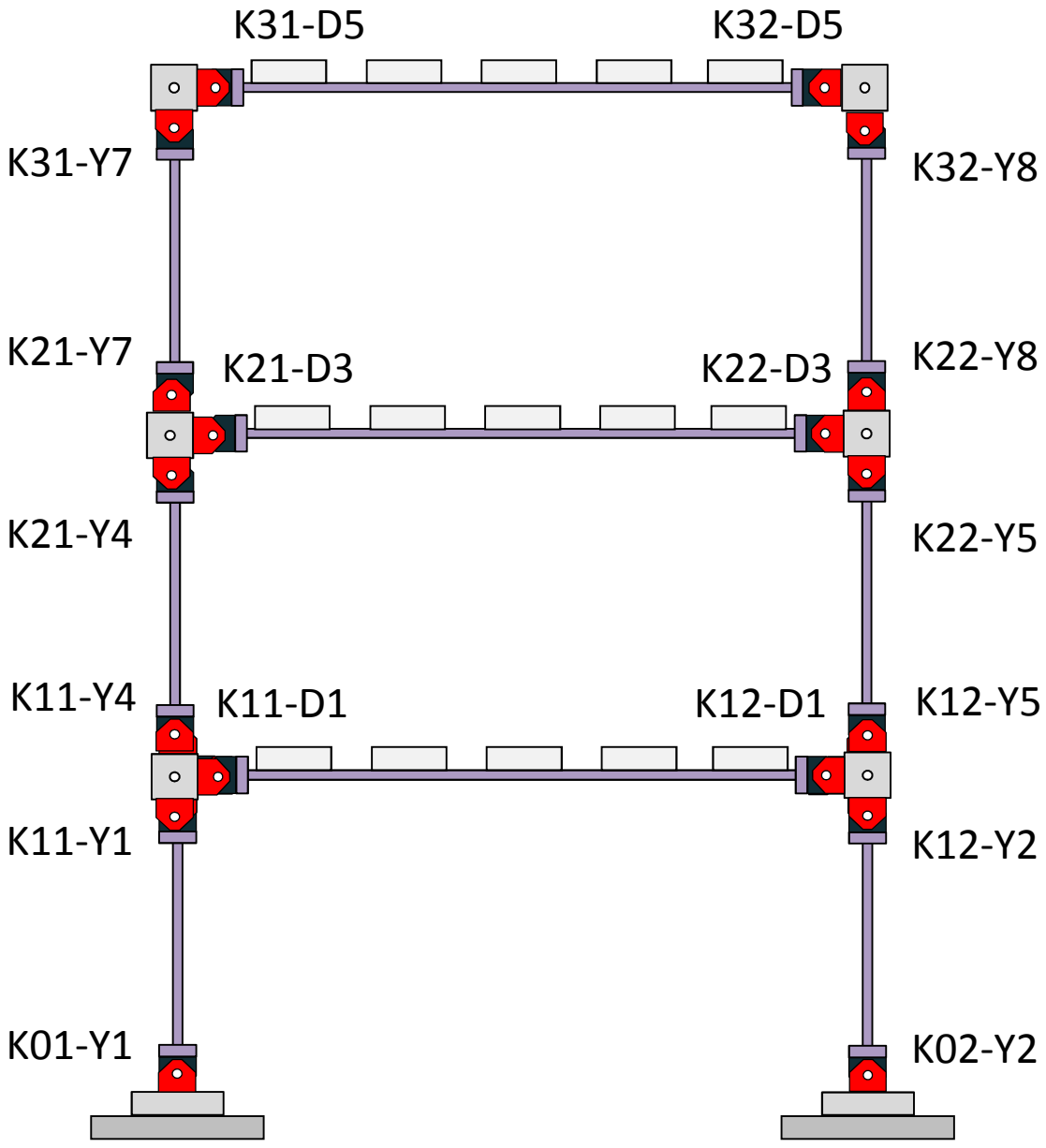

Figure B.1 Schematic illustration of model building and the naming of the connections.

(a)

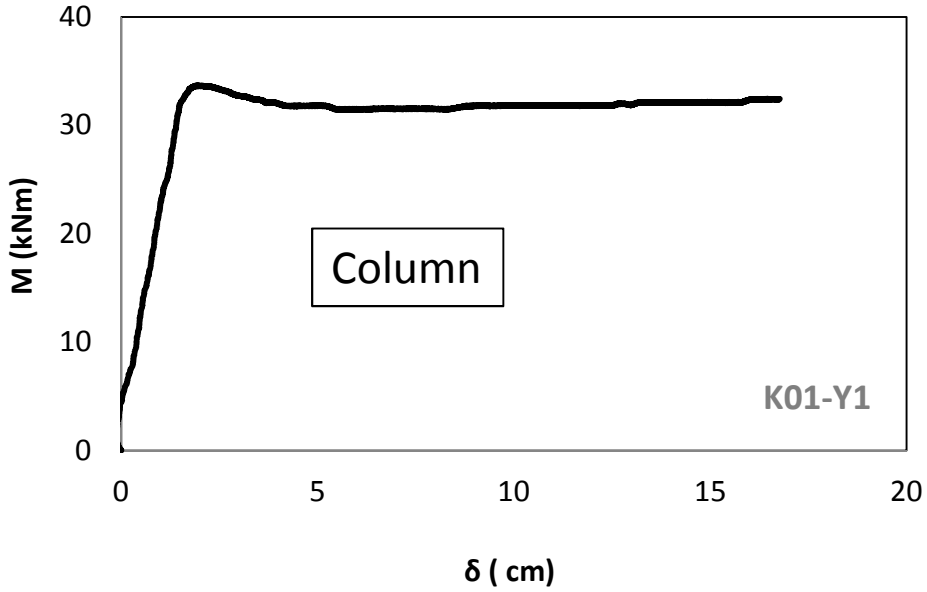

(b)

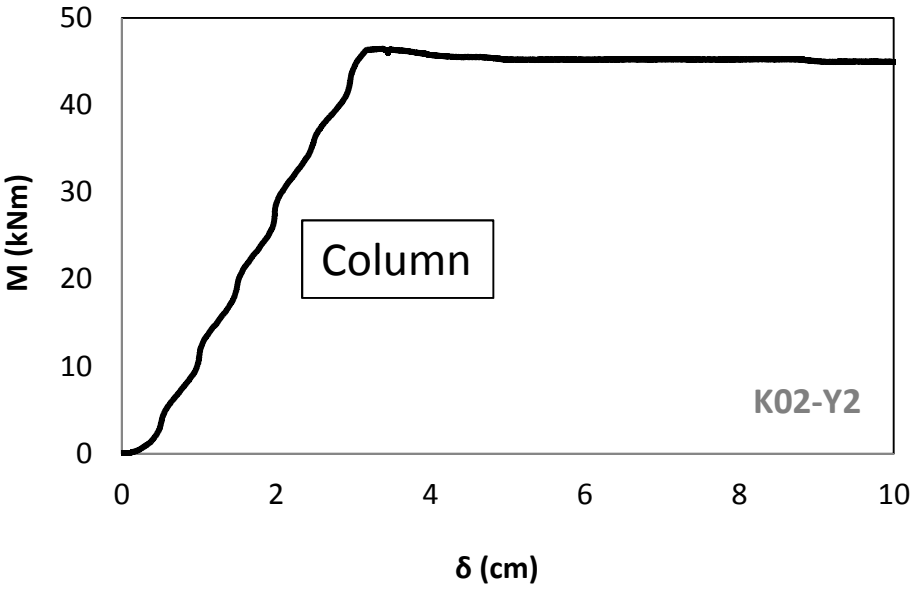

Figure B.2 Bending moment with regard to displacement diagrams derived from the calibration of the artificial plastic hinges for column – footing connections.

(a)

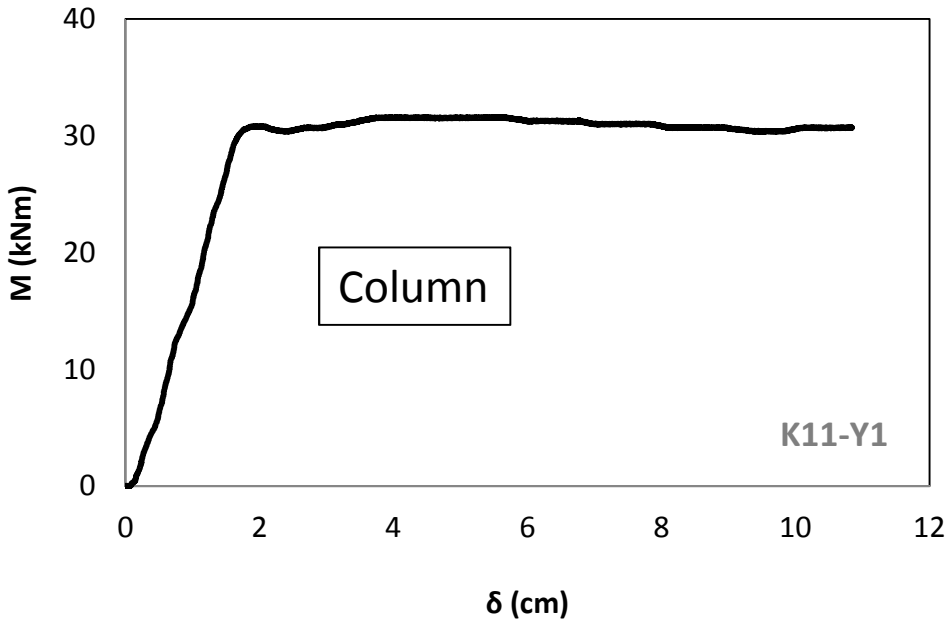

(b)

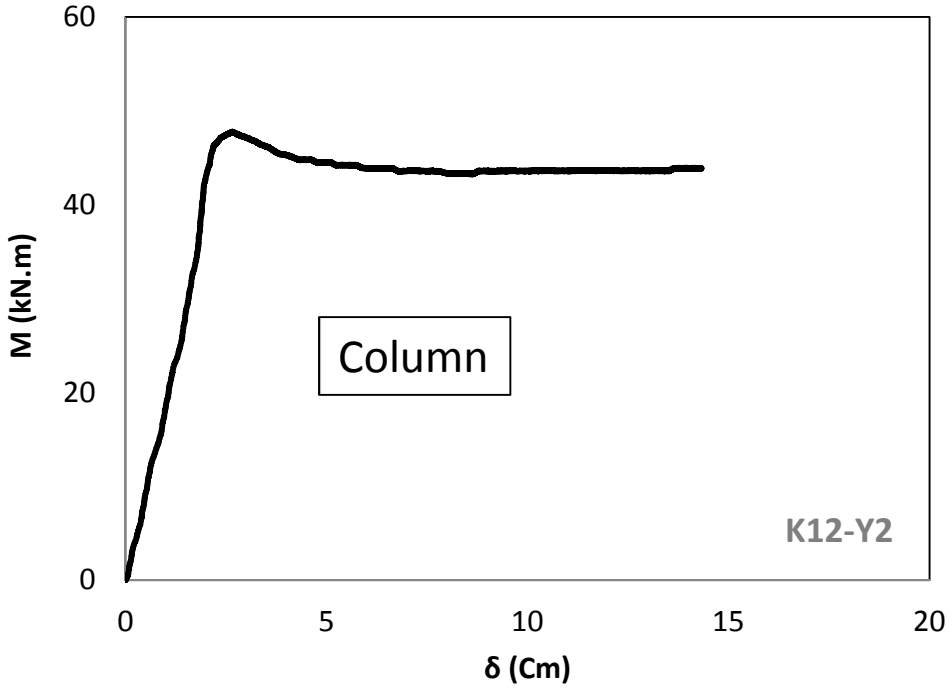

Figure B.3 Bending moment with regard to displacement diagrams derived from the calibration of the artificial plastic hinges for column – beam connections.

(a)

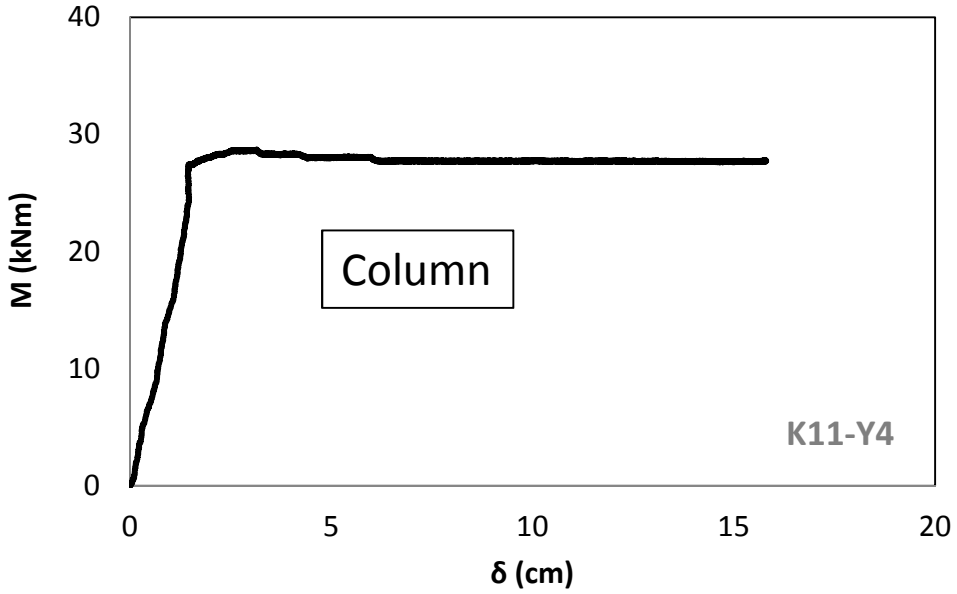

(b)

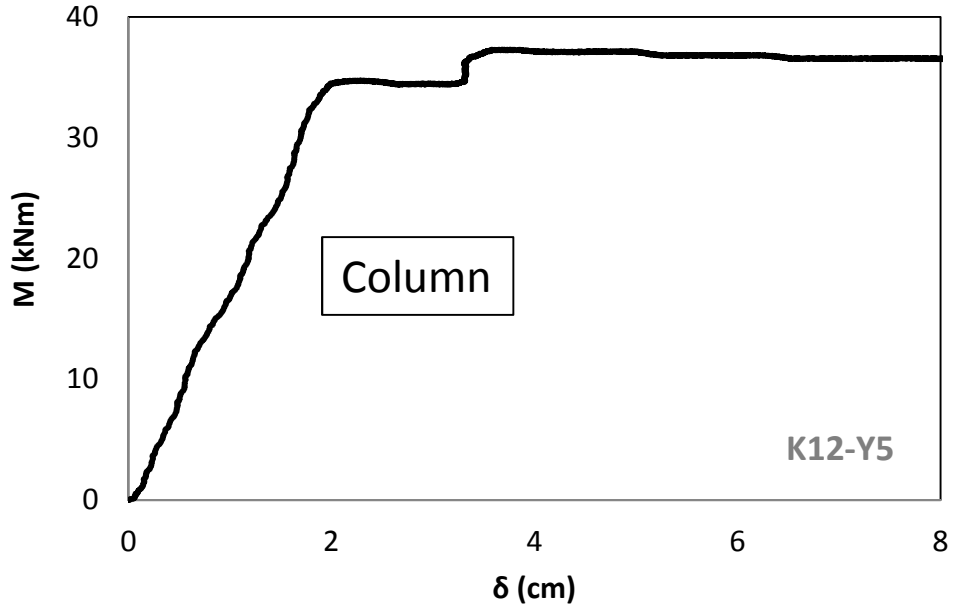

Figure B.4 Bending moment with regard to displacement diagrams derived from the calibration of the artificial plastic hinges for column – beam connections.

(a)

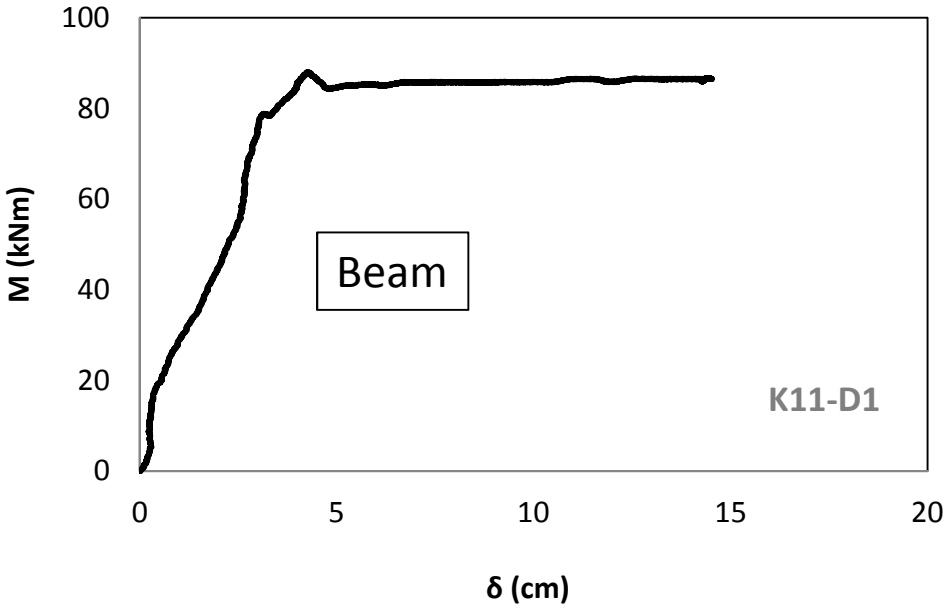

(b)

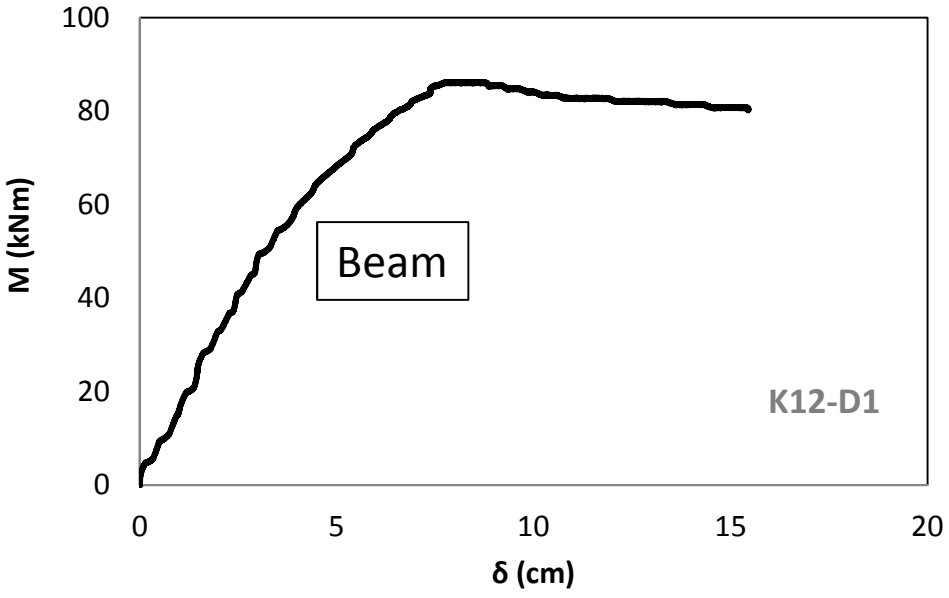

Figure B.5 Bending moment with regard to displacement diagrams derived from the calibration of the artificial plastic hinges for column – beam connections.

(a)

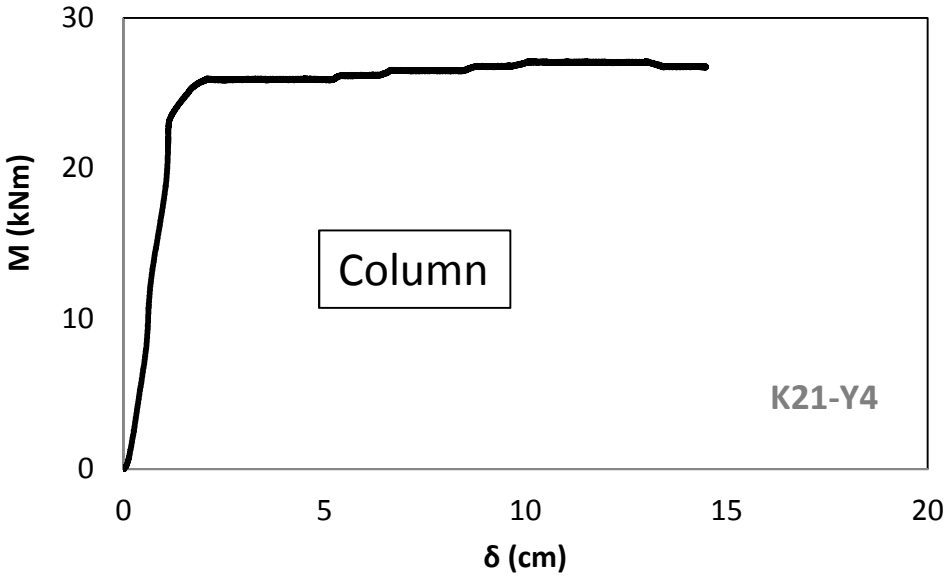

(b)

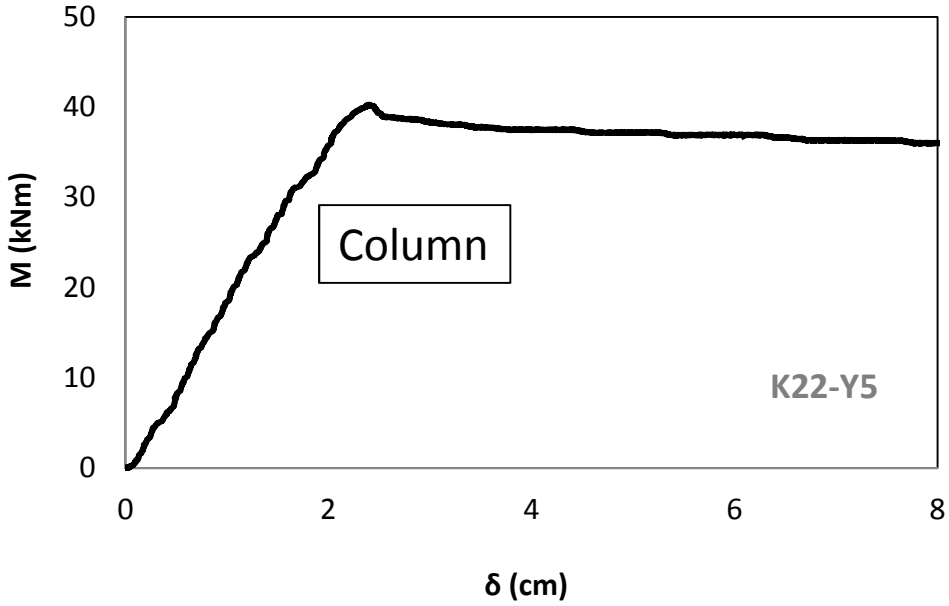

Figure B.6 Bending moment with regard to displacement diagrams derived from the calibration of the artificial plastic hinges for column – beam connections.

(a)

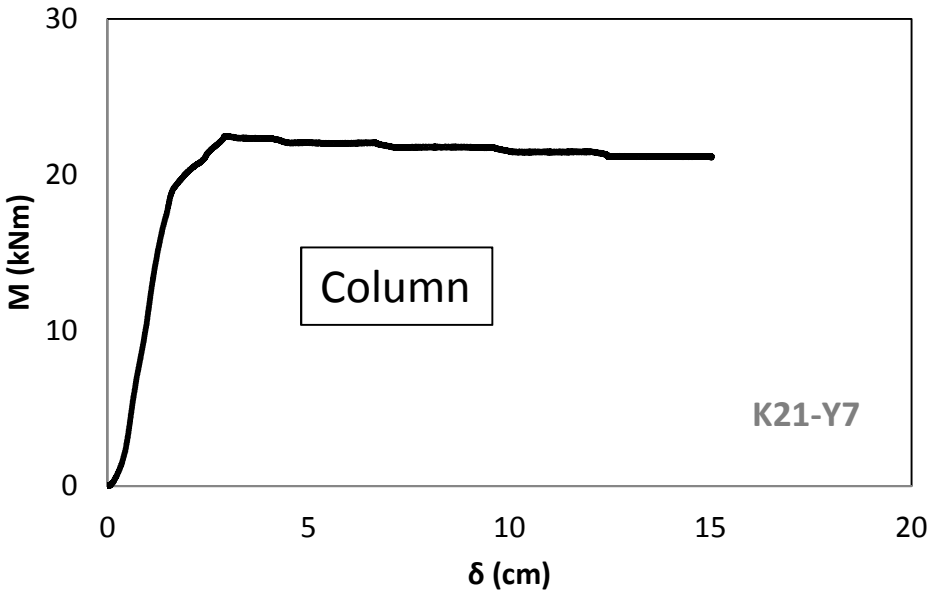

(b)

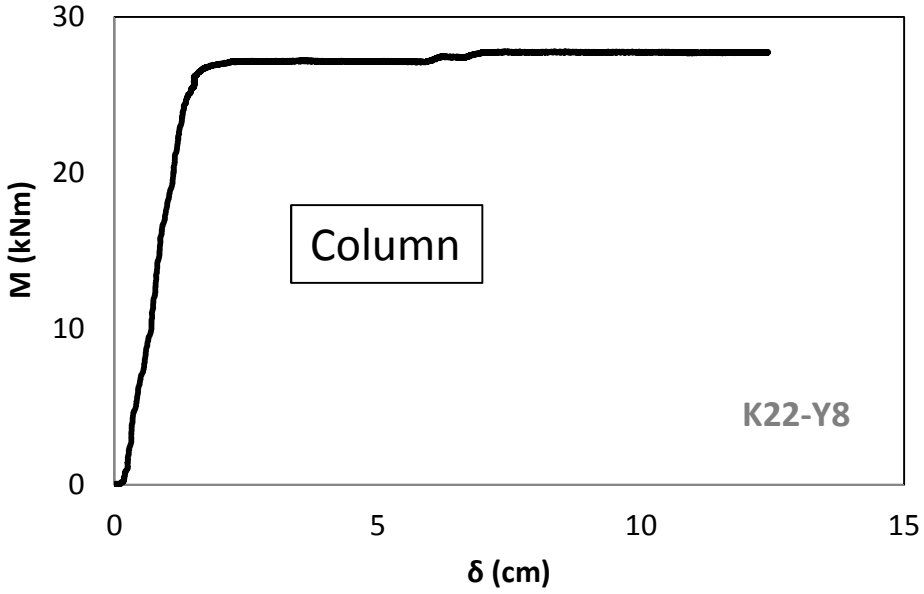

Figure B.7 Bending moment with regard to displacement diagrams derived from the calibration of the artificial plastic hinges for column – beam connections.

(a)

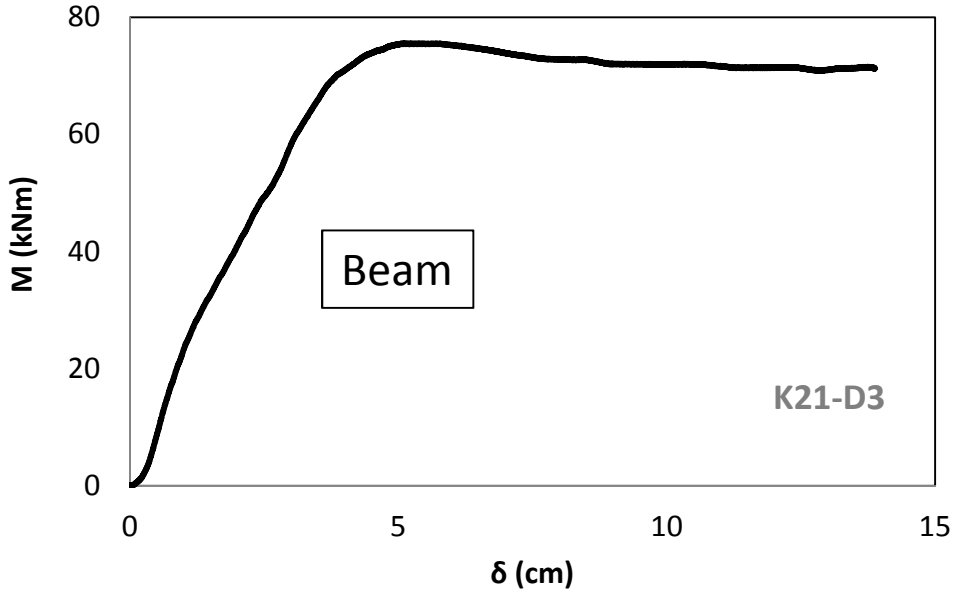

(b)

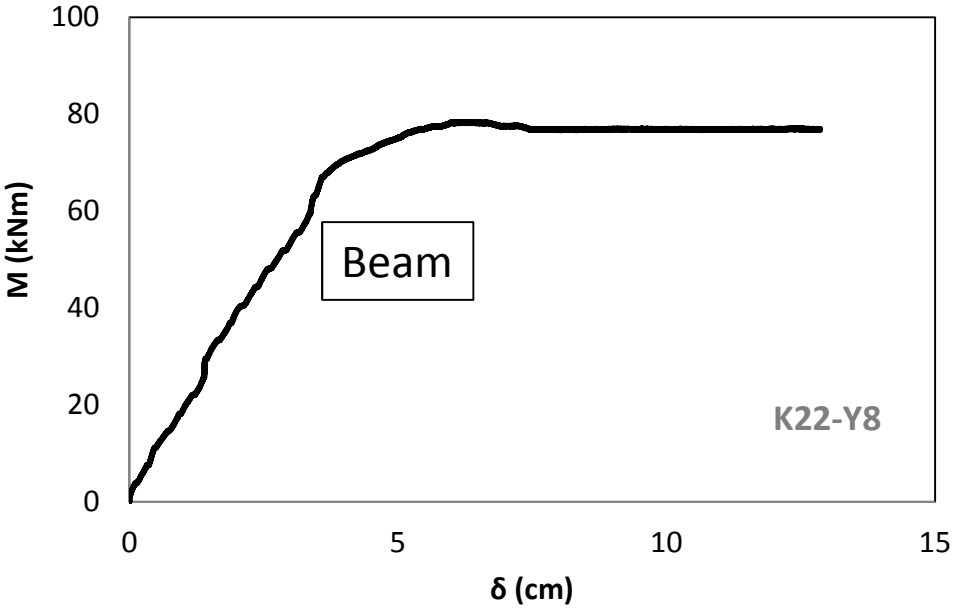

Figure B.8 Bending moment with regard to displacement diagrams derived from the calibration of the artificial plastic hinges for column – beam connections.

(a)

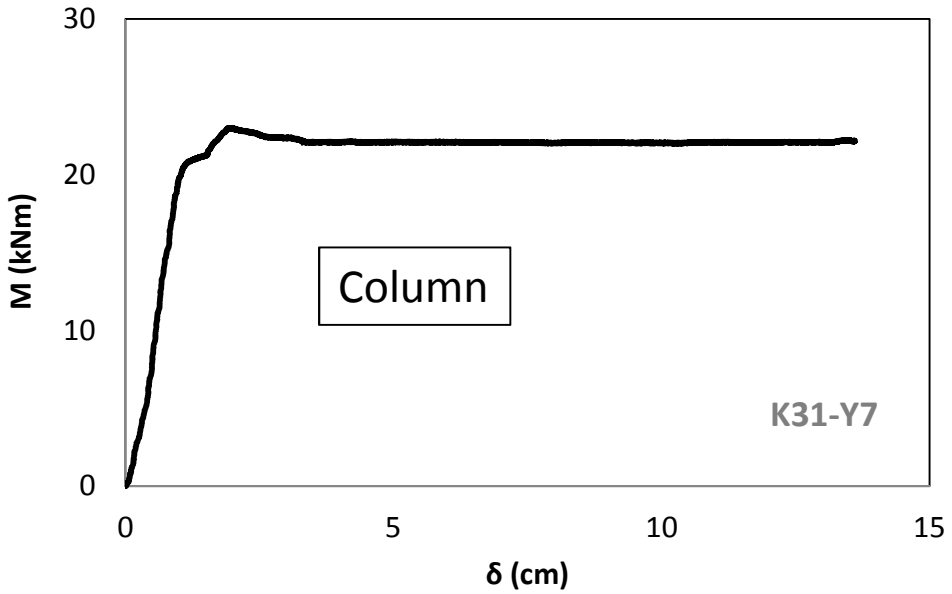

(b)

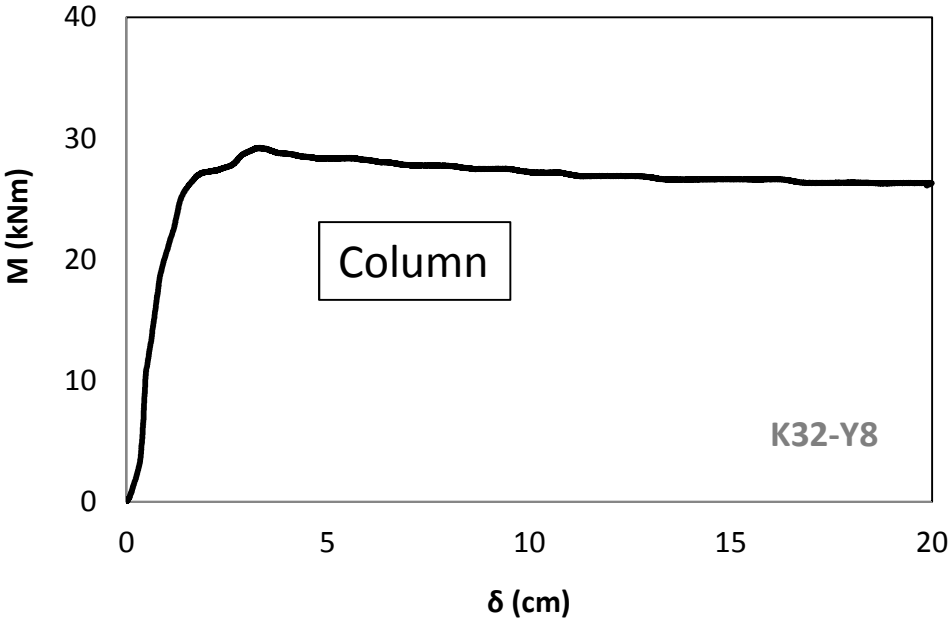

Figure B.9 Bending moment with regard to displacement diagrams derived from the calibration of the artificial plastic hinges for column – beam connections.

(a)

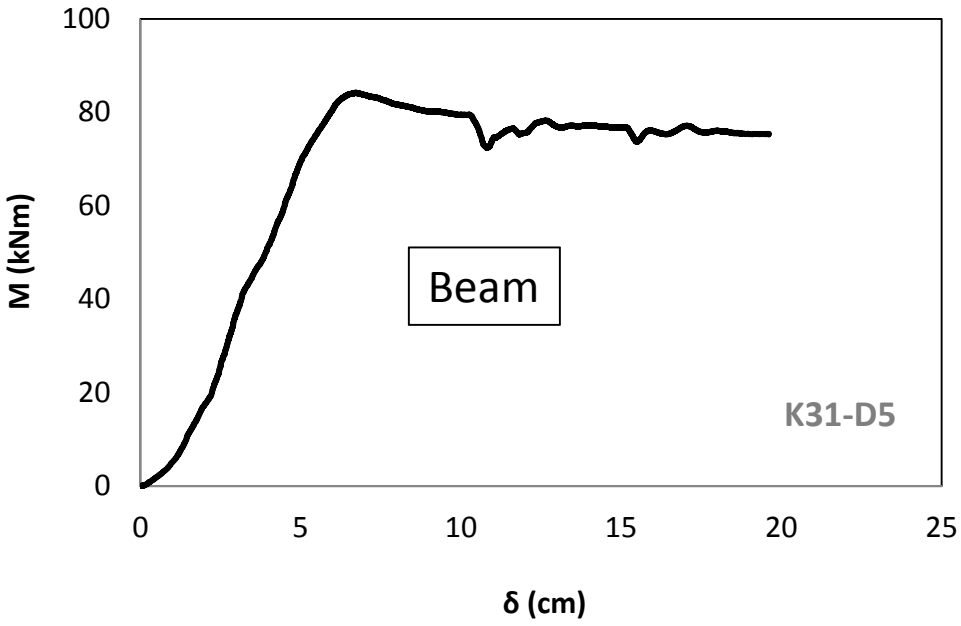

(b)

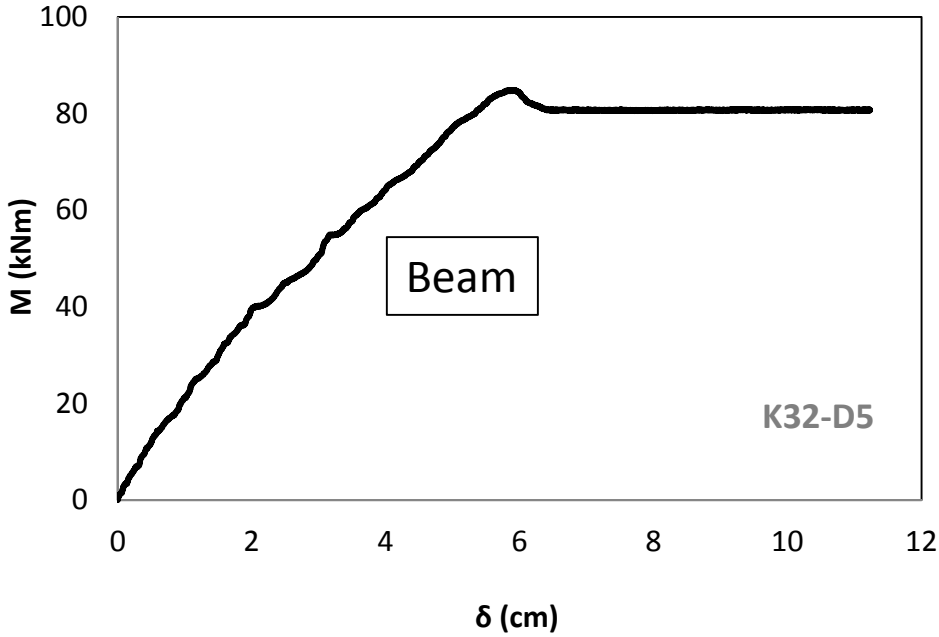

Figure B.10 Bending moment with regard to displacement diagrams derived from the calibration of the artificial plastic hinges for column – beam connections.